TRANSFORMATION OF 2-LINE FERRIHYDRITE AND ITS EFFECT ON ARSENIC ADSORPTION

A Dissertation

by

NAMRYONG HER

Submitted to the Office of Graduate Studies of
Texas A&M University
in partial fulfillment of the requirements for the degree of

DOCTOR OF PHILOSOPHY

August 2007

Major Subject: Civil Engineering

TRANSFORMATION OF 2-LINE FERRIHYDRITE

AND ITS EFFECT ON ARSENIC ADSORPTION

A Dissertation

by

NAMRYONG HER

Submitted to the Office of Graduate Studies of
Texas A&M University
in partial fulfillment of the requirements for the degree of

DOCTOR OF PHILOSOPHY

Approved by:

Co-Chairs of Committee,	Robin Autenrieth
	Richard H. Loeppert
Committee Members,	Ralph A. Wurbs
	Bruce Herbert
Head of Department,	David V. Rosowsky

August 2007

Major Subject: Civil Engineering

ABSTRACT

Transformation of 2-Line Ferrihydrite and Its Effect on Arsenic Adsorption.

(August 2007)

Namryong Her, B.S., Korea University, South Korea;

M.S., Korea Advanced Institute of Science and Technology, South Korea

Co-Chairs of Advisory Committee: Dr. Robin Autenrieth
Dr. Richard H. Loeppert

Although the impacts of foreign species on aqueous transformations and arsenic adsorption by 2-line ferrihydrite (FH2) have been extensively studied, much less is known about the impact of transformation inhibitors on solid-state transformation of FH2 and arsenic adsorption. In this study, the influence of inhibitors (Si(IV), Mg(II), Al(III), Ti(IV), and Ci(citrate)), aging time, and heat treatment on FH2 transformation and arsenic adsorption was investigated. The FH2s were synthesized by mixing Fe(III) salts with an inhibitor at pH 7.5 and air drying for 2 d. With increases in Al/Fe molar ratio, FH2, poorly crystalline Al hydroxide, gibbsite, and bayerite were formed in the FH2-Al series, whereas FH2 was formed in the other FH2s. Heat treatment had a more considerable impact on the transformation, structure, and PZC of FH2 than aging at RT for 235 d. Upon heating the FH2s at 360 ^{o}C, most of the amorphous Fe oxide was transformed into hematite, whereas Si and Al had stronger retarding effects on transformation than the other inhibitors. Hematite and FH2 were identified with increases in Si/Fe molar ratio, whereas with increasing Al/Fe molar ratio, FH2 remained, gibbsite and bayerite were decomposed, and boehmite appeared as a trace component. However, the effect of Si was much more pronounced than that of Al in retarding the transformation. The adsorption density for As(III) on the FH2s (at pH 7) decreased in the order: FH2-Mg-

2 > FH2 > FH2-Al-1, whereas As(V) followed the order: FH2-Al-1 > FH2-Mg-2 > FH2. Compared to aging at RT for 235 d, heat treatment at 360 ^{o}C resulted in significantly reduced arsenic adsorption. The heated FH2 showed a smaller adsorption capacity for arsenic compare to that of the other FH2s. In contrast, the heated FH2-Al and FH2-Si series showed much higher adsorption capacities for As(V) than any other FH2, whereas the heated FH2-Mg series exhibited the largest adsorption capacity of As(III) among the heated FH2s. It is concluded that the use of the FH2-Al, FH2-Mg, or FH2-Si series instead of pure FH2 as filter media in water treatment might achieve more efficient arsenic removal and enhance arsenic retention at waste-disposal sites.

DEDICATION

This dissertation is dictated to Dr. Timothy A. Kramer, now with God. I thank and appreciate Dr. Timothy A. Kramer for the advice, inspiration, suggestions, criticism and support throughout the whole course of this investigation.

He was a truly kind and generous person.

May he rest in peace!

ACKNOWLEDGEMENTS

I wish to extend my faithful thanks and appreciation to the following individuals. I would like to extend my sincere thanks to Dr. Robin Autenrieth, Dr. Richard H. Loeppert, and Dr. Bruce Herbert for their patience, time commitments, and helpful comments as my committee members.

Further, I thank all my colleagues and fellow research group members for their friendship, support, generosity, and time sharing. My special thanks to Dr. Jin-Wook Kim who has been always with me about everything for last five years.

Finally, I am sincerely grateful to my father, mother, brothers, sister, and two sons, Yong and Bin. A very special thanks goes to my wife, Sung-Nyun Choi, who encouraged and supported me to reach my goal during our College Station life of five years.

TABLE OF CONTENTS

CHAPTER Page

CHAPTER Page

LIST OF TABLES

TABLE Page

LIST OF FIGURES

FIGURE Page

FIGURE Page

FIGURE Page

FIGURE Page

NOMENCLATURE

p	=	the partial pressure of the adsorbate
p_0	=	the equilibrium vapor pressure
p/p_0	=	the relative pressure or the adsorption isotherm
v	=	the volume of gas adsorbed
v_m	=	the volume of gas adsorption in a monolayer
c	=	a BET constant
K_a^s	=	conditional acidity constant
$K_{a(\text{int})}^s$	=	intrinsic acidity constant
σ_{tot}	=	total charge
σ_{H^+}	=	net proton charge due to the binding of protons or OH^- ions
σ_{IS}	=	inner-sphere complex charge
σ_{OS}	=	outer-sphere complex charge
$\hat{Y}$	=	the mean of particle size (μm)
S_X, S_Y	=	standard deviation
θ	=	the Bragg angle
d	=	the distance between successive scattering planes of atoms
R^2	=	regression coefficient
$\overline{X}$, $\overline{Y}$	=	mean
$\hat{\sigma}_{X,Y}$	=	estimated covariance
$\hat{\rho}_{X,Y}$	=	estimated correlation
n	=	number of sample
$[Fe_o]$	=	the ammonium oxalate-extractable Fe content at any given time
$[Fe_t]$	=	the total Fe content
k	=	transformation rate constant
k_T	=	transformation constant of temperature dependence
t	=	time (days)
T	=	temperature (^oC)
$T_{75\%}$	=	75 % conversion-temperature
$q_{e,max}$	=	maximum arsenic adsorption capacity
SS_{Error}	=	sum of squared errors
SS_{Model}	=	model sum of squares
SS_{Total}	=	total sum of squares
Y_i	=	observed value
$\hat{Y}_i$	=	predicted value

CHAPTER I

INTRODUCTION

1.1 Characteristics of 2-line Ferrihydrite

Ferrihydrite (FH), a reddish-brown iron oxide, is a common iron oxide in low-temperature surface environments such as water wells, hot- and cold-spring deposits, and lake-bottom sediments [1]. FH occurs predominantly in bands in unconsolidated quaternary rocks, ferriferous springs, acid mine water deposits, bog ores, and lake waters [2]. FH can be expected in relatively young soils or in those where its transformation to more crystalline oxides is inhibited or retarded because of kinetic inhibitions [2]: ground water and stagnant water soils (gleys and pseudogleys), podzols in cool regions, and paddy soils [3]. FH is important in environmental geology due to its common occurrence in mine-waste environments as well as its demonstrated ability to adsorb or coprecipitate with organic compounds and the ions of various elements [1, 4].

1.1.1 Crystal Structure

Ferrihydrite, named by Chukhrov [5], is a poorly crystalline iron oxide. Two extremes of crystal order are referred to as 2-line ferrihydrite (FH2) and 6-line ferrihydrite (FH6) based on the number of broad X-ray peaks that they give [2]: FH2 for material that exhibits poor crystallinity and FH6 for that which is well crystallized. The FH2 shows two extremely broad XRD (X-ray diffraction) peaks at 0.25 nm and 0.15 nm due to the presence of hexagonally close-packed oxygens [6], whereas FH6 shows

---

This dissertation follows the style of Journal of Colloid and Interface Science.

broadened six- to seven-line XRD patterns and was first prepared by Towe and Bradley [7].

Although several different structures of FH have been proposed, its structure is not yet fully understood due to the low degree of crystalline order [2, 8]. From XRD results, Towe and Bradley [7] and Chukhrov et al. [9] proposed the original models of FH6 that involved a defective hematite structure based on a hexagonal close packing array of anions with vacant Fe (III) sites and a considerable amount of water. Compared to hematite, their structural models differ in that the Fe (III) ions are randomly distributed over the interstices, and these models have less Fe (III) and more OH^- and H_2O in FH than in hematite.

Eggleton et al. [10] suggested a second structural model for FH6 based on double-hexagonal close-packed oxygens, with two adjacent layers of iron in octahedral coordination followed by two layers of tetrahedral iron. They concluded that FH6 contains 36% Fe in tetrahedral sites. However, Manceau et al. [11] concluded that the amount of tetrahedrally coordinated Fe in the interiors of FH6 was too small to be detectable. A third structural model was proposed on the basis of the agreement between experimental and simulated XRD data [12] together with structural data from EXAFS (extended X-ray absorption fine structure) spectra [13]. In the third model, FH6 is a mixture of three structural components: (1) defect-free FH consisting of *AcBcAbCbA*……anion (oxygen or hydroxyl) close arrangement with the Fe atoms randomly distributed only at octahedral sites and with 50% occupancy, (2) defective FH with *AcBcA* and *AbCbA* fragment occurring randomly with equality and the Fe atoms in

each fragments being identically ordered in a hexagonal super-cell (where *A* and *B* are anion positions and *c* and *b* represent Fe sites), and (3) ultradispersed hematite.

Though several attempts have been made to determine the structure of FH2, the results are contradictory. Some studies proposed a local structure based on edge- and corner-sharing Fe octahedra, resembling that of goethite or akaganéite [14~16], whereas other studies reported that many octahedra share faces after aging for several hours at 92 ^{o}C before washing [13, 17]. Also, Waychunas et al. [16] suggested a close structural resemblance between FH2 and the defect-free FH6 proposed by Drits et al. [12]. Based on two bright rings at ~0.15 and 0.25 nm and numerous faint rings in XRD and SAED (selected area electron nano-diffraction) patterns, Janney et al. [18] suggested that FH2 has a two-dimensional structure consisting of a basic tetrameric unit, with disordered stacking of close-packed anion layers and randomly distributed Fe atoms.

Generally all of the Fe(III) ions in the interiors of FH crystals are octahedrally coordinated [14, 16, 17, 19, 20, 21]. However, the presence of some Fe(III) ions with less than 6 coordination at the surface of FH, perhaps as tetrahedra were suggested. The results obtained by Zhao et al. [19] using EXAFS and XANES (X-ray absorption near-edge structure) spectroscopy showed that as much as 20~30% of the total iron in FH6 could be in tetrahedral coordination due to dehydroxylation, although only at the particle surface. The sites with tetrahedral coordination at the surface were coordination-unsaturated. The drier the sample as a result of dehydroxylation, the lower the coordination is at the surface [20]. According to the coordination-unsaturated (CUS) model [19, 20], the core of FH consists of iron in octahedral coordination, whereas the surface contains considerable iron in tetrahedral coordination. The CUS model may help

to explain the seemingly contrasting structural properties and the high adsorptive capacity and chemical behavior of FH. However, based on a reexamination on the results of Zhao et al. [20], Manceau and Gates [21] concluded that the suggested presence of 20~30% tetrahedral sites in FH is excessive. A study by Waychunas et al. [15] led to a conclusion that the structure of FH consists of octahedral chains in which the Fe(III) octahedra are joined by shared edges, forming short double chains. However, with an increase in aging time, the chains lengthen, dioctahedral chains become more abundant, and these link to other chains by sharing corners to form a cross-linked structure, resulting in crystal growth; i.e., reducing the number of available adsorption sites. Although none of the contemporary models for the FH structure is incontrovertible, there seems to be a universal agreement that the fundamental structure unit within FH is the $Fe(O, OH)_6$ octahedron with Fe at the center and O, OH, and OH_2 as ligands [4]. The Fe positions may be vacant and the O and OH partially replaced by OH_2, leading to the diffraction pattern broadening.

The main structural difference between FH2 and FH6 is the size of the coherently diffracting domains [12, 13]. High-resolution transmission electron microscopy (HRTEM) images showed 2-4 nm coherently diffracting domains in FH2 and 5-6 nm crystallity in FH6 [22]. HRTEM results indicated that FH6 appears as single crystals with a hexagonal outline and appreciable internal order, whereas both of these characteristics are less well demonstrated in the 2-line variety [22].

FH2 forms by fast hydrolysis of a $Fe(NO_3)_3$ solution at pH 7~8 and room temperature (RT), whereas FH6 is synthesized by forced acid hydrolysis of a $Fe(NO_3)_3$ solution at OH/Fe = 0 and 75 ^oC for 10~12 min [2]. There is ambiguity in the structural

and genetic relationship between FH2 and FH6. However, although these two forms of FHs are synthesized under different conditions, Lewis and Cardile [23] showed that acid hydrolysis of dilute $Fe(NO_3)_3$ solutions (10^{-4}~10^{-2} M) at RT can result in FH6 with some FeOOH at slow hydrolysis as well as FH2 after quick hydrolysis. Also a complete series of FHs between 2- and 6-line varieties were prepared by: (1) varying the rate of hydrolysis of a 0.1 M $Fe(NO_3)_3$ solution (at pH 7 and RT) and (2) oxidizing an 0.1 M $FeCl_2$ solution (at pH 6.5 and RT) containing up to 73 mmol Si(IV)/L [24]. Experiments at RT and pH 7 by Kukkadapu et al. [25] have shown that FH6 eventually dominated in an FH2 suspension containing Ni(II) upon continued aging under aerobic conditions, and the transformation of FH2 containing Ni(II) to FH6 was considerably faster under anaerobic conditions.

A structural investigation [26] of FH2 doped with Si(IV) using XRD and TEM showed that with an increase in the Si/Fe molar ratio, crystallinity decreased and the particle size increased. A model was proposed in which doped Si^{4+} ions are not substituted for Fe^{3+} ions but are chemisorbed on the FH2 surface as Si-O-H and Si-O-Fe groups. A structural study [27] with FH2 containing Ti(IV) suggested that with increasing Ti/Fe molar ratio, two broad XRD peaks of FH2 slightly shifted to the left, a newly weak peak was detected at 2θ = 45 degree, the particle size decreased, and surface area increased. A long-term (16~20 y) experiment [28] of Al(III)-containing FH2 at 25 ^{o}C and at pH values from 4 to 7 showed that aluminum retards the crystallization of FH2 and promotes the formation of hematite over goethite. Fe(III)-Al(III) oxides (Fe/Al molar ratios of 1 ~ ∞) synthesized at pH 5.5 showed very broad XRD peaks characteristic of FH6, whereas the XRD pattern of the sample in the absence of iron showed poorly

crystalline gibbsite [29]. The XRD patterns of Al(III)-containing FH2 showed that Al/Fe molar ratios > 0.25 lead to bayerite and gibbsite with broad background peaks indicative of poorly crystalline hydroxide [30].

Towe and Bradley [7] originally suggested $Fe_5HO_8 \cdot 4H_2O$ as the bulk formula for FH. Its formula is still being debated. In addition, five proposals as alternatives are $5Fe_2O_3 \cdot 9H_2O$ [31], $Fe_6(O_4H_3)_3$ [32], $Fe_2O_3 \cdot 2FeOOH2.6H_2O$ [33], $Fe_4(O,OH,H_2O)_{12}$ for the 2-line variety, and $Fe_{4.6}(O,OH,H_2O)_{12}$ for the 6-line type [10]. However, no exact formula has been widely accepted because of difficulties in separating precisely structural OH and H_2O from adsorbed water [2].

1.1.2 Specific Surface Area

Specific surface area is the surface area of a unit mass of material. The surface area is inversely related with particle size. The specific surface area of FH can influence its reactivity, interaction with adsorbents, phase transformation, and thermodynamic stability [1, 2]. The surface area and particle size of FH is strongly governed by the conditions under which crystal growth occurs [1, 2]. Many factors can influence the surface area of FH: temperature, source of iron, the presence of interfering ions or organics, and even stirring. Also the surface area depends on the method used to measure it. Various methods have been used for determining surfaces area of FH: BET (N_2, Argon, and H_2O) [34], EGME (ethylene glycol monoethyl ether) and negative adsorption of Mg^{2+}, Na^+, and phosphate. The particle size of FH was reported to be 1~3 nm for FH2 and 5~6 nm for FH6 [22]. Thus FH has a high surface area. The reported specific surface area of FH as determined by various techniques and adsorbents ranged from 100 to 700 m^2/g.

However, surface areas of about 200~400 m^2/g seem to be typical of the values obtained by BET analysis (Table 1.1). To measure the surface area of FH, BET analysis using N_2 as an adsorbate is by far the most common method, because the method is generally recognized as a standard. The degree of adsorption of N_2 (at the boiling temperature of liquid N_2 – 77 ^oK) on the outgassed sample is measured as a function of the relative pressure, p/p_0, i.e., an adsorption isotherm. In linearized form the BET method reads

$$\frac{p}{v(p_0 - p)} = \frac{1}{v_m \cdot c} + \frac{(c-1)}{v_m \cdot c} \cdot \frac{p}{p_0} \tag{1.1}$$

where p is the partial pressure of the adsorbate, p_0 its equilibrium vapor pressure, v the volume of gas adsorbed, v_m the volume of gas adsorption in a monolayer, and c is a BET constant. The specific surface area is then calculated from v_m using the area occupied by one molecule of the adsorbate, e.g., 0.162 nm^2/molecule for N_2 [1, 2].

Owing to the aggregation of particles, there are some difficulties in measuring surface area, that is, the internal area is not completely accessible to measurement techniques [1, 2]. The physical pretreatment of sample such as grinding and temperature during the outgassing procedure may also cause an additional problem in measuring surface area. The outgassing, which removes physically adsorbed water, may lead to a phase change and hence an alteration in the specific surface area, especially in the case of amorphous and poorly crystalline materials such as FH [2]. Clausen and Fabricius [35] reported that FH2 was outgassed for 19 hr at RT, at which temperature, stable BET surface areas of between 215 and 229 m^2/g were obtained. The FH2 showed a maximum specific surface area (301 m^2/g) at temperatures between 150 and 250 ^oC, whereas a color

change in FH2 was observed at temperatures between 100 and 150 ^{o}C. It was recommended that temperatures between 90 and 120 ^{o}C are necessary to prevent structural transformation of the FH2 during the outgassing procedure [36].

Table 1.1 Specific Surface Area of 2-line Ferrihydrites by the BET Method

Method	Specific surface area (m^2/g)	Reference
BET-Argon	215~270	Van der Giessen, 1966 [37]
	68~425	Carlson et al., 1981 [38]
BET-H_2O	300 (± 50)	Davies-Colley et al., 1984 [39]
	320~455	Hofmann et al., 2004 [40]
BET-N_2	340	Eggleton et al., 1988 [10]
	122~185[a]	Stanjek et al., 1992 [41]
	269	Hansen et al., 1994 [42]
	230	Axe et al., 1995 [43]
	176~313	Weidler et al., 1997 [36]
	206	Raven et al., 1998 [44]
	170	Martìnez et al., 1999 [45]
	215~301	Clausen et al., 2000 [35]
	205	Larsen et al., 2001 [46]
	245 (± 10)	Scheinost et al., 2001 [47]
	277	Leone et al., 2001 [48]
	368~437[b]	Ishikawa et al., 2002 [27]
	253	Grafe et al., 2002 [49]
	~260	Voegelin et al., 2003 [50]
	365~379	Hofmann et al., 2004 [40]

[a]Samples were not outgassed.
[b]Fe-Ti mixed oxide with different atomic ratios in Ti/Fe from 0 to 4 have been prepared by hydrolysis of aqueous solutions and a freezing method with N_2.

1.1.3 Surface Functional Groups

According to the CUS model [10, 19, 20], the surface of FH under dry conditions may contain considerable iron atoms in tetrahedral coordination. The sites with

tetrahedral coordination at the surface may be coordination-unsaturated. In aqueous systems, surface Fe atoms, which function as Lewis acids, coordinate Lewis bases (hydroxyl ion, H_2O or NH_3) which share their electron pairs with iron [1, 2]. Upon adsorption of water molecules, they usually dissociate, leading to a surface covered by OH groups coordinated to Fe atoms [1, 2]. After hydroxylation of FH, further adsorption of water molecules hydrogen-bond to the surface OH groups can occur. Owing to possession of a double pair of electrons together with a dissociable hydrogen atom from the surface OH group, FH can react with both acids and bases, i.e., the FH is amphoteric (Eqs. 1.2 and 1.3) [1, 2]. The surface OH groups can be coordinated by one, two, or three underlying Fe atom [1, 2]. If each Fe-O bond assigns a charge of +1/2 due to a sixfold coordination of the Fe atom, these singly, doubly and triply coordinated groups possess charges of -1/2, 0 and +1/2, respectively. The reactivity of these different types of OH groups should vary according to the number of underlying Fe atoms coordinated to the surface functional groups. The overall density of these groups varies according to the crystal structure as well as the degree of development of the different crystal faces [1, 2]. From acid/base titration studies, Charlet et al. [51] suggested that the reasonable value for the average density of OH groups on FH is 1.97 sites/nm^2. The dissociation of the surface OH groups leads to charge on the FH surface [1, 2]. The reactions as acid/base equilibria are expressed by the following dissociation reactions (≡ denotes the surface):

$$\equiv FeOH_2^+ \Leftrightarrow \equiv FeOH + H^+ \qquad K_{a1}^s = \frac{\{\equiv FeOH\}[H^+]}{\{\equiv FeOH_2^+\}} mol/dm^3 \qquad (1.2)$$

$$\equiv FeOH \Leftrightarrow \equiv FeO^- + H^+ \qquad K_{a2}^s = \frac{\{\equiv FeO^-\}[H^+]}{\{\equiv FeOH\}} mol/dm^3 \qquad (1.3)$$

where { } = surface species; [ ] = solution species, and K_a^s = conditional acidity constant obtained by combining acid/base titration data with the site density.

1.1.4 Point of Zero Charge

The ionization of the surface OH group results in the development of charge on iron oxides, and the charge is balanced by a layer of counter ions of opposite charge located in the aqueous phase [1, 2]. This charged surface, combined with the diffuse layer of counter ions in solution phase, comprises the electrical double layer. The surface-charge density can depend on the potential gradient and a number of conceptual and mathematical models have been used to describe the distribution of charges in the double layer [1, 2]. Although iron oxides possess little or no permanent surface charge ($\sigma_O \cong 0$) resulting from isomorphous substitution, they may generate cation and anion exchange capacity due to the adsorption of potential-determining ions (usually H^+ and OH^-) [52]. One of the important features of iron oxides is the development of surface charge that depends on pH, which is referred to as variable charge or pH-dependent charge [53]. The total charge of the iron oxide surface is described by the following equation [1, 2]:

$$\sigma_{tot} = \sigma_{H^+} + \sigma_{IS} + \sigma_{OS} \qquad (1.4)$$

where σ_{H^+} = net proton charge due to the binding of protons or OH^- ions, σ_{IS} = inner-sphere complex charge, and σ_{OS} = outer-sphere complex charge.

The pristine point of zero charge (PPZC) is defined as the pH value where the charge on the surface arising from all sources is zero [54]. Without specific adsorption, this pH is also often termed the point of zero charge (PZC) or the isoelectric point (iep). The point of zero net proton charge (PZNPC) is the pH at which net adsorption of potential determining ions (H^+ and OH^-) on the surface is zero. Two methods are generally used to characterize electrochemical behavior: 1) potentiometric titration and 2) electrophoresis [1, 2]. The PZNPC is determined by potentiometric titration of iron oxides in an indifferent electrolyte and is taken as the pH value where the titration curves obtained by plotting the amount of acid or base versus the pH value for several different concentrations intersect. Electrophoresis is related to the movement of charged particles relative to a stationary solution in an applied potential gradient; the particles move acording to their charge. A negative particle migrates to the cathode, whereas a positively charged particle moves towards the anode. Therefore, the charge on the particles and hence the direction of movement varies according to the pH of the solution; the pH value where there is no movement is termed the iep. The intrinsic acidity constants of the surface groups are able to predict the PZC value of iron oxides by the well-known relationship [1, 2]:

$$pH_{pzc} = 1/2(pK_{a1(\text{int})} + pK_{a2(\text{int})}) \tag{1.5}$$

where $K_{a(\text{int})}$ = intricsic acidity constant.

Although the exact relationship depends on the model adopted for describing the acid/base behavior of a solid surface in electrolytic solutions, the PZC value provides an

estimate of the acidity of the iron oxide surface. The relationship between the pH of solution and the distribution of surface OH groups shows that negative, positive and neutral functional groups can coexist on the iron oxide surface [1, 2].

FH has PZC's in the pH range of 7.8~8.9 [51, 55~58]. However, the value of PZC is influenced by factors such as the temperature and the presence of foreign species in the system. Dehydroxylation of iron oxides induced a decrease in concentrations of surface OH groups, resulting in an acid shift in the PZC [59]. Increase in temperature of the suspension from 25 ^{o}C to 90 ^{o}C resulted in lowering the PZC of magnetite form 6.5 to 5.4 [60]. This acid shift in the value of PZC may have partly resulted from both changes in the ionization constant of water due to an increase in temperature and changes in the relative affinity of protons for the surface. When the hematite synthesized by wet precipitation was heated to a temperature above 1000 ^{o}C, the PZC value dropped by three pH units [61].

Specifically adsorbed ions, forming inner-sphere complexes, modify the surface charge on iron oxides and hence induce a shift in the PZC/iep [62]; e.g., phosphate, silicate, selenite, arsenite, chloride, fluoride, citrate, and oxalate. After leaching chloride ions by extended washing with NaOH, the iep of hematite prepared from Fe(III) chloride solution increased from 5.5 to 7.2 [63]. The PZC value of FH coprecipitated with a small amount of silicate was shifted from 7 to 5.3 [64, 65]. The iep value of hematite coated with silicate dropped from 7 to 3 [66], whereas the value of that coated with aluminum or chromium oxide was raised [67]. The PZSE (point of zero salt effect) values of FH2 and Al(III)-containing FH2 (Al/Fe molar ratio = 1) were 7.6 and 8.7, respectively [30]. Specific adsorption of Si(IV) and Mg(II) on goethite particle surfaces resulted in a shift

of iep to a more acidic pH for Si(IV) and a more basic pH for Mg(II) [68, 69]. Owing to surface CO_2 removal, the purging of goethite with N_2 for two months increased the PZC from 8.1 to 9.0 [70, 71]. Adsorption of arsenate on FH2 shifted the PZC from 8.5 to 6.1 [72].

1.2 Transformation of 2-line Ferrihydrite

Two-line ferrihydrite (FH2) is known to combine with heavy metals in aqueous systems through adsorption or coprecipitation [1, 2, 73]. Especially owing to its large surface area, high adsorption capacity, and low costs, FH2 has been used as an effective adsorbent for removing heavy metals from water or wastewater. FH2 formed initially is poorly crystalline [1, 2, 4, 38]. However, FH has pK_{sp} values in the range of 37~39 and is thermodynamically unstable with respect to goethite and hematite, with pK_{sp} values of 41 to 43, respectively. FH, therefore, will ultimately transform to goethite or hematite, depending on the prevailing solution conditions (temperature, pH, and the presence of foreign species) [74, 75]. The vulnerability of goethite and hematite to microbial iron reduction may be considerably decreased due to their lower solubility [76]. Judging from the long-term stability of heavy metal binding, the transformation of amorphous FH to crystalline iron oxides (goethite or hematite) may be advantageous. The crystalline iron oxides, however, are likely to have diminished capacity to combine with heavy metals [77]. The transformation of FH to iron oxides is summarized in Table 1.2 [1, 2].

1.2.1 Aqueous Transformation of 2-line Ferrihydrite to Other Iron Oxides

FH is known be an important precursor for iron oxide formation in various natural

Table 1.2 Transformation of Ferrihydrite to Other Iron Oxides

Precursor	Product	Type of transformation	Preferred medium
FH	Hematite, Maghemite	Thermal dehydration/ dehydroxylation	Gas/vacuum
	Goethite	Dissolution/reprecipitation	Aqueous solution at pH 4 &11
	Akaganéite	″	Acid media; presence of Cl
	Lepidocrite	″	pH 6, presence of cysteine
	Hematite	Aggregation, short-range crystallization within FH aggregate	Aqueous solution at pH 6-8
	Substituted magnetite	Dissolution/reprecipitation	Alkaline solution with M^{II}

surface environments [1, 2]. As a result of FH transformation, goethite and hematite often form together in the end product due to their similar thermodynamic stabilities [1, 2]. Aqueous transformation of FH into crystalline iron oxides is widely believed to proceed by two competing mechanisms [1, 2, 78, 79, 80]. Goethite formation results from the dissolution of FH followed by nucleation and precipitation of the crystalline oxide, whereas hematite formation occurs through dehydration and internal atomic arrangement of the solid FH, with less dependence on the dissolution mechanism. The proportion of each iron oxide (goethite or hematite) in the end product depends on the reaction kinetics and hence the reaction conditions [1, 2]. Compared with XRD, Mössbauer spectroscopy, and EXAFS, net transformation can be monitored more conveniently by a single extraction with acid oxalate solution in the dark (AOD) [81, 82] where residual FH is dissolved and the crystalline product left intact. The degree of transformation at any time is expressed as the ratio $[Fe_o]/[Fe_t]$, in which $[Fe_o]$ is the acid oxalate soluble iron (i.e., the FH) and $[Fe_t]$ is the total iron in the system.

Temperature and pH play important roles in FH transformation [8]. Generally increases in both temperature and pH accelerate the transformation reaction. Temperature

and pH can also affect the goethite/hematite ratio. As shown in Figure 1.1 [8], the dominant factor (in the pH range of 2~12 and the temperature range of 4~30 ^{o}C after 3392~4596 days of storage) that determines the ratio is pH. Hematite predominates over goethite at about pH 7~8 over a wide temperature range (4 to at least 90 ^{o}C), whereas goethite forms as the sole product at pH 12~14. Since goethite forms by dissolution of the FH, the proportion of goethite in the end product parallels the solubility of FH which is at a minimum at the PZC (about pH 7~8). It was suggested by Schwertmann et al. [8] that nano-particle aggregation was required to induce transformation of FH to hematite. The extent of FH aggregation is at a maximum near the pH of zero net charge of the FH surface (pH 7~8), and crystallizing hematite nuclei are apparently provided by a short-range dissolution process involving the FH aggregates. As the pH shifts to either direction from the PZC, the proportion of goethite increases. Hematite, however, dominates again at pH values < 4 and > 14. A speciation change from monovalent to higher valent species which are less conducive to goethite formation might outweigh the increasing solubility of FH [79, 83, 84].

The transformation of FH to goethite is straightforward nucleation/crystallization in the bulk solution. Small, soluble units such as $Fe(OH)_2^+$ are involed in growth in the acid, whereas $Fe(OH)_4^-$ in the alkaline range [6, 85~87]. Monovalent species are the most appropriate growth units since they need to donate only one unit of charge upon incorporation into the crystal. The mechanism of hematite formation from FH in an aqueous system seems more complicated than that of goethite formation. A combination of aggregation-dehydration-rearrangement process induces hematite formation for which the presence of water appears essential [2].

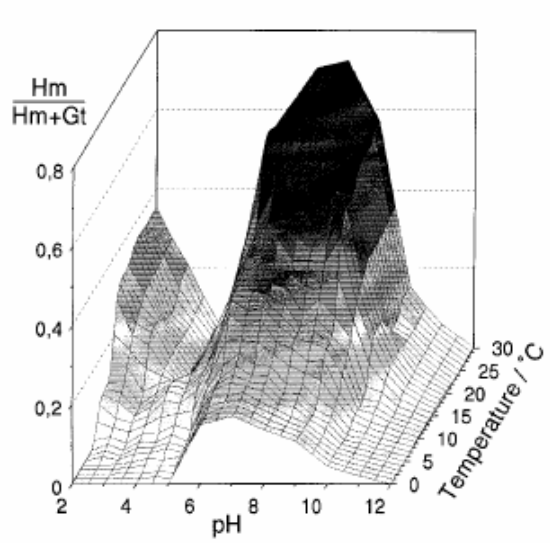

Figure 1.1 Hematite (Hm) and Goethite (Gt) Formation from 2-line Ferrihydrite in the pH Range of 2~12 and the Temperature Range of 4~30 ^{o}C after 9.3~12.6 Years of Storage in Water [8].

EXAFS results [14, 17] showed structural details about this process at 92 ^{o}C: face-sharing between Fe octahedra appeared before XRD showed any indication of hematite. It is accompanied by internal redistribution of vacancies in the anion framework and by further dehydration. The dehydration process induces removal of a proton from an OH group and causes elimination of a water molecule, resulting in formation of an oxo linkage. The local charge imbalance resulting from proton loss is compensated for by migration and redistribution of Fe(III) within the cation sublattice.

The mechanism of hematite formation from FH in aqueous systems is fundamentally different from that for solid-state transformation by dry heating [1, 2]: Some adsorbed water is necessary for the non-thermal transformation of FH to hematite. During the transformation of FH to hematite, TEM [88] shows that the nano particles of FH gradually coalesce to denser aggregates, finally forming 50 nm-sized single hematite crystals. Hematite nucleation is likely to take place in these FH aggregates. In other

words, aggregation seems to facilitate or even to be a prerequisite for the non-thermal transformation of FH to hematite. There was no hematite formation from a stable sol held at pH 4 and 5 for 16-17 yr at 24 ^{o}C [8, 28]. This result differs from the maximum hematite formation at neutral pH, i.e., close to the PZC in which the solubility of FH is at a minimum, whereas aggregation is at a maximum. Compared with the gradual peak sharpening observed during dry heating of FH, the XRD peaks of hematite are relatively sharp at the very beginning of transformation in aqueous systems [8, 41]. Bao and Koch [89] showed a direct proof for the involvement of free water in the transformation to hematite. The oxygen of the hematite transformed from FH2 in the presence of water with $\delta^{18}O$ of -8.0 ‰ showed the same isotopic ratio as this water, demonstrating that the oxygen resulted predominantely from the water present during the transformation and not from the FH precursor.

In summary, hematite can form from aggregated FH in the presence of water by a short-range crystallization process. Even adsorbed water is enough for the conversion of of FH to hematite to take place. There is significant evidence to support the above concept [1, 2]. The evidence is: (1) aggregation is essential, (2) a minimum amount of adsorbed water is necessary (ca. 100~150 g/kg of FH) below which no transformation occurs, (3) a nucleation phase precedes the transformation of FH to hematite, (4) the hematite is fairly well crystalline from the beginning, i.e., the XRD peaks of hematite are relatively sharp from the very beginning of the transformation, and (5) ^{18}O from the free water added to the system is detected in the hematite structure.

1.2.2 Effect of Foreign Species on the Aqueous Transformation of 2-line Ferrihydrite

Foreign species can influence the transformation behavior of FH, that is, some species can stabilize FH for long periods of time since they show a high affinity for surface groups of FH [1, 2]. Generalil foreign species can have two different influences on the conversion of FH to other iron oxides, either through changing the rate of the conversion, usually by delaying the process, or changing the composition (mainly the hematite/goethite ratio) and properties of the end product [1, 2]. There are two principal mechanisms of interaction between FH and foreign species [1, 2]: (1) Foreign species retained either via adsorption (ligands) or by structural incorporation can suppress the reactivity of FH towards internal ordering and/or dissolution; (2) foreign species in solution can impede nucleation or growth of goethite by competing with soluble Fe(III) species for sites on the subcritical nucleus or the growing crystal. This later mechanism is not related to the presence of FH.

The retardation of FH conversion can involve the formation of a covalent bond between the coprecipitated metal and structural OH groups at the iron oxide surface although this mechanism has not been precisely confirmed [90]. In the formation of goethite, retardation of the structural transformation is related to inhibition of FH dissolution due to sorption of a foreign metal. This mechanism was supported by others [90, 91] who showed the inhibitory effect of metal sorption on the proton-promoted dissolution of iron (hydr)oxides. In contrast, in the hematite formation, retardation may be rationalized by suggesting that the initial metal-Fe coprecipitate has a more energetically stable structure than pure FH [1, 2].

Inorganic poly-valent anions (silicate, phosphate, and arsenate) that form strong innersphere complexes with FH surface inhibit markedly the FH crystallization [1, 2]. At a low Si(IV)/Fe(III) of 0.005 and a high pH of 12, silicate combines strongly with FH surface which is negatively charged and thereby induces hematite formation over goethite formation [92]. Addition of goethite surmounted the effects of very low levels of silicate (Si(IV)/Fe(III) = 0.0001), whereas it was not effective at higher Si(IV) concentrations indicating that this ligand operates by stabilizing FH against dissolution. However, where silicate does not interfere with the dissolution of the FH, its principal action is in solution where it hinders the nucleation of goethite [92]. There was 55% transformation to goethite after 660 days at RT and a pH of 12.5 in the presence of 0.01 M silicate, whereas none with 0.1 and 1 M silicate; addition of goethite at high silicate concentrations had no seeding effect [92, 93]. Adsorbed Si(IV) stabilizes FH and strongly retards its dissolution [38], whereas soluble Si(IV) hinders nucleation of goethite leading to fewer, larger crystals [94]. Adsorbed silicate decreased the dissolution rate in oxalate probably by blocking surface Fe sites [95].

Compared to ligands, cations influence the transformation of FH over a wider pH range than do ligands and are often incorporated in the FH structure [1, 2]. Cations need higher mole ratios (M/[M + Fe] = 0.05~0.1) to influence the kinetics and end products of the reaction, whereas ligands are often in effect at hundredfold lower concentrations. Al(III) enhances the hydrolysis of Fe(III) during initial precipitation, that is, the precipitation of mixed Fe(III)-Al(III) solution required more OH^- to achieve the same pH than separate solutions [28, 96]. In a long-term (16~20 y) experiment [28], Al(III) retarded crystallization and promoted the formation of hematite over goethite since

Al(III) in ferrihydrite lowered ferrihydrite solubility. The transformation rate of FH with a coprecipitated Al(III) to goethite/hematite at 25 ^{o}C and at pH 4; 5; 6 and 7 decreased from 1 to 0.03/yr with increasing the Al(III)/[Fe(III) + Al(III)] from 0 to 0.1. The effect becomes less with an increase in pH. Coprecipitated Al(III) hinders the FH transformation through blocking the dissolution of FH and impedes nucleation/growth of goethite so that hematite can form competitively. An Al(III)/[Al(III) + Fe(III)] of 0.025 was enough to inhibit goethite completely in favor of hematite at pH 7 even at 25 ^{o}C and this effect became pronounced with increasing the pH from 4 to 7. Air-dried storage of FH2 from a series with different Al(III) content containing 115 mg H_2O/g FH2 of the initial water content (weight loss between air-dry and 150 ^{o}C) at room temperature for 20.4 years in closed vessels induced partial transformation to fairly well crystalline hematite with small amounts of goethite, which is qualitatively similar to results for the aqueous system [8]. As Al(III) concentration increase and OH^- concentration decreases, the range of hematite formation becomes wider at 70 ^{o}C [97]. In contrast, titanium(IV) promotes the formation of goethite over hematite although it hinders the transformation of FH at pH 6~11 [98].

All divalent, first row transition elements (M) except for Mn(II) and Fe(II) hinder the conversion of FH and modify the composition of the end product [1, 2]. The reciprocal half transformation time of FH with a coprecipitated Ni(II) to crystalline oxides was reduced linearly from 8 to 3 x 10^{-3}/min with an increase of Ni(II) concentration from 0 to 0.016 M [99]. At M(II)/[M(II) + Fe(III)] < 0.15 and 70 ^{o}C, Co(II), Ni(II) and Zn(II) promoted hematite over goethite indirectly by stabilizing FH against dissolution for long sufficient to encourage hematite to nucleate, whereas Mn(II) induced

relatively more goethite than did the control (at pH > 10) [90]. In all cases with M(II)/[Fe(III) +M(II)] > 0.15 at pH 12 and 70 ^{o}C, a spinel phase (MFe_2O_4) was formed and Cu(II) and Ni(II) precipitated as separate phases above the ratio of 0.33 [90]. The FH coprecipitated with the transition element may contain M-O/OH-Fe and M-O/OH-M as well as Fe-O/OH-Fe linkages. The capacity of the transition elements stabilizing FH decreases in order Zn(II) > Cu(II) > Co(II) > Ni(II) > Mn(II) [90, 100]. However, whether the foreign element is incorporated or only adsorbed may be significant. Although Ni(II) forms less stable surface complexes with FH2, coprecipitated Ni(II) hinders the transformation of FH2 to goethite at pH 6 and 11 and 70 ^{o}C more than did Pb(II) because Ni(II) may incorporate into FH and Pb(II) may not [101]. In the presence of a dissimilatory iron-reducing bacterium at 25 ^{o}C in bicarbonate-buffered solution at circumneutral pH, the partial transformation of FH2 coprecipitated Ni(II) was observed [102]. At RT and pH 7, FH6 dominated in Ni(II)-containing FH2 solution with continued aging under aerobic conditions and the transformation of FH2 to FH6 was considerably faster under anaerobic conditions [25].

Organic ligands have an effect on the transformation of FH depending on the pKs of the ligands, the type and number of functional groups [1, 2]. Acyclic molecules such as citrate stabilize FH to a greater degree than do cyclic molecules with the same functional groups [103]. Adsorbed ligands which tend to be polydentate and form binuclear, inner-sphere complexes hinder goethite formation through stabilizing FH against dissolution [1, 2]. Owing to blocking the aggregation of the FH particles, hematite formation may be impeded. Organic ligands either combine with the particles to form an immobile network or increase the electrostatic repulsion between the particles [80, 104, 105]. Hydroxyl

carboxylic acids hinder the transformation of FH in the pH range 9~11 in the order citric > *meso*-tartaric > L-tartaric » lactic [80]. Adsorption may cause retardation of FH transformation by impeding FH aggregation and dissolution, restricting the release of Fe (III) species into solution, and producing conditions favorable for the nucleation of hematite so that the presence of organic anions usually promotes hematite over goethite in the transformation product [104]. The retarding effect of organic ligands generally falls with increasing the pH and decreasing their concentration. FH2 with citrate/Fe(III) = 3% was transformed to mixtures of hematite with FH6 and a magnetic phase by hydrothermal conversion at 150 ^{o}C for 2 weeks. Complete transformation into hematite occurred within 120 days [106].

1.2.3 Thermal Transformation of 2-line Ferrihydrite to Other Iron Oxides

Thermal transformation, which takes place within the solid phase, is related to internal atomic rearrangements with a single crystal of the initial phase being transformed into a single crystal of another phase [1, 2]. The solid-state conversion in the dry state usually occurs only at elevated temperatures and it involves a certain mobility of atoms. Under the influence of either heat or mechanical stress, iron hydroxides (FeOOH or FH) can be dehydrated to other iron oxides [1, 2],

$$2FeOOH \rightarrow Fe_2O_3 + 2H_2O \qquad (1.6)$$

It is often difficult to distinguish precisely differences between a transformation in the “dry state” and that in the presence of water since the minimum amount of water with

which a via-solution transformation is still possible may be very small [1, 2]. This is more and more marked in poorly ordered and nano-sized oxides such as FH with high surface areas and high amounts of adsorbed water. Hematite is generally the end product of the dehydroxylation of pure phases, forming lepidocrocite, maghemite as an intermediate phase [1, 2]. Thermal dehydroxylation depends on the nature of the compound, its crystallinity, the extent of isomorphous substitution, and the presence of foreign species [38, 107]. During the dehydroxylation of all iron hydroxides, micropores develop initially owing to the expulsion of water [1, 2]. At higher temperatures, these micropores coalesce into mesopores. The pore formation leads to an increase in surface area. However, when iron hydroxides are heated at above 600 ^{o}C, the surface area falls markedly. The dehydroxylation causes oxo-bonds originated from hydro-bonds, develops a face-sharing arrangement between octahedra, resulting in a dense structure. Thermal transformation of FH to hematite, which contains a combination of dehydration/ dehydroxylation and atomic rearrangement processes, causes a gradual structural ordering within the FH particles into the direction of the hematite structure [1, 2].

Upon heating FH2 at 127 ^{o}C for 1180 h, the ratio of H_2O/Fe_2O_3 fell from 2.64 to 1.23 without much change in the peaks of XRD [41]. This result indicates that significant amounts of water can be evolved. The oxalate solubility ($[Fe_o]/[Fe_t]$) was analogous to the water loss and remained at 1.0 for the FH2. In the N_2-adsorption isotherms, FH2 shows type I and then gradually transit to type V with an increase in heating time [108]. The porosity increased considerably (55%), whereas the surface area slightly decreased. During heating the FH2 at 227 ^{o}C or 327 ^{o}C, the FH2 transformed easily into hematite and the closure point of the isotherms shifted to higher p/p_o with an increase in heating

time. The XRD patterns showed that hematite gradually formed at 227 ^{o}C. Small amounts of water have significant effect on the transformation of FH [36]: a FH2 was resistant up to 170 ^{o}C during 6h of outgassing, whereas another FH2 exposed to the air for 1 h at RT, during which it adsorbed water, converted into hematite at 130 ^{o}C. The result means that temperatures between 90 and 120 ^{o}C are required to inhibit structural conversion of the FH during the outgassing procedure. From the gradual sharpening of all XRD peaks with increasing temperature, it can be concluded that a continuous increase in crystal size and order leads to the decrease in weight and surface area [41, 109]. During heating FH2, the crystal size of formed hematite increased from 24 (at 340 ^{o}C) to 126 (at 672 ^{o}C) and then to 700 nm (at 995 ^{o}C) and the occupancy of Fe sites increased from 11.2 to 11.5 and then to 11.7 per unit cell (full occupancy = 12). The results mean that the amount of OH in the structure fell over this temperature range [110].

In spite of many studies, the mechanism of thermal transformation has not been fully understood. Stanjek and Weidler [41] have proposed that with gradually expelling OH groups in FH, the average coordination number around Fe dropped, causing charge imbalance and structural strain, and then reaching a point at which no more defects can be tolerated and a structural rearrangement (e.g. face-sharing) is eventually initiated resulting in forming hematite. The activation energy for the process is considerably high (390~500 kJ/mol) so the temperature must be high to enable cation diffuse sufficiently [111]. In contrast, Watari et al. [112] suggested that the special morphology such as a very large specific surface area keeps hematite still in a high energy state and the large amount of energy stored as surface energy is the principal driving force for further

ordering and for decreasing the surface area. The exothermic DTA peak may be attributed to the release of this energy.

Considerably higher temperatures are required to transform FH to hematite since foreign species may inhibit the transformation [1, 2]. It has been reported that FH transforms to hematite between 300~400 ^{o}C [38, 41]. However, the precipitation of FH with Si(IV) is known to increase the thermal stability of FH so that the transformation of FH to hematite is delayed by several hundred degrees [109, 113]. Based on differential thermal analysis, the presence of Si(IV) added both during and after the synthesis of FH2 increased the temperature of its transformation to hematite from 340 ^{o}C without Si to 740 ^{o}C at a Si/[Si + Fe(III)] mole ratio (X_{Si}) of 0.270 [110]. A FH2 with X_{Si} = 0.11 remained essentially unconverted after heating at 600 ^{o}C under oxidizing conditions, whereas it transformed completely to hematite at 850 ^{o}C [114]. Upon heating, the characteristic IR Si-O band at 960/cm shifted to 982/cm at 600 ^{o}C and to 1055/cm at 850 ^{o}C.

The higher thermal stability of Si-rich FH was attributed to surface effects of Si(IV), i.e., the formation of Si-O-Fe bonds that hinder the dehydroxylation and the subsequent atomic rearrangement to hematite [20, 113]. FH and Si-rich FH may, however, dehydroxylate without transforming into hematite [41, 109]. In contrast, another possibility is that Si substitution results in increased stability. On the basis of XPS (X-ray photoelectron spectroscopy) data, Vempati et al. [115] assumed that Si(IV) is structure bound in FH. Upon heating FH2 coprecipitated with Si(IV) at $X_{Si} \leq 0.0679$ and temperature $\leq$ 800 ^{o}C, small amounts of Si(IV) is likely to incorporated into the structure of hematite, probably compensating for the Fe(III) deficit [110]. On the other hand, Yoshinaga and Kanasaki [116] prepared FH coprecipitated with Si and Ge, which have

significantly different ionic radii, and concluded from the similarity in *d*-values that these elements did not substitute in the FH structure. Parfitt et al. [117] and Soma et al. [118] suggested that Si(IV) tends to bridge the surfaces of crystalline domains within FH and combine with particles within aggregates. The Si(IV) in those particles hinders the rearrangement of the Fe(III) octahedra to form hematite. Based on surface and structural data, Si(IV) is located near the particle surface in which it prevents Fe(III) octahedra from rearranging to form hematite [114].

1.3 Adsorption of Arsenic on 2-line Ferrihydrite

Arsenic contamination of groundwaters concerns several countries around the world and has been reported by the World Health Organization as a first priority issue [119]. Arsenic is classified as one of the most toxic and carcinogenic chemical elements [20] and its ingestion may deleteriously affect the gastrointestinal tract, cardiac, vascular system and central nervous system [121]. Arsenite is 25~60 times more toxic than arsenate [122]. Arsenite and arsenate are primary forms of arsenic in natural waters and soils [123]. In most natural water, the concentration of arsenic species depends mainly on redox potential and pH [124~126]. Arsenate is present normally as H_3AsO_4, $H_2AsO_4^-$, $HAsO_4^{2-}$, and AsO_4^{3-} in oxidized surface water whereas arsenite exists in forms of H_3AsO_3, $H_2AsO_3^-$, $HAsO_3^{2-}$, and AsO_3^{3-} under reducing conditions such as groundwater [123, 125]. However, both arsenate and arsenite often exist in soils without reference to the redox conditions due to the relatively slow arsenic redox transformation [126]. Generally, arsenate species exist in the forms of an anion at the normal pH range (6~9) of natural water, whereas arsenite species have dominantly a neutral charge in this pH range.

The neutral charge causes the arsenite species to be more mobile and less absorbable than the arsenate [126], which is an important characteristic in arsenic removal by adsorption.

1.3.1 Methods of Arsenic Removal from Drinking Water

Various treatment methods have been developed for arsenic removal to achieve the new concentration limit. The principle aim is to find the Best Available Technology for arsenic removal from drinking water. Generally arsenic removal technologies fall into three major classes: chemical coagulation-precipitation, adsorption and membrane separation. The commonly used technologies are as follows: coagulation and precipitation with iron and aluminum salts [124, 127], adsorption on activated alumina [125, 128], activated carbon and activated bauxite [129], ion exchange [128, 130], ultrafiltration, nanofiltration, and reverse osmosis [131~135].

Some recent treatment technologies were based on oxidation and adsorption: activated carbons [136], iron oxide coated sand [137], manganese dioxide coated sand [138], ferruginous manganese ore [139], ferrihydrite [72], clay minerals [140], and zero-valent iron [121, 141, 142]. Since coagulation, precipitation, and adsorption using activated alumina and activated carbon have been reported to be not as efficient at arsenite removal as for arsenate removal, thus oxidation of arsenite to arsenate has been suggested. Although the use of external oxidizing agents tends to bring down the water quality, the efficiency of oxidation processes is not completely known [143]. It was reported that ferric hydroxides, ferrihydrite, and goethite adsorb strongly arsenic [44, 72, 124, 127, 141]. Adsorption/ coprecipitation with iron (III) oxides is the most common technique for arsenic removal from water because the method is effective and cheap

compared with other methods [125, 144~147] and the oxidation of arsenite to arsenate favors coagulation-precipitation and adsorption [125].

1.3.2 Adsorption of Arsenic on 2-line Ferrihydrite

Adsorption plays a critical role in the transport, bioavailability, and fate of arsenic. Arsenic adsorption has been studied using a wide range of metal oxides such as iron (III) oxides. Iron oxides have a strong affinity for both arsenite and arsenate. Adsorption studies [44, 148~159] of arsenite and arsenate on iron oxides have been extensively investigated because of their abundant occurrence in the natural system and their higher adsorption capacity of arsenic. Recently ferrihydrite, a poorly or little crystalline iron hydroxide, has received as much attention as an attractive adsorbent for removing arsenic from water because of its large surface area and its high adsorption capacity [44, 72, 148~154, 160].

Adsorption of both arsenite and arsenate is highly pH dependent. Within the pH range of 4~9, adsorption of arsenite increases with a rise in pH, while that of arsenate is greater at low pH [44, 150, 151, 155]. Arsenate reacts with amorphous iron oxides much faster than arsenite [151]. In contrast, after initial rapid adsorption of arsenate on ferribhydrite, slow adsorption kinetics of arsenate has been reported to be attributable to a diffusion-controlled rate-determining step [148]. However, there was only a 10 % increase in the amount of sorption of arsenate on ferrihydrite after 12 months compared with that after 4 min [159]. It was also reported that arsenite reacts with ferrihydrite faster than arsenate at relatively high arsenic loadings, whereas arsenate reacts faster at low As loadings and low pH [44]. From previous EXAFS results [15, 141, 161], it is possible

that the formation of bidentate complexes at high arsenate surface coverage is slower than the monodentate reactions at low arsenate surface coverage. The maximum adsorption on 2-line ferrihydrite was 0.6 for arsenite and 0.25 mol As/mol Fe for arsenate at pH 4.6, respectively, whereas the maximum was 0.58 and 0.16 mol As/mol Fe at pH 9.2 [44]. The adsorption envelopes crossed in the region of pH 6-7.5 at initial arsenic concentrations of 0.27~0.80 mol As/kg 2-line ferrihydrite. At a high arsenic loading (13.3 mol As/kg ferrihydrite), an adsorption maximum was observed for arsenite at about pH 9.0, whereas the amount of arsenate adsorbed was lower than that of arsenite and decreased linearly with increasing pH from 3 to 11 [44].

The molecular structure of arsenic surface complexes on iron oxides has been investigated using spectroscopic techniques. According to EXAFS data, oxyanions (e.g. arsenite and selenite) can form two types of bidentate, inner sphere complexes on iron oxides depending upon the surface site at which they adsorb [161, 162]. A binuclear, bidentate complex binds to the surface hydroxyls at the corners of two adjacent $Fe(OH)_6$ octahedra through a double corner linkage (^2C), whereas the mononuclear, bidentate complex binds to the groups along the edge of a $Fe(OH)_6$ octahedron via an edge linkage (^2E). These edge sites which are high energy sites are preferentially occupied at low surface coverage. The ratio of edge sites to corner sites is considered to be responsible for differences in the types of surface complexes found on different iron oxides [163]. Both arsenite and arsenate form inner sphere complexes on iron oxides. Many studies have suggested strongly that both arsenite and arsenate are adsorbed on iron oxides predominantly by forming bidentate binuclear complexes [15, 155, 159, 161, 164~167]. However, the amount of H^+ or OH^- released per mol arsenic adsorbed on 2-line

ferrihydrite varied with As surface coverage, indicating that a monodentate arsenate complex on 2-line ferrihydrite was present above pH 8 [72]. An EXAFS result also suggested that the speciation of arsenate changed from monodentate to bidentate complexes on goethite with an increase in the extent of adsorption [141]. In addition, a study using Raman, FTIR, and electrophoretic mobility proposed that both inner and outer sphere complexes of arsenite on ferrihydrite formed, depending on the pH [168].

1.3.3 Adsorption of Foreign Species on 2-line Ferrihydrite

Inorganic anions and organic compounds, which can function as the electron donor in a coordinate bond on the surface of iron oxides, may adsorb on iron oxides either specifically or non specifically [1, 2]. Specific adsorption, designated inner sphere adsorption or chemisorption, is related to displacement of the surface OH groups by the adsorbing ligand (L), that is, direct coordination of the ligand to the surface iron atom by a covalent bond [1, 2], i.e.

$$\equiv FeOH + L^- \quad \Leftrightarrow \quad \equiv FeL + OH^- \tag{1.7}$$

$$\equiv (FeOH)_2 + L^- \quad \Leftrightarrow \quad \equiv Fe_2L^+ + 2OH^- \tag{1.8}$$

Specifically adsorbed ligands (silicate, citrate, phosphate, and arsenite), which usually tightly bound, lead to a shift in the PZC through modification of the surface charge on iron oxides [1, 2]. Nonspecific adsorption, which is termed outer sphere adsorption, is governed by the electrostatic contribution to the free energy of adsorption. In the nonspecific adsorption of an anion, there is at least one water molecule between the

anion and the surface [1, 2]. Anions (arsenite) that form outer-sphere surface complexes on amorphous Al(III) oxide exhibit decreasing adsorption with an increase in solution ionic strength whereas anions (arsenate) that form inner-sphere surface complexes on both amorphous Fe(III) and Al(III) oxide show little ionic strength dependence or show increasing adsorption with increasing solution ionic strength [168]. The surface must have an overall positive surface charge in order for anion adsorption to occur as electrostatics control adsorption (i.e. nonspecific adsorption). Therefore, the maximum anion adsorption takes place between the pK_a of the acid and the PZC of the iron oxide. On the other hand, for specific anion adsorption, an overall positive surface charge is not required (only $FeOH_2^+$ and FeOH groups), which explains why the anion adsorption can occur at pH's above the PZC [1, 2]. Specifically adsorbed ligands are coordinated the iron oxide surface through forming mononuclear-monodendate, mononuclear-bidentate, binuclear- monodendate, or binuclear-bidentate complexes [1, 2]. Direct information about the nature of the surface species and their mode of coordination can be obtained by FTIR (Fourier transform infrared) and EXAFS (Extended x-ray absorption fine structure) data [1, 2].

Silicate binds covalently at hydrous surfaces of Fe (III)-(hydr)oxides and then forms an inner-species surface complex [169]. Compared with proton adsorption on the 2-line ferrihydrite, equilibration with silicate was rather slow due to the diffusion controlled reaction [57]. According to the two-layer model, the surface complexation constant for adsorption of orthosilicate on 2-line ferrihydrite ($\equiv FeOSi(OH)_3$) was determined to be log K_{Si} = 3.62 [57]. Adsorption isotherms revealed that twice as much silicate was adsorbed at pH 5 as at pH 3. The Si-O stretching infrared (IR) variation at 940~960 cm^{-1} resulted

from Fe-O-Si bonding. With increasing the amount of silicate adsorbed, the shift of the Si-O stretching frequency to higher wavenumbers may be attributed to the formation of siloxane linkages (Si-O-Si bonds) between adjacent orthosilicate molecules on the 2-line ferrihydrite surface [57]. This strong chemisorption between H_4SiO_4 and ferrihydrite was also observed by other workers [38, 65, 170~173]. The presence of citrate during the formation of iron oxides can significantly influence the kinetics of Fe (II) oxidation and the hydrolysis of Fe (III), resulting in modifying the crystalline structure of the hydrolytic products [174, 175]. Citrate formed a bidentate, inner sphere complex on goethite [176], while earlier adsorption and infrared data showed a tridentate complex on goethite and amorphous Fe (III) hydroxide [177]. The sorption of citrate on ferrihydrite increased strongly with decreasing pH [178]. Adsorption of citrate on goethite is highest at pH 3 and decreases with an increase in pH. The maximum amount of citrate adsorbed on hematite was higher than that adsorbed on goethite [177, 179].

Specific adsorption of cations is related to interaction with deprotonated surface hydroxyl groups to form mono- and bi nuclear inner sphere complexes (Eqs. 1.9 and 1.10), while specific adsorption of anions causes displacement of the surface OH groups by the adsorbing ligand (Eqs. 1.7 and 1.8) [1, 2]. For example, trivalent cations such as Al (III) appear to adsorb on iron oxides as surface hydroxo species (Eq. 1.11), i.e.

$$\equiv FeOH + M^{z+} \quad \Leftrightarrow \quad \equiv FeOM^{(z-1)+} + H^{+} \tag{1.9}$$

$$\equiv (FeOH)_2 + M^{z+} \Leftrightarrow \quad \equiv (Fe-O)_2 M^{(z-2)+} + 2H^{+} \tag{1.10}$$

$$\equiv FeOH + Al^{3+} + H_2O \quad \Leftrightarrow \quad \equiv Fe-O-AlOH^{+} + 2H^{+} \tag{1.11}$$

Cation adsorption on iron oxides is followed by release of protons with the number of protons released per cation being termed *z* [1, 2]. Complexation of Al(III) at the surface of goethite occurred over the pH range 3~8.5 and then the adsorption of Al(III) resulted in a change from goethite surface to an Al(III) surface [180, 181]. According to the constant capacitance model, two very stable monodentate surface hydroxo complexes ($FeOAlOH^+$ and $FeOAl(OH)_2$) formed consecutively with an increase the pH [180, 181]. The Al(III) desorption was extremely slow and exhibited poor reversibility whereas the acid base reactions were completely reversible [180]. Generally, Al(III) is known to have to extensively substitute for Fe(III) in the goethite structure [182]. Therefore, the strong affinity of Al(III) for the goethite surface was considered the first step in the formation of an Al(III) substituted goethite [180, 181]. Also adsorption of Al(III) on lepidocrocite induced the formation of two very stable surface hydroxo complexes [183]. Bleam et al. [184] observed that Mg(II) started to adsorb at relatively few, isolated sites on the goethite surface at about pH 7.6~7.9, below the isoelectric point (IEP) of goethite. The specific adsorption of Mg(II) on goethite enhanced a shift of the IEP to a more basic value [68, 69]. After aging Fe(III) and Ti(IV) coprecipitates at 70 ^oC and pH 5.5 for 70 days, goethite and anatase were identified in turn with an increase in the Ti(IV)/(Ti(IV) + Fe(III)) ratio [98]. The short-range structure of 2-line ferrihydrite was disturbed due to the addition of Ti(IV) [27, 185].

1.3.4 Adsorption of Arsenic on 2-line Ferrihydrite in the Presence of Foreign Species

The presence of anions can reduce the amount of arsenic adsorption on iron oxides by competing for adsorption sites. Silicate adversely affects the adsorption of arsenite and

arsenate by coprecipitattion with hydrous ferric oxide [186~190]. Silicic acid was considered to adsorb on ferrihydrite as a monomer at the total Si/Fe mole ratio below 0.1. The effect of silicic acid on the adsorption of arsenite and arsenate was minimal at the total Si/Fe mole ratio of 0.1 and pH < 9. H_4SiO_4 adsorption hindered arsenic adsorption to a greater extent than H_4SiO_4 polymerization [187]. In balance of Fe(III)-Si(IV) binary oxide adsorbent strength and arsenic adsorption capacity, an optimum Si/Fe molar ratio was suggested to be about 0.33 [186]. In the presence of Mg^{2+} and Ca^{2+} the adverse effect of silicate on arsenate removal was reduced due to the neutralization of negative surface charges [188]. The adsorption capacity of a Fe(III)-Si(IV) binary oxide adsorbent with a Fe/Si molar ratio of 0.33 was 21.1 for arsenite and 11.3 mg As/g for arsenate at 20 ^{o}C, respectively. Arsenite adsorption was clearly less dependent on the pH in the range of 3 to 9, while arsenate adsorption decreased considerably at pH > 7.5 [191]. The adsorption of arsenite and arsenate on goethite and ferrihydrite was reduced in the presence of citric acid [49, 192]. The decrease in arsenic adsorption may be attributable to the presence of functional groups present on citrate, which has three COOH groups and one OH groups as functional groups. Compared with the more chemical adsorption of dissolved organic carbon (DOC) on goethite, that of ferrihydrite may be more physical in nature [193]. Hence, the adsorption of DOC materials on ferrihydrite is probably weaker.

The adsorption of arsenite and arsenate on coprecipitated Al(III):Fe(III) hydroxides was reduced with increasing the Al/Fe molar ratio [30]. In contrast to the adsorption of arsenic on pure 2-line ferrihydrite, the decrease in arsenic adsorption may be due to the greater extent of crystallinity, the lower surface adsorption sites, the lower surface reactivities, and the weaker affinity of gibbsite and bayerite [30, 168, 194, 195]. At an

Al:Fe molar ratio of 1, compared with the adsorption of arsenate, the very low adsorption of arsenite may be influenced by the modes of bonding. Arsenite forms predominantly outer-sphere complexes on amorphous Al oxide [168] and inner- or outer-sphere complexes on crystalline Al oxides (gibbsite) at a pH of > 5.5 [196], while the predominant mode of arsenate is inner-sphere complexation by both amorphous [168] and crystalline [196] Al oxides. For 0:1, 1:4, and 1:1 Al(III):Fe(III) hydroxides, maximum adsorption of arsenite occurred at pH 7~9, while that of arsenate was observed at pH 3~7 [30]. In contrast, concurrent coprecipitation of arsenate with Fe(III) and Al(III) at a 1:1 Al:Fe molar ratio led to enhance arsenic removal compared to either Fe(III) or Al(III) alone at circumneutral pH [197].

Adsorption capacity of arsenate on titanium dioxide suspensions is high at pH 4 while that of arsenite is high at pH 9 [198]. In the presence of Mg^{2+} and Ca^{2+} as cations, the adsorption of arsenate on sulfate modified iron-oxide coated sand was enhanced [199]. However, Ca^{2+} was more effective than Mg^{2+} due to the formation of $Ca_3(AsO_4)_2$ as insoluble solids and $Mg_3(AsO_4)_2$ as soluble solids [200]. The presence of Mg^{2+} and Ca^{2+} reduced the adverse effect of silicate on the removal of arsenate on ferric chloride due to neutralization of the negative surface charges [188].

1.3.5 Adsorption of Arsenic on Granular Ferric Hydroxide

Adsorption/coprecipitation with iron(III) oxides is the most common technique for arsenic removal from water because the method is effective and cheap compared with other methods [125, 144~147]. However, most iron oxides are generally used as fine powders or hydroxide floc/gel in aqueous solution. Therefore, these iron oxides are

limited to reactor configurations consisting of large sedimentation and filtration units. Such conditions can cause difficulty in separation and regeneration of the iron oxides. Furthermore, these iron oxides possess the characteristics of low hydraulic conductivity [186, 201, 202]. For those reasons, the iron oxides in forms of fine powders or hydroxide floc/gel are not adequate as a filter medium for column adsorption. The alternative methods are the granulation of the iron oxides [58, 156, 157, 186, 191, 201~204] or the coating the iron oxides on a substrate such as sand or a polymeric material [137, 199, 205, 206]. Generally, there are several prerequisites for adsorbent for column adsorption of arsenic: (1) granular type, (2) efficient arsenic removal, (3) high capacity, selectivity, and rate of adsorption, (4) high physical strength in water, (5) regenerable, and (6) low cost [186].

In order to increase the physical strength of adsorbents, silica, sand and proprietary materials were used [137, 186, 191, 199, 201~203, 205~208]. It has been reported that the alternative methods were used for removing arsenic form water [137, 156, 157, 186, 191, 199, 204, 205, 207]. As reported in previous studies [156, 157], a granular ferric hydroxide (GFH) was developed for removal of arsenic. Although arsenic adsorption on GFH was lower than the adsorption on freshly prepared ferric hydroxide, column studies showed that nearly 1,100 and 30,000 bed volumes were treated, keeping the effluent As concentration at 5 and 10 μg As/l, respectively. Driehaus [156] and Thirunavukkarasu [157] suggested that GFH based filtration may be appropriate and advantageous to small water utilities due to simplicity, ease of construction, operation and maintenance.

CHAPTER II

OBJECTIVES

The transformation of FH2 into crystalline oxides is known to lead to diminished adsorption capacity of heavy metals. In order to retard the aqueous transformation of FH2, various transformation inhibitors have been studied. FH2 with a coprecipitated transformation inhibitor might be advantageous for both removing arsenic from water and managing arsenic waste due to a slower rate of dissolution with respect to pure FH2. Little information has, however, been found regarding the effects of aging and heat treatment on the solid-state transformation of FH2 containing a transformation inhibitor and the adsorption of arsenic on the FH2. A better understanding of the effects of aging and heat treatment is needed to evaluate the potential utility of FH2 for its potential application as a filter medium for adsorption of arsenic.

The goal of this research was to obtain fundamental information on the characteristics and solid-state transformation of FH2 containing transformation inhibitors (Si(IV), Mg(II), Al(III), Ti(IV), or Ci(citrate)) and evaluate the adsorption capacity of arsenic on the FH2. The goal was achieved by accomplishing the following objectives: (1) to investigate the characteristics of the FH2 using the following analyses: XRD, particle size, specific surface area, PZC, and mechanical strength, (2) to investigate the influence of inhibitor, aging, and heat treatment on the transformation, structure, and PZC of FH2, (3) to investigate the influence of inhibitor, aging, heat treatment, and pH on the adsorption of arsenic on the FH2, and (4) to evaluate the adsorption capacity of arsenic on the FH2 at high arsenic loadings.

CHAPTER III

METHODOLOGY

3.1 Chemicals

Ferric nitrate ($Fe(NO_3)_3 \cdot 9H_2O$, 99.7%, J.T. Baker) was used for synthesizing 2-line ferrihydrite. Five species were used as transformation inhibitors of the FH2: sodium silicate ($Na_2SiO_3 \cdot 9H_2O$, 99.989%, Fisher), magnesium chloride ($MgCl_2 \cdot 6H_2O$, 99.8%, Mallinckrodt), aluminum nitrate ($Al(NO_3)_3 \cdot 9H_2O$, 98.7%, Mallinckrodt), titanium (IV) isopropoxide ($Ti[OCH(CH_3)_2]_4$, 99.999%, Sigma-Aldrich), and citric acid ($C_6H_8O_79$, 99.5%, EM). Hydrochloric acid (HCl, 37.5%, Fisher) and sodium hydroxide (NaOH, 97+%, Sigma-Aldrich) were used in the PZC determination of FH2 for adjusting the pH of the suspension with different sodium chloride (NaCl, 99.0%, EM) concentrations.

Ammonium oxalate ($(COONH_4)_2 \cdot H_2O$, 99~101%, EMD) buffered to pH 3 by oxalic acid ($H_2C_2O_4 \cdot 2H_2O$, 99.5~ 102.5%, EMD) was used in the 2 h ammonium oxalate in the dark (AOD) procedure for extracting the amorphous iron oxide fraction of the FH2s. In addition, hydrochloric acid (HCl, 37.5%, Fisher) was used as a parallel extraction agent. The total iron concentration of the FH2s was determined by the sodium dithionite-citrate-bicarbonate (DCB) procedure using the following chemicals: sodium dithionite ($Na_2S_2O_4$, 89.9%, J.T. Baker), sodium citrate ($C_6H_5Na_3O_7 \cdot 2H_2O$, 100.1%, Calbiochem), sodium bicarbonate ($NaHCO_3$, 99.9%, J.T. Baker), and sodium chloride (NaCl, 99.0%, EM). Standard solutions for analysis of iron were prepared by diluting a stock solution of iron (1,000 mg/L, AA standard, CertiPUR) with deionized (DI) water. Arsenic (III) oxide (As_2O_3, 99.99%, Aldrich) and arsenic (V) oxide (As_2O_5, 99%, Aldrich) were used in

adsorption studies of target compounds. DI water (Barnstead, NANOpureII) above 17.8 MΩ-cm was used in the preparation of chemical solutions and for dilution purposes.

3.2 Sample Preparation

3.2.1 Sample Synthesis

Twenty types of FH2 were prepared with different proportions of iron and a transformation inhibitor following a slightly modified procedure of Cornell and Schwertmann [2]. Five species were used as inhibitors to investigate the effect on transformation of the FH2 to other iron oxides: (a) silicate (Si (IV)) as an anion, (b) Mg (II), Al (III), or Ti (IV) as a cation, and (c) citrate as an organic ligand. The FH2s were synthesized by dissolving 40 g of $Fe(NO_3)_3 \cdot 9H_2O$ in 250~500 ml of DI water and mixing the $Fe(NO_3)_3$ solution with an inhibitor (or a solution containing an inhibitor). To the mixed suspension, 130~580 ml of 1 N NaOH were added at a fixed rate of addition of about 23 ml/min using a burette, during vigorous stirring at a level of five with a magnetic stirrer (Corning PC-520) for about 20 min. After the pH of the suspension was adjusted to 7.5 by the dropwise addition of 1 N NaOH, the suspension was centrifuged at 500×g (International Equipment Company) until the supernatant was flocculated. The resulting centrifugation sediment was dialyzed against DI water by continuous dialysis using dialysis tubing (molecular weight cut-off of 12,000~14,000) to remove salts remaining in the sediment. DI water was added to a dialysis tank at a feed rate of 1.5 l/h with a master flux pump (Cole-Parmer Instrument Co.) for 2 days until the conductivity of the tank dropped below 5 μS/cm. After dialysis, the slurry was centrifuged for 10 min, and the centrifugation sediment was air-dried in a light-free environment using an

electrical fan at room temperature (RT) for 2 days. The effects, if any, of air-drying at RT on mineral transformation were assumed to be minimal. To produce the homogenous FH2s, the air-dried solids were ground gently in a mortar and sieved to a grain size of smaller than the No. 100 (0.15 mm) sieve prior to each experiment. In addition, pellets were prepared to evaluate the mechanical strength of the FH2s. After preparing the centrifugation sediment using the same synthesis procedure, the resulting sediment was granulated to in cylindrical molds 4.5 mm diameter × 3.5 mm long, air-dried in a light-free environment using an electrical fan at RT for 2 days, and then sieved to a pellet size with a diameter of 0.85~2 mm. The chemical recipes for synthesizing twenty types of FH2 are summarized in Table 3.1. The FH2s used in this study were designated, for example, FH2-Si-0.025 or FH2-Mg-2, according to the name of inhibitor and the initial molar ratio of inhibitor/iron.

A reference adsorbent, hydrotalcite-like compound (HTlc), was used in comparison experiments. HTlc is structurally composed of brucite ($Mg(OH)_2$)-like layers where some divalent metal cations have been substituted by trivalent metal cations (Fe^{3+}, Al^{3+}, etc) to form permanent positively charged sheets [209]. HTlc was synthesized by a coprecipitation method [210~212]. A mixed solution of magnesium (II) and iron (III) was prepared in an initial molar ratio of 2:1. The final pH of the suspension was adjusted to 9.5 with 1 M NaOH under vigorous stirring conditions. The suspension was aged in the mother solution at RT for 2 h, centrifuged at 500×g until the supernatant was flocculated, and then washed again in DI water using continuous dialysis for 2 days to remove the electrolytes. After centrifuging the slurry for 10 min, the centrifugation sediment was dried at 80 ^{o}C in a muffle furnace (Modern Laboratory Equipment Co., Inc.) for 24 h.

Finally the dried HTlc was ground to pass through a 0.15 mm mesh sieve for future use. The chemical recipe for synthesizing the HTlc is presented in Table 3.1.

Table 3.1 Chemical Recipes of 2-line Ferrihydrite Synthesis

Type of FH2	Preparation of transformation inhibitor			$Fe(NO_3)_3 \cdot 9H_2O$ hydrolysis	1 N NaOH[b]
	Chemical formula	In/Fe ratio[a]	Preparation		
FH2				40 g in 500 ml DI water	≤ 330 ml
FH2 -Si	$Na_2SiO_3 \cdot 9H_2O$	0.025, 0.05, 0.075, 0.1	0.704~2.814 g in 200 ml 1 N NaOH[c]	40 g in 500 ml DI water	≤ 130ml[c]
FH2 -Mg	$MgCl_2 \cdot 6H_2O$	0.1, 0.5, 1, 2	2.01~40.26 g in 87 ml DI water	40 g in 413 ml DI water	≤ 330 ml
FH2 -Al	$Al(NO_3)_3 \cdot 9H_2O$	0.1, 0.25, 0.5, 1	3.75~37.5 g in 250 ml DI water	40 g in 250 ml DI water	318~580 ml[d]
FH2 -Ti	$Ti[OCH(CH_3)_2]_4$	0.025, 0.05, 0.1, 0.2	0.725~5.803 ml in 500 ml Fe solution[e]	40 g in 500 ml DI water	≤ 330 ml
FH2 -Ci	$C_6H_8O_7$	0.001, 0.01, 0.1	0.019~1.902 g in 50 ml DI water	40 g in 450 ml DI water	≤ 330 ml
HTlc (= H)	$MgCl_2 \cdot 6H_2O$	2	40.26 g in 87 ml DI water	40 g in 413 ml DI water	460~485 ml[f]

[a] Initial molar ratio of inhibitor to iron.
[b] The pH of the mixed suspension was adjusted to 7.5 with 1 N NaOH.
[c] In the synthesis of FH2-Si series, appropriate amounts of $Na_2SiO_3 \cdot 9H_2O$ were added to 200 ml of 1 N NaOH to obtain charged forms of Si (IV) before adjusting the pH of the mixed suspension to 7.5.
[d] In order to adjust the pH of the mixed suspension to 7.5, appropriate amounts of 1 N NaOH were added to the suspension: 318 ml for FH2-Al-0.1, 362 ml for FH2-Al-0.25, 439 ml for FH2-Al-0.5, and 580 ml for FH2-Al-1, respectively.
[e] In the synthesis of FH2-Ti series, appropriate amounts of $Ti[OCH(CH_3)_2]_4$ were added directly to 500 ml of the $Fe(NO_3)_3$ solution.
[f] The final pH of the suspension was adjusted to around 9.5.

3.2.2 Aging and Heat Treatment

Based on the results of screening adsorption experiments for fresh samples (aged for 10~30 days) at low arsenic loading rates, some samples were aged or heat-treated before use. The FH2s were allowed to age for a defined period ranging from a day to 650 days in a light-free environment at RT to determine the effect of aging time on water content, structure, transformation, and arsenic adsorption. Experimental conditions for aging the FH2s are summarized in Table 3.2.

It is known that the effects of foreign species on transformation of FH2 are particularly strong at RT, where the crystallization can be retarded for months or even years, whereas the effects become weaker as the temperature increases [1, 2]. For this reason, some FH2s aged at RT for periods ranging from 16 to 400 days were heat-treated at temperatures of 150, 240, and 360 ^{o}C in a muffle furnace (Modern Laboratory Equipment Co., Inc.) for 12 h to evaluate the effect of heat treatment on structure, point of zero charge (PZC), transformation and arsenic adsorption. The heat-treated samples were cooled to RT in a desiccator prior to future use. Table 3.3 presents the experimental conditions for heat treatment of the FH2s.

Table 3.2 Experimental Conditions for Aging 2-line Ferrihydrite

Experiment	Type of FH2 and inhibitor/Fe ratio	Aging Time (day)		
		1st	2nd	The others[a]
Specific gravity	FH2, FH2-Si-0.1, FH2-Mg-2, H	650		
	FH2-Al-0.1,-0.5	195		
Particle size	FH2, FH2-Si-0.1, FH2-Mg-2, FH2-Al-1, H	190		
Surface area	FH2, FH2-Si-0.1, FH2-Mg-2, FH2-Al-1, H	240		
PZC	FH2, FH2-Si-0.1, FH2-Mg-2, FH2-Al-1	165		
Mechanical strength	FH2, FH2-Si-0.1, FH2-Mg-2, FH2-Al-1, H	10		
Extraction with HCl[b]	FH2, FH2-Si[c], FH2-Mg[c], FH2-Ti[c], FH2-Ci-0.001,-0.01, H	15		
DCB[d]	FH2, FH2-Si[c], FH2-Mg[c], FH2-Ti[c], FH2-Ci-0.001,-0.01, H	400		
	FH2-Al[c]	100		
Effect of pH on As adsorption	All the FH2s[e], H	20[f]		
High loading As adsorption	FH2, FH2-Mg-2, FH2-Al-1, H	40		
Water content	FH2, FH2-Si-0.1, FH2-Mg-2, H	2	650	
	FH2-Al-1	2		
	FH2-Al-0.5		190	
XRD	FH2, FH2-Si[c], FH2-Mg[c], FH2-Ti-0.025, -0.05, -0.1, FH2-Ci-0.001,-0.01, H	20	385	
	FH2-Al[c]	135		
AOD[g]	FH2, FH2-Si[c], FH2-Mg[c], FH2-Ti[c], FH2-Ci-0.001,-0.01, H	1	2	4, 6, 15, 30, 60, 165, 235[a]
	FH2-Al[c]	40		
Screening adsorption[h]	FH2, FH2-Si[c], FH2-Mg[c], FH2-Ti[c] FH2-Ci[c], H	30[f]	235	
	FH2-Al[c]	10		

[a] In the transformation experiment using the AOD procedure, the amorphous iron fraction of FH2 was monitored as a function of aging time ranging from 1 to 235 days.
[b] A 30-min extraction of FH2s with 0.4 M HCl.
[c] The FH2-inhibitor indicates all the inhibitor/Fe molar ratios shown in Table 2.1.
[d] Sodium dithionite-citrate-bicarbonate (DCB) procedure.
[e] Twenty types of FH2s.
[f] Each FH2 was used in the adsorption studies within 20 or 30 days of its aging.
[g] Standard 2 h ammonium oxalate in the dark (AOD) procedure.
[h] Screening adsorption study was conducted to evaluate arsenic removal capability of all the FH2 and HTlc at low arsenic loading rates ranging from 0.5 to 8 mg arsenic/g FH2 as a preliminary experiment.

Table 3.3 Experimental Conditions for Heat Treatment of 2-line Ferrihydrite

Experiment	Type of FH2 and inhibitor/Fe ratio	Heat treatment		
		Aging Time (day)[a]	Temperature (^{o}C)	Duration (h)
XRD	FH2, FH2-Si, FH2-Mg, FH2-Ti-0.025, -0.05, -0.1, FH2-Ci-0.001,-0.01, H	130	360	12
	FH2-Al	16		
PZC	FH2, FH2-Si-0.1, FH2-Mg-2, FH2-Al-1	165	360	
AOD	FH2, FH2-Si, FH2-Mg, FH2-Ti, FH2-Ci-0.001,-0.01, H	205	150	
		275	240	
		170	360	
	FH2-Al	17	150	
			240	
			360	
Screening adsorption	FH2, FH2-Si, FH2-Mg, FH2-Ti, FH2-Ci, H	300~400	360	
	FH2-Al	17		

[a] The FH2s were aged in a light-free environment at RT before heat treatment.

3.3 Experimental Procedure

3.3.1 Characteristics of 2-line Ferrihydrite

3.3.1.1 X-ray Diffractometry

The identity of the samples was confirmed by powder X-ray diffraction (XRD) analysis. As shown in Table 3.2 and 3.3, XRD analysis was carried out using the following experimental conditions for aging time and heat treatment: (a) 20 ("fresh") and 385 day aging for FH2, FH2-Si, FH2-Mg, FH2-Ti-0.025, -0.05, 0.1, FH2-Ci-0.001, -0.01, and HTlc, (b) 135 day aging for FH2-Al, (c) heat treatment at 360 ^{o}C for 12 h after 130 day aging for FH2, FH2-Si, FH2-Mg, FH2-Ti-0.025, -0.05, -0.1, FH2-Ci-0.001, -0.01, and HTlc, and (d) heat treatment at 360 ^{o}C for 12 h after 16 day aging for FH2-Al. Each

sample was pressed onto silicon sample holders previously coated with a thin layer of vaseline. Diffraction patterns were recorded on a computer controlled, Rigaku D/Max 111VB powder diffractometer using CuK_α radiation with a counter equipped with a graphite monochromator. All scans were obtained at conditions of 40 kV and 20 mA, for Bragg angles of 2.1 to 70.0^o 2θ with a step size of 0.03° 2θ and a scan speed of 2.0° 2θmin^{-1}.

3.3.1.2 Water Content and Specific Gravity

The water content of FH2s was determined by a modified procedure of the direct heating method as described in ASTM STANDARDS (D 4959) [213]. As shown in Table 3.2, six types of samples (FH2, FH2-Si-0.1, FH2-Mg-2, FH2-Al-0.5, FH2-Al-1, and HTlc) were tested to determine water content. In order to evaluate the effect of aging time on water content, the samples were aged for two different lengths of time: (a) 2 days ("fresh") for FH2, FH2-Si-0.1, FH2-Mg-2, FH2-Al-1, and HTlc and (b) 190 days for FH2-Al-0.5 or 650 days for FH2, FH2-Si-0.1, FH2-Mg-2, and HTlc. About 1 g of each sample was placed in a small open porcelain dish and dried at 110 ^{o}C in a muffle furnace (Morden Laboratory Equipment Co., Inc.) for about 24 h until the change between two consecutive mass determinations had an insignificant effect on the calculated water content: a change of 0.1% or less of the dry mass of the sample for last two determinations. After cooling the sample to RT in a desiccator, the mass of the porcelain dish before and after drying the sample was determined with a balance (Mettler Toledo, AB54-S) of 0.0001 g readability. The water content determination was performed in duplicate.

The specific gravity of FH2s was determined by means of a picnometer as described in ASTM STANDARDS (D 854) and Standards Methods, with little modification [213, 214]. Six types of aged samples were used in the test as mentioned in Table 3.2: FH2-Al-0.1 and FH2-Al-0.5 aged for 195 days and FH2, FH2-Si-0.1, FH2-Mg-2, and HTlc aged for 650 days. About 4 g of each sample were placed in a 50-mL picnometer and DI water was added to fill the bottle to about three-fifths volume (30 ml). In order to remove entrapped air, the bottle was boiled gently in a water bath at around 80 ^{o}C for 10 h while occasionally shaking the bottle to assist in the removal of the air. After boiling, the bottle was cooled to RT (around 21 ^{o}C) and filled with DI water to the mark (30 ml). The mass of the bottle and the sample was measured and the specific gravity based on water at 4 ^{o}C was calculated. Samples in duplicate were used for determining the specific gravity.

3.3.1.3 Particle Size Distribution

After grinding in a motar, sieving to a grain size of smaller than the No. 100 (0.15 mm) sieve, and then aging at RT for 190 days, the particle-size distribution of five samples (FH2, FH2-Si-0.1, FH2-Mg-2, FH2-Al-1, and HTlc) was analyzed by a photograph/ image analysis system (FlowCAM Portable Imaging Flow Cytometer, Fluid Imaging Technology). Each sample was mixed with DI water to obtain 0.01 g/l sample solution. The sample solution was carried into a flow cell (2 mm × 0.1 mm) using milliGAT pump system (Global FIA) consisting of the piston type pump, motor, gear assembly, a MicroLynx-4 controller, and a linear power supply. Pump flow rate was fixed at 0.5 ml/min. Pump and controller was connected with an RS-232 serial port and input and output signals were achieved by using a window communication terminal.

Plastic tubing was used in the fluid line connections. The pump inlet was placed after flow cell to avoid aggregate break-up during sampling and run. Instrument software was used for image processing and analysis. All measurements were made at 10× objective magnification and a CCD camera (DFW-X70, Sony) with a resolution of 0.6666 μm per pixel triggered at a constant rate (7 frames per second) over a known time for each run.

3.3.1.4 BET Specific Surface Area

The specific surface area of five types of samples (FH2, FH2-Si-0.1, FH2-Mg-2, FH2-Al-1, HTlc) aged at RT for 240 days was determined from multipoint BET (Brunauer, Emmet, and Teller) isotherms [34] with an Autosorb-6 instrument (Quantachrome) using nitrogen (99.99%) as an adsorbate at 77 ^{o}K. About 100 to 200 mg of sample was used for measuring the specific surface area. For metastable minerals such as 2-line ferrihydrite, a low outgassing temperature was chosen to avoid crystallization of the sample during measurement. For the N_2 gas adsorption/desorption isotherms, samples except HTlc were first outgassed on the autosorb degasser at 50 ^{o}C for 12 h. However, HTlc was outgassed at 50 ^{o}C for 24 h due to difficulty in removing water. For each determination, seven measurements were made in the relative pressure range $0.05 < p/p_0 < 0.3$ according to the original paper [34], and the specific surface area was then calculated by the instrument software from the BET plot according to the isotherm equation.

3.3.1.5 Potentiometric Titration

The point of zero charge was evaluated for four types of aged samples before and after heat treatment from the intercept of acid-base titration curves [55, 56, 73, 211, 212, 215]: (a) FH2, FH2-Si-0.1, FH2-Mg-2, and FH2-Al-1 aged at RT for 165 days, (b) FH2, FH2-Si-0.1, FH2-Mg-2, and FH2-Al-1 heat-treated at 360 ^{o}C for 12 h after 165 day aging at RT. Prior to acid-base titration, it is essential to exclude CO_2 from the system (by outgassing with N_2) because CO_2 adsorbs ferrihydrite surfaces, raises the negative charge and lowers the PZC. NaCl solutions of different concentrations (0.001, 0.01, 0.1 N) were purged with 99.99 % nitrogen for 2 h in an atmosphere and then purged for 12 h in an anaerobic chamber (Coy Laboratory Products Inc.) in which the atmosphere was filled with a mixed gas containing 5% hydrogen and 95% nitrogen. One hundred ml of NaCl solution was added to a 125-ml HDPE bottle and the samples were then mixed with NaCl solutions in the chamber to obtain 1 g/l suspension. After preequilibrating the suspension at RT for 24 h on a shaker (VWR, OS-500), appropriate amount of 0.1 N HCl or 0.1 N NaOH was added to give a final pH value ranging from 3 to 11. The amount of acid or base added and the pH value of the suspension were recorded and used to calculate the adsorption amounts of H^+ and OH^- after the bottles were again kept at RT for 24 h on the shaker. Finally, potentiometric titration curves were obtained by plotting the amount of acid or base versus the pH value for different NaCl concentrations.

3.3.1.6 Mechanical Strength

The mechanical strength is considered an important factor because a certain level of strength is required for adsorbents to be used in column adsorption. Due to few methods

being available to test the granulate strength in a wet state, the strength of samples in this study was evaluated according to the procedure proposed by Zeng [186], with little modifications. Five types of samples aged at RT for 10 days were tested in this study: FH2, FH2-Si-0.1, FH2-Mg-2, FH2-Al-1, and HTlc. Also granular goethite (Bayoxide 33, Bayer Chemical), a reference iron oxide, was used in the experiment. About 0.2 g of pellets with a diameter of 0.85~2 mm and 100 ml of DI water were placed into a 125-ml HDPE bottle. Each bottle was placed on a shaker (VWR, OS-500) at 110 stroke/min during the first 24 h run and at 150 strokes/min during the rest 24 h run. After shaking for both 24 h and 48 h, the turbidity of the solution was measured using a turbidity meter (HACH 2100AN). Also after shaking for 48 h, the remaining pellets were dried at 110 ^{o}C in a muffle furnace (Modern Laboratory Equipment Co., Inc.). The dried pellets were sieved to a size with a diameter of 0.85~2 mm and the mass of the sieved pellets was then determined to estimate the weight loss. The mechanical strength determination was performed in duplicate.

3.3.2 Transformation of 2-line Ferrihydrite

3.3.2.1 AOD (2 h Ammonium Oxalate in the Dark) Procedure

As shown as in Table 3.2, the following samples were used in this study to quantify the amorphous fraction of FH2s during the course of aging at room temperature (RT) in a light-excluded environment: (a) FH2, FH2-Si, FH2-Mg, FH2-Ti, FH2-Ci-0.001, -0.01 and HTlc aged at RT for 1, 2, 4, 6, 15, 30, 60, 165, and 235 days and (b) FH2-Al aged at RT for 40 days. Also the following samples treated at high temperatures were tested to evaluate the effect of heat treatment on the transformation of FH2: (a) FH2, FH2-Si,

FH2-Mg, FH2-Ti, FH2-Ci-0.001, -0.01 and HTlc heat-treated at 150, 240, and 360 ^{o}C for 12 h after aging at RT for a defined period (170~275 days) and (b) FH2-Al heat-treated at 150, 240, and 360 ^{o}C for 12 h after aging at RT for 17 days. The rate of transformation from FH2 to other iron oxides was monitored by periodically subjecting the samples to an extraction procedure that selectively dissolved FH2. The ratio of ammonium-oxalate extractable Fe ([Fe_o]) to total Fe ([Fe_t] (the [Fe_o]/[Fe_t] activity ratio) is often used to determine the degree and rate of transformation of amorphous to crystalline iron oxides. The following 2 h ammonium oxalate in the dark (AOD) procedure was used in this study to quantify the amorphous fraction of samples [81]. Ten mg of sample was added to a reaction vessel containing 50 ml of 0.2 M ammonium oxalate buffered to pH 3 using 0.2 M oxalic acid. Light was excluded by wrapping the reaction vessel in aluminium foil to prevent other iron oxides such as goethite and hematite from dissolving into the extraction solution. After agitating the vessel on a wrist action shaker (Berrell, Model 75) at RT for 2 h, 10-ml suspension was filtered through a 0.2 μm nylon membrane filter (Pall Corporation) and acidified with 17.5 μl concentrated HNO_3 (trace metal grade). The ammonium-oxalate extractable iron was analyzed using a Thermo Elemental Solaar M6 flame atomic absorption spectrometer (FAAS). In addition, a parallel extraction method for the following samples aged for 15 days at RT was performed using a 30-min extraction with 0.4 M HCl at RT to confirm whether the potential for precipitation of inhibitor-oxalate phase in the AOD procedure was avoided or not [74, 81]: FH2, FH2-Si, FH2-Mg, FH2-Ti, FH2-Ci-0.001, -0.01, and HTlc. The iron content extracted was also determined using the FAAS. The iron content determination using both the AOD procedure and HCl was performed in duplicate.

3.3.2.2 DCB (Sodium Dithionite-Citrate-Bicarbonate) Procedure

The following samples were tested in this study to quantify the amount of total iron [Fe_t]: (a) FH2, FH2-Si, FH2-Mg, FH2-Ti, FH2-Ci-0.01, -0.001, and HTlc aged at RT for 400 days and (b) FH2-Al aged at RT for 100 days. The technique to be used in this study for the determination of total iron is the sodium dithionite-citrate-bicarbonate (DCB) procedure [216]. Eighty ml of 0.3 M Na-citrate and 10 ml of 1 N $NaHCO_3$ were exactly added to a 250-ml reaction vessel containing 20 mg of sample. After warming the sample to a temperature of 75 ^oC in a water bath, 2 g of Na-dithionite was added, the suspension was stirred constantly for 1 min and intermittently another 15 min, and 10 ml of saturated NaCl solution was added to promote flocculation. After centrifuging for 15 min at 500 g (International Equipment Company), 10-ml supernatant was filtered through a 0.2 μm nylon membrane filter (Pall Coporation) and then acidified with 17.5 μl concentrated HNO_3 (trace metal grade). The total iron obtained using the DCB procedure was also analyzed using the FAAS. Duplicate DCB runs were carried out for each sample.

3.3.3 Arsenic Adsorption on 2-line Ferrihydrite

3.3.3.1 Screening Adsorption Experiments

Screening adsorption experiments were conducted as preliminary studies to evaluate arsenic removal capability of all the samples and compare their arsenic adsorption capability with that of other granular ferric hydroxides at low arsenic loading rates (mg arsenic/g sample) of 0.50, 1.00, 1.33, 2.00 and 4.00 (corresponding to 0.0067, 0.0133, 0.0178, 0.0267, and 0.0534 mol As/kg sample) for As (III) and 1.00, 2.00, 2.67, 4.00 and 8.00 (corresponding to 0.0133, 0.0267, 0.0356, 0.0534, 0.1068 mol As/kg sample) for As (V). The arsenic removal capability was evaluated before and after heat treatment as well

as before and after aging for the following samples: (a) FH2, FH2-Si, FH2-Mg, FH2-Ti, FH2-Ci, and HTlc aged at RT for ~30 days ("fresh") and 235 days, (b) FH2-Al aged at RT for 10 days ("fresh"), (c) FH2, FH2-Si, FH2-Mg, FH2-Ti, FH2-Ci, and HTlc heat-treated at 360 ^{o}C for 12 h after aging at RT for 300~400 days, and (d) FH2-Al heat-treated at 360 ^{o}C for 12 h after 17 day aging at RT. In the experiments, a series of varying initial amounts of samples (0.01~0.08 g) were loaded in each 250-ml HDPE bottle containing 192 ml (for As (V)) or 196 ml (for As (III)) of 0.01 N $NaNO_3$ and rehydrated to account for slow proton buffering on a rotary shaker at RT and 3.3 rpm for 24 h. After rehydrating, each solution was spiked with 4 ml (for As (III)) or 8 ml (for As (V)) of 10 mg arsenic/l and the solution pH was adjusted manually to 7 with 0.01, 0.025, 0.1 and 1 N HNO_3 or NaOH. Agitation was accomplished by means of a magnetic stirrer (Corning PC-250). The bottles were capped and placed on the rotary shaker at RT and 3.3 rpm for 48 h. The solution pH was manually readjusted after both 12 and 24 h. After 48 h of the reaction period, 10-ml of the suspension was filtered through 0.2 μm nylon membrane filter (Pall Corporation) and acidified with 17.5 μl concentrated HNO_3 (trace metal grade). Arsenic analysis was carried out using a Thermal Elemental Solaar M6 graphite furnace atomic absorption spectrometer (GFAAS). The data obtained from the screening experiments were used to select samples for other studies.

3.3.3.2 Effect of pH on Arsenic Adsorption

All the samples aged at RT for ~20 days were tested to investigate arsenic adsorption at different pH values. The effect of pH on arsenic adsorption was obtained for both As (III) and As (V) in 0.01 N $NaNO_3$ at low arsenic loading rates of 1.33 mg As

(III)/g sample (corresponding to 0.01780 mole As/kg) and 1.67 mg As (V)/g sample (corresponding to 0.02225 mole As/kg), respectively. The experimental setup was the same as for the screening experiments, except that the solution pH was adjusted to a desired value (pH 3, 5, 7, or 9). In each test, 30 mg of sample was loaded in each HDPE bottle containing 196 ml of 0.01 N $NaNO_3$ and rehydrated on a rotary shaker at RT and 3.3 rpm for 24 h. After adding 4 ml of 10 mg arsenic/l to the bottle, the pH of the solution, which was agitated with a magnetic stirrer (Corning PC-250), was adjusted manually to a defined value with 0.01, 0.025, 0.1 and 1 N HNO_3 or NaOH and then the bottle was placed on the rotary shaker at RT and 3.3 rpm for 48 h. The solution pH was readjusted after both 12 and 24 h. After the 48 h reaction period, 10-ml of the suspension was filtered through a 0.2 μm nylon membrane filter (Pall Corporation), acidified with 17.5 μl concentrated HNO_3 (trace metal grade), and analyzed for arsenic using the GFAAS.

3.3.3.3 Effect of High Arsenic Loading on Arsenic Adsorption

Based on results of the screening adsorption experiments, four types of samples (FH2, FH2-Mg-2, FH2-Al-1, and HTlc) aged at RT for 40 days were selected as adsorbents to evaluate their adsorption densities. Adsorption isotherms were obtained at initial arsenic loading rates in the range of 5, 10, 20, 50, 100, 150, 200, and 400 mg arsenic/g sample (corresponding to 0.06674, 0.13347, 0.2669, 0.6674, 1.3347, 2.0021, 2.6694, and 5.3389 mol As/kg). The FH2s are aimed to be applied in drinking water plants; therefore the experiments were conducted at pH 7 and RT. The experimental setup was the same as for the screening experiments for arsenic adsorption except that initial arsenic concentrations of 0.5, 1, 2, 5, 10, 15, 20, and 40 mg/l were used. Twenty mg of

sample was placed in each 250-ml HDPE bottle containing 118, 158, 168, 178, 188, 194, 196, and 197 ml of 0.01 N $NaNO_3$ and rehydrated on a rotary shaker at RT and 3.3 rpm for 24 h before each isotherm experiments. After adding 1, 2, 4, 10, 20, 30, 40, or 80 ml of 100 mg As (III or V)/l to each bottle, the solution pH was adjusted manually to 7 with 0.01, 0.025, 0.1 and 1 N HNO_3 or NaOH on a magnetic stirrer (Corning PC-250) and then the bottles were capped and shaken at RT and 3.3 rpm on the rotary shaker at RT and 3.3 rpm for a contact time of 48h. After both 12 and 24 h, the pH of the suspension was readjusted to 7. After completion of the contact time, 10 ml of all the samples was passed through a 0.2 μm nylon membrane filter (Pall Corporation), acidified with 17.5 μl concentrated HNO_3 (trace metal grade), and analyzed for arsenic using the GFAAS. The data obtained from the isotherm studies were used to analyze the adsorption isotherms in order to estimate the constants, adsorption density and adsorption maxima. The adherence of the adsorption data to the Langmuir, Freundlich, and Temkin isotherms was tested.

3.3.4 Iron and Arsenic Analyses

3.3.4.1 Measurement of Iron Concentration

The iron content (extracted using the AOD procedure and the DCB procedure and extracted with 0.4 M HCl) was determined using the FAAS, with D2 quadline background correction. The FAAS was equipped with a CETAC auto sampler. All operations of the FAAS were controlled by SOLAAR M Series software. All measurements were performed at 248.3 nm by using a hollow cathode lamp (Thermo Electron Corporation), and the calibration range was 0~10 mg/l of iron ($R^2 > 0.999$). Acetylene (99.6%, 9 psi) and air (Zero K, 30 psi) were used as flame gases.

3.3.4.2 Measurement of Arsenic Concentration

Arsenic was analyzed by the GFAAS, with Zeeman background correction. The GFAAS was equipped with a GF95 graphite furnace and a FS95 furnace auto sampler. All operations of the GFAAS were controlled by SOLAAR M Series software. All measurements were performed at 193.7 nm by using a hollow cathode lamp (Thermo Electron Corporation). Normal electrographite cuvettes (Thermo Elemental) were used in the experiments and argon gas of ultrahigh purity (99.999%, 15 psi) was used to sheath the atomizer and purge it internally. Atomization temperature was 2700 ^{o}C. The calibration range was 0~25 μg/l of arsenic ($R^2 > 0.995$).

CHAPTER IV

CHARACTERISTICS OF 2-LINE FERRIHYDRITE CONTAINING A TRANSFORMATION INHIBITOR

4.1 Introduction

FH2 shows two extremely broad peaks at 0.25 and 0.15 nm due to the presence of hexagonally close-packed oxygen [6]. However, the structure of FH2 is not yet fully understood due to the low degree of order [2, 8]. The particle size of FH2 was reported to be 1~3 nm [22]. FH2 thus has a high surface area. The specific surface area of FH2 obtained by BET analysis is known to vary between 200 and 400 m^2/g [2, 4]. In spite of little or no permanent surface charge, FH2 may generate both anion and cation exchange capacities due to the adsorption of potential-determining ions [52]. FH has PZC's in the pH range of 7.8~8.9 [51, 55~58]. The low crystallinity, small particle size, large surface area, and high reactivity of FH2 make it an important adsorbent of trace metals such as arsenic in surface and groundwater systems. Compared with pure FH2, FH2 with a coprecipitated transformation inhibitor may be very desirable for efficient and economical applications for removing arsenic from water due to the retardation of transformation of FH2 into crystalline iron oxides. The objective of this study, therefore, was to investigate the fundamental characteristics of FH2 containing a transformation inhibitor (Si(IV), Mg(II), Al(III), Ti(IV), or Ci(citrate)). The identity of the FH2 was confirmed by XRD analysis. Water content, specific gravity, particle size, specific surface area, and PZC values were also determined. In addition, mechanical strength was measured to evaluate the potential of the FH2 as a filter medium for column adsorption.

4.2 Results and Discussion

4.2.1 X-ray Diffraction

4.2.1.1 FH2, FH2-Si, FH2-Ti, FH2-Ci, FH2-Mg Series and HTlc

Figure 4.1 and 4.2 depicted XRD patterns of FH2, FH2-Si, FH2-Ti, FH2-Ci, and FH2-Mg series at an initial aging time (20 days). The XRD patterns revealed the presence of two broad peaks at 35 (d = 0.26 nm) and 62^{o} 2θ (d = 0.15 nm) characteristic of poorly crystalline 2-line ferrihydrite as a sole phase formed. These XRD patterns agree approximately with those reported for 2-line ferrihydrite by others [8, 20, 24~27, 30, 40]. Although the XRD lines were broad because of poor crystallinity, no significant differences in peak position were ascertained. The XRD pattern of HTlc is shown in Figure 4.2. From this pattern, it was observed that the peaks were sharper than those of the FH2s and hence well crystallized. This XRD pattern allowed the product to be assigned as an Mg/Fe HTlc with peaks at 12.03, 23.38, 34.39, 38.78, 46.08, 59.66, and 61.35^{o} 2θ, close to the literature values [212].

4.2.1.2 FH2-Al Series

For FH2-Al series aged at room temperature for 135 days, broad background peaks were observed at 35 (d = 0.26 nm) and 62^{o} 2θ (d = 0.15 nm), indicative of poorly crystalline 2-line ferrihydrite and broader than those of the FH2, FH2-Si, FH2-Ti, FH2-Ci, and FH2-Mg series aged at room temperature for 20 days (Figure 4.2). The XRD pattern of FH2-Al-0.1 was almost identical to that of FH2 (2-line ferrihydrite) although FH2-Al-0.1 showed two broader peaks with respect to FH2. However, peaks, indicative of crystalline Al hydroxides, appeared as a trace in FH2-Al-0.25 and as distinct bands in

FH2-Al-0.5 and FH2-Al-1. Gibbsite (α-$Al(OH)_3$) and bayerite (β-$Al(OH)_3$) were present as crystalline Al hydroxides at Al/Fe molar ratios ≥ 0.25, although broad background peaks indicative of poorly crystalline 2-line ferrihydrite were also evident with these phases. Although the peaks of the XRD patterns shifted to slightly lower positions in this XRD analysis, the 21.3, 23.6, 44.1, and 23.9^o 2θ peaks were the result of gibbsite while the 47.5, 21.9, 23.7, and 62.5^o 2θ peaks were the result of bayerite [217].

In general, when Al(III) salt solutions are neutralized with base, the hydrolysis of Al(III) results in the initial formation of amorphous and poorly crystalline Al hydroxides, which will transform into crystalline Al hydroxides upon aging: rapid precipitation usually yields bayerite, nordstrandite or both, whereas slow crystallization producs gibbsite [218]. It was reported by other researches [30, 219] that gibbsite and bayerite were identified as products through both coprecipitation of Fe(III) with Al(III) at pH 7.5 [30] and addition of Al(III) salt solution to FH at pH 7.5 [219]. Masue et al. [30] concluded that Al(III) was largely incorporated into the FH2 structure as a solid solution to form a poorly crystalline bimetal hydroxide (Al-substituted FH2) at Al/Fe molar ratios ≤ 0.25, whereas goethite and baterite were formed at Al/Fe molar ratios ≥ 0.43. In the binary Fe(III)-Al(III) systems (coprecipitaed at a 1:1 molar ratio at pH 8) [220], Al(III) becomes relatively enriched in the $Fe(OH)_3$ particles' surface layers: the most likely process for this involves partial dissolution of the $Al(OH)_3$ particles and adsorption or reprecipitation on the surface of the $Fe(OH)_3$. A yellow-brown Fe (III)-Al (III) sol was reported to be formed by reaction of FH2 with Al (III) hydroxy species at pH 4.0~4.2 and was shown to be stable at the pH over long periods [96]. Al(III) adsorption on goethite occurs in the pH range of 3~8.5 and then two very stable monodentate surface hydroxo

complexes ($FeOAlOH^+$ and $FeOAl(OH)_2$) form consecutively as the pH increased [180, 181]. Al(III), which is known to have the ablity to extensively substitute for Fe(III) in the goethite structure [182], can be expected to be very strongly bound at the goethite surface once adsorbed. Therefore, the strong adsorption of Al(III) on the goethite surface might be considerd the first step in the formation of an Al(III) substituted goethite [180, 181].

In summary, for FH2-Al-0.1, Al(III) species might form initially complexes with Fe(III) at the 2-line ferrihydrite surface, and then result in being largely incorporated into the 2-line ferrihydrite structure to form Al-substituted 2-line ferrihydrite. For FH2-Al-0.25, FH2-Al-0.5 and FH2-Al-1, Al (III) species might be involved in the formation of poorly crystalline or crystalline Al hydroxides (gibbsite and bayerite) as separate phases as well as forming stable complexes with 2-line ferrihydrite. Therefore, it may be suggested that Al-substituted 2-line ferrihydrite formed in FH2-Al-0.1, whereas FH2-Al-0.25, FH2-Al-0.5, and FH2-Al-1 consisted of poorly crystalline 2-line ferrihydrite, gibbsite/bayerite, and poorly crystalline Al hydroxide.

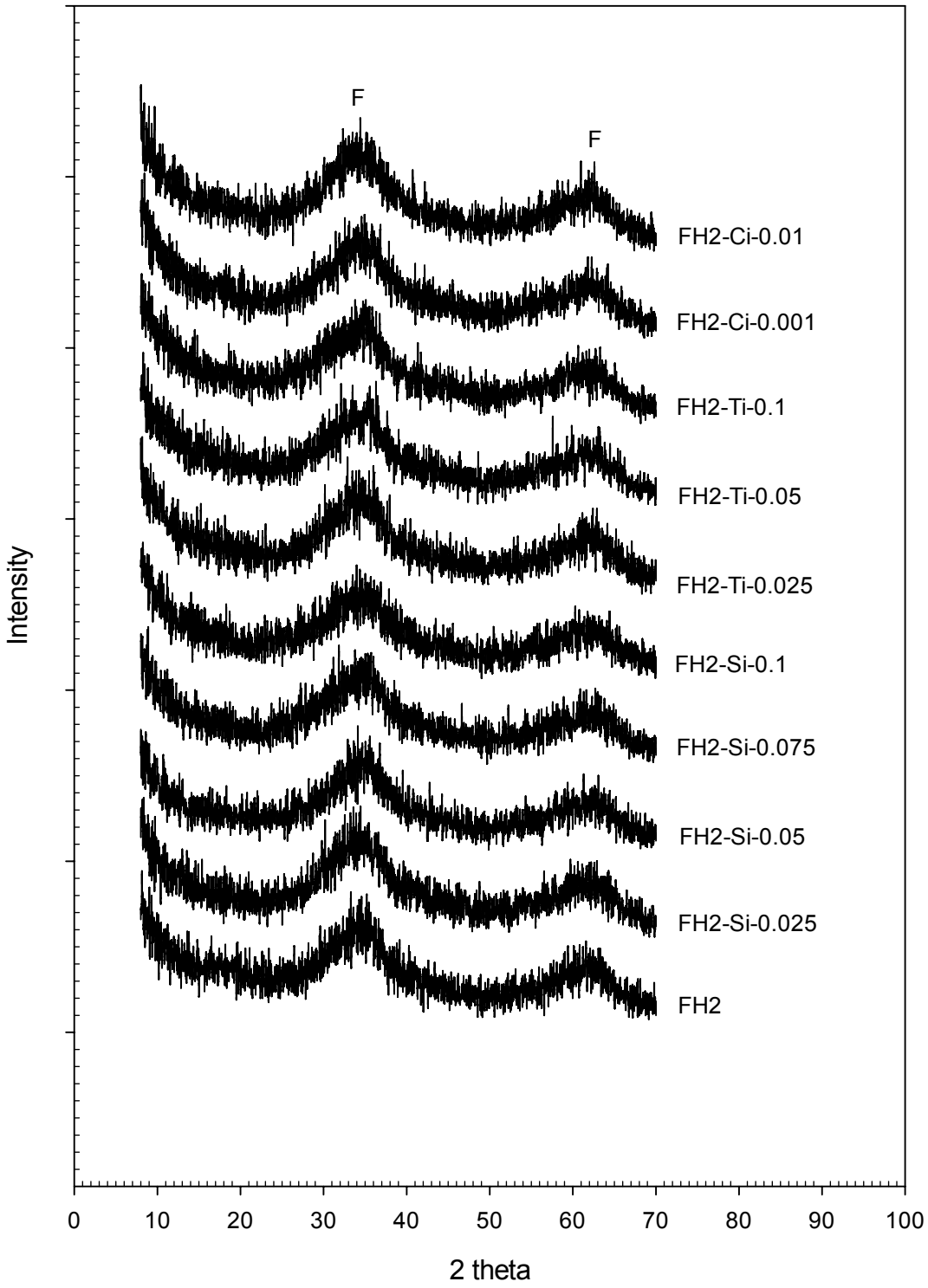

Figure 4.1 XRD Patterns of FH2-Si, FH2-Ti, and FH2-Ci Series at an Initial Aging Time (20 Days). Major Peaks due to 2-line Ferrihydrite are indicated as F.

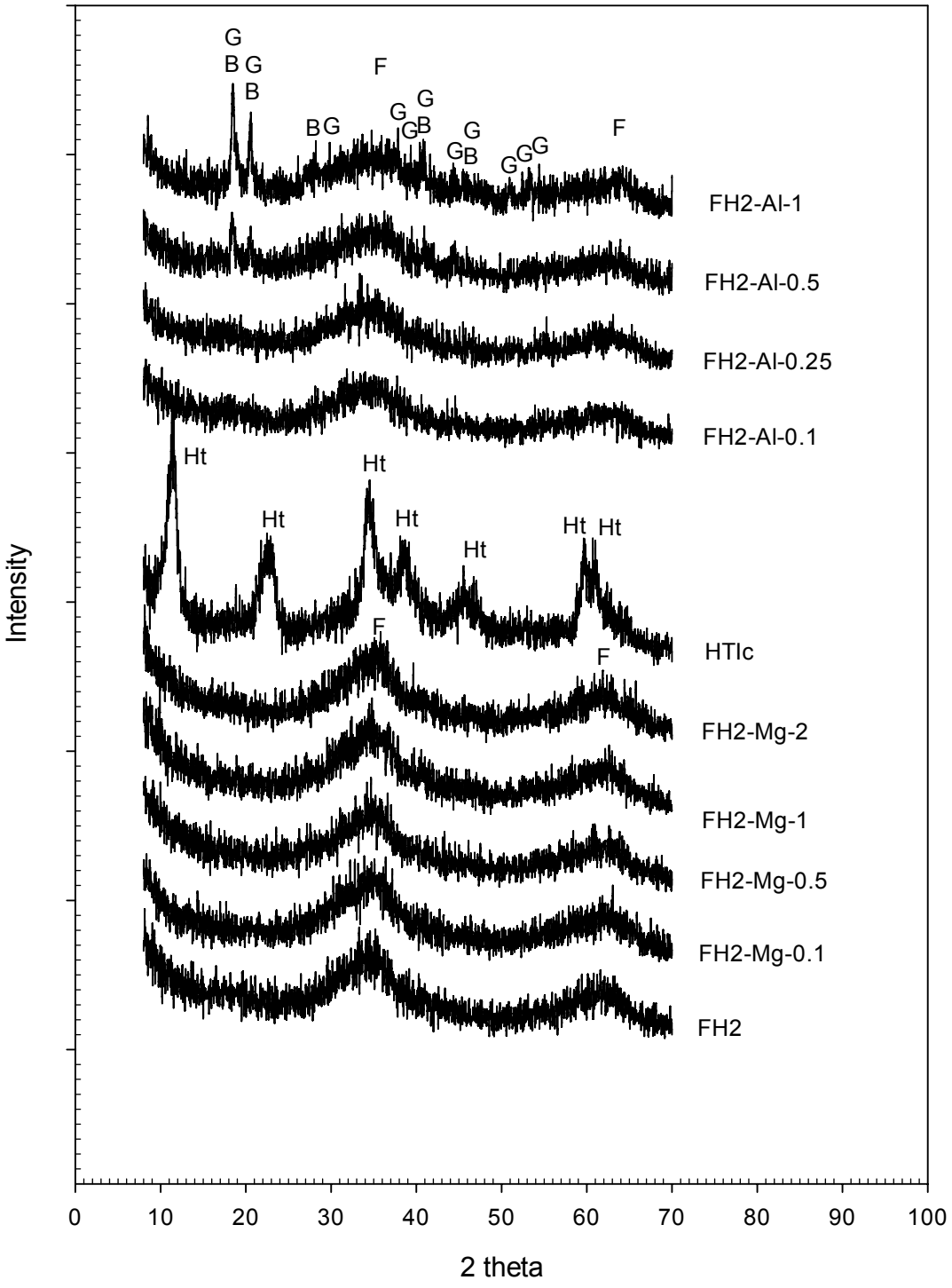

Figure 4.2 XRD Patterns of FH2-Mg, FH2-Al Series and HTlc at an Initial Aging Time (20 Days for FH2-Mg Series and HTlc and 135 Days for FH2-Al Series). Major Peaks due to 2-line Ferrihydrite, HTlc, Gibbsite, and Bayerite are Indicated as F, Ht, G, and B, Respectively.

4.2.2 Water Content and Specific Gravity

The water content of the fresh FH2, FH2-Si-0.1, and FH2-Mg-2 ranged from 24.52 to 26.00% (Table 4.1). Aging at room temperature (RT) for 650 days resulted in lower water contents of 18.67 to 21.18%. The results indicate that during air-drying for 650 days, a small amount of residual water was evaporated from the FH2s and part of the hydrous 2-line ferrihydrite transformed into other iron oxides. The water content of the fresh HTlc (H) was 12.04%, which was less than 50% of the values for the fresh FH2, FH2-Si-0.1, and FH2-Mg-2, due to water loss during heat treatment at 80 ^{o}C in the preparation of the HTlc. In contrast to the aged FH2, FH2-Si-0.1, and FH2-Mg-2, air-drying of the HTlc at RT for 650 days caused an increase in water content by 2.20% over the fresh HTlc. The increase may be attributed to readsorption of water during the exposure of HTlc to the air for 650 days. The water content of the fresh FH2-Al-1 was determined to be 15.61%, which was less than that of the fresh FH2, FH2-Si-0.1, and FH2-Mg-2. This result indicates that the formation of polymorphs of $Al(OH)_3$ such as gibbsite and bayerite could have been induced during the coprecipitation of Al^{3+} and Fe^{3+} [30, 219] to lead to a decrease in the proportion of hydrous 2-line ferrihydrite in FH2-Al-1 and resulting in a decrease in the water content of FH2-Al-1.

Schwertmann et al. [8] reported that air-dried FH2s from a series with different Al contents had initial water contents of 11.5% (weight loss between air-drying and 150 ^{o}C), and even after 21.4 years of storage the water content (weight loss after heating at 150 ^{o}C for 300 h) increased from 13.0 to 17.6% within an Al range of 0 to 0.20 mol_{Al}/mol_{Al+Fe} Schwertmann et al. [8] and Cornell et al. [2] suggested that FH with 100~150 mg water/g FH transforms to hematite through a short-range crystallization process. Therefore, the

water content for both the fresh and the aged samples might be sufficiently low to allow non-thermal transformation of 2-line ferrihydrite to hematite.

The specific gravity (density) of five types of FH and HTlc was determined by means of a picnometer. The densities of FH2, FH2-Mg-2, and FH2-Al-0.1 were 3.18, 3.13, and 3.22 g/cm^3, respectively, whereas the density decreased slightly with an increase in the Si/Fe mole ratio (FH2-Si-0.1) or the Al/Fe mole ratio (FH2-Al-0.5). The density of FH2 was lower than that of both dry ferric hydrous oxide (3.96 g/cm^3) [7] and iron (III) oxide-hydrate gel (3.80 g/cm^3) [37]. Differences between the literature data and the results of the current study might be partly due to the efficiency with which entrapped air was removed during boiling of the sample in the water bath before picnometer analysis.

Table 4.1 Water Content and Specific Gravity of 2-line Ferrihydrites

Type of FH2		FH2	FH2-Si-0.1	FH-Mg-2	FH2-Al-0.1	FH2-Al-0.5	FH2-Al-1	H
Water Content (%)	Fresh[a)]	26.00	24.52	25.13			15.61	12.04
	Aged	18.67[b)]	21.18[b)]	19.80[b)]		18.75[c)]		14.24[b)]
	Decrement[d)]	- 7.33	- 2.97	- 5.33				2.20
Specific gravity (Density (g/cm^3))[e)]		3.18	2.75	3.13	3.22	2.55		2.69

[a)] "Fresh" samples were tested after 2 day aging at room temperature (RT).
[b), c)] Water content was determined after 650 day[b)] and 190 day[c)] aging at RT, respectively.
[d)] Difference between water content of the fresh sample and that of the aged sample.
[e)] Specific gravity was measured after 190 day aging at RT. Before calculating the specific gravity (at 4 ^{o}C), a temperature correction factor of 0.99806 (at 21 ^{o}C) was used. Density was calculated from the relationship between specific gravity and water density.

4.2.3 Particle Size Distribution

The particle-size distribution of five samples sieved to a grain size of smaller than the No. 100 (0.15 mm) sieve was analyzed by a photograph/ image analysis system. The

average diameters of FH2, FH2-Si-0.1, FH2-Mg-2, and FH2-Al-1 ranged from 2.175 to 2.389 μm, whereas HTlc had an average diameter of 2.797 μm (Figure 4.3 and Table 4.2). The difference in diameter between HTlc and the other samples might be due to the heat treatment in the synthesis of samples and the degree of grinding. The centrifugation sediment of HTlc became hardened by heat treatment at 80 ^{o}C so that the hardened aggregates were difficult to grind.

From the analysis of particle-size using the skewness and kurtosis coefficients, each distribution of the samples was unimodal, right-skewed, and somewhat heavily-tailed with volume means of 2.175~2.797 μm and standard deviations of the distributions of 1.467~2.044 μm (Table 4.2). FH2-Mg-2 was slightly more skewed and right-tailed than any other sample due to the extent of grinding. According to the empirical rule [221], FH2 exhibited a normal size distribution since 95.15% of the data was between the values $\hat{Y} - 2S_Y$ and $\hat{Y} + 2S_Y$ and 99.05% of the data was between the values $\hat{Y} - 3S_Y$ and $\hat{Y} + 3S_Y$. No clear trend could be observed among FH2, FH2-Si-0.1, FH2-Mg-2, and FH2-Al-1. It was, however, observed that the addition of the inhibitor to the FH2 tended to decrease the mean of diameter.

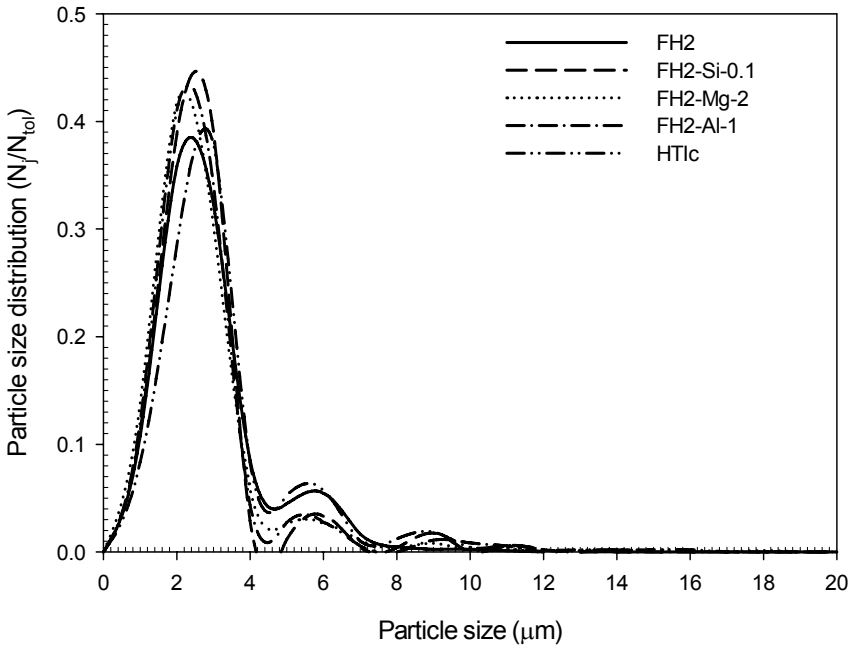

Figure 4.3 Particle Size Distributions of 2-line Ferrihydrites Aged at Room Temperature for 190 Days after Grinding.

Table 4.2 Analysis of Particle Size Distribution Shape

Type of sample[a)]	FH2	FH2-Si-0.1	FH2-Mg-2	FH2-Al-1	H
Mean ($\hat{Y}$: μm)	2.389	2.251	2.175	2.198	2.797
Range (μm)	0.727~ 10.910	0.727~ 13.091	0.727~ 17.455	0.727~ 10.182	0.727~ 15.273
Standard deviation (S_Y)	1.467	1.637	1.642	1.533	2.044
Skewness Coefficient[b)]	1.621	3.042	3.596	2.738	2.494
Kurtosis Coefficient[c)]	6.425	14.833	23.246	12.467	11.686
$\hat{Y} \pm 2S_Y$ (%)[d)]	95.15	94.96	95.68	96.45	95.54
$\hat{Y} \pm 3S_Y$ (%)[d)]	99.05	97.07	97.91	97.54	97.97

[a)] All samples were ground gently and sieved to a grain size of smaller than the No. 100 (0.15 mm) sieve before analysis.

[b)] The skewness coefficient is $\frac{1}{n}\sum_{i=1}^{n}(\frac{Y_i - \hat{Y}}{S_Y})^3$, This measures asymmetry. Coefficients bigger than 1 or less than -1 indicate a fair amount of skewness.

[c)] The kurtosis coefficient is $\frac{1}{n}\sum_{i=1}^{n}(\frac{Y_i - \hat{Y}}{S_Y})^4$, This measures heaviness of the tails. Coefficients bigger than 4 indicate somewhat heavier tails.

[d)] The empirical rule, based on the classic bell-shape curve (normal distribution), says that for many datasets one will find that about 95% of the data are between the values $\hat{Y}$ - $2S_Y$ and $\hat{Y}$ + $2S_Y$, and about 99% of the data are between the values $\hat{Y}$ - $3S_Y$ and $\hat{Y}$ + $3S_Y$.

4.2.4 Effect of Inhibitor on the Specific Surface Area

The N_2 adsorption isotherms, BET plots, and specific surface areas obtained after the outgassing of samples at 50 ^oC are presented in Figures 4.4 and 4.5 and Table 4.3. According to International Union for Pure and Applied Chemistry (IUPAC) classification [148], the N_2 adsorption isotherms for all samples can be assigned to Type I (Langmuir-type isotherm) (Figure 4.4). The BET plots are linear for all samples in the relative pressure range examined, and the R^2 values for the regression lines are greater than 0.998 (Figure 4.5, Table 4.3). These observations show that the BET equation is valid in the applied relative pressure range ($0.05 < p/p_0 < 0.3$).

The specific surface areas were determined to be 325.8 for FH2, 393.8 for FH2-Si-0.1, 340.2 for FH2-Mg-2, and 229.3 m^2/g for FH2-Al-1, in agreement with the typical values (200~400 m^2/g) for 2-line ferrihydrite obtained by the BET analysis as shown in Table 1.1. The specific surface areas of both FH2-Si-0.1 and FH2-Mg-2 were greater than that of FH2. As discussed in section 4.2.3, the particle sizes of FH2-Si-0.1 and FH2-Mg-2 ranged from 2.175 to 2.251 μm, whereas for FH2 it was found to be 2.389 μm. Therefore, compared to FH2, the bigger particle sizes of FH2-Si-0.1 and FH2-Mg-2 might be in part responsible for their larger surface areas.

In contrast, the specific surface area of FH2-Al-1 was smaller than that of the other FH2s. It was reported that amorphous iron oxides showed greater surface area than amorphous aluminum oxides [220, 222], and an increase in a Fe/Al molar ratio in mixed (or coprecipitated) iron-aluminum oxide corresponded to an increase in the specific surface area, although the maximum value was obtained at a Fe/Al molar ratio =1 [220, 223]. Potter et al. [223] and Anderson et al. [220] suggested that adsorbed SO_4^{2-} formed

bridges between metal ions and thus resulted in inhibiting the growth of large particles during oxide precipitation [223] and soluble $Al(OH)_3$ species led to redispersion of preciously agglomerated $Fe(OH)_3$ particles, significantly decreasing the average size of these particles, and resulting in increasing their surface areas [220]. Contrary to what was previously observed for amorphous iron-aluminum oxides [220, 223], in the current study the specific surface area of FH2-Al-1 (Al/Fe molar ratio = 1) was lower than that of the other FH2s. The result can be explained by both the XRD analysis and the measurement of total iron content. From the XRD pattern for the aged FH2-Al-1 for 135 days (Figure 4.2), crystalline Al hydroxides (gibbsite and bayerite) were detected along with two broad background peaks indicative of 2-line ferrihydrite. The specific surface area of gibbsite in soils [196, 218, 224~225] and bayerite [217, 226] was reported to be about 19~90 and 6~85 m^2/g, respectively, which are much lower than that of FH2. As will be discussed in detail later (section 5.2.1), the total iron content of FH2-Al-1 represents half the content of FH2. Therefore, the formation of the crystalline Al hydroxides was likely responsible for the lower specific surface area of FH2-Al-1.

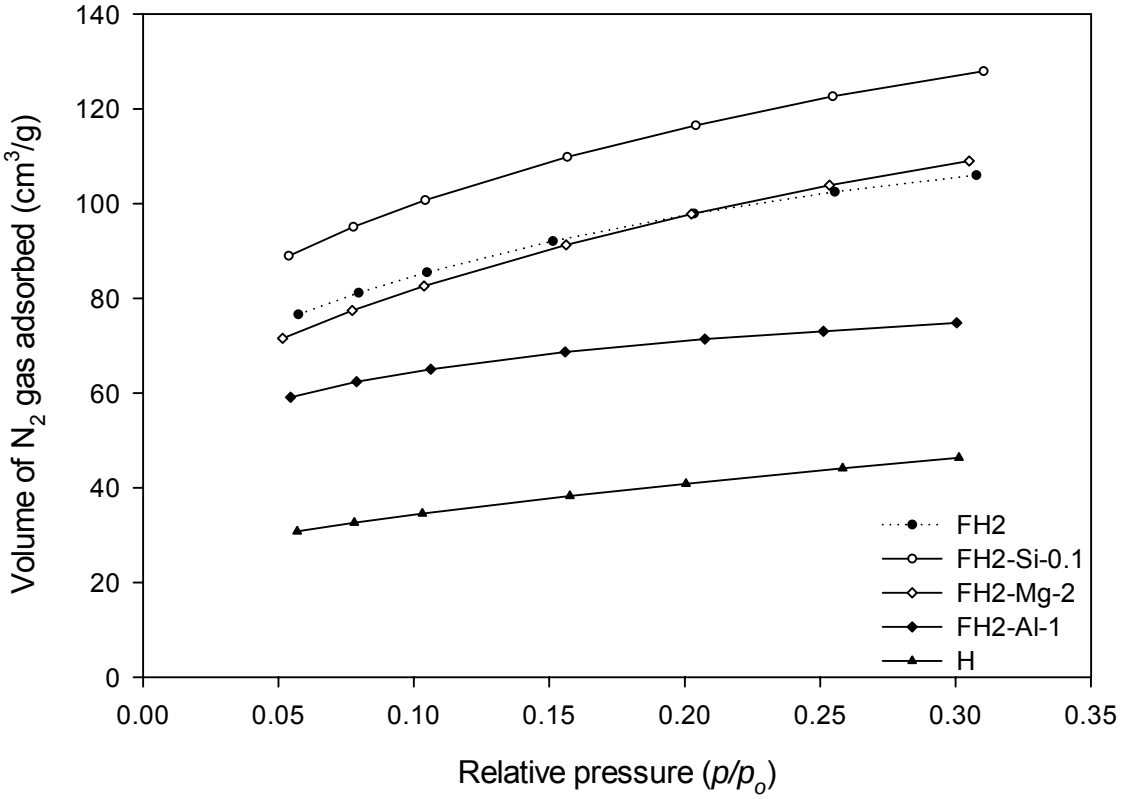

Figure 4.4 N_2 Gas Adsorption Isotherms for 2-line Ferrihydrites Aged at Room Temperature for 240 Days after Grinding.

Table 4.3 Specific Surface Area of 2-line Ferrihydrites

Type of FH2	FH2	FH2-Si-0.1	FH2-Mg-2	FH2-Al-1	H
Outgassing temperature (^oC)	50	50	50	50	50
Outgassing time (h)	12	12	12	12	24
Specific surface area (m^2/g)	325.8	393.2	340.2	229.3	144.9
R^2 value[a)]	0.9985	0.9988	0.9993	0.9981	0.9998

[a)] A regression coefficient of the linearized BET equation.

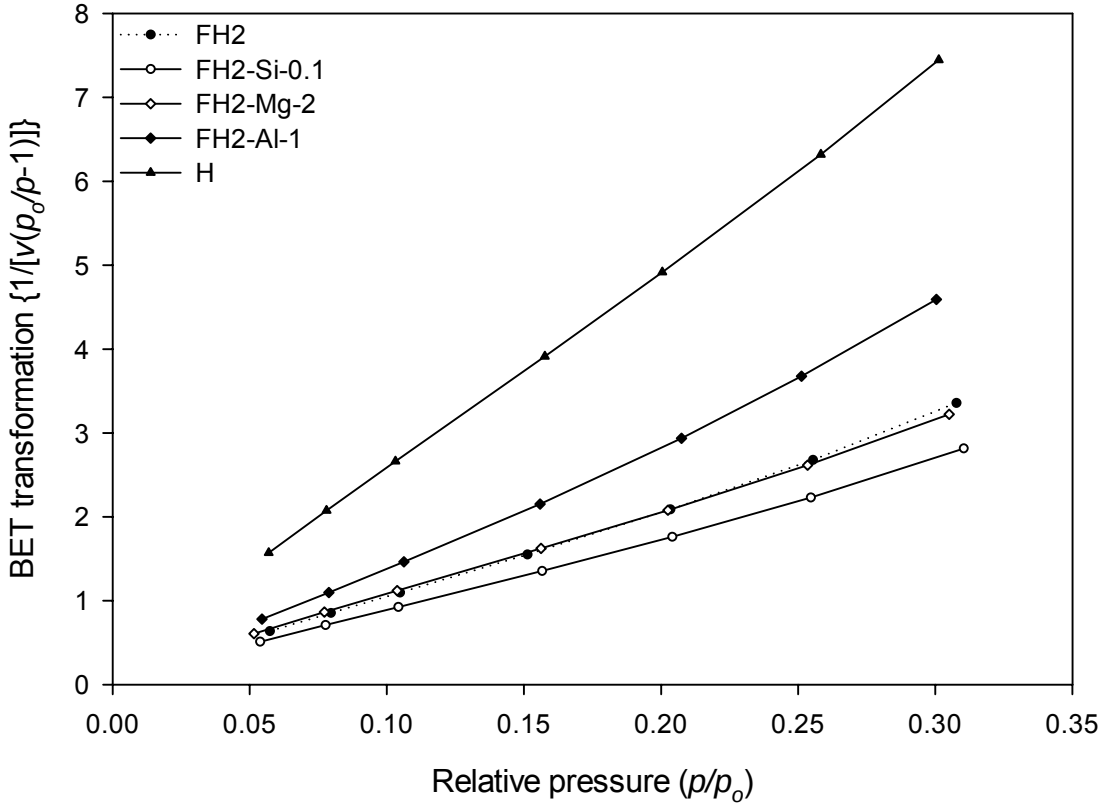

Figure 4.5 BET Plots for 2-line Ferrihydrites Aged at Room Temperature for 240 Days after Grinding.

4.2.5 Effect of Inhibitor on the Point of Zero Charge

The PZC of FH2 was found to be 7.82 (Figure 4.6), which fell within the range of PZC values reported by other researchs [19, 20, 51, 55~58, 72]. FH2-Si-0.1, an FH2 coprecipitated with silicate, had a PZC of 6.90, lower than that of FH2. The lower PZC may be explained by the occurrence of at least part of the coprecipitated Si(IV) at the surface mineral [114]. Generally the coprecipitated Si(IV) is known to modify the surface charge on the iron oxides and hence induce an acid shift in the PZC [64, 65, 114]. The mechanism responsible for lowering the PZC is similar to that occurring during specific adsorption of Si(IV) on the iron oxide surface. The soluble Si(IV) could have modified

the charge characteristics of ferrihydrite by changing proton acceptor FeOH groups into proton donor SiOH groups [113]. The formation of 2-line ferrihydrite and monosilicic acid (H_4SiO_4) could have occurred simultaneously at pH 7.5 to result in the formation of silicato-iron (III) surface complexes through the polymerization of silicic acid on the 2-line ferrihydrite surface. When the Si/Fe molar ratio is high, siloxane linkages (Si-O-Si) form on the 2-line ferrihydrite surface [115, 187, 227]. The specific adsorption of Si(IV) on 2-line ferrihydrite lowers the PZC by increasing the negative charge on the 2-line ferrihydrite surface, thus requiring increased proton adsorption (i.e., lower pH) to neutralize the surface charge [2]. It was also reported that the PZC decreased with an increase in the Si(IV)/(Si(IV)+Fe(III)) molar ratio [64, 65]. The addition of Si(IV) after ferrihydrite precipitation caused slightly lower PZC values than the coprecipitation of Si(IV) with Fe(III), since more of the Si(IV) was located at the ferrihydrite surface [64].

The PZC value of FH2-Al-1 was determined to be 8.70 (Figure 4.7), which was greater than that of FH2. The result indicates that the coprecipitation of FH2 with Al(III) promoted a shift of the PZC to a more positive value. A basic shift of PZC (8.7 and 9.1) was reported by other researchs [30, 221] when Al(III) and Fe(III) salts were coprecipitated at a 1:1 molar ratio at pH 7~8. The shift of PZC of FH2-Al-1 to the more basic value suggested the following possible scenarios. First, the higher value of PZC of FH2-Al-1 than that of FH2 indicates that at least part of Al (III) species located at the surface of 2-line ferrihydrite surface formed stable complexes with Fe (III) [96, 180, 181], which caused an increase in the PZC value of FH2-Al-1. Anderson et al. [220] suggested that the coprecipitation of Fe(III) with Al(III) (at a 1:1 molar ratio and pH 8) caused partial dissolution of $Al(OH)_3$ particles, resulting in adsorption or reprecipitation of

soluble Al(III) species on the surface of the $Fe(OH)_3$. The soluble Al(III) species controlled the chemical interaction between the particles' surface and the solution phase (e.g., the PZC), that is, an increase in PZC (9.1) was observed compared to that (7.2) of $Fe(OH)_3$ alone. Second, from the XRD pattern of FH2-Al-1 as shown in Figure 4.2, the formation of poorly crystalline and crystalline Al hydroxides (gibbsite and bayerite) might contribute to the higher value of PZC. It has been reported that the PZC values of poorly crystalline Al hydroxide (8.5~9.4) [168, 228], gibbsite (9.0~9.9), and bayerite (9.1) [196, 228~230] were higher than that of FH2.

The adsorption of Mg resulted in a shift of the PZC to 7.90 (Figure 4.8). Specific adsorption of Mg(II) on goethite has been reported by several authors [68, 69, 184]. With an increase in the concentration of Mg(II), the zeta potential values became more positive and hence the PZC shifted to a basic pH, which reflected an increase in the specific adsorption of Mg(II) onto the sample surface. Bleam et al. [184] reported that the adsorption of Mg(II) started at about pH 7.6~7.9, below the isoelectric point (9.0 ± 0.2) of goethite. Therefore, in the current study, the slight shift of PZC from 7.82 to 7.90 might be due to a small amount of Mg(II) adsorption on the FH2.

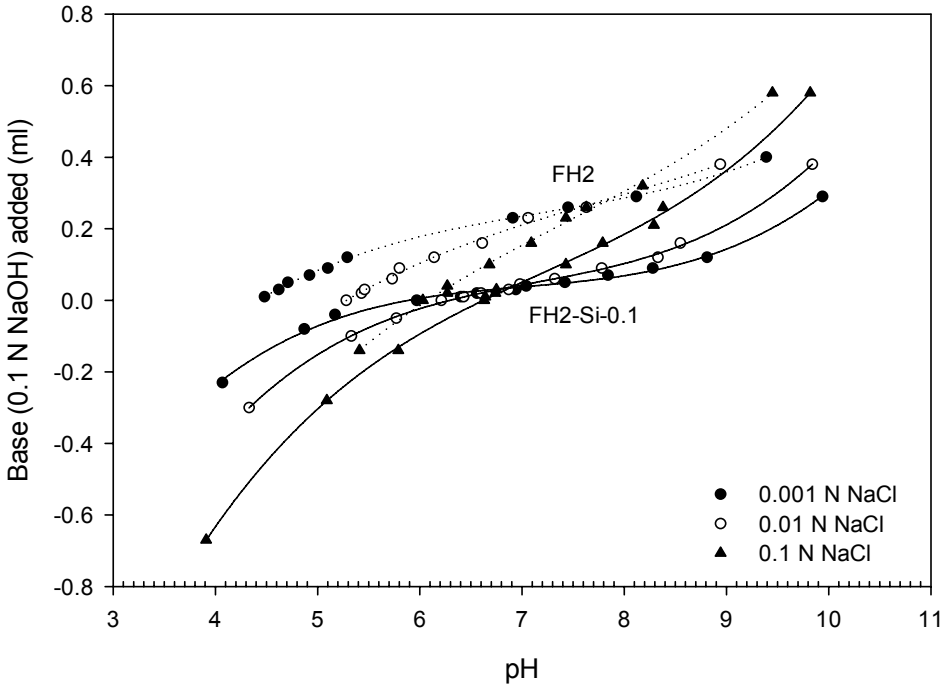

Figure 4.6 Potentiometric Titration Curves of 2-line Ferrihydrite and Si-Containing 2-line Ferrihydrite (FH2-Si-0.1) Aged at Room Temperature for 165 Days.

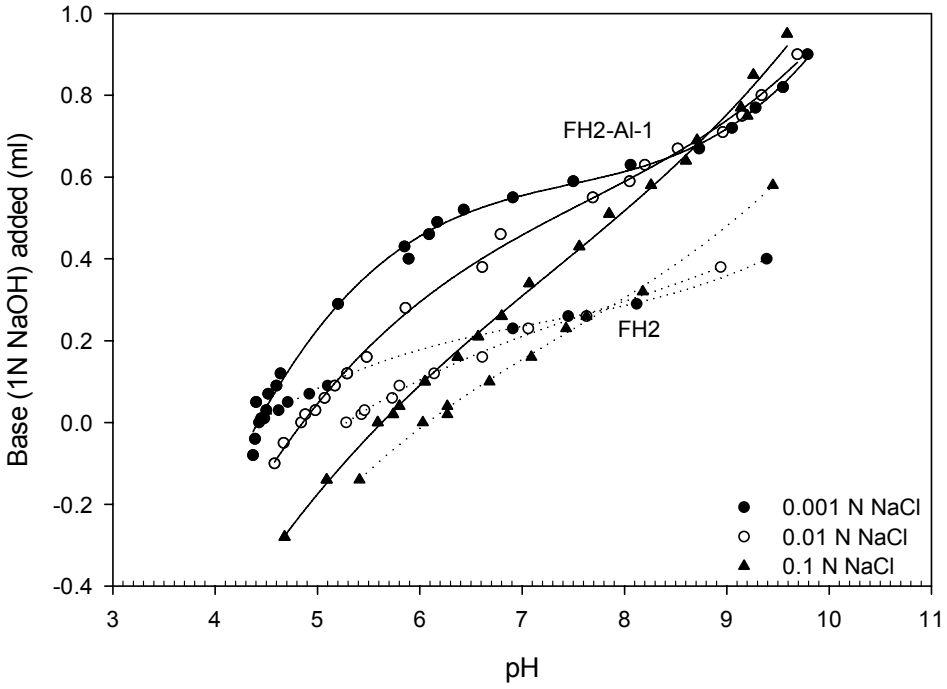

Figure 4.7 Potentiometric Titration Curves of 2-line Ferrihydrite and Al-Containing 2-line Ferrihydrite (FH2-Al-1) Aged at Room Temperature for 165 Days.

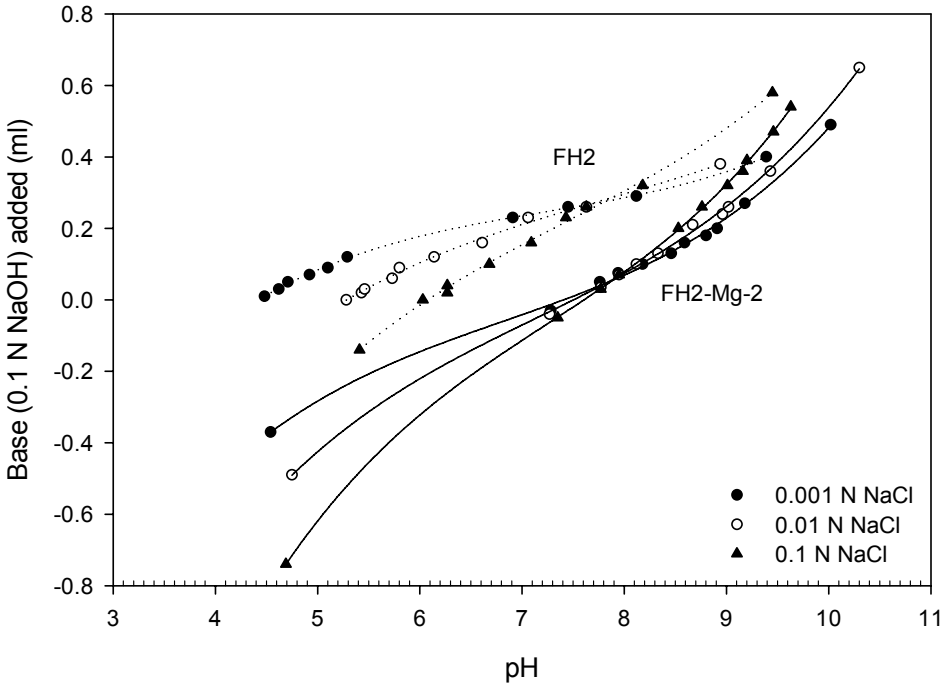

Figure 4.8 Potentiometric Titration Curves of 2-line Ferrihydrite and Mg-Containing 2-line Ferrihydrite (FH2-Mg-2) Aged at Room Temperature for 165 Days.

4.2.6 Effect of Inhibitor on Mechanical Strength

The mechanical strength of granulated samples in a wet state was evaluated by measuring both the turbidity of the solution and the amount of the dried residual of samples (initially sieved to a size with a diameter of 0.85~2.00 mm) after shaking 0.2 g of pellets in 100 ml of DI water for 48 h. After 48 h shaking, the solution of FH2-Si-0.1 exhibited the lowest turbidity, whereas, the highest turbidity was obtained for the solution of commercial goethite (Figure 4.9). The turbidities for FH2-Si-0.1, FH2-Mg-2, and FH2-Al-1 were lower than that for FH2, while the turbidity for the goethite and HTlc were higher than that for FH2. The sample with lower turbidity had higher mechanical strength. Therefore, 48 h shaking caused goethite to disintegrate significantly into the solution, resulting in a higher concentration of suspended colloidal matter. FH2-Si-0.1 was

physically stronger than any other sample. The positive effect of Si on the mechanical strength was in agreement with the results obtained by Zeng [186].

To determine the weight of the dried residual of samples after 48 h shaking, the remaining pellets were dried at 110 ^{o}C and then sieved to a size with a diameter of 0.85 to 2 mm. As shown in Figure 4.10, the percentage residual decreased in the order of HTlc (68.75%) > FH2-Si-0.1 (57.94%) > FH2 (54.20%) > FH2-Mg-2 (53.73%) > goethite (48.74%) > FH2-Al-1 (16.07%). FH2-Si-0.1 and HTlc disintegrated less than FH2 in water. Obviously, the positive effect of inhibitor on the mechanical strength was obtained only for FH2-Si-0.1. This result appears to be in agreement with the result of turbidity for FH2-Si-0.1. It was reported that granulated hydrous ferric oxide (FeOOH) with addition of silica was stronger than granular FeOOH without silica [186]. The positive effect of Si on the mechanical strength is likely attributed to the concept that polymerization of silicic acid ($Si(OH)_4$) on FeOOH forms silicato-iron (III) surface complexes between Si(IV) and Fe(III) [115, 187, 227]. Therefore, the complexation between Si(IV) and Fe(III) might enhance the binding of FeOOH microns, resulting in an increase in the physical strength of the FeOOH.

The percentage residual for initial pellets was found to be 68.75% for HTlc, which exhibited the highest mechanical strength among all samples. However, a significant strength discrepancy between results of the turbidity and the percentage residual for HTlc is likely attributed to a fact that although HTlc contained considerable amounts of suspended and colloid matters, which was responsible for high turbidity, it had the least disintegration into the solution due to hardening during heat treatment at 80 ^{o}C. The

percentage residual of FH2-Mg-2 was slightly lower than that of FH2, although it showed a lower turbidity with respect to FH2.

There was a significant strength dicrepancy between results of the turbidity and the percentage residual for FH2-Al-1, that is, although it exhibited a low turbidity the percentage residual was the lowest value of 16.07%. This discrepancy between results of the turbidity and the percentage residual for FH2-Al-1 can be explained by both a visual observation of disintegration and the XRD analysis of FH2-Al-1. After 48 h shaking, the significant disintegration of FH2-Al-1 to smaller particles (with a diameter less than 0.85 mm), which were not suspended and colloid matters which caused turbity in solution, was visually observed. From the XRD pattern of FH2-Al-1 shown in Figure 4.2, 2-line ferrihydrite and poorlt crystalline/crystalline Al hydroxides were identified as separate solid phases. An implication of the visual observation and the XRD pattern is that although the physical separation of FH2-Al-1 into 2-line ferrihydrite and Al hydroxide particles was responsible for the lowest percentage residual, the disintegration did not lead to high turbidity in solution since the 2-line ferrihydrite and Al hydroxide particles remained as solid phases even after 48 h shaking. Therefore, the optimum Al/Fe molar ratio (probably less than 1), with a balance of mechanical strength, extent of transformation and arsenic adsorption capacity deserves further detailed evalution.

To quantify the relationship between turbidity and percent residual, the correlation between them was estimated using Pearson's correlation coefficient ($\rho_{X,Y}$) [231]. The correlation between them was determined to be 0.2103, which indicates a very weak positive correlation (Table 4.4 and Figure 4.11). However, a strongly negative correlation between them was expected, that is, if the percent residual is large then the turbidity

should tend to be small and vice versa. It is worth noting that the mechanical strength obtained from the measurement of percent residual might be more reasonable and realistic than that from turbidity. Hence FH2-Si-0.1 and HTlc can be considered as better adsorbents than FH2. However, before any realistic application as adsorbents, these materials need to be further evaluated for mechanical strength, extent of transformation, and arsenic adsorption capacity.

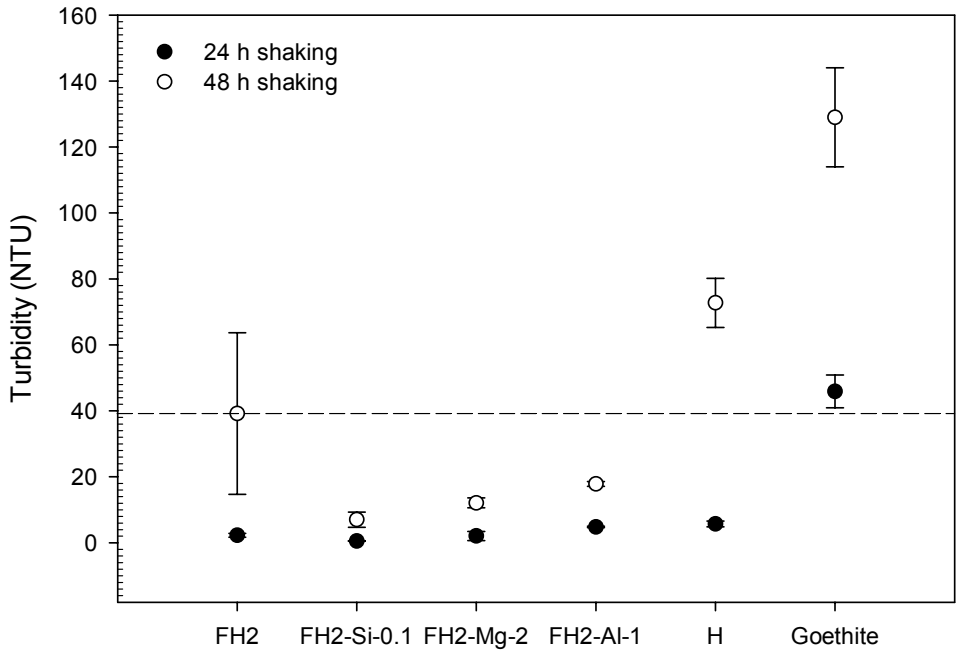

Figure 4.9 Turbidity of the Solution after 24 and 48 h Shaking of 2-line Ferrihydrites Aged at Room Temperature for 10 Days.

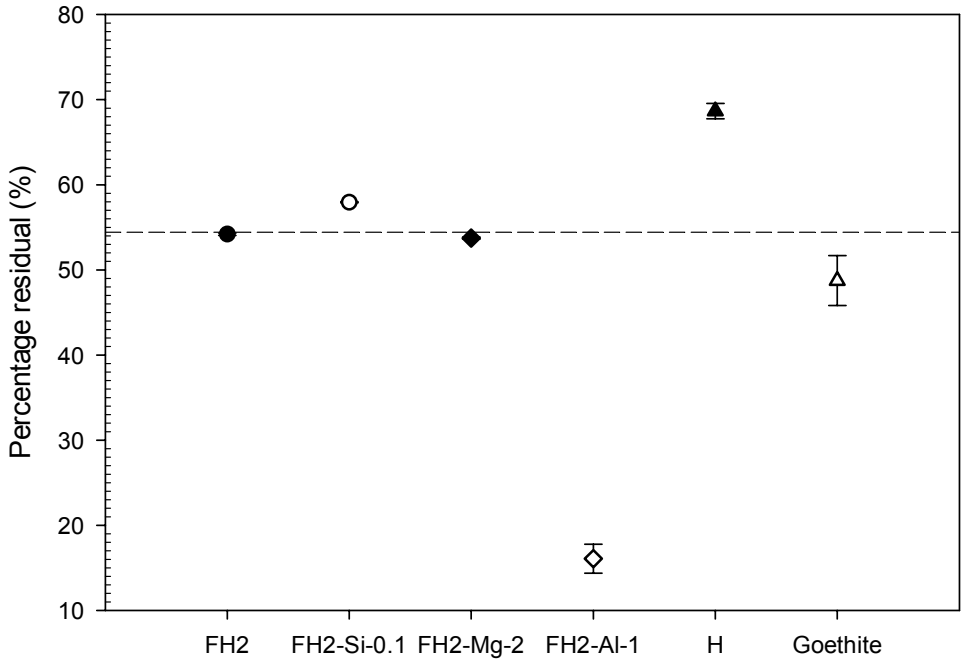

Figure 4.10 Percentage Residual with a Diameter of 0.85~2 mm after 48 h Shaking of 2-line Ferrihydrites Aged at Room Temperature for 10 Days.

Table 4.4 Correlation between the Turbidity and the Percentage Residual

$\overline{X}$ [a]	$\overline{Y}$ (%)[b]	$\hat{\sigma}_{X,Y}$ [c]	S_X [d]	S_Y (%)[e]	$\hat{\rho}_{X,Y}$ [f]
46.3208	49.8883	177.0405	47.1399	17.8616	0.2103

[a] Mean of the turbidity (X) in solution

[b] Mean of the percentage (Y) of the residual to the initial pellets

[c] Estimated covariance: $\hat{\sigma}_{X,Y} = \frac{1}{n-1}\sum_{1}^{n}\left(X_i - \overline{X}\right)\left(Y_i - \overline{Y}\right)$, n = number of sample = 6

[d], [e] Standard deviation of X and Y

[f] Estimated correlation: $\hat{\rho}_{X,Y} = \frac{\hat{\sigma}_{X,Y}}{\hat{\sigma}_X \hat{\sigma}_Y} = \frac{\hat{\sigma}_{X,Y}}{S_X S_Y}$

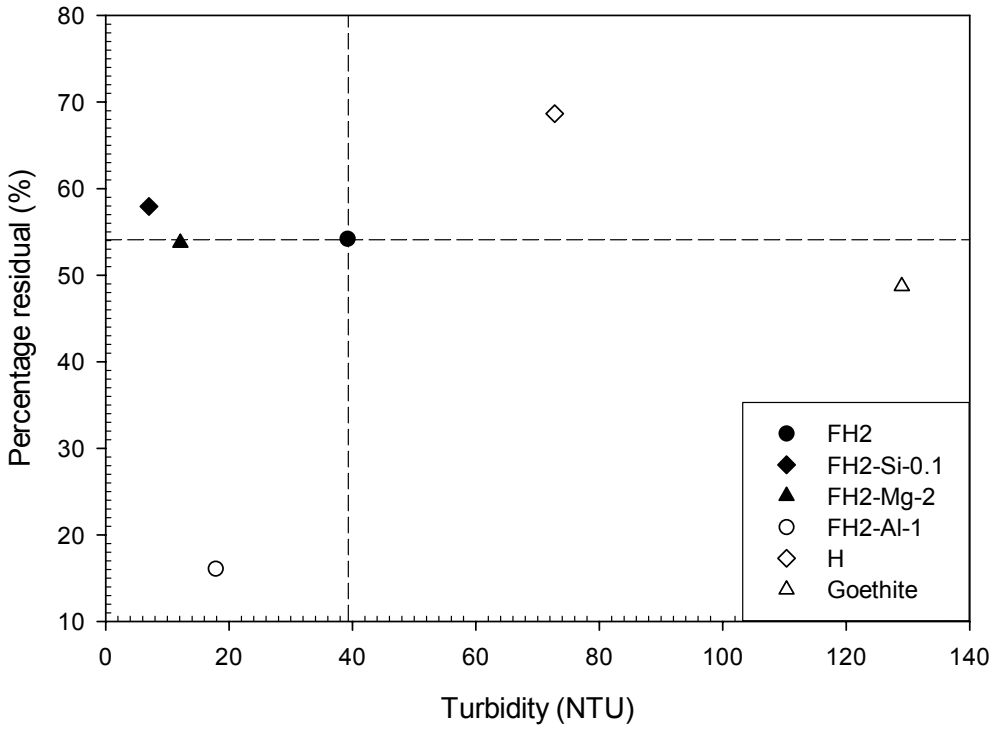

Figure 4.11 Relationship between the Turbidity and the Percentage Residual.

4.3 Conclusions

The FH2 containing Si, Ti, Mg, or Ci(citrate) was identified as a 2-line ferrihydrite, whereas the FH2-Al series consisted of mixed solid phases (2-line ferrihydrite, gibbsite, bayerite, and poorly crystalline Al hydroxide). The water contents of the fresh FH2s and the aged FH2s ranged from 15.61 to 26.00%, which were sufficient for the non-thermal transformation of 2-line ferrihydrite to hematite. For FH2, FH2-Si-0.1, FH2-Mg-2, and FH2-Al-1 sieved to a grain size of smaller than the No. 100 (0.15 mm), each sample exhibited a nearly normal distribution of particle size with volume means of 2.175~2.389 μm while the specific surface area ranged from 229.3 to 393.8 m^2/g, in agreement with the typical values (200~400 m^2/g) for 2-line ferrihydrite obtained by the BET analysis. The formation of crystalline Al hydroxides resulted in lowering the surface area of FH2-Al-1. The PZC of 6.90 for FH2-Si-0.1 was lower than that for FH2 (7.82) due to coprecipitated Si(IV) at the 2-line ferrihydrite surface, whereas the specific adsorption of Mg(II) (FH2-Mg-2) promoted a slight shift of the PZC to a more basic value (7.90). For FH2-Al-1, the shift of the PZC to a more basic value (8.70) was attributable to the formation of Al hydroxides as separate phases as well as the adsorption/reprecipitation of Al(III) species on the 2-line ferrihydrite surface. The positive effect of inhibitor on the mechanical strength was obtained only for FH2-Si-0.1 due to the complexation between Si(IV) and Fe(III). Our results have shown that varying the inhibitor/Fe molar ratio in the FH2s can affect their physical and chemical characteristics. Especially with increasing the Al/Fe molar ratio, the coprecipitaion of Al(III) with Fe(III) played a significant role in determining the characteristics of the FH2-Al series through the formation of crystalline Al hydroxides as well as the adsorption/coprecipitation of Al(III) species.

CHAPTER V

TRANSFORMATION OF 2-LINE FERRIHYDRITE CONTAINING A TRANSFORMATION INHIBITOR

5.1 Introduction

From the viewpoint of the long-term stability of heavy metal binding, the transformation of FH2 into crystalline iron oxides (goethite and hematite) may be advantageous since their vulnerability to microbial iron reduction is considerably decreased due to their lower solubilities and dissolution rates with respect to FH2 [76]. However, FH2 transformation is known to lead to lower the adsorption capacity of heavy metals [77]. Various foreign species have been investigated for retarding the aqueous transformation of FH2. FH2 with a coprecipitated transformation inhibitor might be advantageous for both removing heavy metals from water and managing their waste due to a slower rate of transformation with respect to pure FH2. In spite of much research on the aqueous transformation of FH2 containing foreign species, there was little information about the solid-state transformation of FH2 with a transformation inhibitor. In addition, an improved understanding of the solid-state transformation is needed to assess arsenic adsorption on FH2 containing a transformation inhibitor. Therefore, the objectives of this study were (1) to investigate the effect of aging at RT on both the solid-state transformation and structure of FH2 with a trsnsformation inhibitor, (2) to investigate the effect of heat treatment at high temperatures on the solid-state transformation, structure, and PZC of the FH2, and (3) to relate the inhibitor-specific

influence of transformation of the FH2 during both aging at RT and heat treatment at high temperatures to their structure and PZC.

5.2 Results and Discussion

5.2.1 Total Iron Content

Figure 5.1 shows the total content of iron of samples aged at RT for 400 days for the FH2, FH2-Ci, FH2-Si, FH2-Ti, FH2-Mg series and HTlc and 100 days for the FH2-Al series. Assuming that the chemical formula of FH2 is $Fe_2HO_8 \cdot 4H_2O$ [7], the theoretical content of iron in FH2 can be estimated to be 581.4 mg Fe/g FH2. In this study, the total iron content of FH2 was found to be 623.8 mg Fe/g sample, which is slightly higher than the theoretical value but much higher than the values (419~535 mg Fe/g FH2) reported by Schwertmann et al. [24].

The total iron content of the FH2-Si, FH2-Ti, and FH2-Al series decreased with increasing the inhibitor/Fe molar ratio. The decrease was more evident for the FH2-Al and FH2-Ti series than for the FH2-Si series. From the XRD analysis of the FH2-Al series shown in Figure 4.2, the decrease is attributable to the increase in the proportion of Al hydroxide in the product with the increase in Al/Fe molar ratio. Owing to the formation of Al hydroxides, the total contents of iron for FH2-Al-0.1, -0.25, -0.5, and 1 were determined to be 536.6, 457.2, 407.1, and 318.7 mg Fe/g sample, respectively. The total iron content of FH2-Al-1 corresponded to about half the content of FH2. The total content of iron for the FH2-Ti series decreased from 594.2 for FH2-Ti-0.25 to 491.9 mg Fe/g sample for FH2-Ti-0.2. The result might be due to formation of amorphous titanium hydroxide ($Ti(OH)_4$). It was visually observed that a small amount of white Ti-hydroxide

formed at pH above 3.5 during the synthesis of FH2-Ti-0.2 in this study, as reported by others [232].

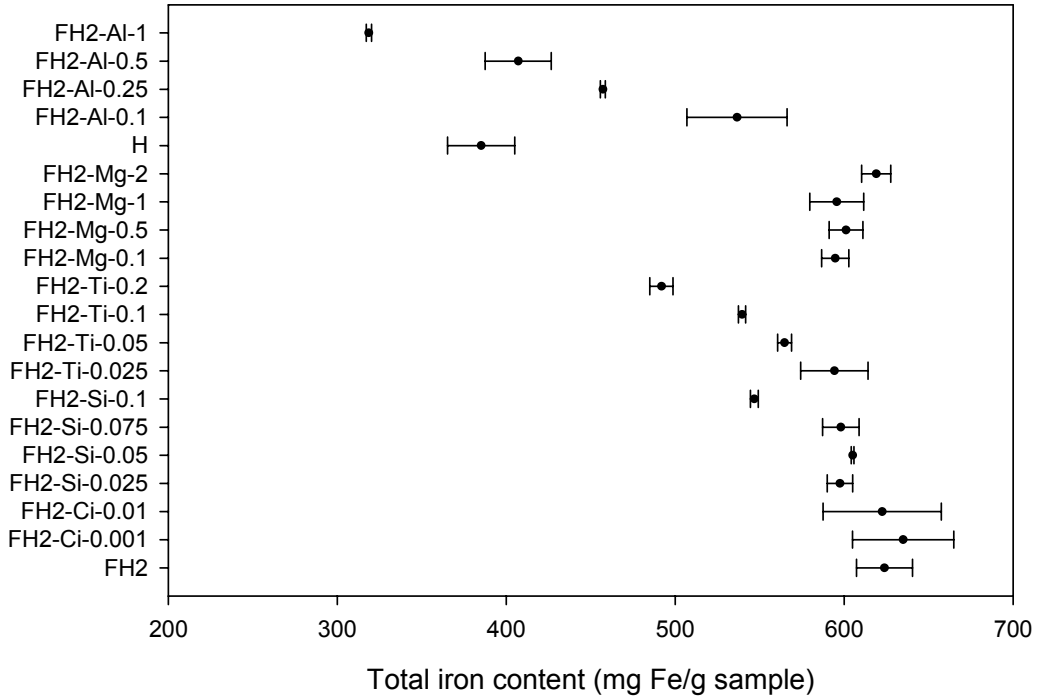

Figure 5.1 Total Iron Content of 2-line Ferrrihydrites Aged at Room Temperature (for 400 Days for FH2, FH2-Ci, FH2-Si, FH2-Ti, FH2-Mg Series, and HTlc for 100 Days for FH2-Al Series).

The total iron content of 546.9 mg Fe/g sample for FH2-Si-0.1 was somewhat lower than those of FH2, FH2-Si-0.025, FH2-Si-0.05, and FH2-Si-0.075. The lower iron content of FH2-Si-0.1 could be attributed to the formation of Fe(III)-Si(IV) complexes on the surface of 2-line ferrihydrite. In this study, the formation of 2-line ferrihydrite and polymerized silica probably occurred simultaneously at pH 7.5 and led to the formation silicato-iron surface complexes through the polymerization of silicic acid on the 2-line ferrihydrite surface [115, 187, 227], resulting in a decrease a proportion of iron content in the product.

The contents of total iron were determined to be 594.7~619.0 for the FH2-Mg series and 622.6~635.0 for the FH2-Ci series, respectively, which were slightly lower than that of FH2. However, the slightly higher content of total iron of the FH2-Ci series compared to that of FH2 cannot be explained. Owing to the formation of a hydrotalcite-like compound, HTlc had a low total iron content of 385.2 mg Fe/g sample, which corresponded to 66.25% of the total iron content for FH2.

5.2.2 Effect of Aging at Room Temperature on the Transformation of 2-line Ferrihydrite

5.2.2.1 Extraction with HCl

For the FH2, FH2-Ci, FH2-Si, FH2-Mg series, and HTlc aged at RT for 15 days, a preliminary 30-min extraction with 0.4 M HCl [74, 81], was performed in parallel with the AOD procedure to test whether the potential precipitation of inhibitor-oxalate phase in the AOD procedure had occurred. Compared to the AOD procedure (92.5~111.7 mg Fe/L), the HCl method extracted smaller amounts of 2-line ferrihydrite ranging from 13.4 to 80.3 mg Fe/L from each of the FH2 samples, while the concentration (68.2 mg Fe/L) of amorphous Fe for the HTlc obtained from the preliminary extraction was similar to that (69.9 mg Fe/L) using the AOD. Therefore, there was no potential for precipitation of inhibitor-oxalate phase since the concentration of amorphous Fe using the AOD procedure was higher than that using the 30-min extraction with 0.4 M HCl.

5.2.2.2 Rate Constant of Transformation within the First 2 Days

The transformation rate of amorphous Fe oxide (as 2-line ferrihydrite) was modeled as an irreversible first order reaction with respect to the fraction of 2-line ferrihydrite

(amorphous Fe) left in the samples during aging at RT in the absence of light. In order to measure the kinetics of transformation, only data collected within the first 2 days were used for derivation of the rate constant (k) because the ln-transformed data remained nearly linear within this time. The nearly linear relationship for a semi-log plot indicates a first-order type of reaction; i.e., the rate of transformation at any time was proportional to the amount of 2-line ferrihydrite remaining during transformation. The transformation can be described as $[Fe]_{amorphous} \rightarrow [Fe]_{crystalline}$, with the expression $-\ln([Fe_o]/[Fe_t]) = k \times t$, where $[Fe_o]$ is the ammonium oxalate-extractable Fe content (determined using the AOD procedure) at any given time, $[Fe_t]$ is the total Fe content (determined by the DCB procedure), and t is time (days). From the slope of a linear regression of $-\ln([Fe_o]/[Fe_t])$ versus time, a transformation rate constant, k, was obtained.

The rate constant of the transformation of FH2 was determined to be 0.0674/day, which was lower than that of the FH2-Ti series, FH2-Mg-0.1, and FH2-Mg-2. However, the rate constant of the FH2-Ci, FH2-Si series, FH2-Mg-0.5, FH2-Mg-1, and HTlc was lower than that of FH2 (Figures 5.2~5.6). FH2-Si-0.1 had the lowest rate constant of 0.0159/day. It may be explained by the fact that Si(IV) located at the 2-line ferrihydrite surface hindered dehydroxylation at the surface of 2-line ferrihydrite and the subsequent atomic rearrangement, resulting in preventing the transformation of 2-line ferrihydrite to hematite [20, 113]. Compared with FH2, the transformation of 2-line ferrihydrite was retarded in the presence Ci (k = 0.0183~0.0447/day), Si (k = 0.0159~0.0645/day), and Mg (k = 0.0349~0.0358/day) during the initial aging time (2 days), however, the long-term effect of the inhibitors need further examination.

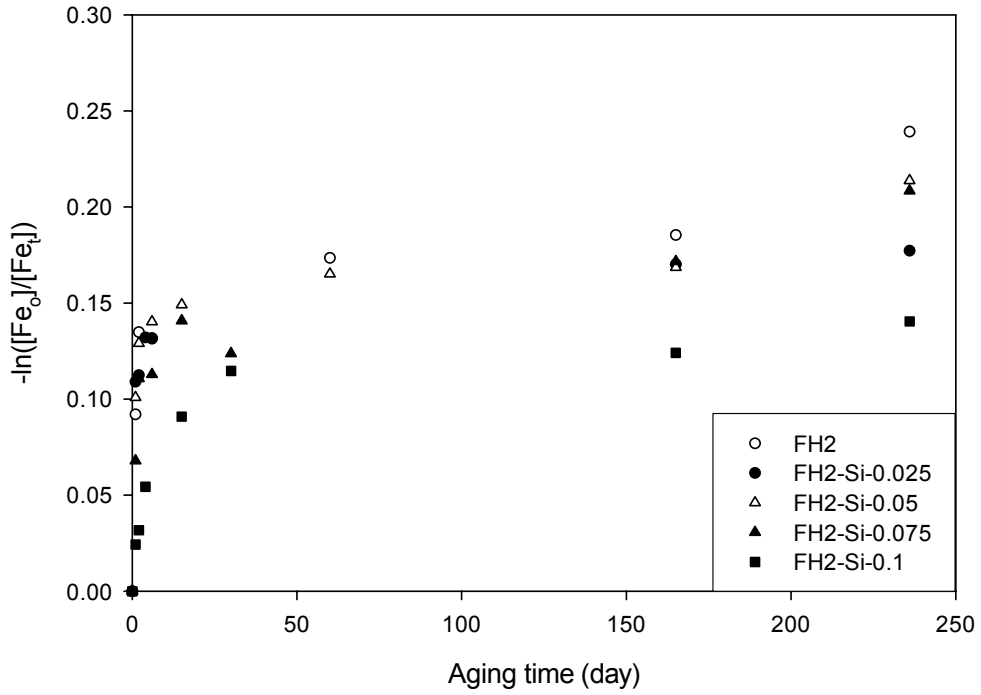

Figure 5.2 Transformation of FH2-Si Series at Room Temperature in a Light-Excluded Environment for 235 Days.

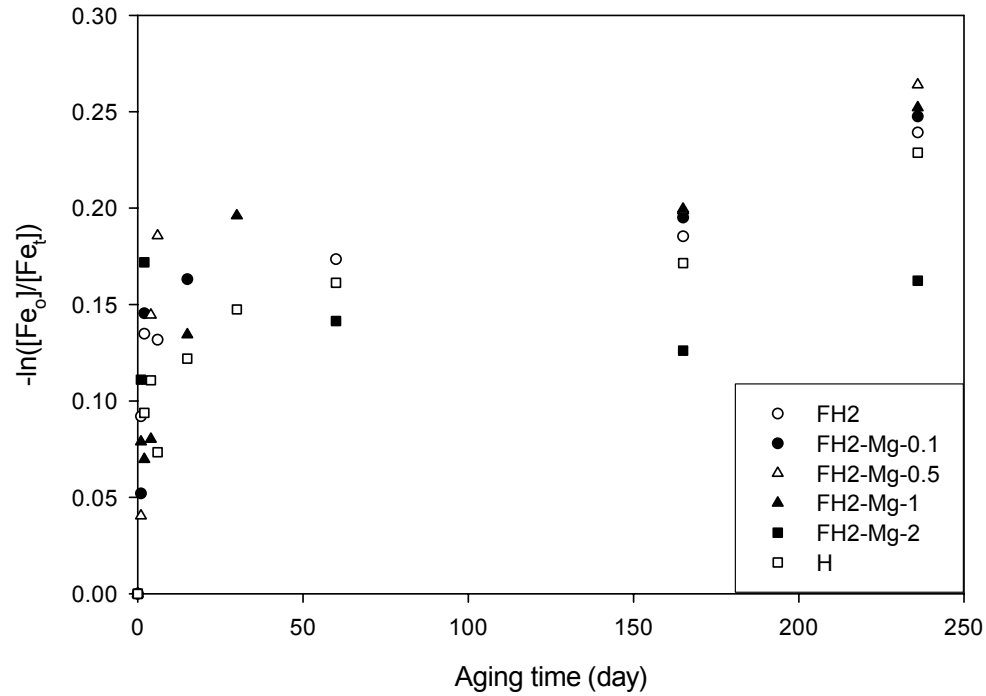

Figure 5.3 Transformation of FH2-Mg Series and HTlc at Room Temperature in a Light-Excluded Environment for 235 Days.

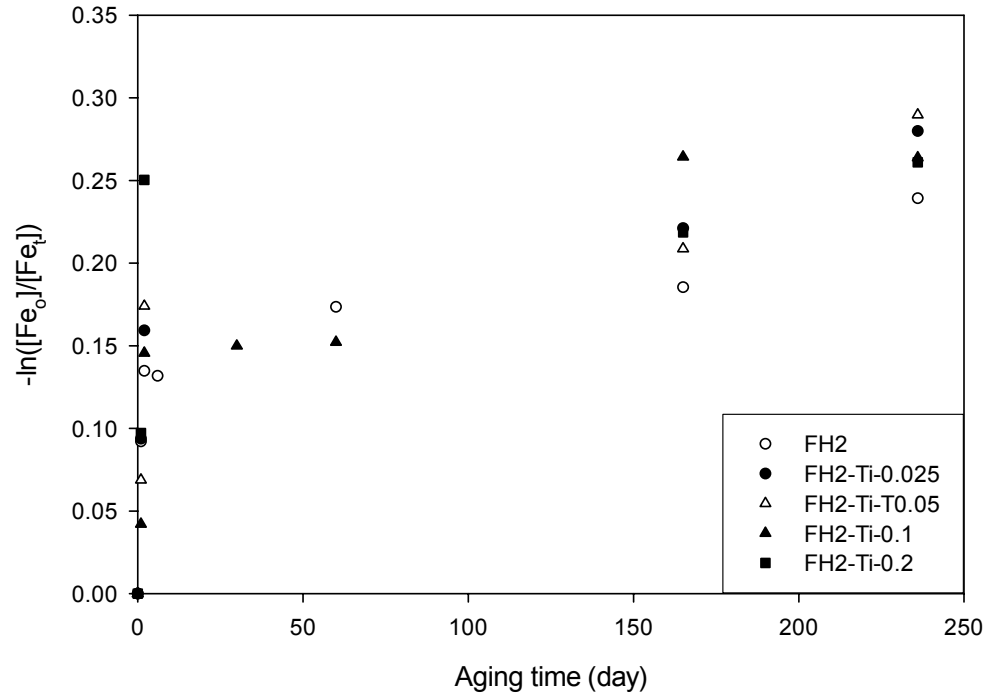

Figure 5.4 Transformation of FH2-Ti Series at Room Temperature in a Light-Excluded Environment for 235 Days.

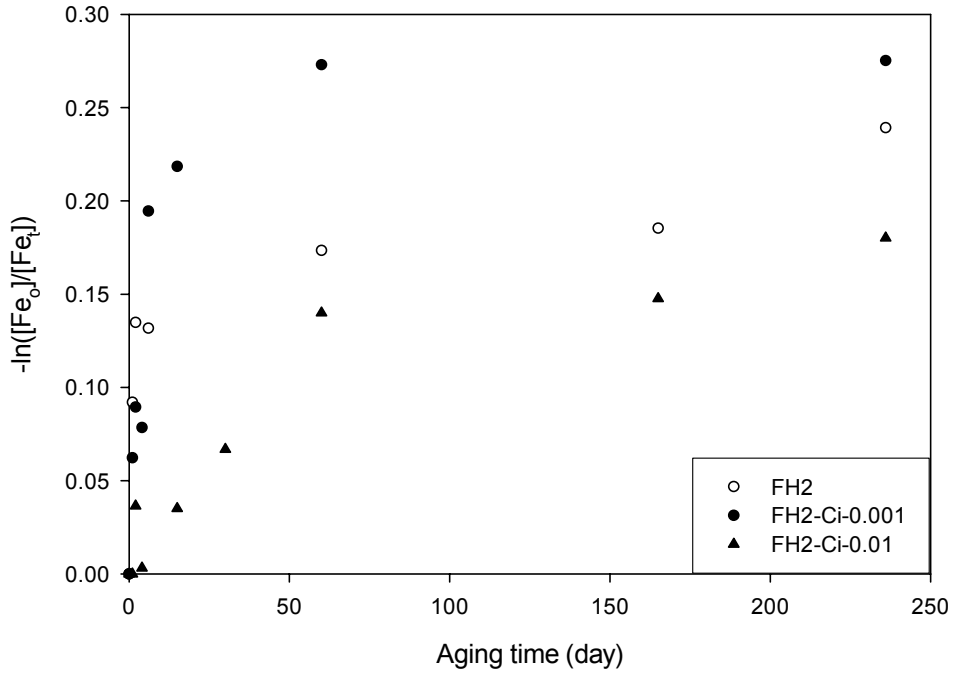

Figure 5.5 Transformation of FH2-Ci Series at Room Temperature in a Light-Excluded Environment for 235 Days.

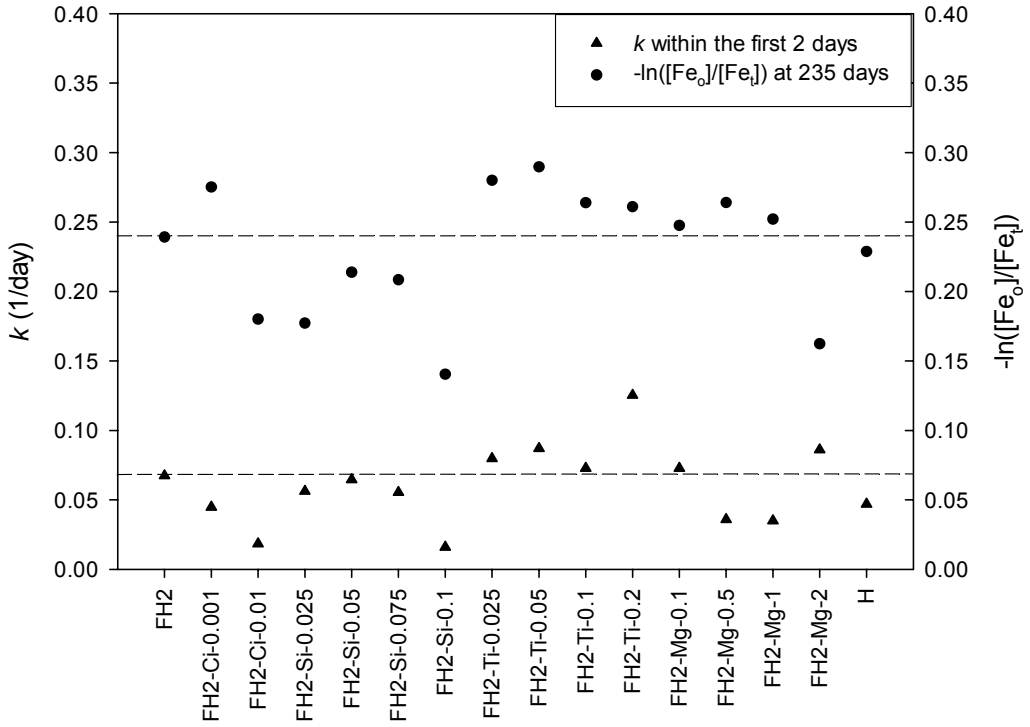

Figure 5.6 The Rate Constant (k) of Transformation within the First 2 Days and the ln-Transformed Value (-ln([Fe$_o$]/[Fe$_t$])) at 235 Days.

5.2.2.3 Transformation during 235 Day Aging at Room Temperature

After aging for 235 days, the [Fe$_o$]/[Fe$_t$] value of FH2 was 78.73 %, which corresponded to 21.27% transformation of 2-line ferrihydrite to other iron oxides. The result indicates that even after aging for 235 days at RT, the transformation of 2-line ferrihydrite to other iron oxides occurred. The [Fe$_o$]/[Fe$_t$] value was 67.73~69.70% for the FH2-Ti series, 75.94~83.52% for the FH2-Ci series, 76.80~ 85.01% for the FH2-Mg series, and 80.75~ 86.90% for the FH2-Si series, respectively.

The effect of inhibitors (except Al) on the transformation of 2-line ferrihydrite for a long period of time was evaluated in detailed using the ln-transformed value (–ln([Fe$_o$]/[Fe$_t$])) as shown in Figures 5.2~5.5. During 235 day aging at RT in the absence

of light, there was a rapid increase in the ln-transformed value ($-\ln([Fe_o]/[Fe_t])$) within the first 6 days, and the value increased gradually thereafter. After aging for 235 days, the ln-transformed value of the FH2s was 0.2392 for FH2, 0.1801 for FH2-Ci-0.01, 0.1404 for FH2-Si-0.1, 0.2610 for FH2-Ti-0.2, and 0.1624 for FH2-Mg-2. Compared with FH2, the transformation of 2-line ferrihydrite was slightly accelerated in the presence of Ti (FH2-Ti series) and for FH2-Ci-0.001, FH2-Mg-0.1, FH2-Mg-0.5, and FH2-Mg-1. In contrast, the transformation of 2-line ferrihydrite was somewhat retarded in the presence of Si (FH2-Si series) and high levels of Ci (FH2-Ci-0.01) and Mg (FH2-Mg-2). The extent of retardation decreased in order FH2-Si-0.1 (0.1404) > FH2-Mg-2 (0.1624) > FH2-Si-0.025 (0.1772) > FH2-Ci-0.01 (0.1801) > FH2-Si-0.075 (0.2084) > FH2-Si-0.05 (0.2138) > FH2 (0.2392).

The transformation of amorphous Fe oxide to other iron oxides may be due to the presence of CUS (coordination-unsaturated) sites [19] at the 2-line ferrihydrite surface where the CUS sites can easily absorb water molecules to fill the CUS sites. At low temperatures, the CUS sites with adsorbed water molecules are considered the crystal growth sites [20]. The exposure of FH2 to the air for 235 days caused water molecules to evolve from the FH2 particle contacts, induce the particles to agglomerate, resulting in the transformation of FH2 to other iron oxides such as hematite [233]. As discussed in section 4.2.2, the evolution of water was observed for FH2 after aging for 650 days at RT. The water content of FH2 decreased from 26.00% for the fresh FH2 to 18.67% for the aged FH2. According to a minimum of water content (10~15%) suggested by Schwertmann et al. [8] and Cornell et al. [2], the water contents for both the fresh and the aged FH2 appeared to be sufficient for the non-thermal transformation of FH2 to hematite.

Therefore, the transformation of FH2 at RT depends on the coverage of water molecules at the FH2 surface. In addition, the slower transformation for FH2-Si series, FH2-Ci-0.01, and FH2-Mg-2 might be due to the sorption mechanism of inhibitor which hindered the transformation pathway to highly ordered iron oxides. Anions may be more favorably adsorbed on the CUS sites at the 2-line ferrihydrite surface than water molecules, to form a Fe-O-anion layer, thereby blocking the crystal growth sites [20].

It was reported by Schwertmann et al. [79] that half-conversion times of 2-line ferrihydrite solution aged at 24 ^{o}C were 70 and 110 days for solutions with pH values of 8 and 7, respectively, and a half-conversion time for 2-line ferrihydrite solution with a pH value of 7.5 was estimated to be about 100 days. Compared with the results obtained Schwertmann et al. [79], the extent of transformation of the air-dried FH2s in my study was much lower. Therefore, the half-conversion time, which corresponds to the ln-transformed value of 0.6931, could not be interpolated in this study since the FH2s showed low values, ranging from 0.1404 to 0.2899.

5.2.2.4 Relationship between the Rate Constant (*k*) and the ln-Transformed Value

Figure 5.7 depicts the relationship between the rate constant (*k*) of transformation within the first 2 days and the ln-transformed value ($-\ln([Fe_o]/[Fe_t])$ at 235 days. In order to quantify the dependence between the rate constant (*X*) and the ln-transformed value (*Y*), the correlation between them was estimated according to Pearson's correlation coefficient ($\rho_{X,Y}$) [231]. The correlation between the rate constant of transformation and the ln-transformed value was determined to be 0.4087. This result shows a moderately strong positive relationship between them, although a strongly positive correlation between them

was expected, that is, if the rate constant of transformation is high then the ln-transformed value will tend to be high and vice versa. The moderately strong positive relationship can be attributed to FH2-Ci-0.001 (0.0447, 0.2752), FH2-Ti-0.2 (0.1253, 0.2610), FH2-Mg-0.5 (0.0358, 0.2639), FH2-Mg-1 (0.0349, 0.2521), and FH2-Mg-2 (0.086, 0.1624). However, except for these five FH2s, the correlation was determined to be 0.8858, which indicates fairly strong positive correlation between k and $-\ln([Fe_o]/[Fe_t])$ (Figure 5.7 and Table 5.1).

Table 5.1 Correlation between the Rate Constant (k) of Transformation within the First 2 Days and the ln-Transformed Value ($-\ln([Fe_o]/[Fe_t])$) at 235 Day

$\overline{X}$ a)	$\overline{Y}$ b)	$\hat{\sigma}_{X,Y}$ c)	S_X d)	S_Y e)	$\hat{\rho}_{X,Y}$ f)
0.057891	0.224427	0.000946	0.0223152	0.046130	0.885766

a) Mean of the rate constant (X) of transformation within the first 2 day
b) Mean of the ln-transformed value (Y) at 235 day
c) Estimated covariance: $\hat{\sigma}_{X,Y} = \frac{1}{n-1}\sum_{1}^{n}\left(X_i - \overline{X}\right)\left(Y_i - \overline{Y}\right)$, n = number of sample = 11
d), e) Standard deviation of X and Y
f) Estimated correlation: $\hat{\rho}_{X,Y} = \frac{\hat{\sigma}_{X,Y}}{\hat{\sigma}_X \hat{\sigma}_Y} = \frac{\hat{\sigma}_{X,Y}}{S_X S_Y}$

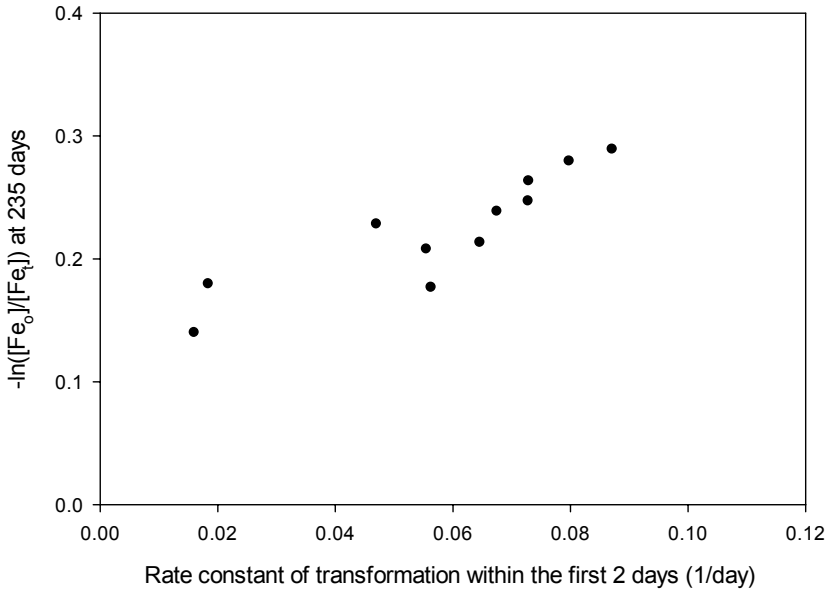

Figure 5.7 Relationship between the Rate Constant (k) of Transformation within the First 2 Days and the ln-Transformed Value ($-\ln([Fe_o]/[Fe_t])$) at 235 Days.

5.2.3 Effect of Aging at Room Temperature on the Structure of 2-line Ferrihydrite

Figures 5.8 and 5.9 depict the XRD patterns for the FH2, FH2-Si, FH2-Ti, FH2-Ci, and FH2-Mg series aged at RT for 385 days. After aging for 385 days, all the FH2s consisted of a single solid phase that was identified as typical 2-line ferrihydrite [8, 20, 24~27, 30, 40]. The XRD patterns for all the FH2s revealed the presence of two broad peaks at 35 (d = 0.26 nm) and 62^o 2θ (d = 0.15 nm). Compared to the XRD patterns of the fresh samples at an initial aging time (20 days), neither significant change in peak position nor chemical conversion was found after aging for 385 days. Therefore, the XRD patterns for the fresh samples agree fairly well with those for the samples aged for 385 days. The finding indicates that the transformation of FH2s was not evident after 385 day aging.

From the results of the transformation of FH2s discussed in section 5.2.2, after aging for 235 days, the proportion ([Fe_o]/[Fe_t]) of FH2s ranged from 67.73 to 86.90%. The results indicated that 13.10~32.27% of amorphous Fe oxide transformed to other iron oxides. However, after aging for 385 days, no sharp diffraction peaks of other iron oxides were detected in the XRD patterns of the FH2s. This XRD behavior might be explained by the assumption that traces of other iron oxides were obscured by the two broad 2-line ferrihydrite peaks due to small amounts of other iron oxides. A detailed interpretation of a relationship between the extent (expressed as [Fe_o]/[Fe_t]) of 2-line ferrihydrite transformation and the emergence of sharp diffraction peaks in XRD patterns of other iron oxides will be given later (sections 5.2.4 and 5.2.5).

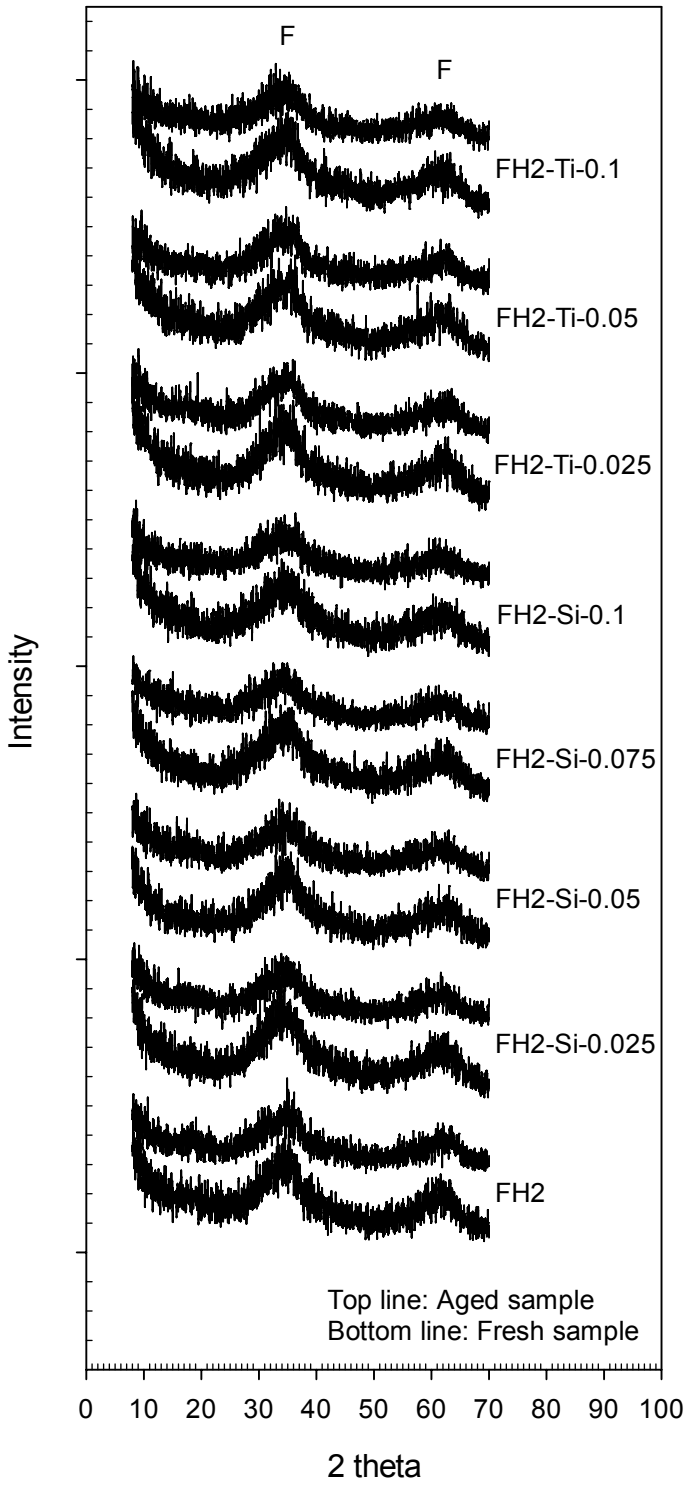

Figure 5.8 XRD Patterns of FH2, FH2-Si, and FH2-Ti Series Aged at Room Temperature for 385 Days. Major Peaks due to 2-line Ferrihydrite are Indicated as F.

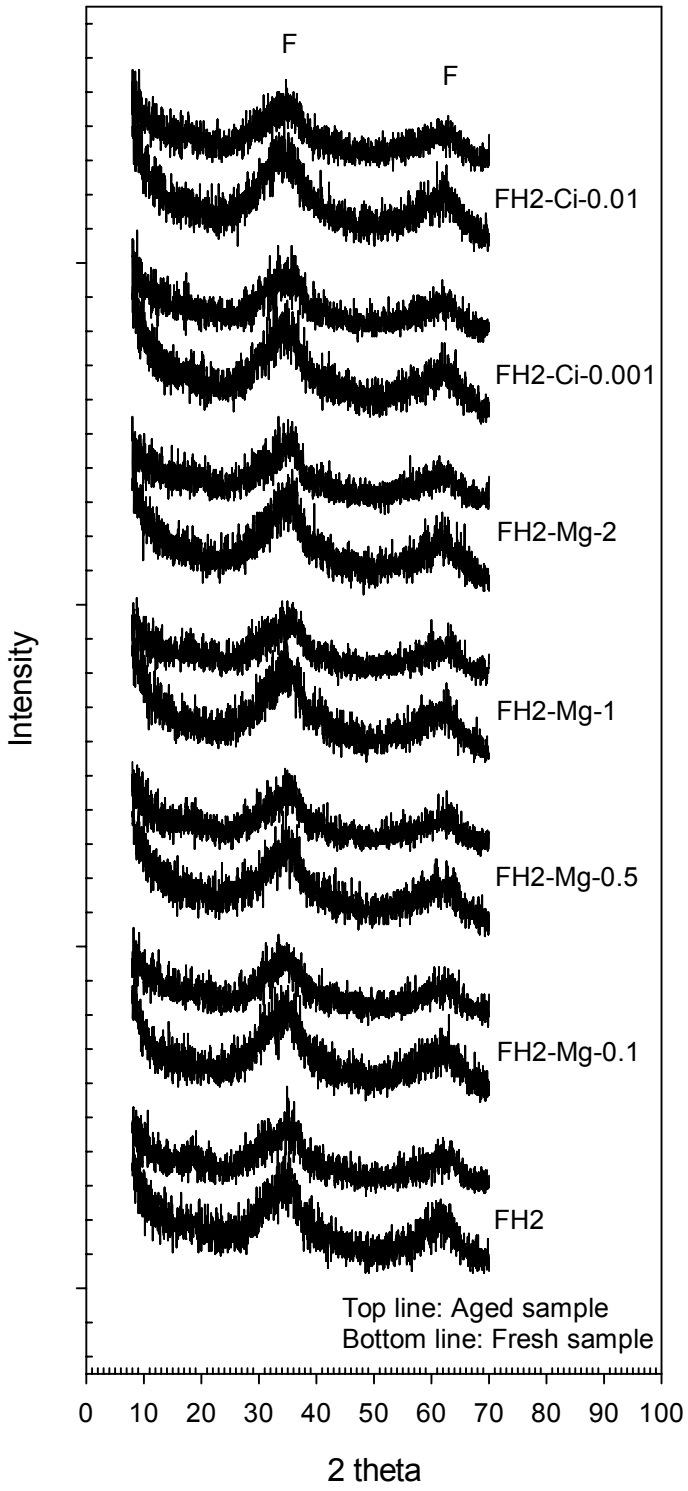

Figure 5.9 XRD Patterns of FH2, FH2-Mg, and FH2-Ci Series Aged at Room Temperature for 385 Days. Major Peaks due to 2-line Ferrihydrite are Indicated as F.

5.2.4 Effect of Heat Treatment on the Transformation of 2-line Ferrihydrite

5.2.4.1 Transformation Constant of Temperature Dependence

In order to accelerate the transformation of amorphous Fe oxide to other iron oxides, all the samples aged at RT were heat-treated in a muffle furnace at high temperatures (20, 150, 240, and 360 ^{o}C) for 12 h. After heating at 360 ^{o}C for 12 h, the $[Fe_o]/[Fe_t]$ value was found to be 0.52% for FH2, 0.42~0.46% for the FH2-Ci series, 0.66~0.95% for the FH2-Ti series, 0.79~1.24% for the FH2-Mg series, 12.79~27.98% for the FH2-Al series, 3.81~42.89% for the FH2-Si series, and 104.93% for HTlc.

The change in the ammonium oxalate-extractable Fe fraction ($-\ln([Fe_o]/[Fe_t])$) against temperature is shown in Figures 5.10~5.14. Compared to the transformation of FH2s after aging at RT for 235 days discussed in section 5.2.2, a plot of the ln-transformed value ($-\ln([Fe_o]/[Fe_t])$) versus temperature for all samples was approximately linear over the range considered. Therefore, the transformation extent of amorphous Fe oxide to other iron oxides was described as an irreversible first order reaction with respect to the fraction of amorphous Fe remaining in the sample. The extent of transformation at any temperature was proportional to the amount of amorphous Fe left during transformation. The transformation by heat treatment can be described as $[Fe]_{amorphous} \rightarrow [Fe]_{crystalline}$ with the expression, $-\ln([Fe_o]/[Fe_t]) = k_T \times T$, where $[Fe_o]$ is the ammonium oxalate-extractable Fe fraction (determined using the AOD procedure) at any given temperature, $[Fe_t]$ is the total Fe content at 20 ^{o}C (determined using the DCB procedure), and T is temperature (^{o}C). From the slope of a linear regression of $-\ln([Fe_o]/[Fe_t])$ versus temperature, a transformation constant of temperature dependence, k_T, was obtained. Another transformation constant was also obtained from data between

150 and 360 ^{o}C for a more linear plot of the ln-transformed value versus temperature (Figure 5.15).

The transformation constant of temperature dependence for FH2 between 20 and 360 ^{o}C was determined to be 0.0157/^{o}C. Compared to FH2, FH2-Ti-0.025 and FH2-Mg-1 showed slightly higher transformation constants (0.0161/^{o}C and 0.0160/^{o}C, respectively), while the other FH2s exhibited lower transformation constants ranging from 0.0022 to 0.0154/^{o}C (Figure 5.15). For most samples, the transformation constant decreased with an increase in inhibitor/Fe molar ratio. This result indicates that high levels of inhibitor/Fe molar ratio strongly retarded the transformation of amorphous Fe oxide to other iron oxides. Upon heating between 20 and 360 ^{o}C, the extent of transformation inhibition decreased in the order of FH2-Si-0.1 (0.0022/^{o}C) > FH2-Si-0.075 > FH2-Al-1 > FH2-Al-0.25 > FH2-Si-0.05 = FH2-Al-0.5 > FH2-Al-0.1 > FH2-Si-0.025 (0.0093/^{o}C). Both Si(IV) and Al(III) had a stronger retarding effect on the transformation of amorphous Fe than did any other inhibitor. The transformation constant was determined to be 0.0022~0.0093/^{o}C for the FH2-Si series and 0.0039~0.0059/^{o}C for the FH2-Al series, respectively.

The plot of the ln-transformed value versus temperature between 150 and 360 ^{o}C was more linear that between 20 and 360 ^{o}C, and the transformation constant of temperature dependence between 150 and 360 ^{o}C was higher than that between 20 and 360 ^{o}C. The transformation constant of temperature dependence for FH2 between 150 and 360 ^{o}C was found to be 0.0219/^{o}C. All the FH2s (FH2-Si, FH2-Al, FH2-Mg, and FH2-Ti series) except the FH2-Ci series showed lower transformation constants ranging from 0.0049 to 0.0217/^{o}C than was observed for FH2 (Figure 5.15). For all the FH2s

except the FH2-Ci series, the transformation constant decreased with an increase in the inhibitor/Fe molar ratio. Upon heating between 150 and 360 ^{o}C, the extent of transformation inhibition decreased in the order of FH2-Si-0.1 (0.0049/ ^{o}C) > FH2-Si-0.075 > FH-Al-1 > FH2-Al-0.5 = FH2-Al-0.25 > FH2-Si-0.05 > FH2-Al-0.1 > FH2-Si-0.025 > FH2-Mg series > FH2-Ti series > FH2 (0.0219/^{o}C) > FH2-Ci series. Both Si(IV) and Al(III) had a stronger retarding effect on the transformation of amorphous Fe oxide than did any other inhibitor. The transformation constant was determined to be 0.0049~0.0155/^{o}C for the FH2-Si series and 0.0062~0.0105/^{o}C for the FH2-Al series, respectively.

In addition, a summary of transformation data was given as a 75% conversion-temperature ($T_{75\%}$) versus FH2 type in Figure 5.16. The 75% conversion-temperatures for FH2-Si-0.075, -0.1, FH2-Al-0.25, and -0.1 were not observed but interpolated. For a first-order reaction the rate of transformation over the range of 20~360 ^{o}C (Figure 5.15) is inversely proportional to the $T_{75\%}$ (Figure 5.16). The $T_{75\%}$ of FH2 was determined to be 198.3 ^{o}C. The $T_{75\%}$ increased with an increase in inhibitor/Fe molar. This result indicates that high levels of inhibitor/Fe molar ratio retarded the transformation of amorphous Fe oxide to other iron oxides. Significant differences between $T_{75\%}$ temperatures for the FH2-Si/Al series and FH2-Ci/Ti/Mg series were evident. The $T_{75\%}$ decreased in the order of FH2-Si-0.1 (385.5 ^{o}C) > FH2-Al-1 > FH2-Si-0.075 > FH2-Al-0.25 > FH2-Al-0.5 > FH2-Si-0.05 > FH2-Al-0.1 > FH2-Si-0.025 (305.2 ^{o}C). This results indicate that Si(IV) and Al(III) had stronger retarding influences on the conversion of amorphous Fe oside than did any other inhibitor. The results of $T_{75\%}$ were fairly compatible with those of the transformation constant (k_T).

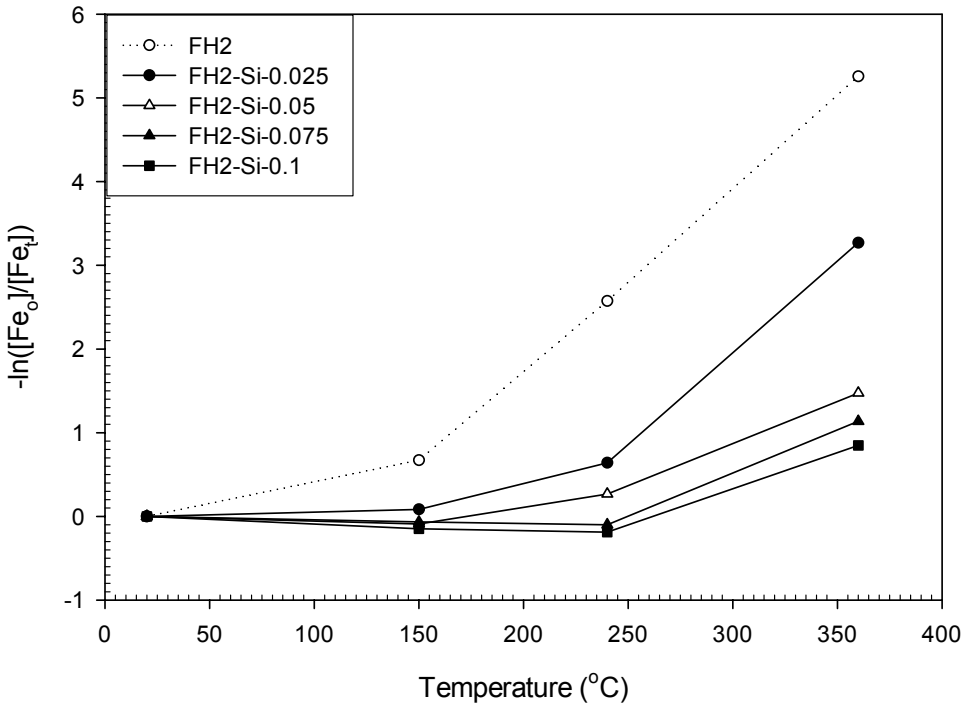

Figure 5.10 Transformation of FH2 and FH2-Si Series by Heat Treatment at 150, 240, and 360 ^{o}C for 12 h.

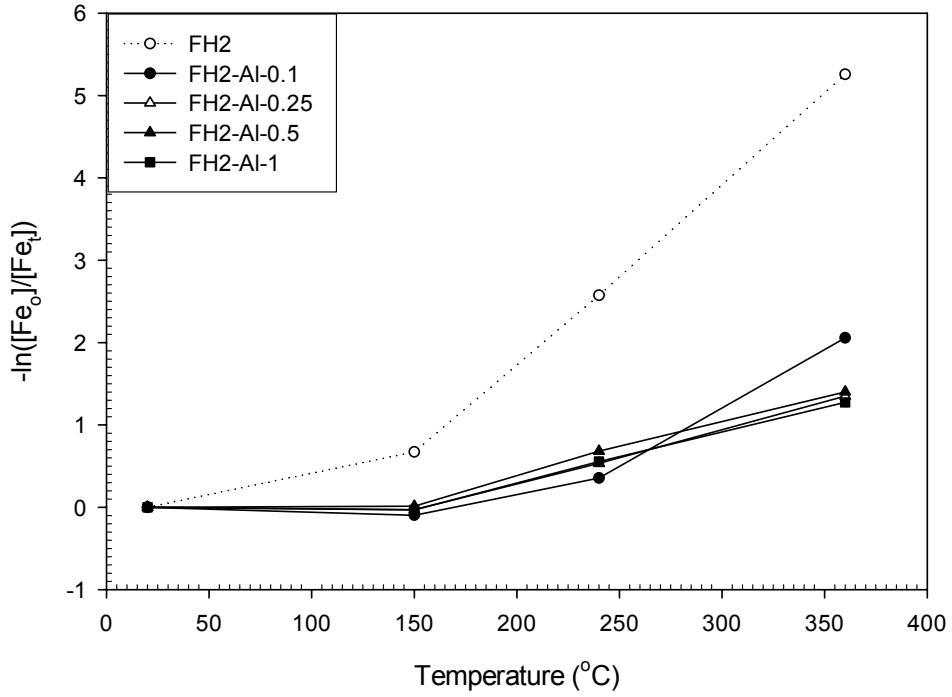

Figure 5.11 Transformation of FH2-Al Series by Heat Treatment at 150, 240, and 360 ^{o}C for 12 h.

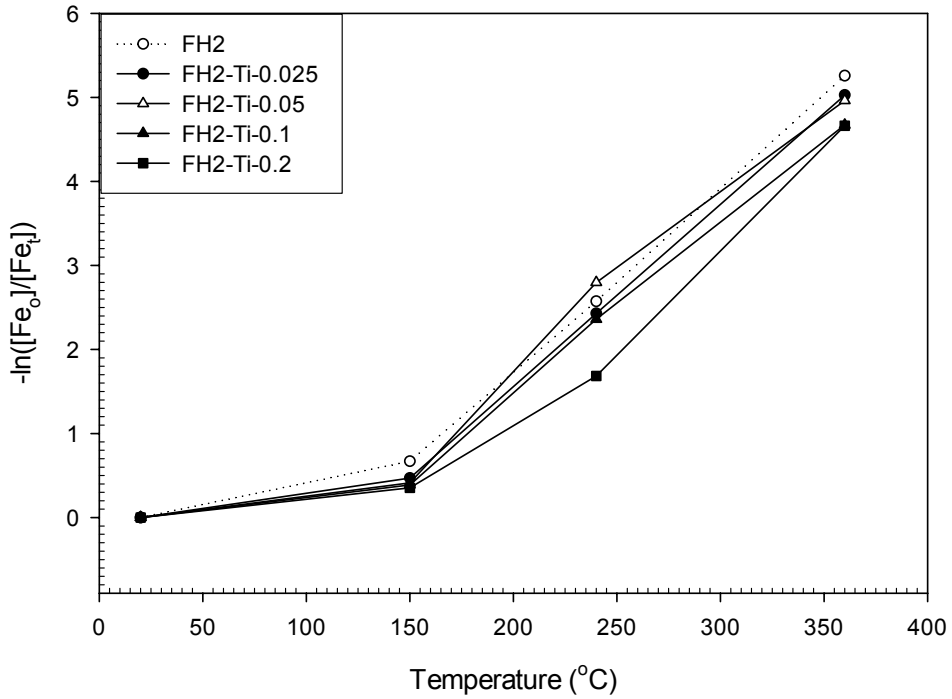

Figure 5.12 Transformation of FH2-Ti Series by Heat Treatment at 150, 240, and 360 ^{o}C for 12 h.

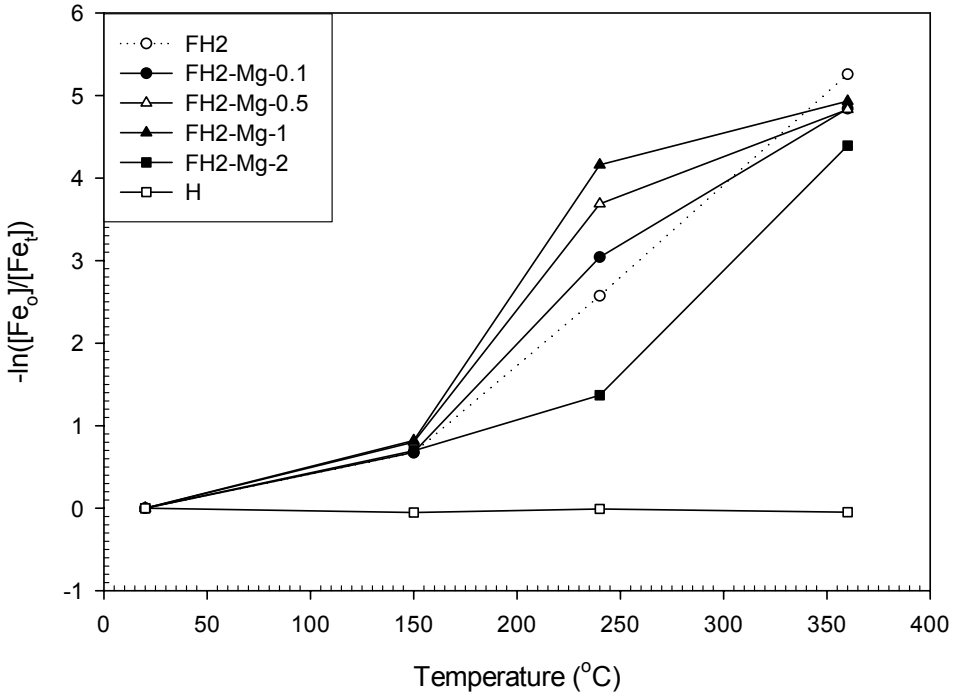

Figure 5.13 Transformation of FH2-Mg Series and HTlc by Heat Treatment at 150, 240, and 360 ^{o}C for 12 h.

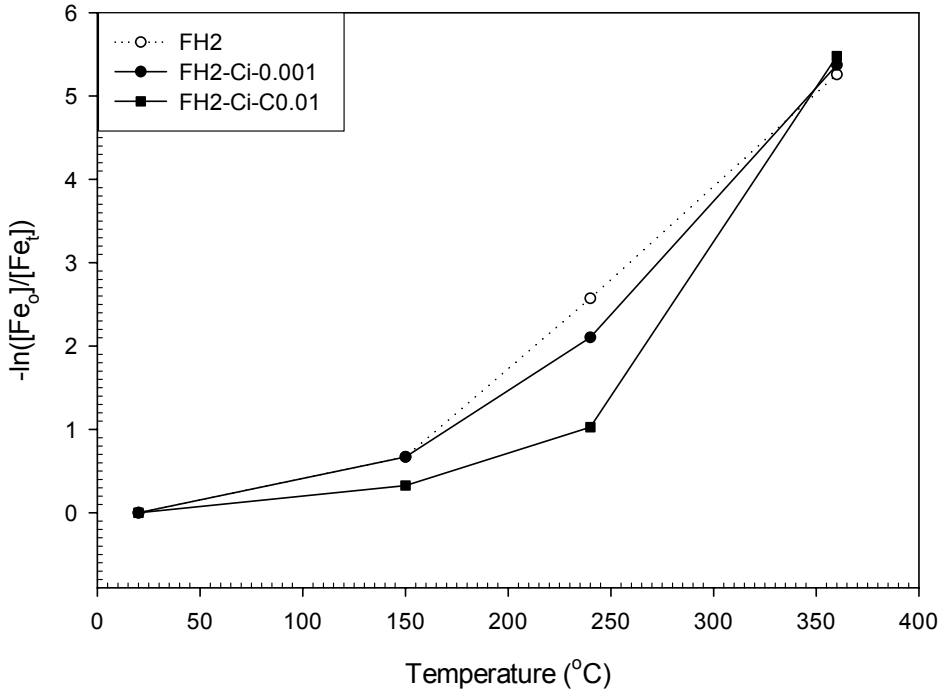

Figure 5.14 Transformation of FH2-Ci Series by Heat Treatment at 150, 240, and 360 ^{o}C for 12 h.

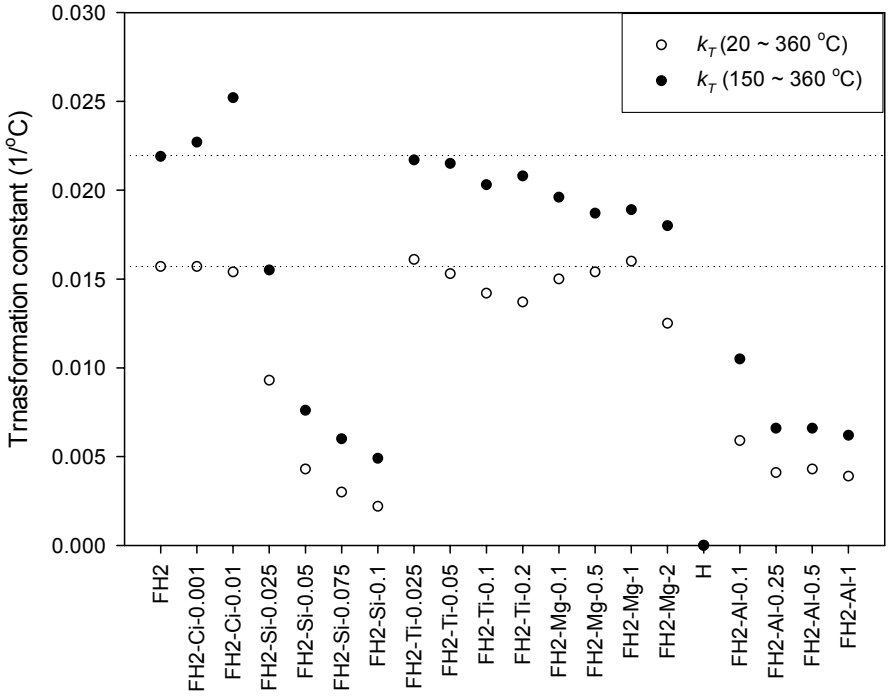

Figure 5.15 Transformation Constant of Temperature Dependence Obtained from Data Both between 20 and 360 ^{o}C and 150 and 360 ^{o}C.

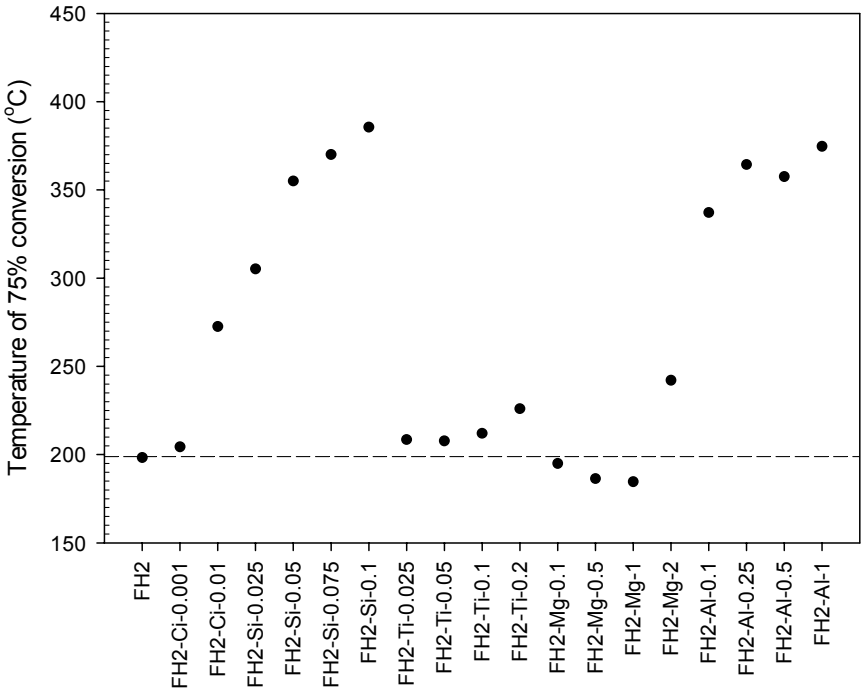

Figure 5.16 Temperature for 75 % Conversion of 2-line Ferrihydrite to Other Iron Oxides.

5.2.4.2 Transformation of Samples with an Inhibitor/Fe Molar Ratio of 0.1

To evaluate in detail the effect of inhibitor on the transformation of amorphous Fe oxide, a summary of transformation data for samples with equimolar ratios (0.1) of inhibitor/Fe is given in Table 5.2. No significant difference between transformation of FH2 and FH2-Ti/Mg-0.1 was evident. However, the retarding effects of Ti(IV) and Mg(II) on the transformation of amorphous Fe oxide increased slightly with an increase in the inhibitor/Fe molar to Ti/Fe 0.2 and Mg/Fe 2, as shown in Figures 5.12 and 5.13. From the data of $[Fe_o]/[Fe_t]$, k_T, and $T_{75\%}$, Si(IV) and Al(III) had stronger retarding effects on the transformation of amorphous Fe oxide than did any other inhibitor (Ti(IV), Mg(II), and citrate).

The pronounced retardation effect of Si(IV) on the transformation of amorphous Fe oxide may be explained by the suggestion that Si(IV) located at the FH2 surface hindered the surface dehydroxylation of FH2 and the subsequent atomic rearrangement, resulting in the prevention of FH2 forming hematite. It has been reported that upon heating, the presence of Si(IV) increased the temperature of ferrihydrite transformation to hematite from 300~400 ^{o}C (for the ferrihydrite without Si) [38, 41] to several hundred degrees [38, 109, 110, 113, 114]. It has been also reported that the presence of Al(III) chemisorbed at 2-line ferrihydrite surface (with an atomic ratio of Al(III):Fe(III) = 0.05) increased the temperature of 2-line ferrihydrite transformation to hematite from 225 to 300 ^{o}C [20]. The significant inhibition effect of Al(III) on the transformation of amorphous Fe oxide indicates that as discussed in sections 4.2.1 and 4.2.5, the formation of stable Al(III) complexes with Fe(III) at the FH2 surface [96, 180, 181] or the adsorption/reprecipitation of soluble Al(III) species on the surface of the $Fe(OH)_3$ surface [220] might result in the retardation of amorphous Fe oxide transformation into other iron oxides.

However, Si(IV) is much more effective than Al (III) in retarding the transformation of amorphous Fe oxide to other iron oxides. The result agrees well with results reported by other research [20]; the phase transformation of 2-line ferrihydrites into hematite was completed at 300 for Al(III) chemisorbed ferrihydrite (with an atomic ratio of Al(III):Fe(III) = 0.05) and 400 ^{o}C for Si(IV) chemisorbe ferrihydrite (with an atomic ratio of Si(IV):Fe(III) = 0.05), respectively. The effect might be partially attributable to the incompatibility of silicate ions and Fe(III) ions during the high temperature treatment [20]. Si(IV) adsorbed at the 2-line ferrihydrite surface might have suppressed crystal growth to form hematite and goethite due to the incompatibility of Si(IV) tetrahedral

symmetry with the octahedral symmetry of the iron oxides, whereas, Al(III) might have easily substituted for Fe(III) to form solid solutions, due to the isostructural properties of Al(III) and Fe(III) [20, 24]. Therefore, upon heating at high temperatures, silicate was much more effective than Al(III) in suppressing the transformation of amorphous Fe oxide to more crystalline phases. It has been reported that the substitution of Al(III) for Fe(III) reached 15% for hematite and 30% for goethite, respectively [2, 31], whereas, 2% of Si was incorporated into the goethite lattice [234].

Table 5.2 Transformation of 2-line Ferrihydrites with an Inhibitor/Fe Molar Ratio of 0.1

Type of FH2	$[Fe_o]/[Fe_t]$				k_T	$T_{75\%}$
	150 °C[a)]	240 °C[a)]	360 °C[a)]	235 days[b)]	(1/°C)[c)]	(°C)
FH2	0.5112	0.0763	0.0052	0.7873	0.0157	198.3
FH2-Si-0.1	1.1599	1.2075	0.4289	0.8690	0.0022	385.5
FH2-Al-0.1	1.1014	0.7005	0.1279	-	0.0059	337.2
FH2-Ti-0.1	0.6787	0.0944	0.0094	0.6951	0.0142	212.0
FH2-Mg-0.1	0.5079	0.0478	0.0072	0.7807	0.0150	195.0

[a)] The fraction was measured after heat-treating samples at 150, 240, and 360 °C for 12 h.
[b)] The fraction was measured after aging samples at room temperature for 235 days.
[c)] The transformation constant was obtained from data between 20 and 360 °C.

5.2.4.3 Comparison of Effects of Aging and Heat Treatment

A comparison of the effects of aging and heat treatment on the transformation of amorphous Fe is shown in Figure 5.17. Compared with the $[Fe_o]/[Fe_t]$ (67.73 ~ 86.90%) after aging at RT for 235 days, the $[Fe_o]/[Fe_t]$ after heat-treating at 360 °C for 12 h ranged from 0.42 to 42.89%. The results indicate that the effect of heat treatment on the transformation of amorphous Fe was much more pronounced than that of aging at RT. The heat-treatment at 360 °C for 12 h caused FH2, FH2-Ti-0.05, FH2-Mg-0.1, FH2-Mg-0.5, and FH2-Mg-1 to transform into other iron oxides (99.20~99.48%). After heat-

treating at 240 ^{o}C, the $[Fe_o]/[Fe_t]$ ratios of the FH2-Ci series, FH2-Ti-0.025, FH2-Ti-0.1, FH2-Ti-0.2, and FH2-Mg-2 were determined to be 8.81~35.77 %, which were higher than that of FH2 (7.63%), whereas, after heat-treating at 360 ^{o}C, the $[Fe_o]/[Fe_t]$ ratios ranged from 0.42 to 1.24%. This results indicates that most of amorphous Fe oxide (98.76~99.58%) was transformed into other iron oxides during heat-treatment at 360 ^{o}C. After heat-treating at 360 ^{o}C, the $[Fe_o]/[Fe_t]$ ratios of the FH2-Si, FH2-Al series and HTlc were determined to be 3.81~42.89, 12.79~27.98, and 100%, respectively. This result indicates that these inhibitors had stronger retarding effects on the transformation of amorphous Fe oxide than did the other inhibitor. After heating at 150 or 240 ^{o}C, the $[Fe_o]/[Fe_t]$ ratios of the FH2-Si series and HTlc were generally higher than those aged at RT for 235 days (Figure 5.17). Also the ln-transformed values ($-\ln([Fe_o]/[Fe_t])$) of the FH2-Si, FH2-Al series and HTlc dropped below zero (Figure 5.10, 5.11 and 5.13). This result might be an indication that significant amounts of water were evolved from the iron oxy-hydroxides without much transformation, due to the strong retarding effects of the inhibitors. The thermal decomposition of hydrotalcite has indicated that only interstitial water was lost reversibly below 200 ^{o}C, whereas, both further water and carbon dioxide from the dehydroxylation were removed between 250 and 450 ^{o}C. However, if the temperature did not exceed 550~600 ^{o}C, the calcined hydrotalcite could reconstruct its original layer structure upon rehydration and sorption of various anions [235].

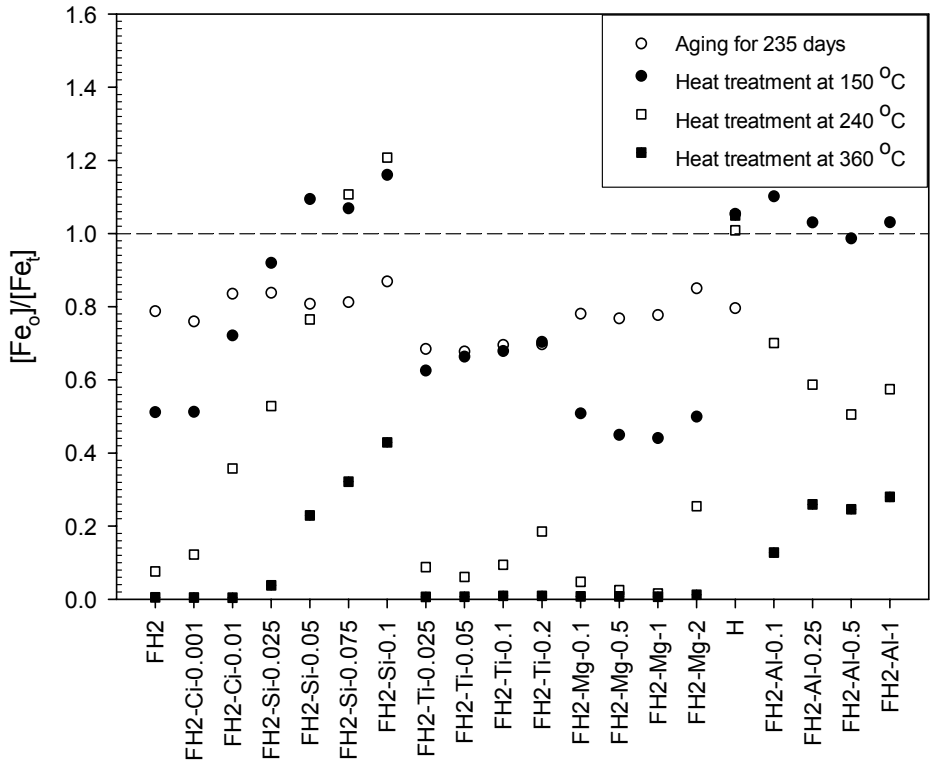

Figure 5.17 Comparison of Effects of Aging at Room Temperature for 235 Days and Heat-Treatment at High Temperatures on [Fe$_o$]/[Fe$_t$].

5.2.5 Effect of Heat Treatment on the Structure of 2-line Ferrihydrite

5.2.5.1 FH2, FH2-Ti, FH2-Ci, and FH2-Mg Series

The XRD patterns of the FH2, FH2-Ti, FH2-Ci, and FH2-Mg series heat-treated at 360 ^{o}C for 12 h are depicted in Figures 5.18 and 5.19. After heat-treating FH2 at 360 ^{o}C for 12 h, the complete decomposition of 2-line ferrihydrite occurred, resulting in the formation of a well ordered hematite as a single solid phase with peaks at 33.15, 35.65, 54.10, 49.95, 24.15, 64.05, 62.45, and 40.85^{o} 2θ (Figure 5.18). Also the color of FH2 changed from dark red-brown for 2-line ferrihydrite to a light red for hematite. The results indicate that the formation of hematite identified by XRD analysis was compatible

with the complete conversion (99.48%) of amorphous Fe oxide to other iron oxides (section 5.2.4), and the temperature of 2-line ferrihydrite transformation to hematite fell within the range (300~400 ^{o}C) reported previously by others [20, 38, 40, 110].

Figure 5.18 depicts the XRD patterns of the the FH2-Ci and FH2-Ti series heat-treated at 360 ^{o}C for 12 h. All of the diffraction peaks in these patterns can be also assigned to a well crystalline iron oxide, hematite. However, when the Ti/Fe molar ratio was increased from 0 to 0.1, the intensity of the peaks became shorter. This finding indicates that FH2-Ti-0.1 had a stronger retarding effect on the transformation of amorphous Fe oxide to hematite than was observed with FH2 and FH2-Ti-0.025, that is, the extent of transformation decreased with an increase in the Ti/Fe molar ratio. The decrease in the extent of transformation was consistent with the decrease in $[Fe_o]/[Fe_t]$ discussed in section 5.2.4. In addition, the XRD patterns for the FH2-Ti series after heat-treating at 360 ^{o}C showed traces of crystalline anatase TiO_2, as indicated by a small diffraction peak near 25.23^{o} 2θ. This peak was evident with increasing Ti/Fe molar ratio. The emergence of anatase can be attributed to the formation of titanium hydroxide, $Ti(OH)_4$. During preparation of the FH2-Ti series in this study, a small amount of white Ti-hydroxide was visually observed at above pH 3.5. It has been reported by others [236] that anatase, TiO_2, can be formed by heat treatment of Ti-hydroxide at 75 ^{o}C for more than 6 h. Upon heating the FH2-Mg series samples at 360 ^{o}C for 12 h, they transformed into hematite (Figure 5.19), and the FH2-Mg-2 sample showed the lowest intensity of peaks among them.

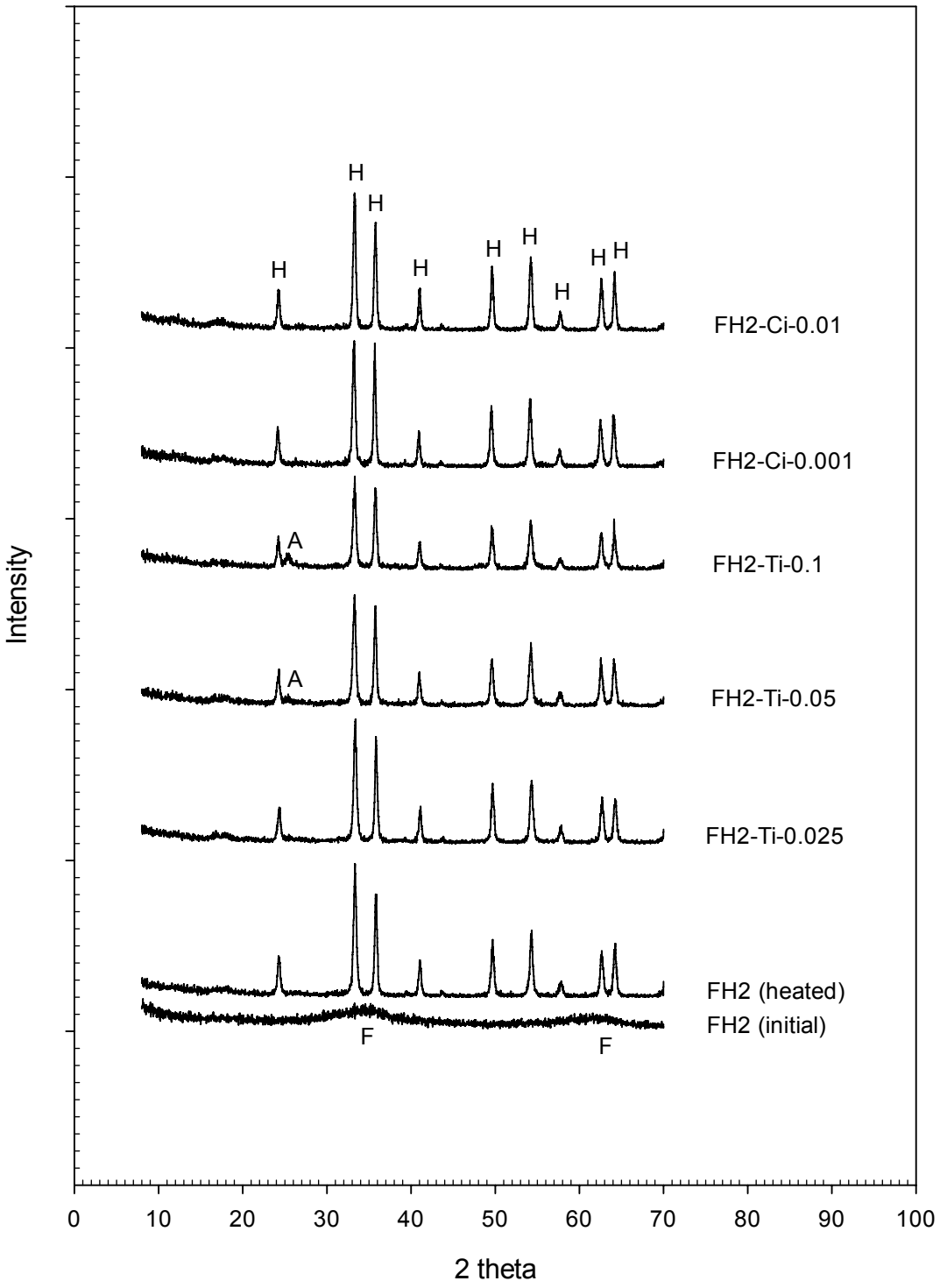

Figure 5.18 XRD Patterns of FH2, FH2-Ti and FH2-Ci Series Heated at 360 ^{o}C for 12 h. Major Peaks due to 2-line Ferrihydrite, Hematite, and Anatase are Indicated as F, H, and A, Respectively.

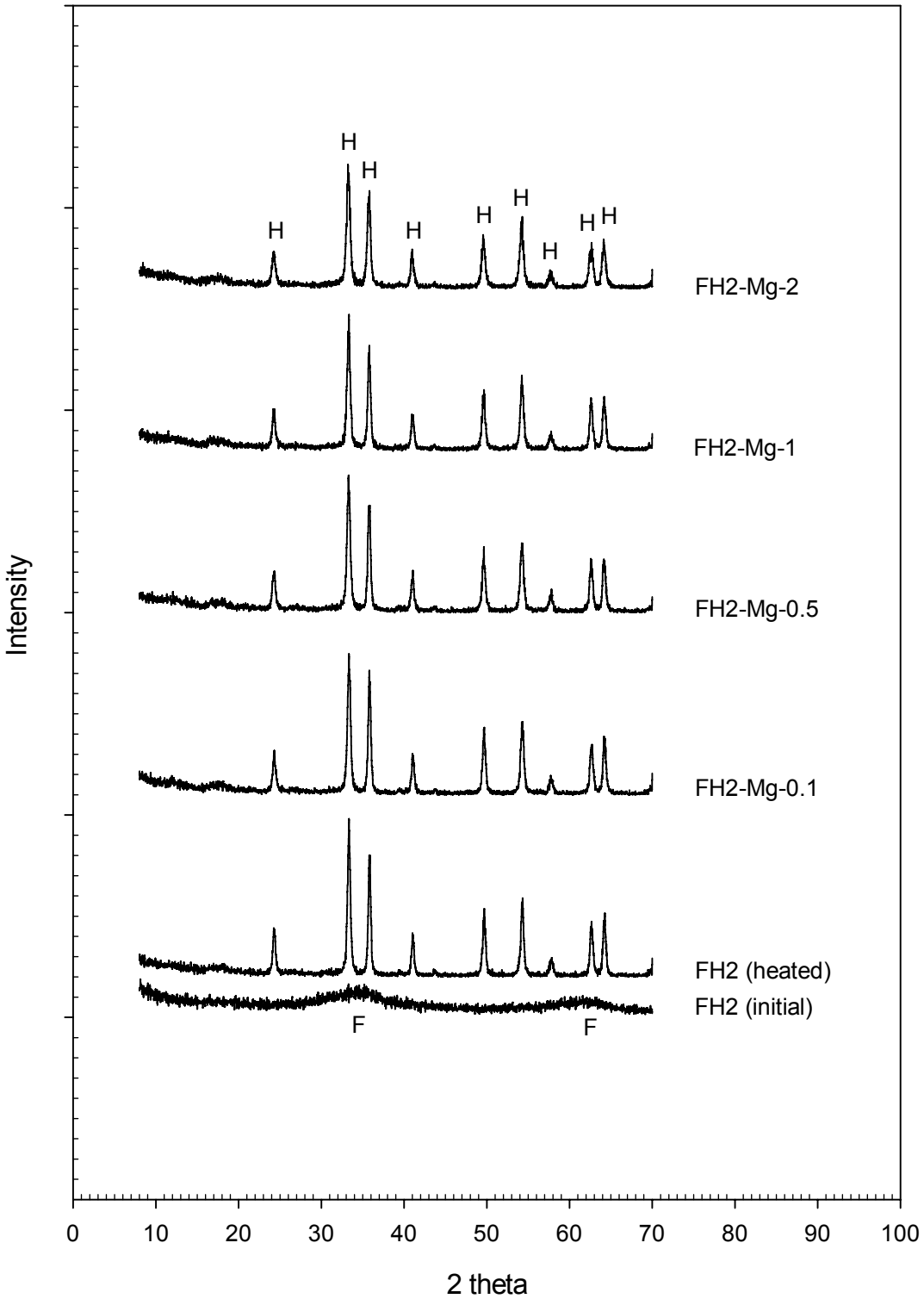

Figure 5.19 XRD Patterns of FH2-Mg Series Heated at 360 ^{o}C for 12 h. Major Peaks due to 2-line Ferrihydrite and Hematite are Indicated as F and H, Respectively.

5.2.5.2 FH2-Si Series

Upon heat-treating the FH2-Si series at 360 ^{o}C for 12 h, peaks indicative of hematite were observed. The hematite peaks were less evident with Si/Fe molar ratio (Figure 5.20). Although the XRD pattern of FH2-Si-0.075 still exhibited the presence of large amounts of 2-line ferrihydrite, the XRD pattern showed traces of crystalline hematite near 33.15, 35.65, 54.10, 49.45, 64.05, and 62.45^{o} 2θ, as indicated by the very tiny diffraction peaks superimposed on the two broad 2-line ferrihydrite peaks. For FH2-Si-0.05 and FH2-Si-0.025 (Si/Fe molar ratio $\leq$ 0.05), the sharp diffraction peaks indicative of hematite appeared as distinct bands. As discussed in section 5.2.4, the $[Fe_o]/[Fe_t]$ ratios of FH2-Si-0.025, FH2-Si-0.05, FH2-Si-0.075, and FH2-Si-0.1 after heat-treating at 360 ^{o}C were 3.81, 22.91, 32.17, and 42.89%, respectively, which corresponded to the conversion of 96.19, 77.09, 67.83, and 57.21% of amorphous Fe oxide into hematite. For FH2-Si-0.075 and FH2-Si-0.1, more than half of the amorphous Fe oxide (67.83 and 57.21%) was transformed into other iron oxides, however, no sharp diffraction peaks for hematite were detected in the XRD patterns. This phenomenon might be explained by the assumption that hematite was forming and that peaks of poorly ordered hematite were superimposed on the two broad 2-line ferrihydrite peaks. The exact nature of the phase transformations in the mineral may not always be determined by direct analysis of the XRD patterns. In order to detect smaller scale differences, extensive mathematical processing of the XRD data might be required. The XRD analysis can yield information on the identity of mineral phases but cannot indicate in detail the extent of 2-line ferrihydrite transformation. Thus, the transformation study is complementary to XRD analysis, each resulting in data ancillary to the other.

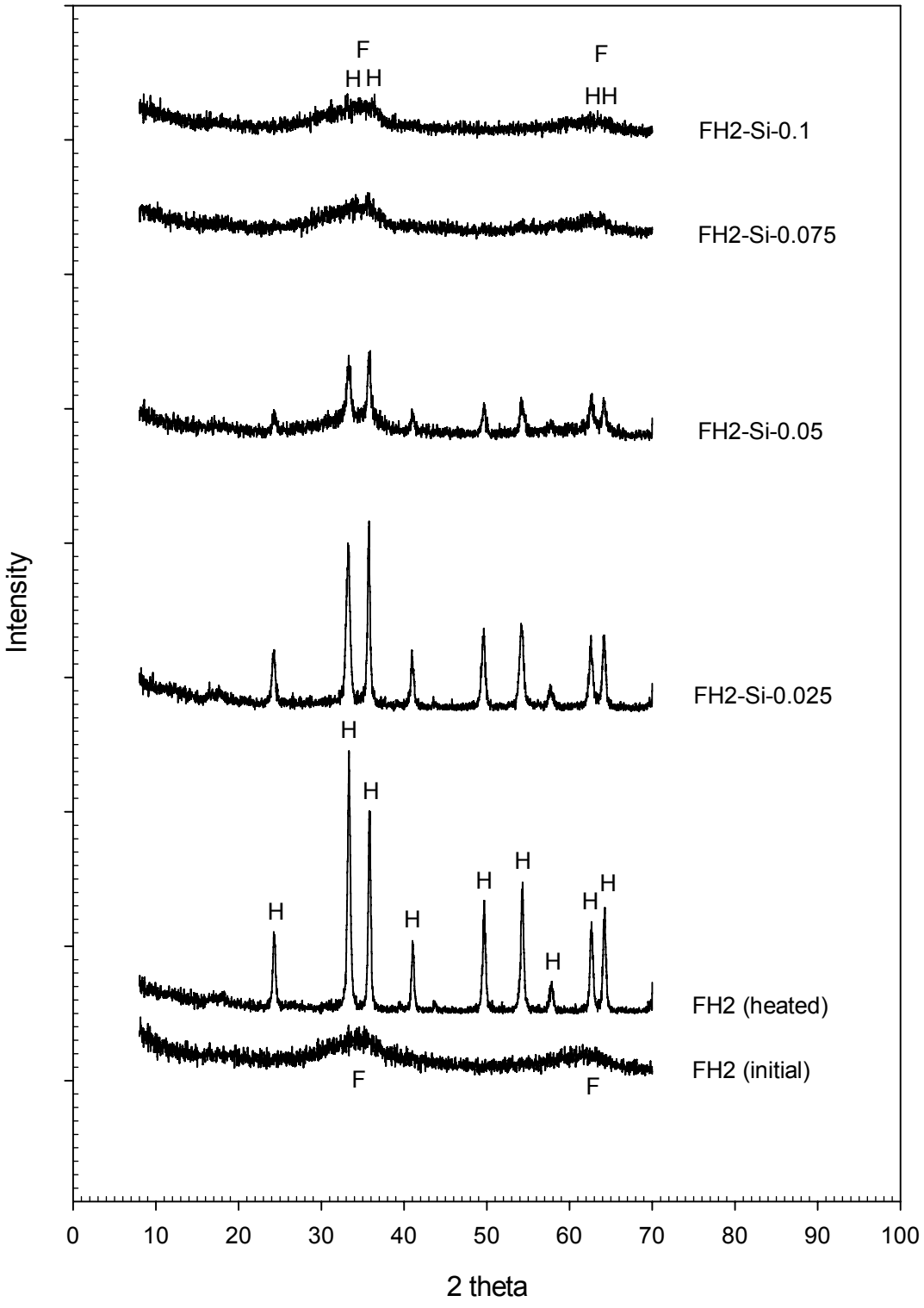

Figure 5.20 XRD Patterns of FH2-Si Series Heated at 360 ^{o}C for 12 h. Major Peaks due to 2-line Ferrihydrite and Hematite are Indicated as F and H, Respectively.

5.2.5.3 FH2-Al Series

Figure 5.21 shows XRD patterns of the FH2-Al series heat-treated at 360 ^{o}C for 12 h. The XRD pattern for FH2-Al-0.1 exhibited sharp diffraction peaks indicative of hematite, whereas, very small diffraction peaks for hematite were detected in the XRD patterns for FH2-Al-0.25, FH2-Al-0.5, and FH2-Al-1. After aging at RT for 135 days, peaks indicative of gibbsite and bayerite, with two broad background peaks typical of 2-line ferrihydrite appeared as a trace in FH2-Al-0.25 and as distinct bands in FH2-Al-0.5 and -1. Following the heat-treatment of FH2-Al-0.25, FH2-Al-0.5, and FH2-Al-1 at 360 ^{o}C for 12 h, the two broad background peaks remained unchanged at around 35 (d = 0.26 nm) and 62^{o} (d = 0.15 nm) 2θ, indicative of poorly crystalline 2-line ferrihydrite. The results might be explained by the fact that during heat treatment the crystalline Al hydroxides were decomposed or transformed into other Al oxyhydroxides, whereas the transformation of the 2-line ferrihydrite into hematite was retarded. The retardation of the 2-line ferrihydrite transformation into hematite could be attributed to the formation of Al (III) complexes on the 2-line ferrihydrite surface [96], the adsorption/reprecipitation of soluble Al(III) species on the surface of the $Fe(OH)_3$ surface [220], and hence the substitution of Al(III) for Fe(III) to form Al(III)-substituted hematite [20, 24, 31]. As discussed previously in section 5.2.4, the $[Fe_o]/[Fe_t]$ ratios of FH2-Al-0.1, FH2-Al-0.25, FH2-Al-0.5, and FH2-Al-1 after heat-treating at 360 ^{o}C were 12.79, 25.96, 24.61, and 27.98%, respectively, which corresponded to the transformation of 87.21, 74.04, 75.39, and 72.02% of amorphous Fe oxide into hematite. For FH2-Al-0.25, FH2-Al-0.5, and FH2-Al-1, a significant amount (72.02~74.04%) of amorphous Fe oxide transformed into hematite, however, no sharp diffraction peaks for hematite were detected in their XRD

patterns. This discrepancy might be explained by an assumption that peaks of poorly crystalline hematite were obscured by the two broad 2-line ferrihydrite peaks.

After heating FH2-Al-0.025, FH2-Al-0.5, and FH2-Al-1 at 360 ^{o}C for 12, the diffraction peaks of gibbsite and bayerite disappeared. For FH2-Al-1 very tiny peaks indicative of boehmite (γ-AlOOH) were evident at 14.43, 49.27, and 67.06^{o} 2θ. It has been generally known that the transformation of aluminum hydroxides into α-alumina in air, termed the Bayer process [237], depends on many factors such as heating rate, water vapor pressure around particles, and especially the particle size of the aluminum hydroxides [238]. Upon heating at temperatures between 300 ^{o}C and 400 ^{o}C for 2 h under atmospheric pressure, previous XRD results have indicated that thermal transformation of aluminum hydroxides proceeded as follows: 1) coarse gibbsite into boehmite and λ-alumina, 2) fine gibbsite (below 1 μm) into λ-alumina, 3) coarse bayerite into boehmite and η-alumina, and 4) fine bayerite (below 1 μm) into η-alumina [239]. It has been generally accepted that the transformation of gibbsite into boehmite is more likely to occur for large gibbsite particles (≥ 50 μm) [238, 240]. Therefore boehmite may not expected to form from small gibbsite particles since water in gibbsite particles escapes without a significant increase in internal pressure [238]. It was, however, reported by Bhattacharya et al. [241] that after heating fine gibbsite (1.5 μm) for 2 h, a boehmite peak was observed at 14.43^{o} 2θ at 250 ^{o}C, and the fine gibbsite transformed completely into boehmite with peaks at 14.43, 28.17, 38.33, 48.98, 49.27, and 67.06^{o} 2θ at 400 ^{o}C. The formation of a boehmite phase was also found after heating finer gibbsite (0.25 μm) at 400 ^{o}C. Compared with boehmite obtained from 1.5 μm particles, the 400 ^{o}C calcined finer particles (0.25 μm) showed reduced peak height and broader peak width.

Bhattacharya et al. [241] suggested that with further reduction in particle size, the boehmite particles will show amorphous characteristics by further reduction in peak height and by peak broadening when gibbsite particles become so small that gibbsite can not produce normal diffraction maxima, boehmite formation might not be a possibility.

For FH2-Al-1, although the particle size was determined to be 2.198 μm (section 4.2.3) and gibbsite and bayerite decomposed after heat-treatment, but there was no distinct sign of boehmite formation. It has been reported by other research [242] that the initiation of gibbsite transformation into boehmite was retarded by the presence of iron. Gong et al. [242] suggested that the presence of additional precipitated iron hydroxide solids should retard water evaporation during the hydrothermal transformation of gibbsite into boehmite at 150 ^{o}C, resulting in affecting the transformation kinectics. Therefore, the Al hydroxides obtained in the transformation of FH2-Al-1 were assumed to be in a transitional stage of structure between gibbsite and boehmite. In summary, the heated FH2-Al-1 was assumed to consist of 2-line ferrihydrie, hematite, gibbsite, and boehmite.

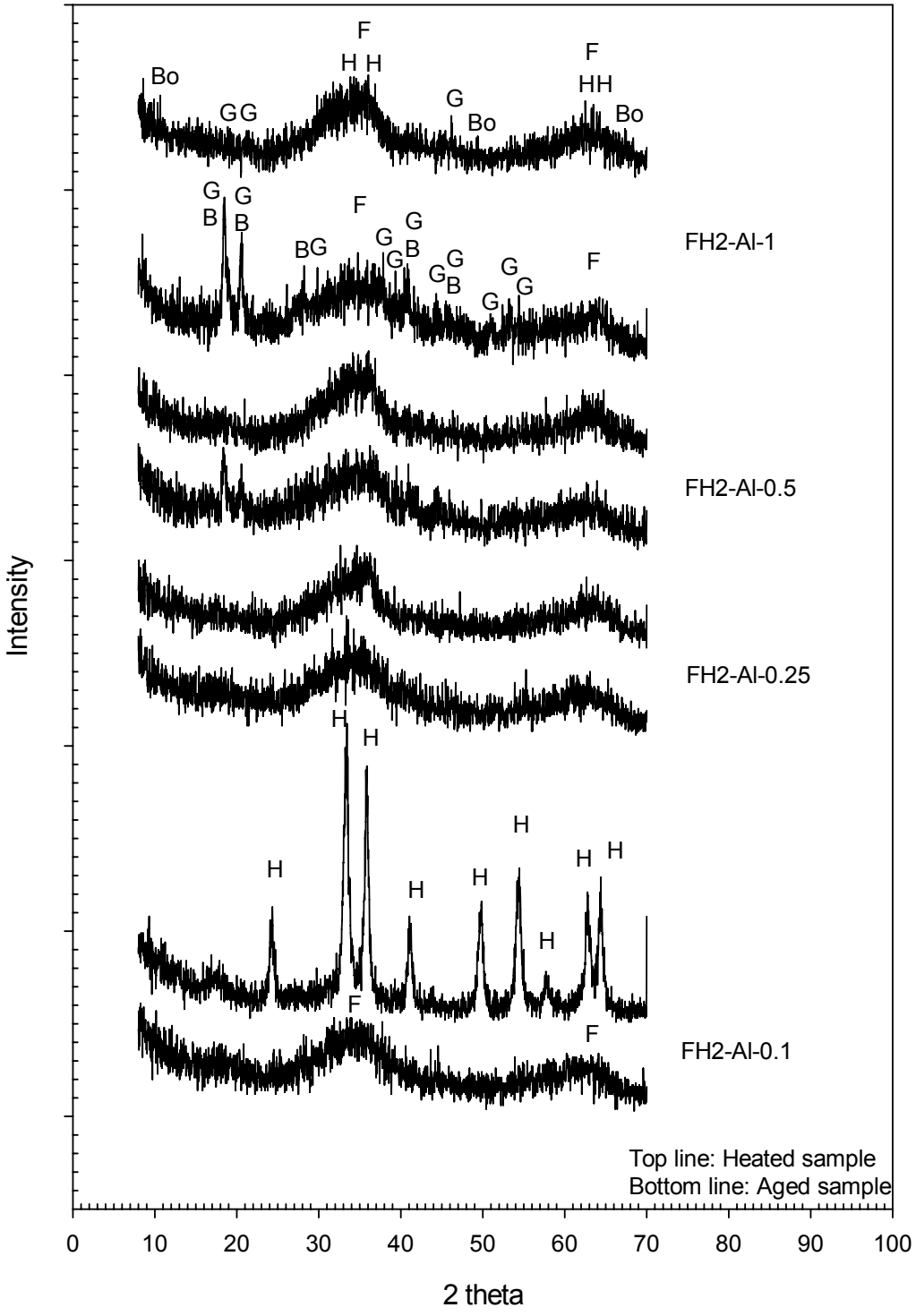

Figure 5.21 XRD Patterns of FH2-Al Series Aged at Room Temperature for 135 Days and Heated at 360 ^{o}C for 12 h. Major Peaks due to 2-line Ferrihydrite, Hematite, Gibbsite, Bayerite, and Boehmite are Indicated as F, H, G, B, and Bo, Respectively.

5.2.6 Effect of Heat Treatment on the Point of Zero Charge

The potentiometric titration curves (cubic-polynomial curves) of FH2, FH2-Mg-2, FH2-Si-0.1, and FH2-Al-1 heat-treated at 360 ^{o}C for 12 h are shown in Figures 5.22, 5.23, 5.24, and 5.25. As shown in these figures, the PZC values of the heated FH2s no longer coincided with those of the FH2s aged at RT for 165 days (Figures 4.6, 4.7, and 4.8). After heat-treatment at 360 ^{o}C, the FH2 was transformed completely into an iron oxide (99.48%) which was identified as hematite by XRD (sections 5.2.4 and 5.2.5). The PZC of FH2 was shifted from 7.82 to 8.70 (Figure 5.22), which fell within the range (8.5~9.5) of PZC values of hematite reported by others [61, 243, 244]. For the heated FH2-Mg-2, the value of PZC was found to be 8.90 (Figure 5.23), which is almost in agreement with the PZC value of the heat-treated FH2. The shift of PZC value of FH2-Mg-2 to a more basic pH can be also attributed to the formation (98.76%) of hematite by heat treatment.

On the other hand, the PZC of FH2-Si-0.1 dropped slightly from 6.90 to 6.30 after heat-treating at 360 ^{o}C (Figure 5.24). As discussed in sections 5.2.4 and 5.2.5, although the heated FH2-Si-0.1 was still identified by XRD as a typical 2-line ferrihydrite with two broad peaks, over half of the amorphous Fe oxide (57.11%) was transformed into hematite through the breakage of the Fe-O-Si bonds [114, 116], that is, the thermal conversion of FH2-Si-0.1 produced two separate phases, hematite and 2-line ferrihydrite, due to the retardation effect of Si at the 2-line ferrihydrite surface on the rearrangement of surface Fe octahedral units to hematite [114]. It has been reported by others [24, 64, 65] that the dehydroxylation and sintering of iron oxides at high temperatures and the presence of Si(IV) on the 2-line ferrihydrite surafec caused an acid shift in PZC. Therefore, the slight shift of PZC to a more acidic pH after heating at 360 ^{o}C might be

attributed to a combined effect of heat-treatment at 360 ^{o}C and Si(IV) on the 2-line ferrihydrite surface, although the product consisted of large amount of hematite which would be expected to result in an increase in the PZC value.

Upon heat-treating at 360 ^{o}C for 12 h, the PZC value of FH2-Al-1 dropped slightly from 8.70 to 8.20 (Figure 5.25). After heating at 360 ^{o}C, a significant amount of the orginal amorphous Fe oxide (72.02%) has transformed into hematite (section 5.2.4), the PZC value of which was reported to range from 8.50 to 9.50 [61, 243, 244]. For the Al hydroxides, boehmite phase was not apparent from XRD patterns, although the diffraction peaks of gibbsite and bayerite disappeared after heating at 360 ^{o}C (section 5.2.5). As discussed in sections 5.2.4 and 5.2.5, the product obtained by heat treatment of FH2-Al-1 at 360 ^{o}C were considered to exist as a mixture of hematite, 2-line ferrihydrite, gibbsite, and boehmite. It has been reported by others [245, 246] that the PZC of boehmite occurs at about 8.6 to 8.8, which are less than those of gibbsite and bayerite. Therefore, the slightly acidic shift in the PZC value of the heated FH2-Al-1 might be attributable to the decomposition of gibbsite and bayerite (PZC value: 9.0~9.9) [196, 228~230], the formation of boehmite (PZC value: 8.6~8.8) [245, 246], and the larger amount of remaining 2-line ferrihydrite (PZC value: 7.82) compared to that of the heated FH2.

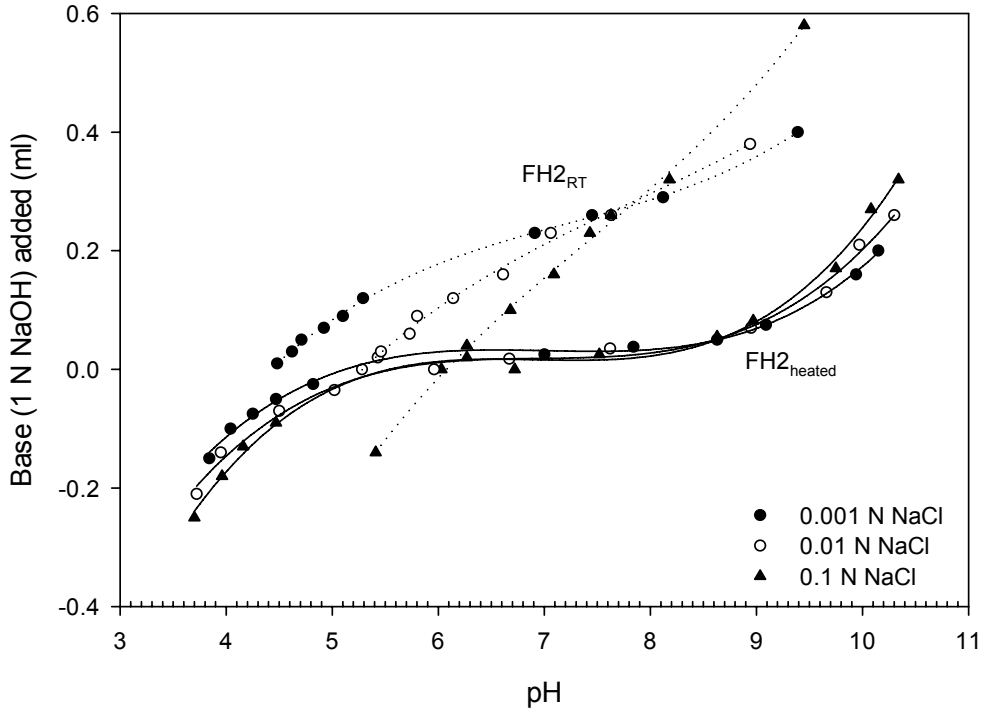

Figure 5.22 Potentiometric Titration Curves of 2-line Ferrihydrite Heated 360 ^{o}C for 12 h.

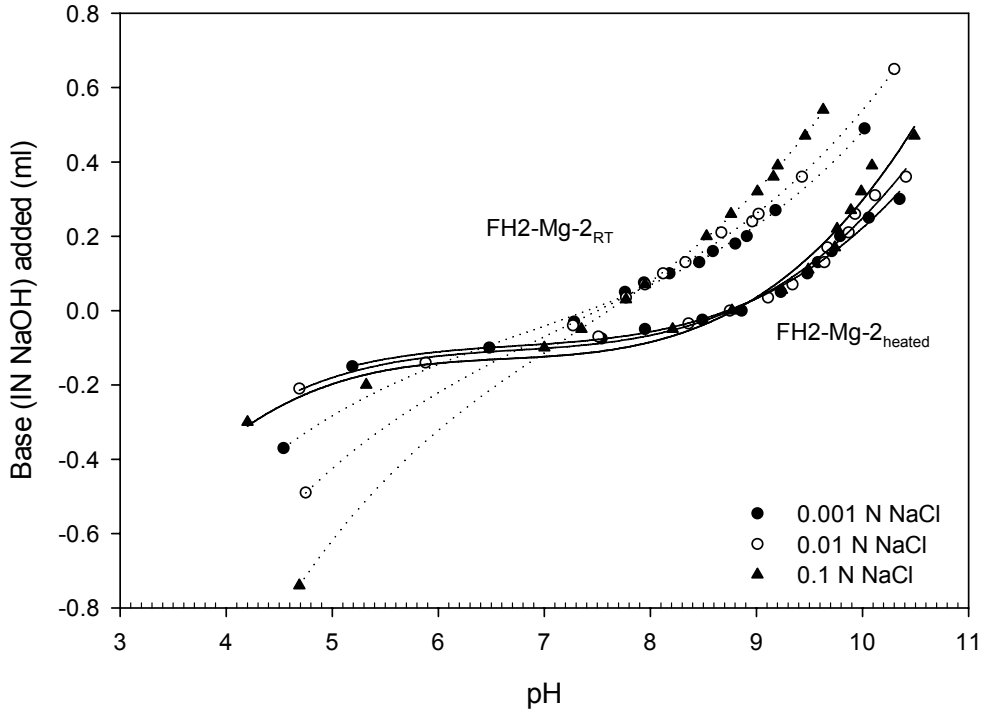

Figure 5.23 Potentiometric Titration Curves of FH2-Mg-2 Heated 360 ^{o}C for 12 h.

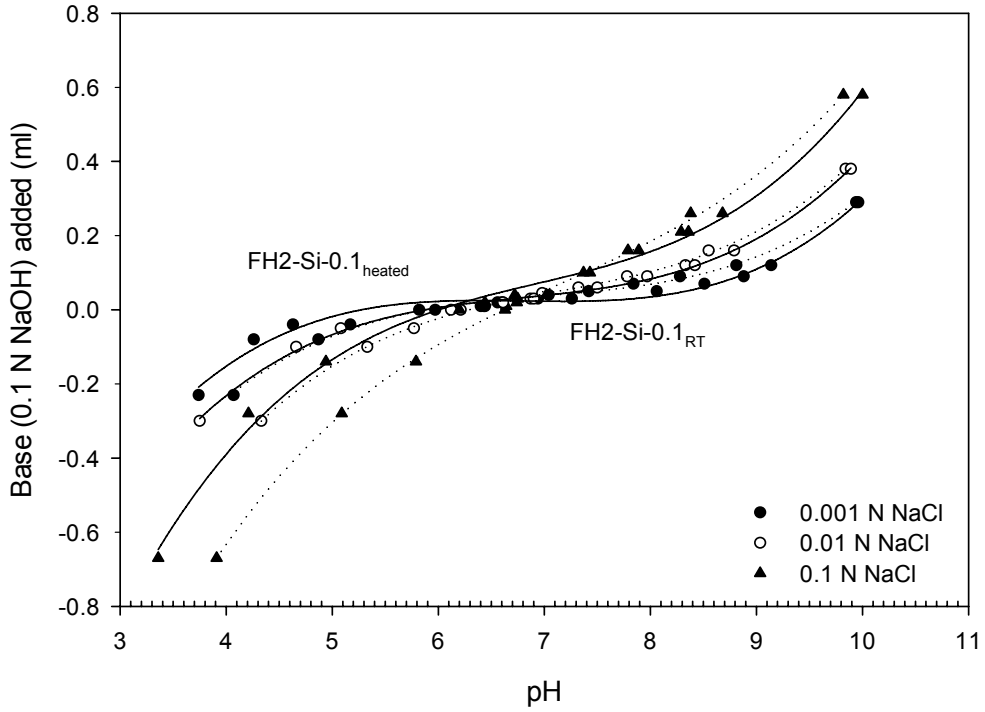

Figure 5.24 Potentiometric Titration Curves of FH2-Si-0.1 Heated 360 ^{o}C for 12 h.

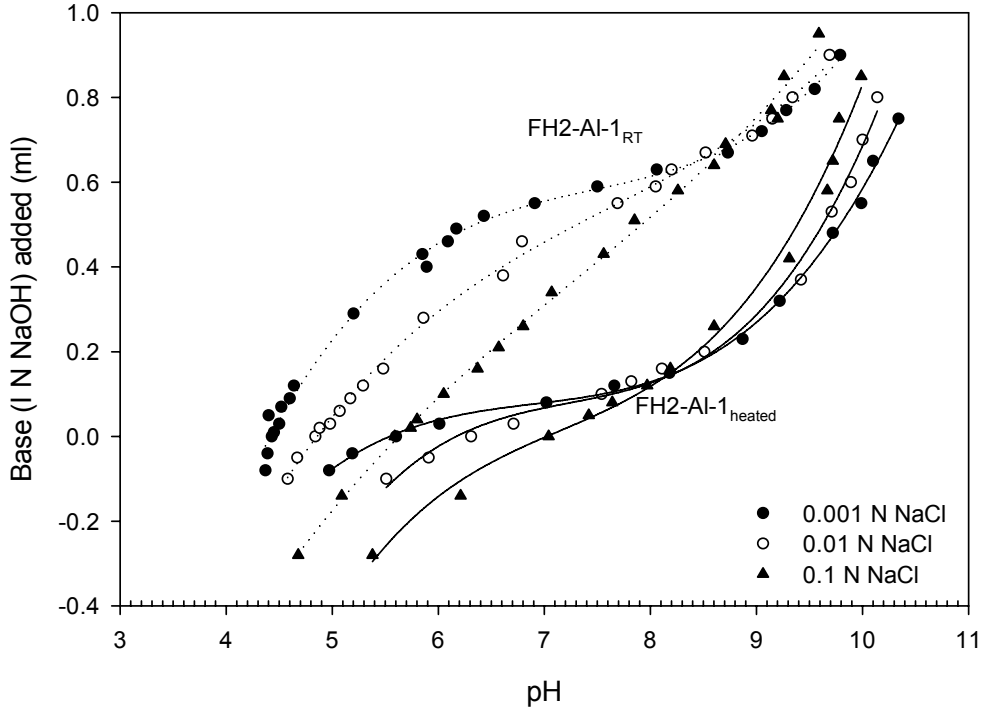

Figure 5.25 Potentiometric Titration Curves of FH2-Al-1 Heated 360 ^{o}C for 12 h.

5.3 Conclusions

During aging the FH2s (except FH2-Al series) at RT for 235 d, the conversion of 13~32% of the amorphous Fe oxide into other iron oxides occurred. The transformation of amorphous Fe oxide was retarded in the presence of Si(IV) or at high molar ratios of Mg(II) and citrate. However, there were neither distinct differences between inhibitor-specific influences (except Si) on the transformation nor indication of other iron oxide in the XRD patterns due to the superimposition of its peaks on 2-line ferrihydrite peaks.

Upon heating the FH2, FH2-Mg, FH2-Ti, and FH2-Ci series at 360 ^{o}C, the amorphous Fe oxide was almost totally transformed into hematite. In contrast, Si(IV) and Al(III) had stronger retarding effects on the transformation of amorphous Fe oxide with respect to the other FH2s due to the presence of Si(IV) and Al(III) at the 2-line ferrihydrite surface. However, Si(IV) was much more pronounced than Al(III) in retarding the transformation of amorphous Fe oxide due to the incompatility of Si(IV) tetrahedral symmetry with the 2-line ferrihydrite structure. The XRD patterns for FH2-Si-0.075 and FH2-Si-0.1 still indicated the presence of large amounts (32~43%) of amorphous Fe oxide, while at higher Al/Fe molar ratios ($\geq$ 0.5), greater than 25 % of 2-line ferrihydrite remained untransformed, gibbsite and bayerite were decomposed, and very tiny peaks indicative of boehmite appeared as a trace component. After heating at 360 ^{o}C, the formation of hematite promoted the shift of the PZC for FH2 and FH2-Mg-2 to a more basic pH, whereas for FH2-Si-0.1 and FH2-Al-1, the PZC dropped to a slightly more acidic pH. Compared to aging at RT, heat treatment at high temperatures had much more noticeable and complicated effects on the transformation, structure, and PZC of the FH2s.

CHAPTER VI

ADSORPTION OF ARSENIC ON 2-LINE FERRIHYDRITE CONTAINING A TRANSFORMATION INHIBITOR

6.1. Introduction

Adsorption of arsenic on iron oxides has been extensively investigated due to their abundant occurrence in the natural system and their higher adsorption capacity for arsenic [44, 148~159]. Recently ferrihydrite, a poorly crystalline iron hydroxide, has received much attention as an effective adsorbent for removing arsenic from water because of its large surface area and high adsorption capacity [44, 75, 148~154, 160]. However, the transformation of FH2 into crystalline iron oxides generally results in lowering the adsorption capacity for heavy metals [77]. Therefore, FH2 containing a transformation inhibitor might be advantageous for removing arsenic from water as well as managing arsenic waste due to a slower rate of transformation with respect to pure FH2. Although various foreign species have been investigated for inhibiting the transformation of FH2 to crystalline oxides, there has been comparatively little information on the adsorption of arsenic on FH2 in the presence of a transformation inhibitor. Therefore, the objectives of this study were (1) to investigate the influence of both aging at RT and heat treatment at 360 ^{o}C on arsenic adsorption on FH2 containing a transformation inhibitor (Si (IV), Mg (II), Al (III), Ti (IV), or Ci(citrate)) at low arsenic loadings, (2) to evaluate the influence of pH on arsenic adsorption on the FH2, (3) to evaluate the inhibitor-specific influence on arsenic adsorption, and (4) to evaluate the influence of high arsenic loadings on arsenic adsorption.

6.2 Results and Discussion

6.2.1 Arsenic Adsorption on Fresh Samples

Screening adsorption experiments for the fresh FH2s were performed at pH 7 and at low arsenic loading rates (0.0067, 0.0133, 0.0178, 0.0267, and 0.0534 mol As (III)/kg sample and 0.0133, 0.0267, 0.0356, 0.0534, 0.1068 mol As (V)/kg sample). After a reaction period of 48 h at pH 7 with an initial arsenite loading of 0.0534 mol As(III)/kg (initial As(III) concentration: 200 μg/L), the equilibrium arsenite concentrations for FH2, FH2-Si-0.05, FH2-Ti-0.025, -0.05, and FH2-Al-0.1 were below 5 μg/L, while FH2-Ci-0.1, FH2-Al-1, FH2-Si-0.1, and FH2-Al-0.5 showed higher arsenite concentrations of 138.35, 21.54, 13.26, and 12.31 μg/L, respectively (Figure 6.1). In contrast, at an initial arsenate addition of 0.1068 mol As(V)/kg (initial As(V) concentration: 400 μg/L), the equilibrium arsenate concentrations of most samples were less than 5 μg/L, whereas those of FH2-Ci-0.1, FH2-Si-0.1, and FH2-Ti-0.2 exceeded 5 μg/L (334.01.71 for FH2-Ci-0.1, 13.69 for FH2-Si-0.1, and 5.06 μg/L for FH2-Ti-0.2, respectively). Especially FH2-Ci- 0.1 showed the smallest adsorption capacity of arsenic.

The adsorption experiments showed that arsenic removal by FH2 was 99.73% for arsenite (at 0.0534 mol As (III)/kg) and 99.68% for arsenate (at 0.1068 mol As (V)/kg), whereas arsenic removal by the other FH2s except FH2-Ci-0.1 was 89.23~98.81% for arsenite (at 0.0534 mol As (III)/kg) and 96.58~100% for arsenate (at 0.1068 mol As (V)/kg) (Figure 6.2). The relatively strong retention of arsenite and arsenate suggests that each arsenic species was adsorbed as an inner-sphere complex. This high capacity for adsorption of both arsenite and arsenate was also reported by other researchers [30, 44,

149, 151]. However, the percentage arsenic removal by FH2-Ci-0.1 was 30.83% for arsenite (at 0.0534 mol As (III)/kg) and 16.50% for arsenate (at 0.1068 mol As (V)/kg).

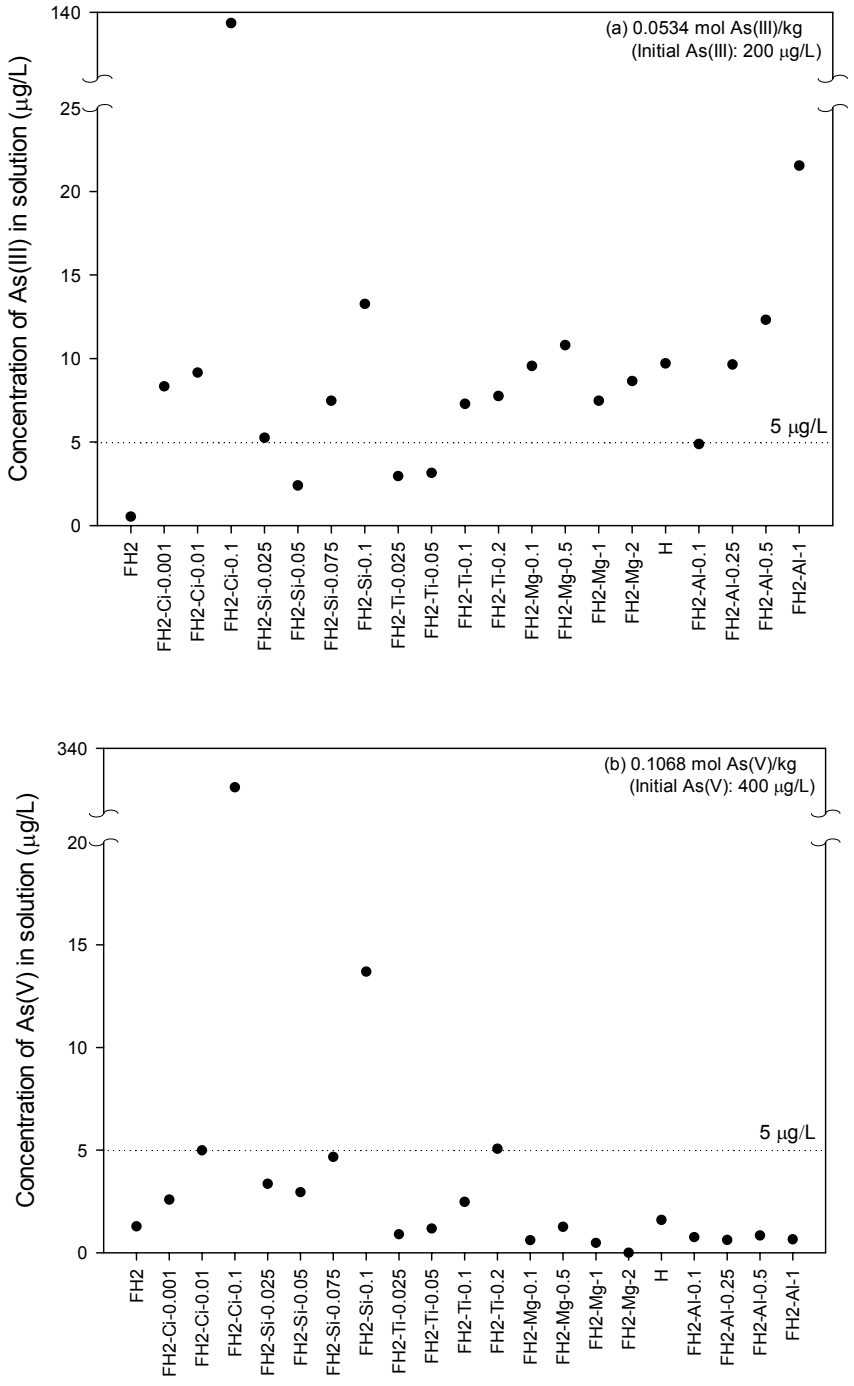

Figure 6.1 Equilibrium Concentration of As(III) (a) and As(V) (b) in Solution after a Reaction Period of 48 h at pH 7.

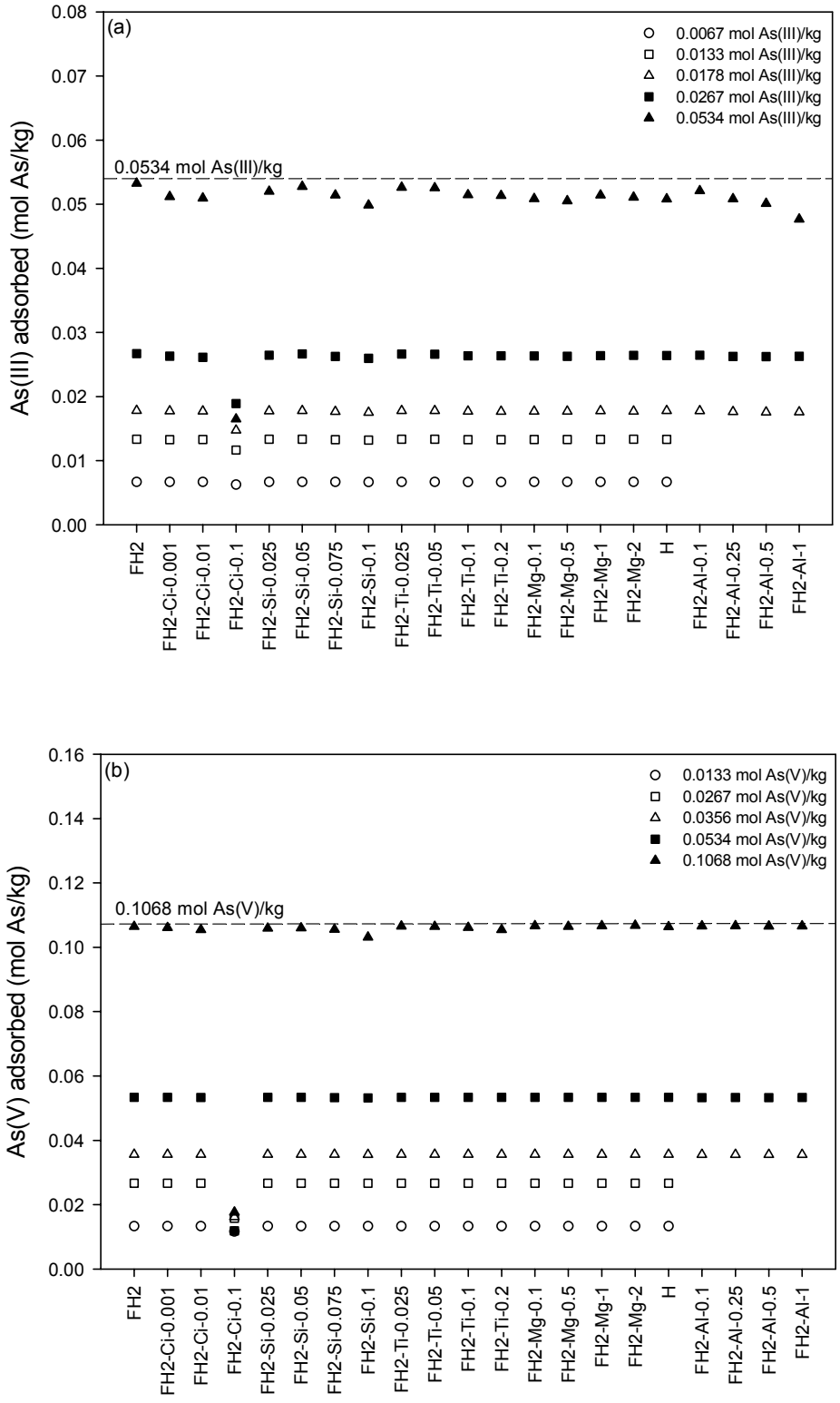

Figure 6.2 Adsorption of As(III) (a) and As(V) (b) on Fresh 2-line Ferrihydrites at pH 7.

A comparison between arsenite adsorption and arsenate adsorption on the fresh FH2s is shown in Figure 6.3. At initial arsenic loadings of both 0.0267 and 0.0534 mol As/kg, arsenate was adsorbed in larger amounts than arsenite. This result is in agreement with other studies using 2-ferrihydrite [44] and Fe (III)-Si binary oxide [191]: arsenate was in larger amounts than arsenite both at an initial low arsenic loading of 0.267 mol As/kg (at pH 7) [44] and at an arsenic equilibrium concentration of smaller than 1.6 mg/L (at initial arsenic loadings of 0~0.3070 mol As/kg and at pH 6.5) [191].

A comparison of arsenic adsorption on the fresh FH2s with an equimolar inhibitor/Fe ratio of 0.1 at pH 7 is shown in Figure 6.4. With arsenite, adsorption capacity on the fresh FH2s decreased in the order of FH2 > FH2-Al-0.1 > FH2-Ti-0.1 > FH2-Mg-0.1 > FH2-Si-0.1 >> FH2-Ci-0.1. The difference in arsenite adsorption between FH2, FH2-Al-0.1, FH2-Ti-0.1, FH2-Mg-0.1, and FH2-Si-0.1 was quite small, but the arsenite adsorption on FH2-Ci-0.1 was much lower. With arsenate, there was no discernable difference in arsenate adsorption between FH2, FH2-Al-0.1, FH2-Ti-0.1, and FH2-Mg-0.1. However, the adsorption of arsenate on FH2-Si-0.1 was somewhat lower while that of arsenate on FH2-Ci-0.1 was considerably lower. The decrease in arsenate adsorption on FH2-Si-0.1 and FH2-Ci-0.1 may be in part attributed to their respective surface charges. At pH 7, the surface of FH2-Si-0.1 and FH2-Ci-0.1 has a net negative charge and would tend to repulse $H_2AsO_4^-$ and $H_2AsO_4^{2-}$ ions in solution [49, 186~192]. Compared with the other FH2s, the addition of citrate to 2-line ferrihydrite apparently led to a considerable decrease in arsenic adsorption capacity. It was reported by others [49, 192] that a decrease in arsenic adsorption on iron oxides may be due to the presence of functional groups (three COOH groups and one OH group) present on citrate. There was

a general trend of decreasing arsenite adsorption with increasing Ci/Fe, Si/Fe, Al/Fe, and Ti/Fe molar ratios as well as decreasing arsenate adsorption with increasing with Ci/Fe, Si/Fe, and Ti/Fe molar ratios (Figures 6.1 and 6.2). A detailed interpretation of effect of inhibitor/Fe molar ratio on arsenic adsorption of the fresh FH2s will be given later in sections 6.2.2~6.2.5.

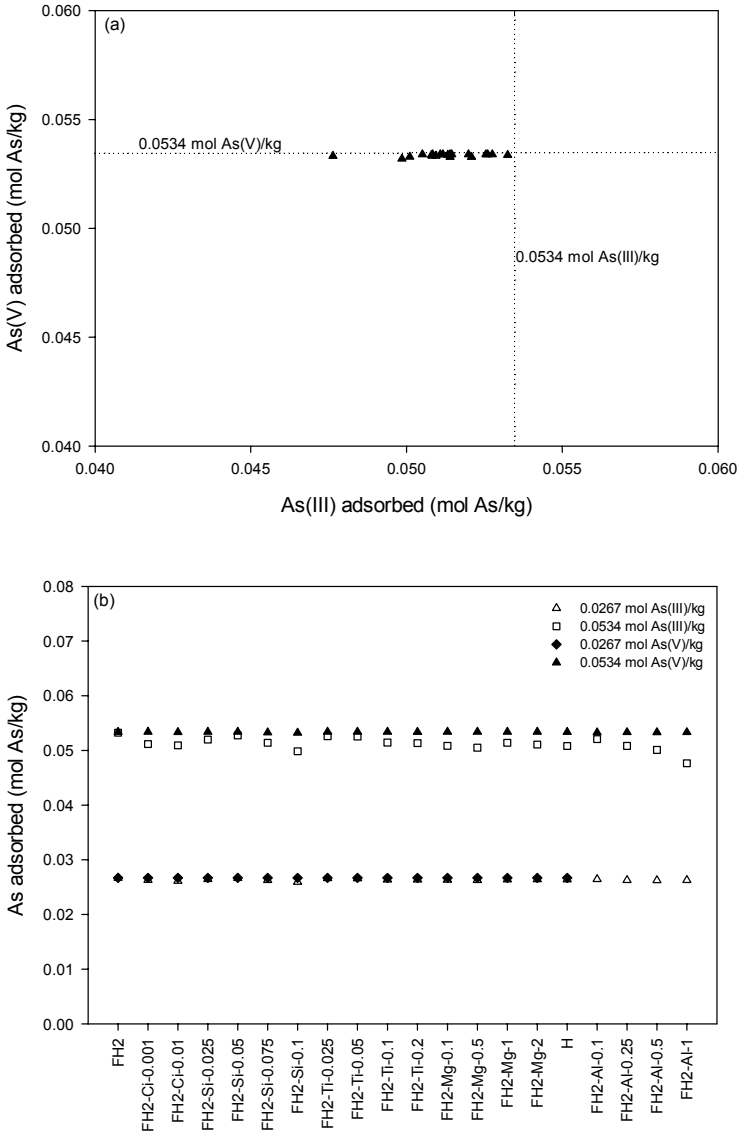

Figure 6.3 Comparison of As(III) Adsorption and As(V) Adsorption on Fresh 2-line Ferrihydrites at pH 7 (Initial As Addition: 0.0534 (a) and 0.0267 and 0.0534 mol As/kg Sample (b)).

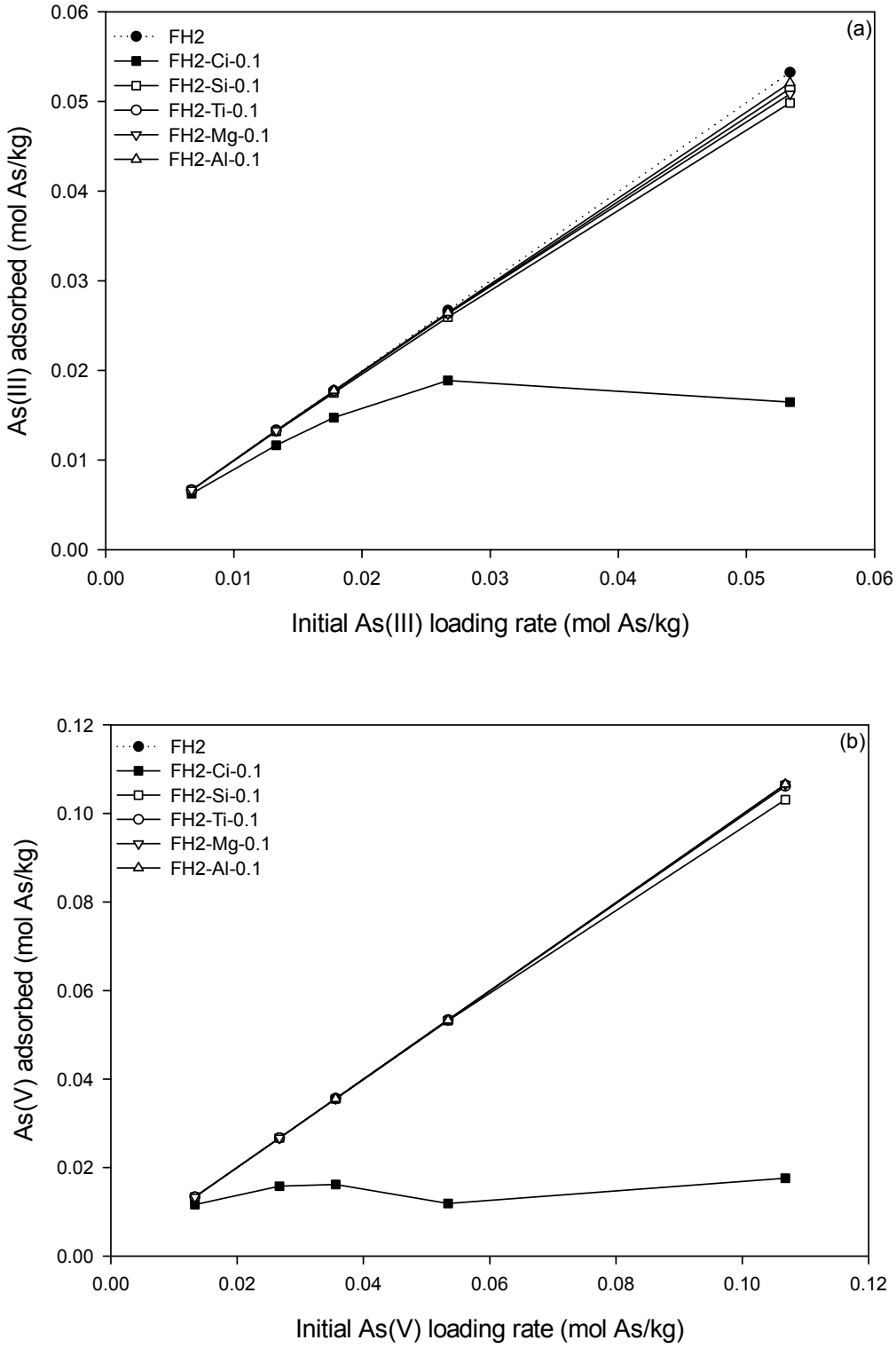

Figure 6.4 Adsorption of As(III) (a) and As(V) (b) on Fresh 2-line Ferrihydrites with an Inhibitor/Fe Molar Ratio of 0.1 at pH 7.

6.2.2 Effect of Aging at Room Temperature on Arsenic Adsorption

Adsorption experiments for the FH2s aged at RT for 235 days were performed at pH 7 and at low arsenic loading rates (0.0178, 0.0267, and 0.0534 mol As (III)/kg sample and 0.0356, 0.0534, 0.1068 mol As (V)/kg sample). The adsorption experiments for the aged FH2s showed that arsenic removal by FH2 was 94.66% for arsenite (at 0.0534 mol As (III)/kg) and 99.89% for arsenate (at 0.1068 mol As (V)/kg), whereas arsenic removal by the other FH2s (except FH2-Ci-0.1) was 78.33~97.19% for arsenite (at 0.0534 mol As (III)/kg) and 97.70~99.93% for arsenate (at 0.1068 mol As (V)/kg) (Figure 6.5). After aging for 235 days, the percentage adsorption for arsneite decreased by 5.07% for FH2 and 0~15.04% for the other FH2s (at 0.0534 mol As (III)/kg) while there was no discernable reduction in the percentage adsorption for arsenate (at 0.1068 mol As (V)/kg).

With arsenite, adsorption capacity (above 0.05 mol As (III) adsorbed/kg) on the aged FH2s decreased in the order of HTlc > FH2-Mg-1 > FH2-Mg-0.1 > FH2 > FH2-Mg-2 > FH2-Ci-0.001 > FH2-Mg-0.5. With increasing the inhibitor/Fe molar ratio, the adsorption capacity of arsenite on both the FH2-Si and FH2-Ci series decreased. Especially, the adsorption capacity of arsenite on FH2-Ci-0.1 decreased considerably. With arsenate, there was no discernable difference in adsorption capacity between the aged FH2s and the fresh FH2s. However, the adsorption capacity of arsenate on FH2-Ci-0.1 was substantially lower.

As discussed in section 5.2.2, the slight reduction in arsenite adsorption is attributable to a decrease in the amount of 2-line ferrihydrite due to the transformation of amorphous Fe oxide to crystalline iron oxide (hematite), where the fraction of transformed Fe oxide ranged from 13.10% for FH2-Si-0.1 to 32.27% for FH2-Ti-0.05

after aging 235 days. Additionally the aged FH2-Ci- 0.1 showed the smallest adsorption capacity of arsenic among the aged FH2s. A comparison between arsenite adsorption and arsenate adsorption on the aged FH2s is shown in Figure 6.6. Compared with adsorption of arsenic on the fresh FH2s, there was the same trend that arsenate was adsorbed in larger amounts than arsenite at an initial arsenic loading of 0.0534 mol As/kg.

The influence of both inhibitor/Fe molar ratio and aging for 235 days on arsenic adsorption for the FH2s at pH 7 is shown in Figures 6.7~6.10. The results of arsenic adsorption on the aged FH-Si series are given in Figure 6.7. The results indicate that the Si/Fe molar ratio affected arsenite adsorption on both the fresh and the aged FH2-Si series whereas the ratio had little influence on arsenate adsorption on both the fresh and the aged FH2-Si series. It was also observed that aging for 235 days had a slight effect on arsenite adsorption on the FH2-Si series while an increase in aging time had little influence on arsenate adsorption on the FH2-Si series. It was reported by Zeng [186] that the tested aging time from 1 to 7 days had trivial influence on the arsenic adsorption for a Fe-Si binary oxide with Si/Fe = 1 mol/mol at 0.28 mg As (III)/g adsorbent and pH 9.4~9.6.

As shown in section 4.2.5, after aging at RT for 165 days, the PZC values of FH2 and FH-Si-0.1 were determined to be 7.82 and 6.90, respectively. As the Si/Fe molar ratio of aged samples increased from 0 to 0.1, the adsorption of arsenite at an initial As addition of 0.0534 mol As(III)/kg decreased by 17%. Gradual decreases in arsenite adsorption on the aged FH2-Si series with increasing the Si/Fe molar ratio may be attributable to the coverage of silicic acid on active sites at the surface of 2-line ferrihydrite, hence resulting in a substantial decrease in arsenite adsorption [186]. The

adsorption of arsenate on the aged FH2-Si-0.1 (with a PZC value of 6.90) at pH 7 may be partly explained by a well-recognized phenomenon [62], that is, maxima in the adsorption envelopes of anions occur at pH values near their pK_a. At pH 7 close to pK_{a2} (6.97) of arsenate, H^+ dissociated from arsenate reacts with OH^- at the 2-line ferrihydrite surface to form the surface OH_2, which is more advantageous than the charged surface OH^- to arsenate exchange. Therefore, the OH_2 surface may in part lead to the adsorption of arsenate.

The influence of both Mg/Fe molar ratio and aging for 235 days on adsorption of arsenic on the FH2-Mg series at pH 7 is shown in Figure 6.8. The results indicate that both Mg/Fe molar ratio and aging for 235 days had little influence on the adsorption of both arsenite and arsenate on the FH2-Mg series. These results can be explained by the fact that the PZC value (7.90) of FH-Mg-2 was closely equal to that (7.82) of FH2 (section 4.2.5). The influence of both Ti/Fe molar ratio and aging for 235 days on the adsorption of arsenic on the FH2-Ti series at pH 7 is shown in Figure 6.9. Although small amounts of amorphous $Ti(OH)_4$ precipitate was visually observed, the results show that both Ti/Fe molar ratio and aging for 235 days had little influence on the adsorption of both arsenite and arsenate on the FH2-Ti series. The results are likely due to the higher concentration of adsorption sites per unit weight of sample with the poorly crystalline 2-line ferrihydrite. Two-line ferrihydrite of both the FH2-Mg series and the FH2-Ti series was still a principal adsorbent for arsenic adsorption.

Compared with FH2, FH2-Ci-0.001 and FH2-Ci-0.01, the adsorption of arsenic on FH2-Ci-0.1 was considerably lower (Figure 6.10). With an increase in the Ci/Fe molar ratio from 0 to 0.1, the adsorption capacity of arsenite at an initial As addition of 0.0534

mol As (III)/kg decreased by 69.00% for the fresh samples and 79.36% for the aged samples while that of arsenate at an initial As addition of 0.1068 mol As (V)/kg 83.50% for the fresh samples and 92.93% for the aged samples. The great decrease in arsenic adsorption may be attributable to a function of the surface activity of the functional groups (three COOH groups and one OH group) on citrate [49, 192].

After aging for 235 days, arsenic adsorption on the aged FH2s at pH 7 with an equimolar inhibitor/Fe ratio of 0.1 was evaluated to compare their capacities of adsorption (Figure 6.11). With arsenite, adsorption capacity decreased in the order of FH2-Mg-0.1 ≥ FH2 > FH2-Ti-0.1 > FH2-Si-0.1 >> FH2-Ci-0.1. There was no discernable difference in arsenite adsorption between FH2-Mg-0.1, FH2, and FH2-Ti-0.1. However, the adsorption of arsenite on FH2-Si-0.1 was lower while FH2-Ci-0.1 showed the smallest adsorption capacity of arsenite. With arsenate, adsorption capacity followed the order: FH2 ≥ FH2-Mg-0.1 > FH2-Ti-0.1 > FH2-Si-0.1 >> FH2-Ci-0.1. There was no distinct difference in arsenate adsorption between FH2, FH2-Mg-0.1, FH2-Ti-0.1, and FH2-Si-0.1. However, the adsorption of arsenate on FH2-Ci-0.1 was significantly lower with respect to the other aged FH2s.

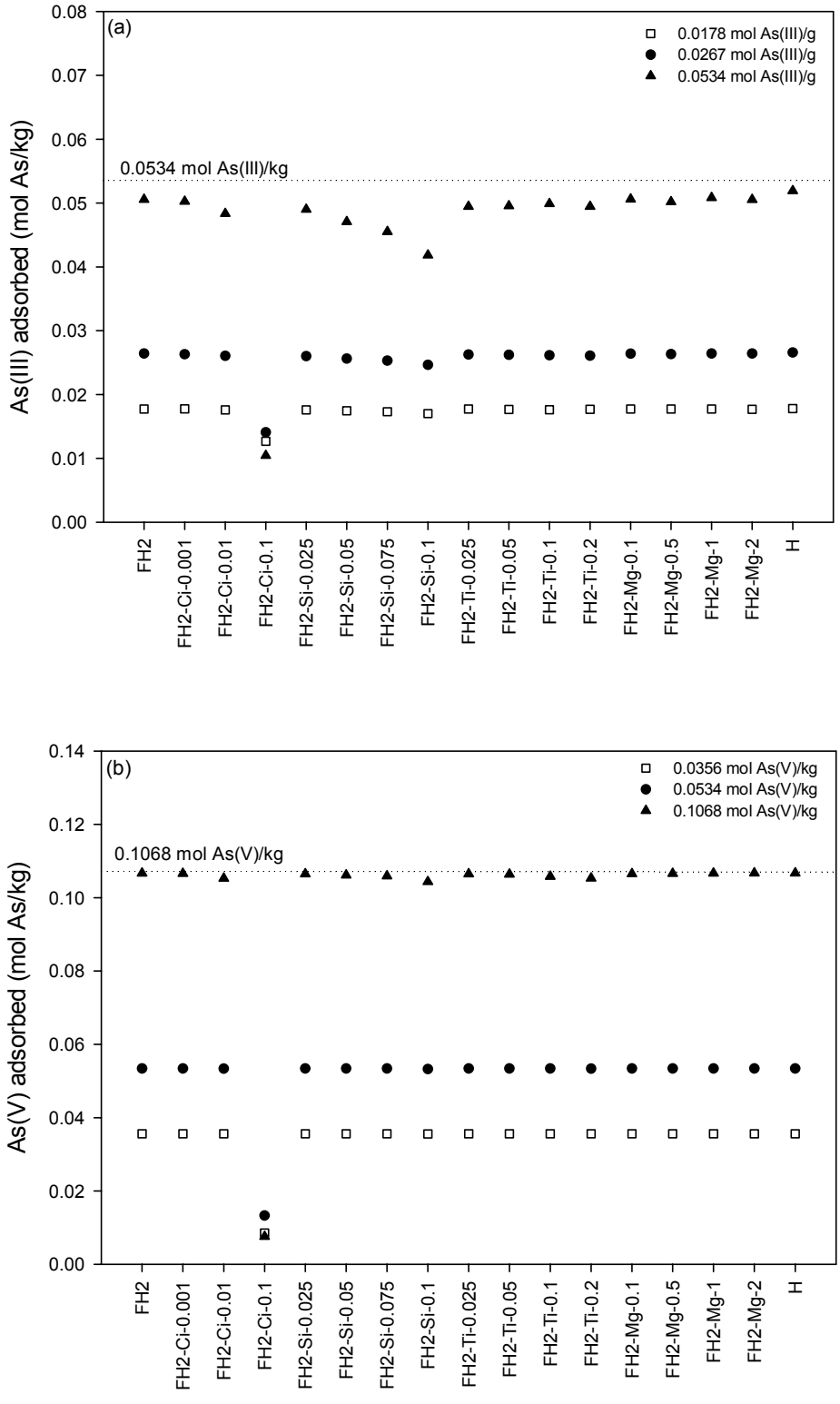

Figure 6.5 Adsorption of As(III) (a) and As(V) (b) on 2-line Ferrihydrites at pH 7 after Aging for 235 Days at Room Temperature.

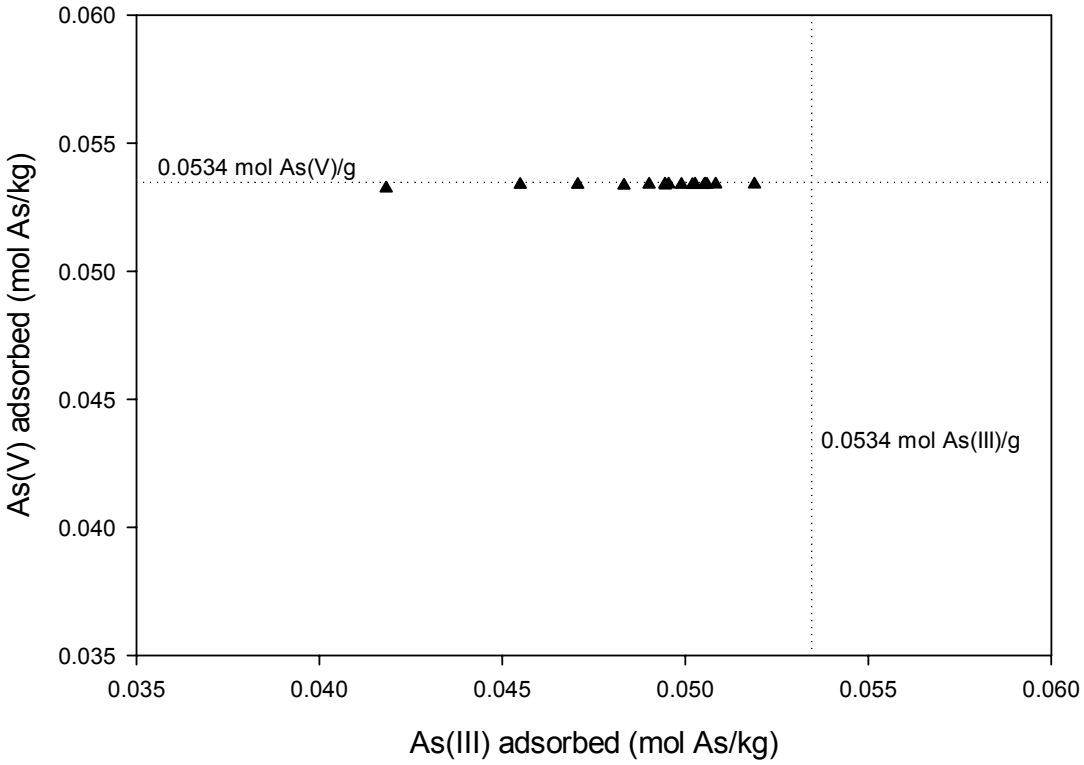

Figure 6.6 Comparison of As(III) Adsorption and As(V) Adsorption on 2-line Ferrihydries with an Initial As Addition of 0.0534 mol As/kg Sample at pH 7 after Aging 235 Days at Room Temperature.

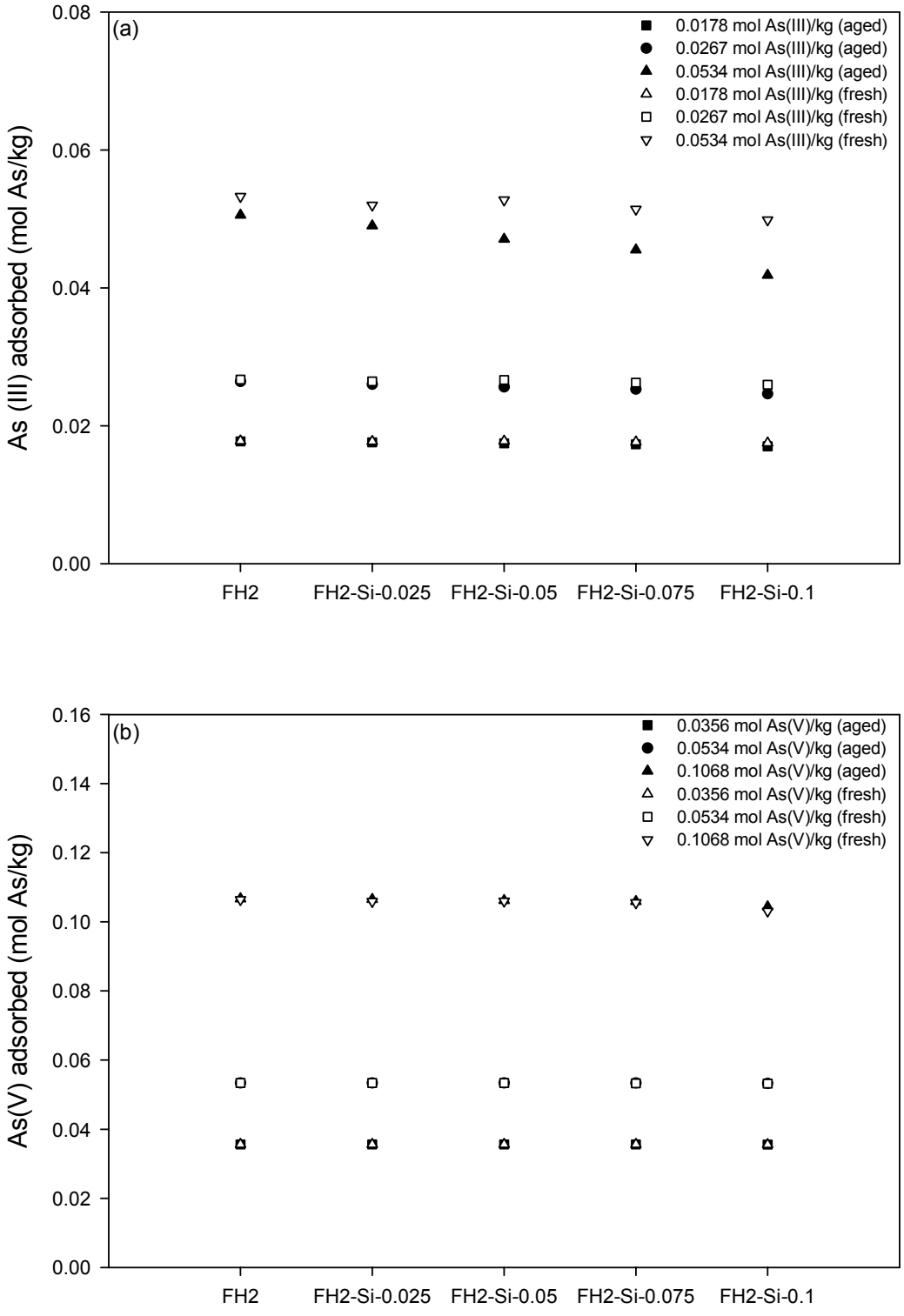

Figure 6.7 Effect of Aging (235 Days) on Adsorption of As(III) (a) and As(V) (b) on FH2-Si Series at pH 7.

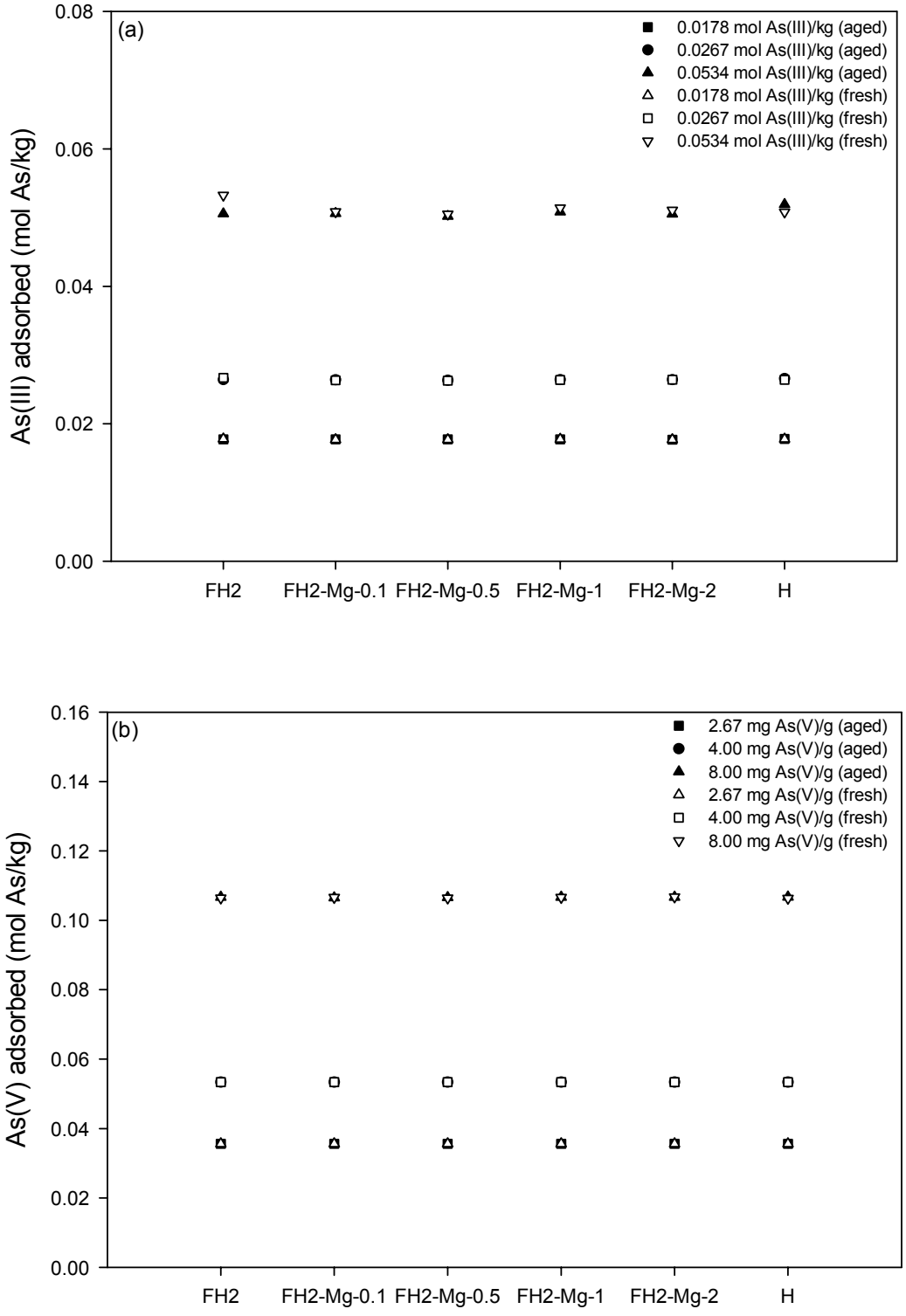

Figure 6.8 Effect of Aging (235 Days) on Adsorption of As(III) (a) and As(V) (b) on FH2-Mg Series and HTlc at pH 7.

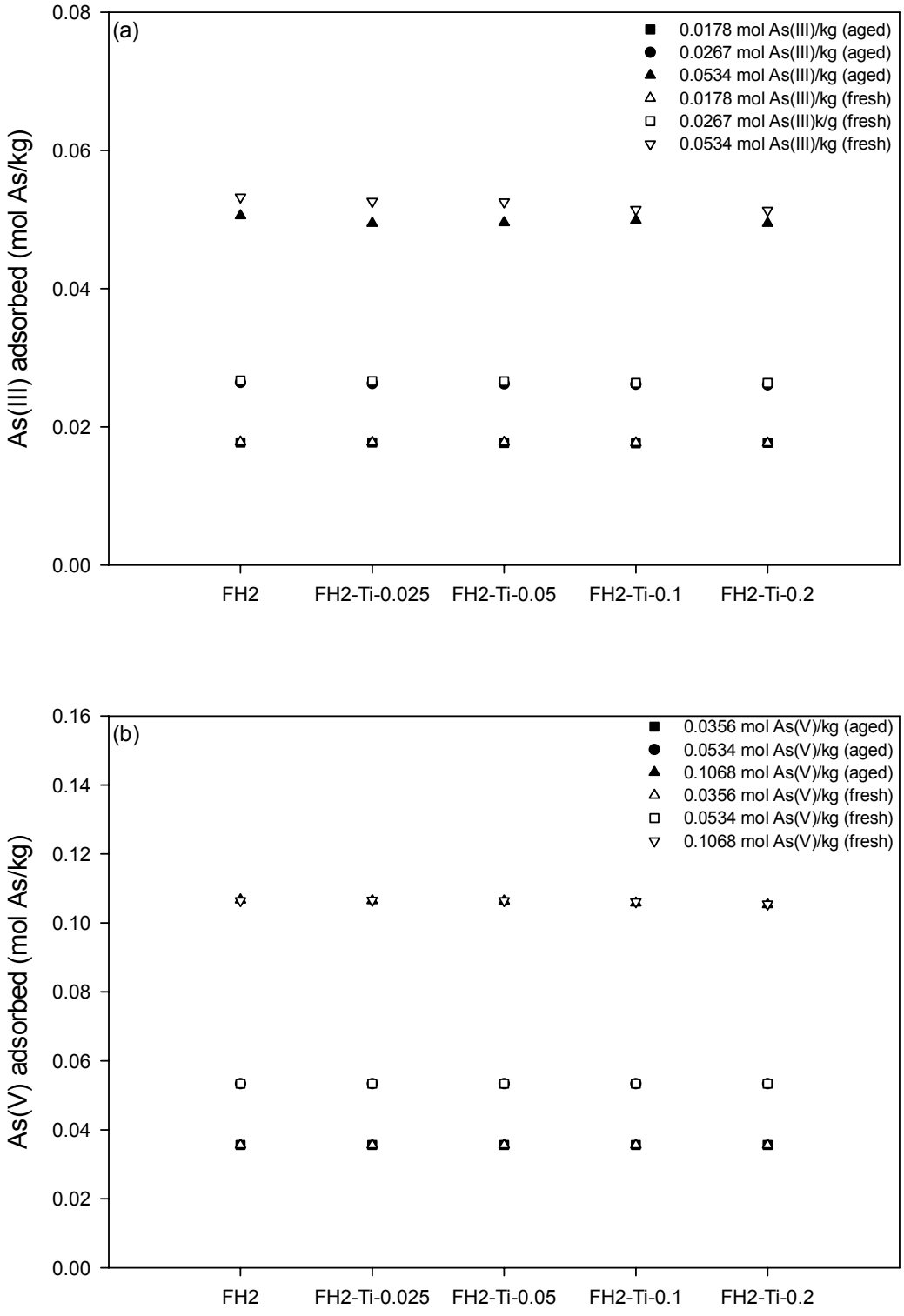

Figure 6.9 Effect of Aging (235 days) on Adsorption of As(III) (a) and As(V) (b) on FH2-Ti Series at pH 7.

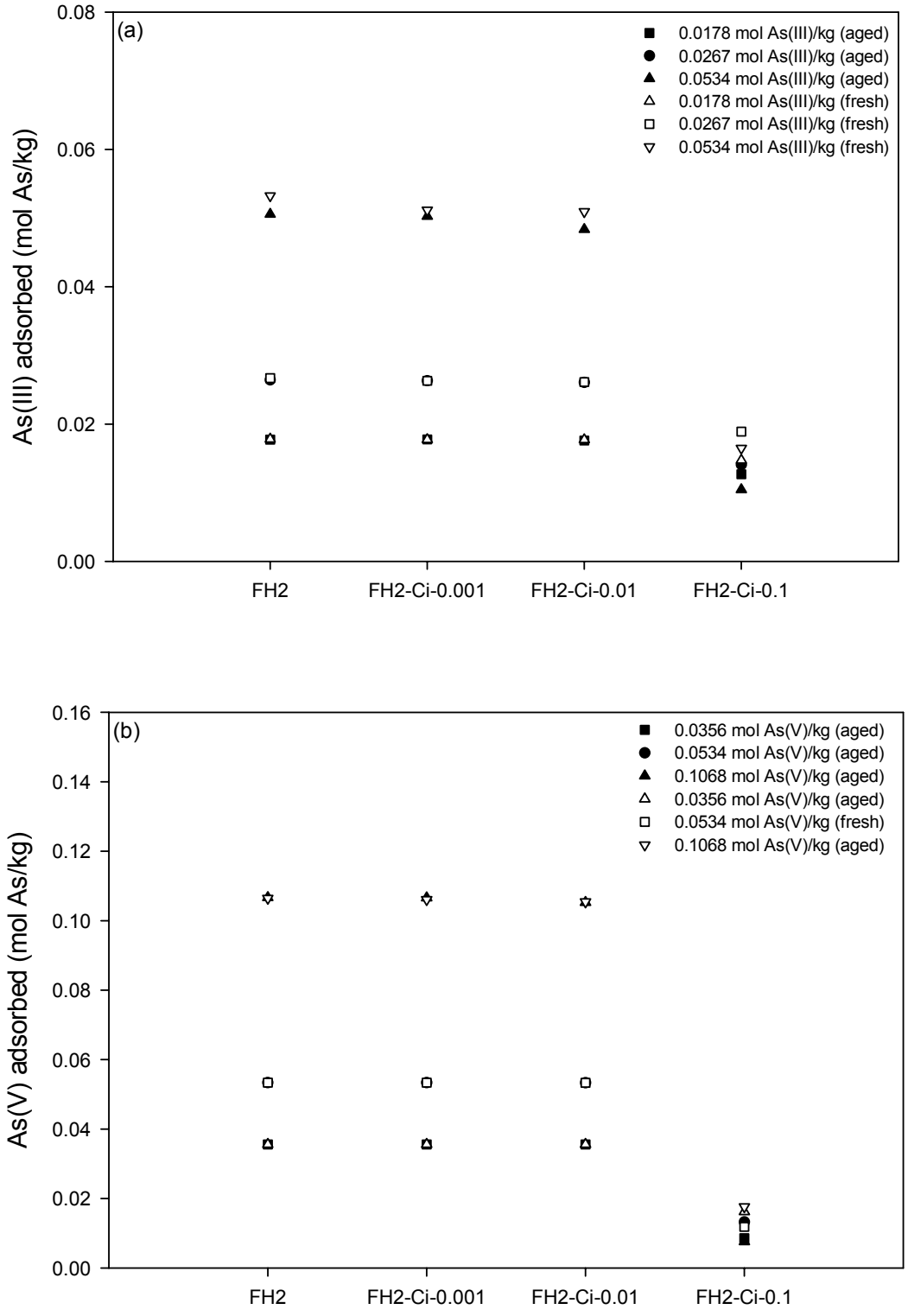

Figure 6.10 Effect of Aging (235 days) on Adsorption of As(III) (a) and As(V) (b) on FH2-Ci Series at pH 7.

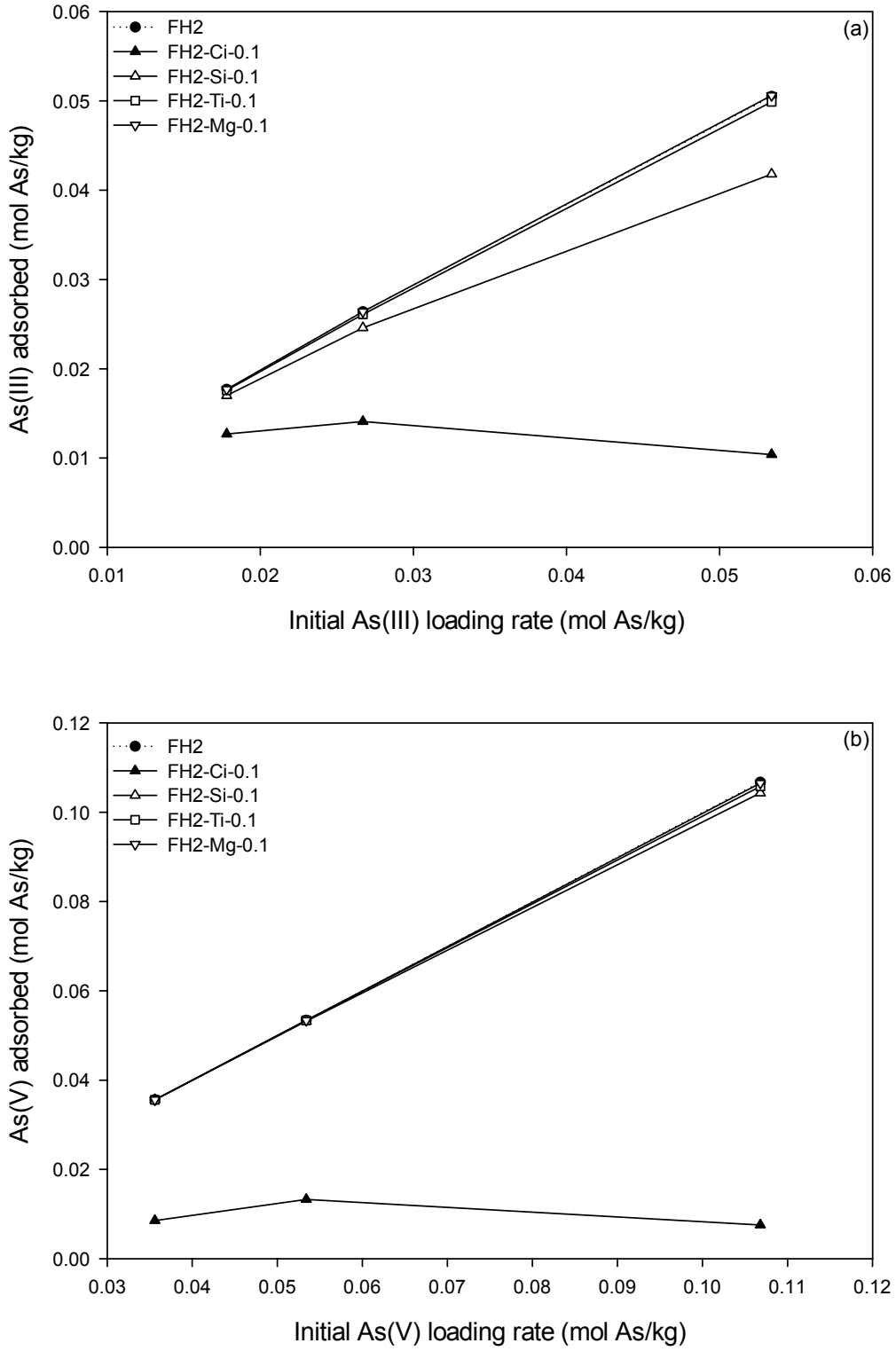

Figure 6.11 Adsorption of As(III) (a) and As(V) (b) on 2-line Ferrihydrites with an Inhibitor/Fe Molar Ratio of 0.1 at pH 7 after Aging 235 Days at Room Temperature.

6.2.3 Effect of Heat Treatment on Arsenic Adsorption

6.2.3.1 An Overview of Arsenic Adsorption on Heat-treated 2-line Ferrihydrites

Adsorption experiments for the FH2s heated at 360 ^{o}C for 12 h were performed at pH 7 and at low arsenic loading rates (0.0178, 0.0267, and 0.0534 mol As (III)/kg and 0.0356, 0.0534, and 0.1068 mol As (V)/kg). The adsorption experiment for FH2-Ci-0.1 was not carried out in this study due to the low adsorption capacity of arsenic as shown in adsorption studies of arsenic on both fresh and aged samples (sections 6.2.1 and 6.2.2).

The adsorption capacity of arsenite on the heated FH2s decreased in the order of HTlc > FH2-Mg-2 > FH2-Mg-1 > FH2-Mg-0.1 > FH2-Mg-0.5 > FH2-Ti-0.1 > FH2-Ti-0.025 > FH2-Si-0.05 > FH2-Ti-0.05 > FH2-Al-0.25 > FH2-Si-0.025 > FH2-Ti-0.2 > FH2-Ci-0.01 > FH2-Si-0.075 > FH2-Al-0.5 > FH2-Si-0.1 > FH2-Ci-0.001 > FH2-Al-1 > FH2 while that of arsenate on the heated FH2s followed the order: HTlc > FH2-Al-1 > FH2-Al-0.5 > FH2-Al-0.25 > FH2-Al-0.1 > FH2-Si-0.05 > FH2-Si-0.075 > FH2-Si-0.1 > FH2-Si-0.025 > FH2-Mg-1 > FH2-Mg-2 > FH2-Ti-0.025 > FH2-Mg-0.1 > FH2-Ti-0.05 > FH2-Ti-0.2 > FH2-Ti-0.1 > FH2-Mg-0.5 > FH2 > FH2-Ci-0.001 > FH2-Ci-0.01 (Figure 6.12). The results indicated that the adsorption capacity of arsenic on the heated FH2 was generally lower than that of arsenic on any other heated FH2.

After heat treatment, the percentage adsorption for arsneite on FH2 at 0.0534 mol As (III)/kg decreased from 99.73% (for the fresh FH2) to 73.24% while that of arsenate on FH2 at 0.1068 mol As (V)/kg reduced considerably from 99.68% (for the fresh FH2) to 49.87%. Compared with the other heated FH2s, the considerable reduction in the percentage adsorption of arsenic on the heated FH2 may be attributed to a decrease in the amount of amorphous Fe oxide through the complete conversion (99.48%) of 2-line

ferrihydrite to hematite, a crystalline iron oxide, which likely contributed to the adsorption of arsenic in smaller amounts than 2-line ferrihydrite. In contrast, after heating 360 ^{o}C, HTlc still showed the high adsorption capacity of arsenic, that is, arsenic removals by HTlc were 96.83% for arsenite (at 0.0534 mol As (III)/kg) and 99.17% for arsenate (at 0.1068 mol As (V)/kg), respectively. Especially the heated HTlc, FH2-Al series, FH2-Si-0.05, FH2-Si-0.075, and FH2-Si-0.1 showed much higher adsorption capacities of arsenate than any other FH2. After heat treatment, the fraction of amorphous Fe oxide was determined to be nearly 100% for HTlc, 12.79~27.98% for the FH2-Al series, and 22.91~42.89% for FH2-Si-0.05, FH2-Si--0.075, and FH2-Si-0.1, respectively. The larger amount of the remaining amorphous Fe oxide may be in part responsible for the higher adsorption capacity of arsenate.

A comparison between arsenite and arsenate adsorptions on the heated FH2s at 0.0534 mol As/kg is shown in Figure 6.13. Compared to the fresh and aged FH2s (Figures 6.3 (a) and 6.6), a trend was observed: arsenate was adsorbed slightly larger than or equal to arsenite after heating at 360 ^{o}C, while arsenate was adsorbed in much larger amounts than arsenite for both the fresh and the aged FH2s (Figure 6.14). The result indicates that the adsorption of arsenate was more greatly affected by heat-treatment at 360 ^{o}C than that of arsenite. Especially, the adsorption capacity of arsenate on the heated FH2, FH2-Ci, FH2-Ti, and FH2-Mg series substantially decreased. The decrease in arsenate adsorption may be in part attributable to the lower fraction of the remaining 2-line ferrihydrite in the heated FH2, FH2-Ci, FH2-Ti, and FH2-Mg series (0.42~1.24%) with respect to the heated Si and Al series (3.81~42.89%).

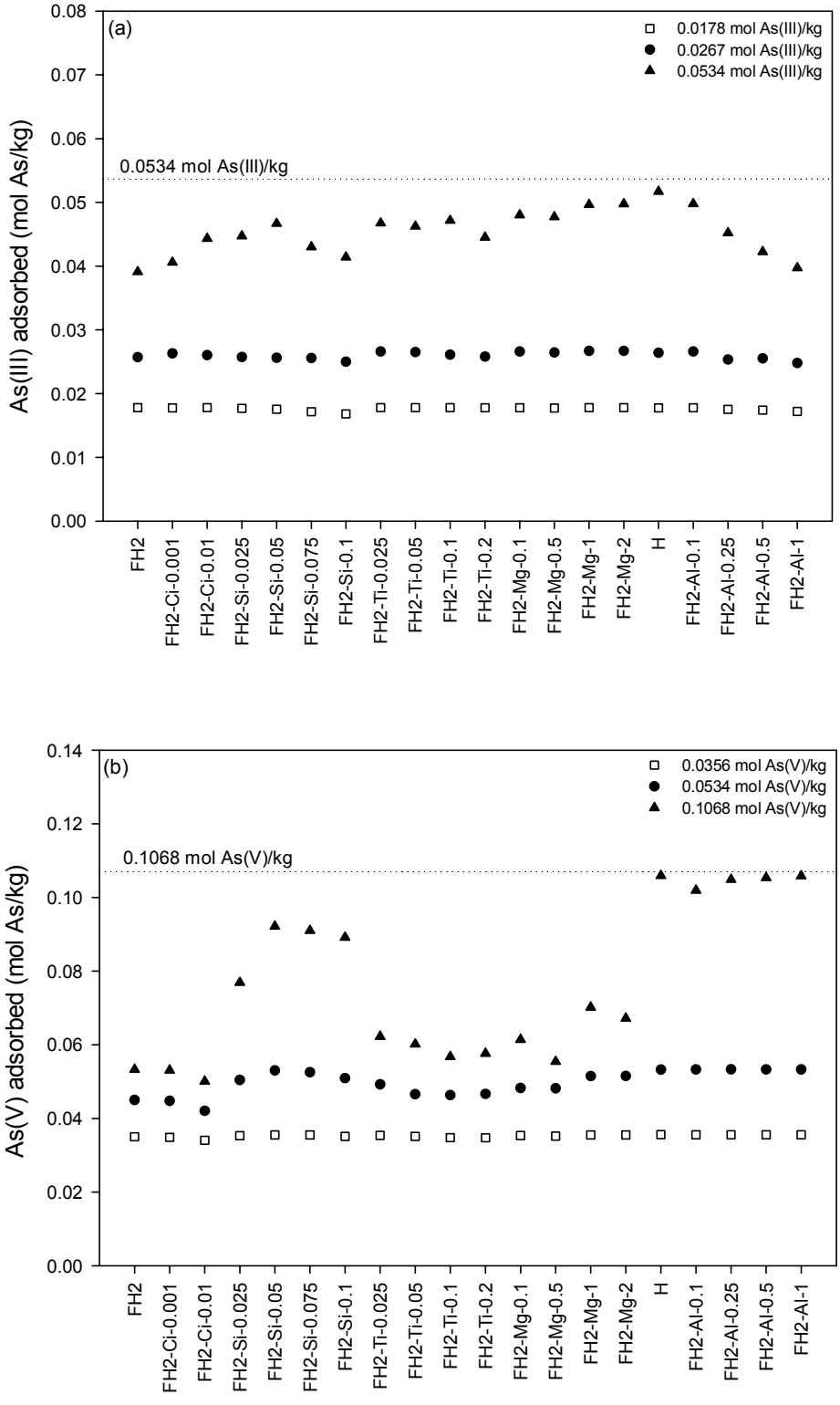

Figure 6.12 Adsorption of As(III) (a) and As(V) (b) on 2-line Ferrihydrites at pH 7 after Heat-Treating at 360 ^{o}C for 12 h.

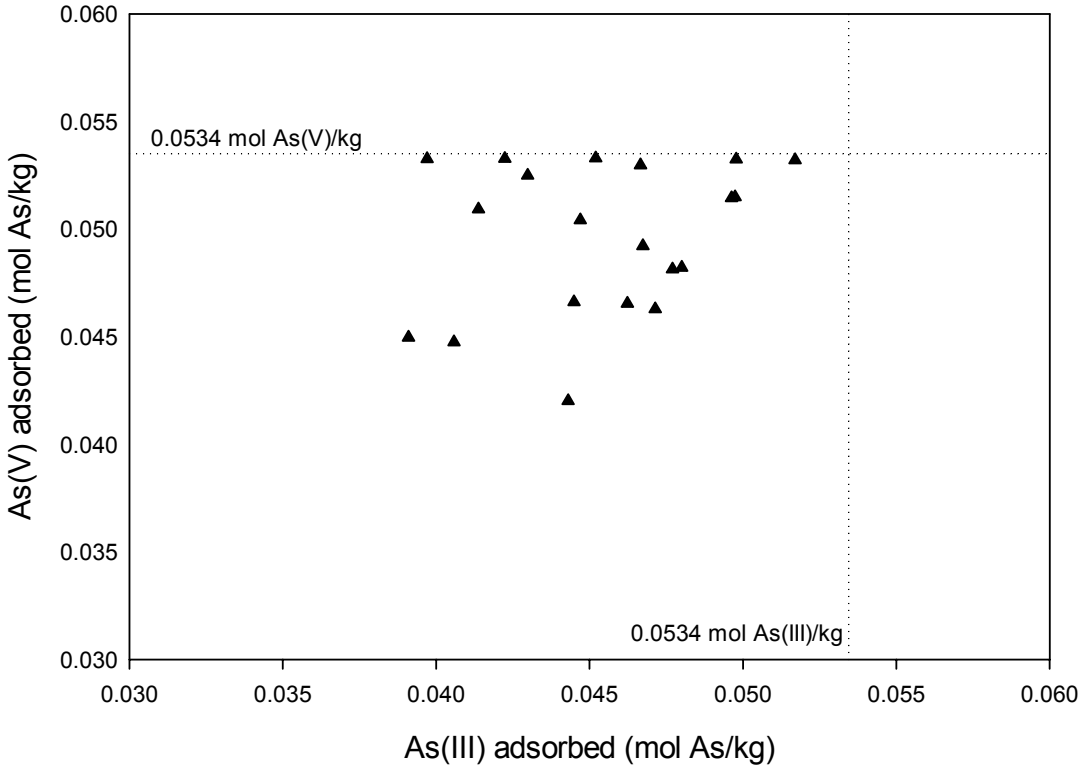

Figure 6.13 Comparison of As(III) Adsorption and As(V) Adsorption on 2-line Ferrihydrites with an Initial As Addition of 0.0534 mol As/kg Sample at pH 7 after Heat-Treating at 360 ^{o}C for 12 h.

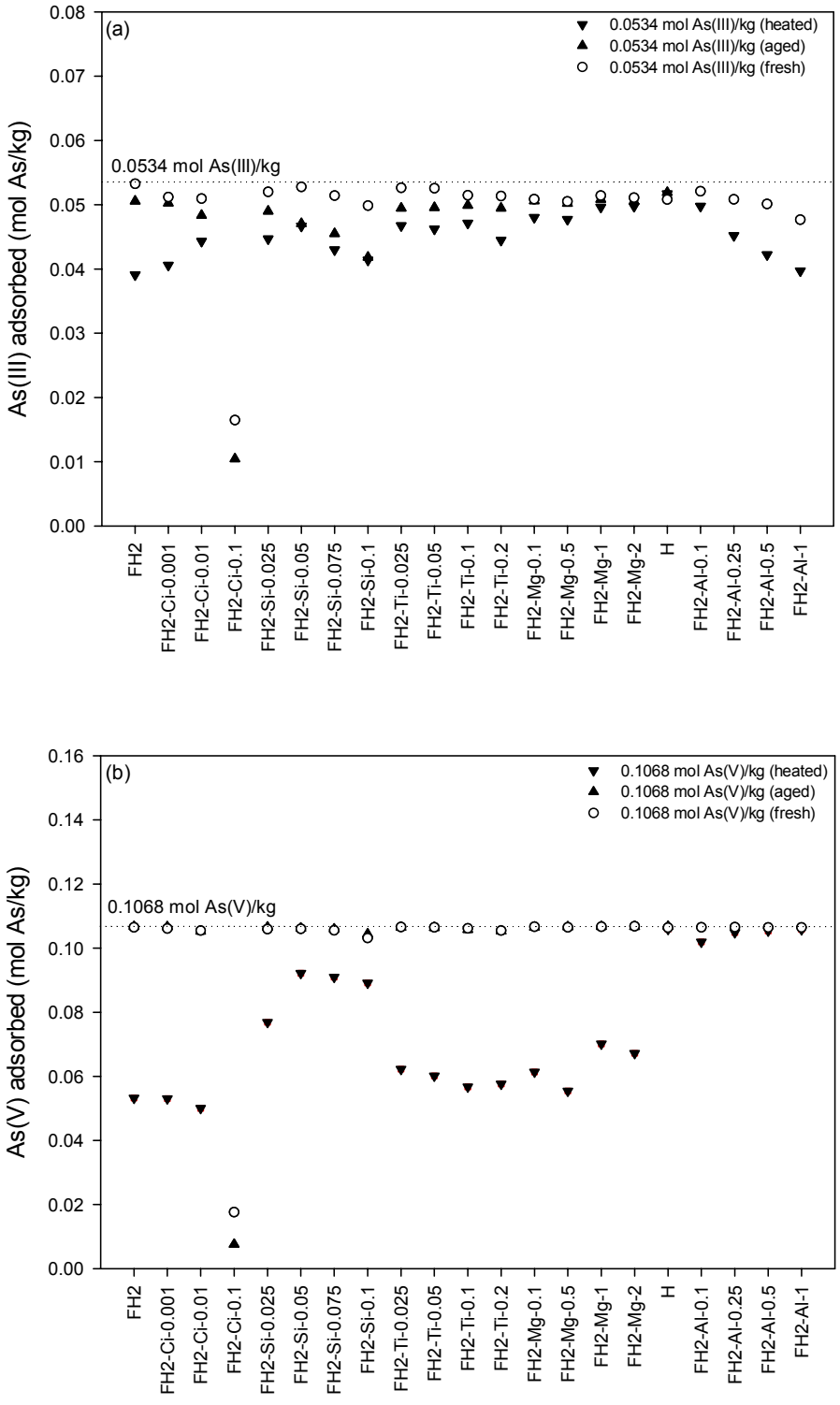

Figure 6.14 Comparison of Aging (235 days) Effect and Heat Treatment (360 ^{o}C) Effect on Adsorption of As(III) (a) and As(V) (b) on 2-line Ferrihydrites at pH 7.

6.2.3.2 Effect of Heat Treatment on Adsorption of Arsenic on FH2-Si series

The results of arsenic adsorption on the heated FH2-Si series at pH 7 are given in Table 6.1 and Figure 6.15. After heat-treating at 360 ^{o}C for 12 h, compared with the adsorption of arsenic on the fresh FH2-Si series, the percentage adsorption for arsenite at 0.0534 mol As (III)/kg decreased by 26.57% for FH2 and 11.55~17.00% for the FH2-Si series, respectively while that for arsenate at 0.1068 mol As (V)/kg was reduced by 49.77% for FH2 and 13.07~27.40% for the FH2-Si series, respectively. The heated FH2-Si-0.05 showed the largest adsorption capacity of both arsenite and arsenate. Although adsorption capacity of both arsenite and arsenate on all heated FH2-Si series was larger than that of the heated FH2, there was no trend between Si/Fe molar ratio and the adsorption capacity of arsenic.

Table 6.1 Adsorption of Arsenic on FH2-Si Series at pH 7 and the Fraction ($[Fe_o]/[Fe_t]$) of Amorphous Iron of FH2-Si Series after Heat-treating at 360 ^{o}C for 12 h.

Type of FH2		FH2	FH2-Si-0.025	FH2-Si-0.05	FH2-Si-0.075	FH2-Si-0.1
As(III)	As(III) adsorbed (mol As/kg sample)[a)]	0.0391	0.0447	0.0467	0.0430	0.0453
	Percentage decrease in adsorption (%)[b)]	26.57	14.02	11.55	16.37	17.00
As(V)	As(V) adsorbed (mol As/kg sample)[a)]	0.0533	0.0769	0.0921	0.0910	0.0891
	Percentage decrease in adsorption (%)[b)]	49.77	27.40	13.07	13.81	13.57
$[Fe_o]$ (mg amorphous Fe/g sample)[c)]		3.24	22.77	138.62	192.38	234.54
Percentage $[Fe_o]/[Fe_t]$ (%)		0.52	3.81	22.91	32.17	42.89

[a)] The adsorption of arsenite and arsenate was performed at an initial As loading of 0.0534 mol As(III) and 0.1068 mol As(V)/g sample, respectively.
[b)] (As adsorbed on fresh sample – As adsorbed on heated sample)/(As adsorbed on fresh sample)
[c)] The remaining amorphous iron content after heat treatment at 360 ^{o} C for 12 h

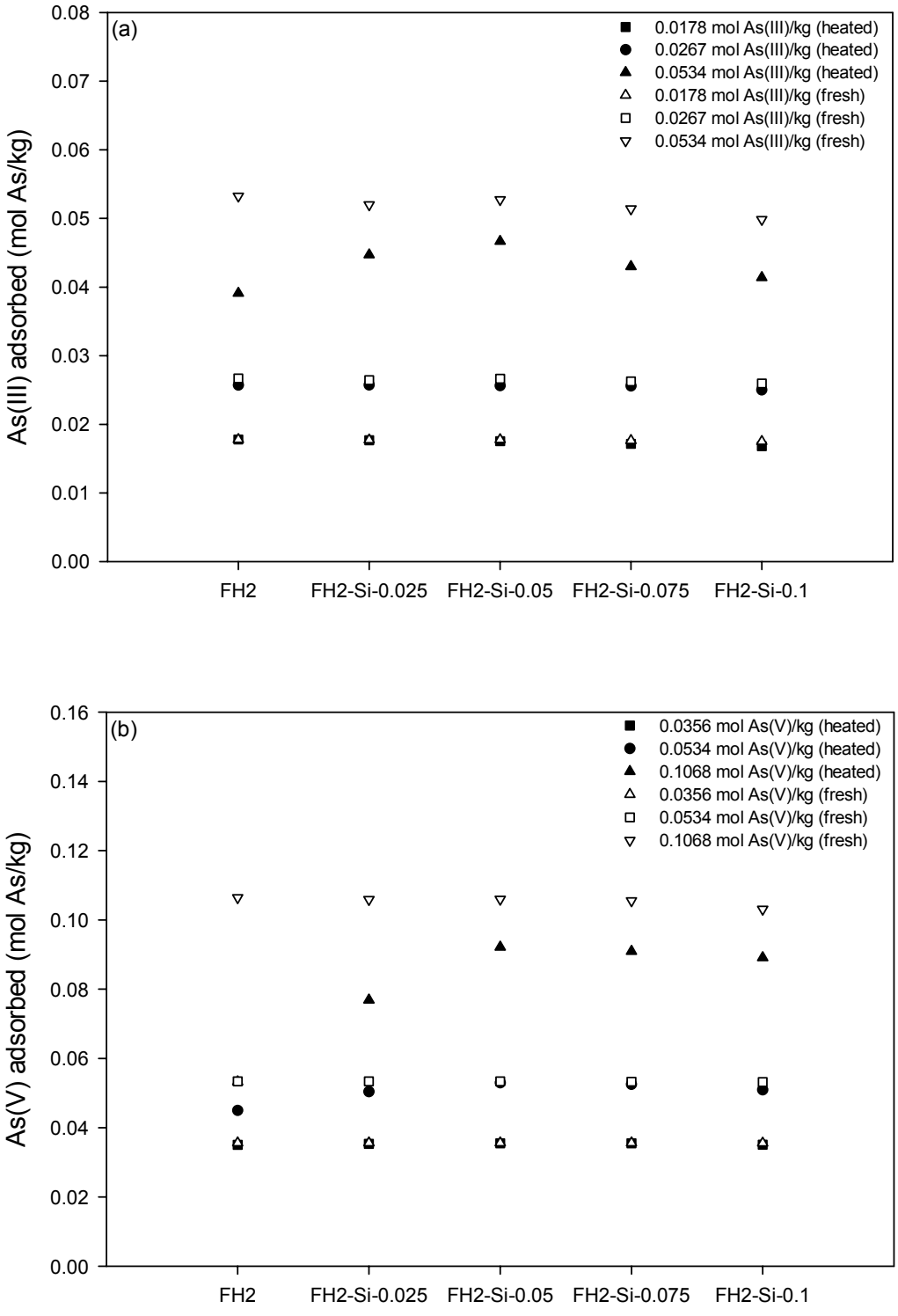

Figure 6.15 Effect of Heat Treatment (360 ^{o}C) on Adsorption of As(III) (a) and As(V) (b) on FH2-Si Series at pH 7.

It was observed in section 5.2.4 that after heating at 360 ^{o}C for 12 h, the fraction ($[Fe_o]/[Fe_t]$) of amorphous Fe oxide decreased to 0.52% for FH2 while for the FH2-Si series it was reduced to 3.81~42.89%. Also the fraction of amorphous Fe oxide for the FH2-Si series increased with increasing the Si/Fe molar ratio and the heated FH2-Si-0.1 showed the highest fraction of amorphous Fe oxide (Table 6.1). It may be assumed by the observation that the heated FH2 consistd nearly exclusively of hematite, a crystalline iron oxide, while the heated FH2-Si-0.1 was made of 42.89% 2-line ferrihydrite and 57.11% hematite. The specific surface area of hematite depends on the synthesis method as well as particle size and shape. The surface area of hematite obtained from solution at less than or about 100 ^{o}C ranges from 10 to 90 m^2/g while for hematite formed by dehydroxylation of ferrihydrite at temperatures lower than 500~600 ^{o}C it is reported up to 200 m^2/g [2], which is lower than that (325.8 m^2/g) of the aged FH2 (section 4.2.4). The formation of hematite through heat treatment can cause a lower specific surface area and then result in a reduction in arsenic adsorption. Therefore, compared with the arsenic adsorption of the heated FH2, higher adsorption capacity of arsenic on the heated FH2-Si series was in part due to larger amounts of the remaining 2-line ferrihydrite after heating.

After heating at 360 ^{o}C for 12 h, the PZC of FH2 shifted from 7.82 to 8.70 whereas for FH-Si-0.1 it moved from 6.90 to 6.30 (section 5.2.6). From the results of PZC determination for the heated FH2 and FH2-Si-0.1, it may be suggested that the PZC values of FH2-Si-0.025, FH2-Si-0.05, and FH2-Si-0.075 ranged from above 6.30 to below 8.70. Although the PZC of the heated FH2 was higher than that of the heated FH2-Si-0.1, the arsenic adsorption capacity on the heated FH2 was less than that of the heated FH2-Si-0.1. The result may be attributed to the difference between the amounts of the

remaining 2-line ferrihydrite after heating. However, although the heated FH2-Si-0.1 showed the highest content ([Fe_o]) of amorphous iron, the heated FH2-Si-0.05 exhibited the largest adsorption capacity of arsenic. It may be in part explained by an assumption that the PZC of FH2-Si-0.05 was higher than that of FH2-Si-0.1 and a more positive surface charge of the heated FH2-Si-0.05 led to higher adsorption of arsenic. There was no distinct trend between Si/Fe molar ratio and the arsenic adsorption on the heated FH2-Si series while the adsorption of arsenic on both the fresh and aged FH2-Si series decreased with an increase in the Si/Fe molar ratio (section 6.2.2). Therefore, it may be concluded that a combined effect of the fraction of amorphous Fe oxide and the net surface charge had an influence on the adsorption of arsenic on the heated FH2-Si series.

6.2.3.3 Effect of Heat Treatment on Adsorption of Arsenic on FH2-Mg series

The results of arsenic adsorption on the heated FH-Mg series and HTlc at pH 7 are shown in Table 6.2 and Figure 6.16. After heat treatment at 360 ^{o}C, compared to the adsorption of arsenic on the fresh FH2-Mg series, the percentage adsorption for arsenite at 0.0534 mol As (III)/kg decreased by 2.62~5.58% for the FH2-Mg series (26.57% for FH2) while that for arsenate at 0.1068 mol As (V)/kg was reduced by 34.25~47.92% for the FH2-Mg series (49.77% for FH2). A considerable reduction in arsenate adsorption on the FH2-Mg series was observed whereas the adsorption of arsenite on them decreased slightly. The heated FH2-Mg-2 showed the largest adsorption capacity of arsenite while the heated FH2-Mg-1 exhibited the highest adsorption capacity of arsenate. Although adsorption capacity of both arsenite and arsenate on the heated FH2-Mg series was larger than that of the heated FH2, there was no evident trend between the Mg/Fe molar ratio

and the adsorption capacity of arsenic. However, generally the arsenic adsorption capacity for the FH2-Mg series with higher Mg/Fe molar ratios was larger than that for the FH2-Mg series with lower Mg/Fe molar ratios.

Table 6.2 Adsorption of Arsenic on FH2-Mg Series and HTlc at pH 7 and the Fraction of Amorphous Iron of FH2-Si Series and HTlc after Heat-treating at 360 ^{o}C for 12 h.

Type of FH2		FH2	FH2-Mg-0.1	FH2-Mg-0.5	FH2-Mg-1	FH2-Mg-2	HTlc
As (III)	As(III) adsorbed (mol As/kg sample)[a)]	0.0391	0.0480	0.0477	0.0496	0.0497	0.0517
	Percentage decrease in adsorption (%)[b)]	26.57	5.58	5.55	3.43	2.62	-1.74
As (V)	As(V) adsorbed (mol As/kg sample)[a)]	0.0533	0.0614	0.0554	0.0701	0.0672	0.1059
	Percentage decrease in adsorption (%)[b)]	49.77	42.42	47.92	34.25	37.08	0.43
[Fe_o] (mg amorphous Fe/g sample)[c)]		3.24	4.70	4.81	4.29	7.68	385.15
Percentage [Fe_o]/[Fe_t] (%)		0.52	0.79	0.80	0.72	1.24	100

[a)] The adsorption of arsenite and arsenate was performed at an initial As loading of 0.0534 mol As(III) and 0.1068 mol As(V)/g sample, respectively.
[b)] (As adsorbed on fresh sample – As adsorbed on heated sample)/(As adsorbed on fresh sample)
[c)] The remaining amorphous iron content after heat treatment at 360 ^{o} C for 12 h

As discussed in section 5.2.4, after heating at 360 ^{o}C, the fraction ([Fe_o]/[Fe_t]) of amorphous Fe oxide of the FH2-Mg series reduced to 0.72~1.24%, which was slightly larger than that (0.52%) of the heated FH2. The heated FH2-Mg-2 showed the highest fraction of amorphous Fe oxide (Table 6.2). From the results of the transformation study, the FH2-Mg series were assumed to consist nearly of hematite. After heating at 360 ^{o}C, the PZC of FH-Mg-2 shifted from 7.90 to 8.90 due to the formation of hematite by heat treatment (section 5.2.6) and its PZC was slightly higher than that (8.70) of the heated FH2. Based on the results of transformation studies of the FH2-Mg series and the PZC determination of FH2-Mg-2, it may be suggested that higher adsorption capacity of arsenic on the heated FH2-Mg series may be due to both a larger fraction of amorphous

Fe oxide of the heated FH2-Mg series and a higher PZC value of the heated FH2-Mg series with respect to the heated FH2.

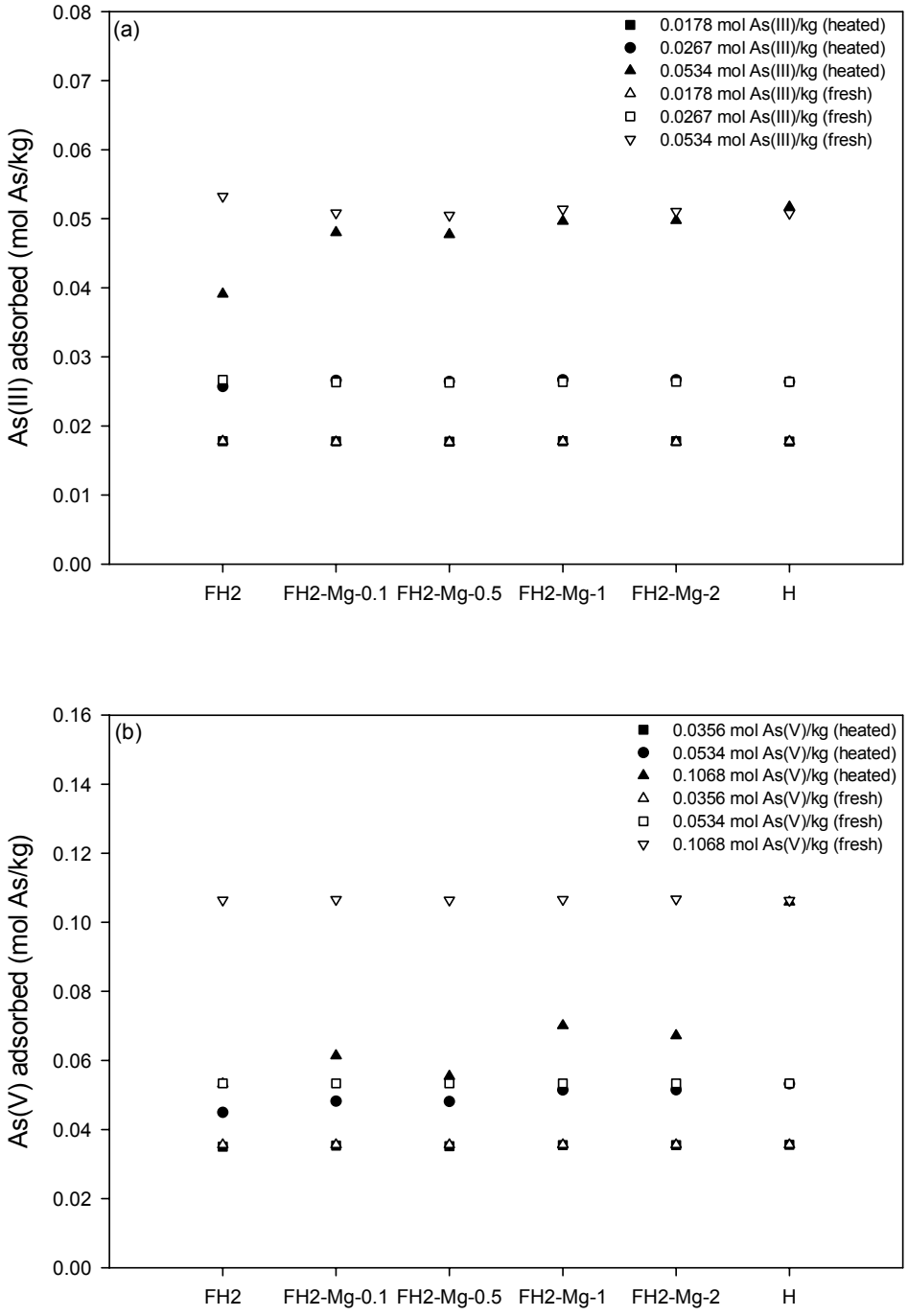

Figure 6.16 Effect of Heat Treatment (360 ^{o}C) on Adsorption of As(III) (a) and As(V) (b) on FH2-Mg Series and HTlc at pH 7.

After heat treatment at 360 ^{o}C, the heated HTlc still showed the high adsorption capacity of arsenic, that is, arsenic removal by the heated HTlc was 96.83% for arsenite (at 0.0534 mol As (III)/kg) and 99.17% for arsenate (at 0.1068 mol As (V)/kg). Upon heating HTlc at 360 ^{o}C, the transformation of amorphous Fe oxide was not observed (section 5.2.4 and Table 6.2). As shown in sections 4.2.3 and 4.2.4, compared with the other aged FH2s, the aged HTlc had a lower specific surface area of 144.9 m^2/g (229.3~325.8 m^2/g for the other aged FH2s) and a larger particle size of 2.797 μm (2.175~2.389 μm for the other aged FH2s). HTlc, a layered double hydroxide, has been known as an inorganic anion-exchanger for removing arsenic, chromates, and humic substances through the intercalation of pollutants into the positively charged innerlayer and the adsorption on hydroxyl groups of the pollutants [247~249]. It has been also known that the main sorption mechanism of calcined HTlc is attributable to the intercalation into the positively charged interlayer whereas for uncalcined material is due to the ion exchange of the interlayer anions (carbonate ions) [250]. Calcined HTlc was reported to be the better sorbent for removing chromium than uncalcined HTlc [247] since the calcination of HTlc resulted in a doubling of surface area through generation of mesopores within the structure and the calcined HTlc (below 500 ^{o}C) could reconstruct its original layer structure with rehydration and sorption of various anions [235, 251]. HTlc bears two types of charges (permanent positive charge and variable charges). The PZC value of HTlc was reported 8.94 with a Mg/Fe molar ratio of 2 [212]. Therefore, the highest adsorption capacity of arsenic on the heated HTlc may be attributable to a combined effect of the intercalation of arsenic into the positively charged interlayer, the increased surface area, and the high PZC value.

6.2.3.4 Effect of Heat Treatment on Adsorption of Arsenic on FH2-Ti series

The results of adsorption of arsenic on the heated FH-Ti series at pH 7 are shown in Table 6.3 and Figure 6.17. Compared with the fresh FH2-Ti series, after heat-treating at 360 ^{o}C, the percentage adsorption for arsenite at 0.0534 mol As (III)/kg decreased by 8.37~13.30% for the FH2-Ti series (26.57% for FH2) while that for arsenate at 0.1068 mol As (V)/kg was reduced by 41.59~46.55% for the FH2-Ti series (49.77% for FH2). A reduction in arsenate adsorption on the FH2-Ti series was much larger than that in arsenite adsorption. The heated FH2-Ti-0.1 showed the largest adsorption capacity of arsenite while the heated FH2-Ti-0.025 exhibited the highest adsorption capacity of arsenate. Although the adsorption capacity of both arsenite and arsenate on the heated FH2-Ti series was larger than that of heated FH2, no distinct trend between the Ti/Fe molar ratio and the adsorption capacity of arsenic was observed. However, the arsenate adsorption capacity for the FH2-Ti series with lower Ti/Fe molar ratios (FH2-Ti-0.025 and FH2-Ti-0.05) was larger than that for the FH2-Ti series with higher Mg/Fe molar ratios (FH2-Ti-0.1 and FH2-Ti-0.2) although FH2-Ti-0.1 and FH2-Ti-0.2 contained slightly larger amounts of amorphous Fe oxide compared to FH2-Ti-0.025 and FH2-Ti-0.05.

After heating at 360 ^{o}C, the fraction ($[Fe_o]/[Fe_t]$) of amorphous Fe oxide of the FH2-Ti series decreased to 0.66~0.95% (section 5.2.4), which was slightly larger than that (0.52%) of the heated FH2. The heated FH2-Ti-0.2 showed the highest fraction of amorphous Fe oxide while the heated FH2-Ti-0.1 exhibited the highest content of amorphous iron (Table 6.2). From the results of the transformation and XRD studies, the heated FH2-Ti series were assumed to consist of hematite with traces of crystalline

anatase TiO_2, peaks of which was evident with increasing the Ti/Fe molar ratio (section 5.2.5). However, the effect of oxidation of arsenite to arsenate by TiO_2 has not been considered in this study because the adsorption study was perform for a short time (48 hr) and the oxidation of arsenite to arsenate has been known to be kinetically a slow process [126]. The PZC of crystalline anatase TiO_2 was to be reported 6.0 [252]. The crystalline anatase TiO_2 may lead to the change of the FH2-Ti series surface charge from positive to more negative charge. Therefore, although FH2-Ti-0.1 and FH2-Ti-0.2 contained slightly larger amounts of amorphous Fe oxide compared to FH2-Ti-0.025 and FH2-Ti-0.05 due to retardation of amorphous Fe oxide transformation by larger amounts of Ti, the formation of larger amounts of TiO_2 led to the shift of the net surface charge to somewhat more negative, resulting in a slight decrease in arsenic adsorption.

Table 6.3 Adsorption of Arsenic on FH2-Ti Series at pH 7 and the Fraction of Amorphous Iron of FH2-Ti Series after Heat-treating at 360 ^oC for 12 h.

Type of FH2		FH2	FH2-Ti-0.025	FH2-Ti-0.05	FH2-Ti-0.1	FH2-Ti-0.2
As (III)	As(III) adsorbed (mol As/kg sample)[a)]	0.0391	0.0467	0.0462	0.0471	0.0445
	Percentage decrease in adsorption (%)[b)]	26.57	11.14	12.02	8.37	13.30
As (V)	As(V) adsorbed (mol As/kg sample)[a)]	0.0533	0.0622	0.0602	0.0567	0.0576
	Percentage decrease in adsorption (%)[b)]	49.77	41.59	43.49	46.55	45.34
$[Fe_o]$ (mg amorphous Fe/g sample)[c)]		3.24	3.92	3.95	5.07	4.67
Percentage $[Fe_o]/[Fe_t]$ (%)		0.52	0.66	0.70	0.94	0.95

[a)] The adsorption of arsenite and arsenate was performed at an initial As loading of 0.0534 mol As(III) and 0.1068 mol As(V)/g sample, respectively.
[b)] (As adsorbed on fresh sample – As adsorbed on heated sample)/(As adsorbed on fresh sample)
[c)] The remaining amorphous iron content after heat treatment at 360 ^{o} C for 12 h

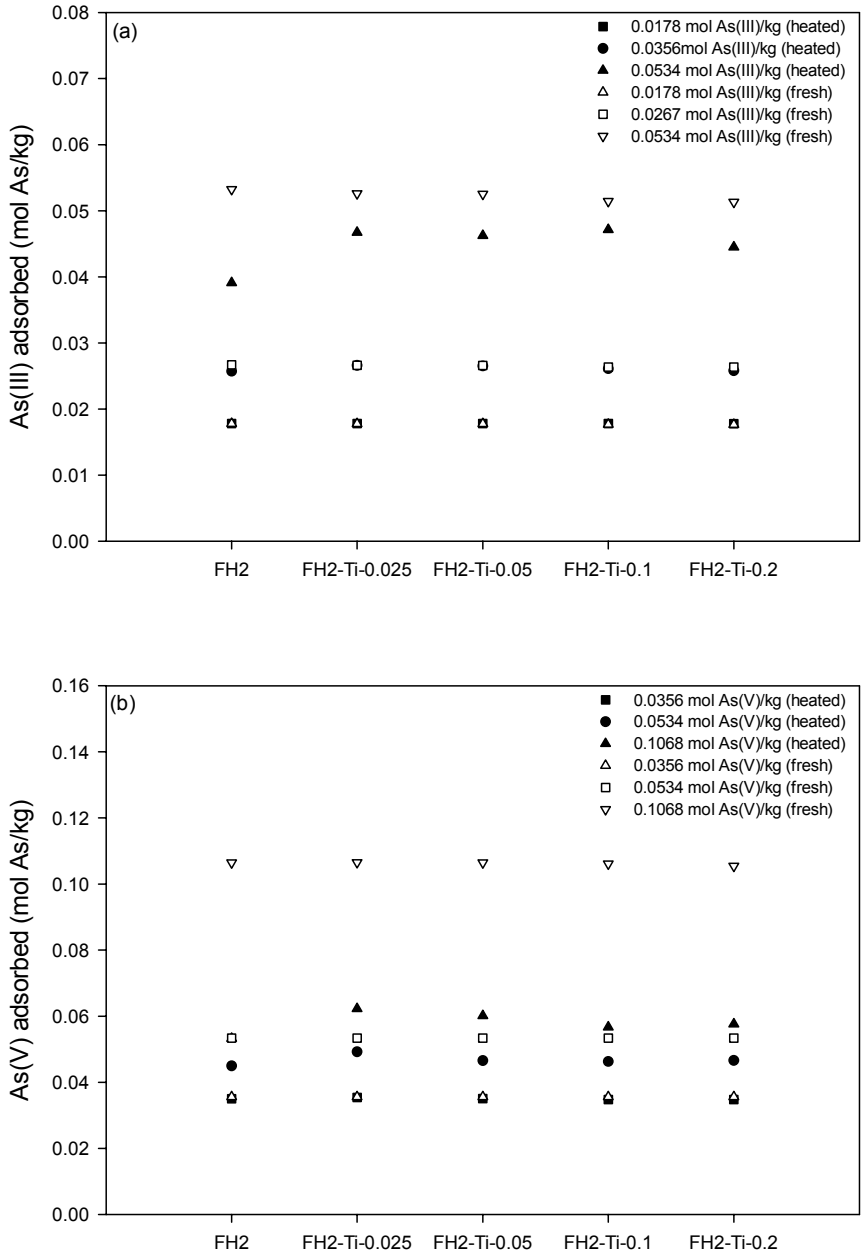

Figure 6.17 Effect of Heat Treatment (360 ^{o}C) on Adsorption of As(III) (a) and As(V) (b) on FH2-Ti Series at pH 7.

6.2.3.5 Effect of Heat Treatment on Adsorption of Arsenic on FH2-Ci series

The results of arsenic adsorption on the heated FH-Ci series at pH 7 are shown in Table 6.4 and Figure 6.18. The adsorption experiment for FH2-Ci-0.1 has not been

carried out in this study due to the lowest adsorption capacity of arsenic as illustrated in adsorption studies of arsenic on both the fresh and aged samples (sections 6.2.1 and 6.2.2). Compared to the adsorption of arsenic on the fresh FH2-Ci series, after heat treatment at 360 ^{o}C, the percentage adsorption for arsenite at 0.0534 mol As (III)/kg decreased by 13.05~20.69% for the FH2-Ci series (26.57% for FH2) while that for arsenate at 0.1068 mol As (V)/kg was reduced by 49.98~52.54% for the FH2-Ci series (49.77% for FH2). Also a decrease in arsenate adsorption on the FH2-Ci series was much larger than that in arsenite adsorption on them. The adsorption capacity of arsenite on the heated FH2-Ci series increased slightly with increasing Ci/Fe molar ratio while that of arsenate decreased somewhat by increasing the ratio. After heating at 360 ^{o}C, the fraction ($[Fe_o]/[Fe_t]$) of amorphous Fe oxide in the FH2-Ci series decreased to 0.42~0.46% (section 5.2.4), which was lower than that (0.52%) of the heated FH2. The heated FH2-Ci series were assumed to consist of crystalline hematite. Based on the results of transformation and adsorption studies, no significant differences between the heated FH2-Ci series and the heated FH2 has not been observed.

Table 6.4 Adsorption of Arsenic on FH2-Ci Series at pH 7 and the Fraction of Amorphous Iron of FH2-Ci Series after Heat-treating at 360 ^{o}C for 12 h.

Type of FH2		FH2	FH2-Ci-0.001	FH2-Ci-0.01
As (III)	As(III) adsorbed (mol As/kg sample)[a)]	0.0391	0.0406	0.0443
	Percentage decrease in adsorption (%)[b)]	26.57	20.69	13.05
As (V)	As(V) adsorbed (mol As/kg sample)[a)]	0.0533	0.0531	0.0500
	Percentage decrease in adsorption (%)[b)]	49.77	49.98	52.54
$[Fe_o]$ (mg amorphous Fe/g sample)[c)]		3.24	2.92	2.61
Percentage $[Fe_o]/[Fe_t]$ (%)		0.52	0.46	0.42

[a)] The adsorption of arsenite and arsenate was performed at an initial As loading of 0.0534 mol As(III) and 0.1068 mol As(V)/g sample, respectively.
[b)] (As adsorbed on fresh sample – As adsorbed on heated sample)/(As adsorbed on fresh sample)
[c)] The remaining amorphous iron content after heat treatment at 360 ^{o} C for 12 h

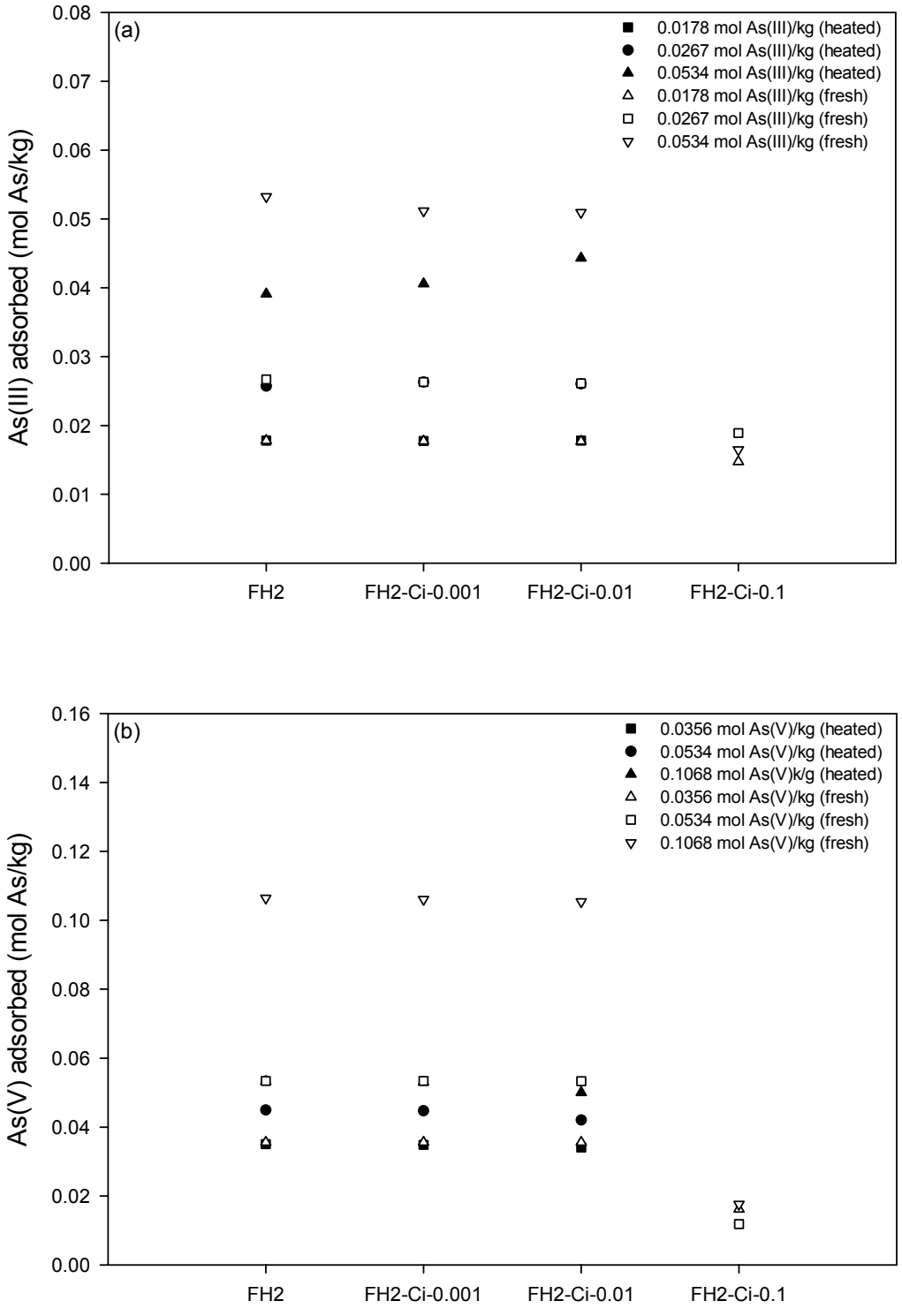

Figure 6.18 Effect of Heat Treatment (360 ^{o}C) on Adsorption of As(III) (a) and As(V) (b) on FH2-Ci Series at pH 7.

6.2.3.6 Effect of Heat Treatment on Adsorption of Arsenic on FH2-Al series

The results of arsenic adsorption on the heated FH-Al series at pH 7 are illustrated in Table 6.5 and Figure 6.19. Compared to the adsorption of arsenic on the fresh FH2-Al series, after heat treatment at 360 ^{o}C, the percentage adsorption for arsenite at 0.0534 mol As (III)/kg decreased by 4.43~16.65% for the FH2-Al series (26.57% for FH2) while that for arsenate at 0.1068 mol As (V)/kg was reduced by 0.75~4.38% for the FH2-Al series (49.77% for FH2). The results indicate that there was a lower decrease in arsenate adsorption compared with that in arsenite adsorption and a much lower reduction in arsenic adsorption with respect to the heated FH2. Specifically, the adsorption capacity of arsenate on the heated FH2-Al series was equal to or slightly less than that of arsenate on the fresh FH2-Al series. The heated FH2-Al-0.1 showed the largest adsorption capacity of arsenite while the heated FH2-Al-1 exhibited the highest adsorption capacity of arsenate.

Table 6.5 Adsorption of Arsenic on FH2-Al Series at pH 7 and the Fraction of Amorphous Iron of FH2-Al Series after Heat-treating at 360 ^{o}C for 12 h.

Type of FH2		FH2	FH2-Al-0.1	FH2-Al-0.25	FH2-Al-0.5	FH2-Al-1
As (III)	As(III) adsorbed (mol As/kg sample)[a)]	0.0391	0.0498	0.0452	0.0422	0.0397
	Percentage decrease in adsorption (%)[b)]	26.57	4.43	11.05	15.70	16.65
As (V)	As(V) adsorbed (mol As/kg sample)[a)]	0.0533	0.1019	0.1048	0.1054	0.1058
	Percentage decrease in adsorption (%)[b)]	49.77	4.38	1.66	1.13	0.75
[Fe_o] (mg amorphous Fe/g sample)[c)]		3.24	68.63	118.69	100.19	89.16
Percentage [Fe_o]/[Fe_t] (%)		0.52	12.79	25.96	24.61	27.98

[a)] The adsorption of arsenite and arsenate was performed at an initial As loading of 0.0534 mol As(III) and 0.1068 mol As(V)/g sample, respectively.
[b)] (As adsorbed on fresh sample – As adsorbed on heated sample)/(As adsorbed on fresh sample)
[c)] The remaining amorphous iron content after heat treatment at 360 ^{o} C for 12 h

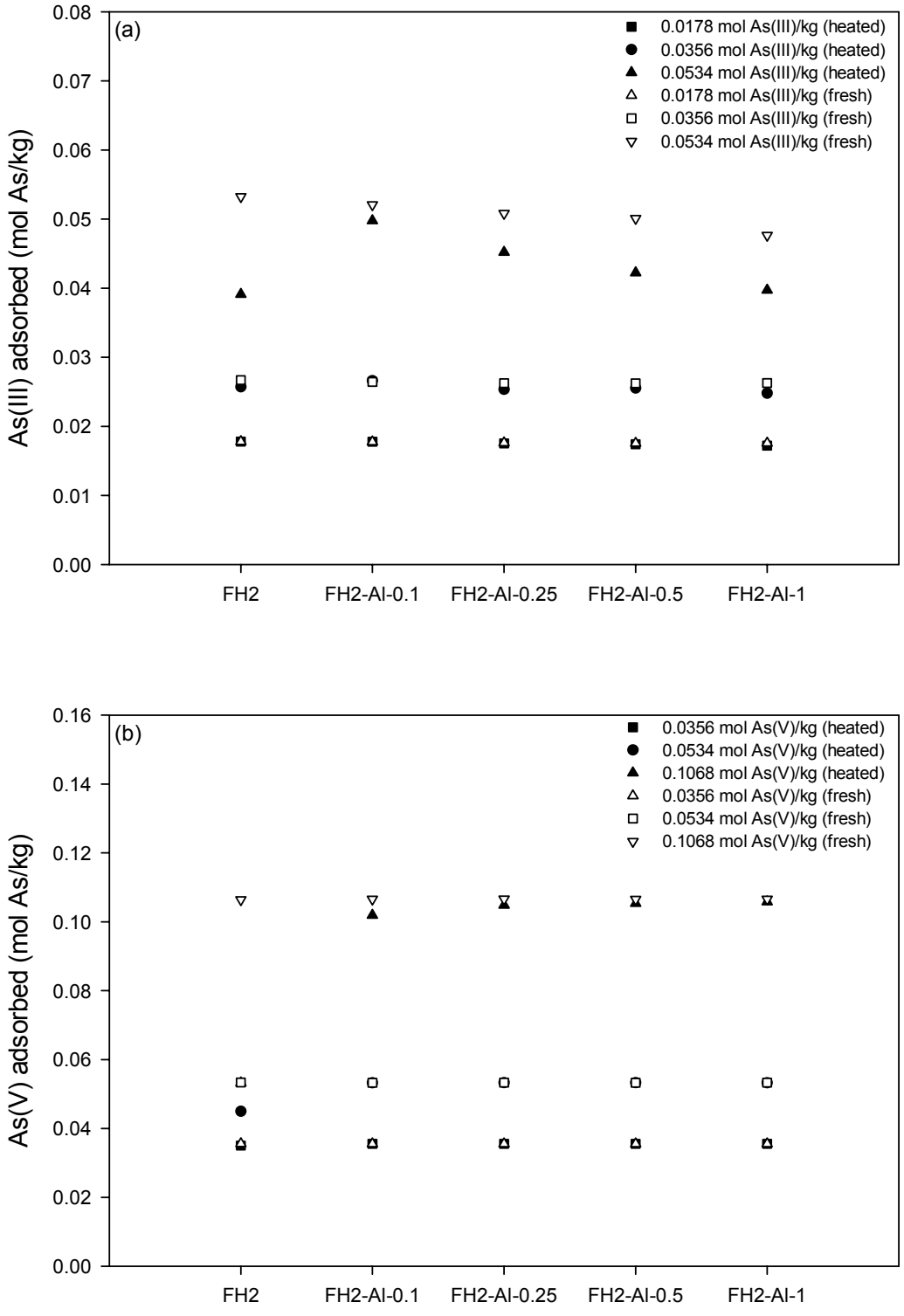

Figure 6.19 Effect of Heat Treatment (360 ^{o}C) on Adsorption of As(III) (a) and As(V) (b) on FH2-Al Series at pH 7.

With arsenite, there was a trend that the adsorption capacity on the heated FH2-Al series decreased with increasing the Al/Fe molar ratio. With increasing the Al/Fe molar ratio, the extent of the decrease was steeper in the heated FH2-Al series with respect to the fresh FH2-Al series. The decrease in arsenite adsorption with increasing the Al/Fe molar ratio indicates that arsenite adsorption at higher Al/Fe molar ratios may be attributable to adsorption by 2-line ferrihydrite [30]. The reduction in arsenite adsorption with increasing the Al/Fe molar ratio may be attributable to the weak affinity for arsenite on Al hydoxides [195] and the mode of bonding of arsenite, outer-sphere complexation by amorphous Al hydroxides [168] and inner-sphere or outer-sphere complexation by crystalline Al hydroxides (gibbsite) at a pH of > 5.5 [196].

In contrast, there were no significant variations in arsenate adsorption on the heated FH2-Al series. However, it has been reported that arsenate adsorption on Al:Fe hydroxides in solution phase decreased with increasing the Al/Fe molar ratio [30]. The disagreement might be attributed to different experimental conditions (adsorbent type and initial As loading rate) and the different extent of transformation of adsorbents by heat treatment. Compared to arsenite adsorption, the high adsorption capacity of arsenate on the heated FH2-Al series may be due to both inner-sphere complexation of arsenate by crystalline Al hydroxides [168] and inner-sphere complexation of arsenate by iron oxides [15, 155, 159, 161, 164~167].

As discussed in sections 5.2.4 and 5.2.5, the FH2-Al series heated at 360 ^{o}C were considered a mixture of 2-line ferrihydrite, hematite, and Al hydroxides in a transitional stage of structure between gibbsite and boehmite. The OH^- groups on the planar surfaces of gibbsite and the corrugated AlOOH sheets of boehmite are fully charge-satisfied and

relatively inert [53, 253]. However, the edges of gibbsite and boehmite crystals have a large amount of unsaturated O atoms that can never be fully charge-satisfied by the addition or removal of a proton [53], are the source of the pH-dependent variable charge of Al hydroxides, and are active sites for sorption reactions [218]. Due to the abundance of highly reactive, unsaturated O atoms on the edges of gibbsite and boehmite, Al hydroxides have been known to be important in the sorption of various metals and both organic and inorganic anions [23]. During the process dehydration of fine gibbsite (1.5 μm), the BET surface area of material was reported to increase initially (30 m^2/g at uncalcined condition), reached a maximum 311 m^2/g at 350 ^oC, and then dropped at higher temperatures [241]. It was also reported that the heat treatment of nanocrystalline boehmite at 350 ^oC induced an increase (up to about 440 m^2/g) in the specific surface area due to water loss [254]. The calcination of boehmite at 500 ^oC resulted in both degradation of the layered crystal structure and formation of the previously amorphous structure and a maximum specific surface area of boehmite was obtained at calcining temperature about 500 ^oC [255]. The 220 ^oC calcined boehmite were able to remove more than 97 % of arsenate from aqueous systems at pH 6.4 and an initial arsenate loading of 0.73 mol As/kg sample [255]. Upon heating boehmite in the temperature range of 200~1150 ^oC, the boehmite calcined at 400 ^oC showed the highest adsorption capacity of arsenious ions as compared with those both uncalcined and calcined at other temperatures [256].

As discussed in section 5.2.4, after heating at 360 ^oC, the fraction ($[Fe_o]/[Fe_t]$) of amorphous Fe oxide of the FH2-Al series reduced to 12.79~27.98%, which were much larger than that (0.52%) of the heated FH2. The fraction of amorphous Fe oxide was the

highest at an Al/Fe molar ratio of 1 and increased with increasing the Al/Fe molar ratio (Table 6.5). However, FH2-Al-0.25 showed the largest content ([Fe_o]) of amorphous iron. Based on the results of total iron content (section 5.2.1) and the transformation studies (section 5.2.4), it can be estimated that the heated FH2-Al-1 consists of 14.27% 2-line ferrihydrite, 36.73% hematite, and 49.00 % Al hydroxides (gibbsite and boehmite). Therefore, the higher adsorption capacity of arsenic on the heated FH2-Al series was in part due to larger amounts of the remaining 2-line ferrihydrite after heating.

Compared with the PZC shift of FH2 from 7.82 to 8.70, after heating at 360 ^oC, the PZC of FH-Al-1 moved from 8.70 to 8.20 (section 5.2.6). From the results of the PZC determination for the heated FH2 and FH2-Al-1, it may be suggested that the PZC values of FH2-Al-0.1, FH2-Al-0.25, and FH2-Al-0.05 are estimated to be above 8.20 since they had lower [Fe_o]/[Fe_t] ratios (higher ratios of hematite to 2-line ferrihydrite) after heat treatment than the heated FH2-Al-1. Therefore, at pH 7, the surface of the heated FH2-Al series has a net positive charge that would attract $H_2AsO_4^-$ and $HAsO_4^{2-}$ ions. Although the aged FH2-Al-1 had a lower specific surface of 229.3 m^2/g than the other aged FH2s (325.8~393.3 m^2/g) as determined in section 4.2.4, the adsorption of arsenate on the heated FH-Al series was larger than any other heated FH2. In summary, the higher adsorption capacity of arsenic on the heated FH2-Al series may be attributable to a combined effect of the high fraction of the remaining 2-line ferrihydrite, the abundance of highly reactive edges of gibbsite and boehmite, and the net positive surface charge.

6.2.3.7 Arsenic Adsorption on Heat-Treated FH2s with an Inhibitor/Fe Molar Ratio of 0.1

A comparison of arsenic adsorption on the heated FH2s (360 ^{o}C) with an equimolar inhibitor/Fe ratio of 0.1 at pH 7 is given in Table 6.6 and Figure 6.20. An evident difference of adsorptions between the heated FH2s was observed although there were no discernable variations between adsorption on the fresh FH2s (section 6.2.1). The adsorption capacity of arsenite on the heated FH2s decreased in the order of FH-Al-0.1 > FH2-Mg-0.1 > FH2-Ti-0.1 > FH2-Si-0.1 > FH2 while the adsorption capacity of arsenate on the heated FH2s followed the order: FH2-Al-0.1 > FH2-Si-0.1 > FH2-Mg-0.1 > FH2-Ti-0.1 > FH2. From the results that the arsenite adsorption capacity of the heated FH2 was lower than those of the other heated FH2s, it was evident that inhibitors have retarded the transformation of 2-line ferrihydrite to hematite. Based on the results of total iron content (section 5.2.1) and the transformation studies (section 5.2.4), it can be estimated that FH2-Al-0.1 was made of 10.99% 2-line ferrihydrite, 75.01 hematite, and 14.00% Al hydroxides (gibbsite and boehmite). Therefore, higher adsorption capacity of arsenic on the heated FH2-Al-0.1 was to due to a combined effect of the high fraction of the remaining 2-line ferrihydrite, the abundance of highly reactive edges of gibbsite and boehmite, and the net positive surface charge (at pH 7).

Table 6.6 Arsenic Adsorption and $[Fe_o]/[Fe_t]$ of 2-line-Ferrihydrite with an Inhibitor/Fe Molar Ratio of 0.1 after Heat-treating at 360 ^oC for 12 h.

Type of FH2		FH2	FH2-Si-0.1	FH2-Mg-0.1	FH2-Ti-0.1	FH2-Al-0.1
As (III)	As(III) adsorbed (mol As/kg sample)[a)]	0.0391	0.0414	0.0480	0.0471	0.0498
	Percentage decrease in adsorption (%)[b)]	26.57	17.00	5.58	8.37	4.43
As (V)	As(V) adsorbed (mol As/kg sample)[a)]	0.0533	0.0891	0.0614	0.0567	0.1019
	Percentage decrease in adsorption (%)[b)]	49.77	13.57	42.42	46.55	4.38
$[Fe_o]$ (mg amorphous Fe/g sample)[c)]		3.24	234.54	4.70	5.07	68.63
Percentage $[Fe_o]/[Fe_t]$ (%)		0.52	42.89	0.70	0.94	12.79

[a)] The adsorption of arsenite and arsenate was performed at pH 7 and an initial As loading of 0.0534 mol As(III) and 0.1068 mol As(V)/g sample, respectively.
[b)] (As adsorbed on fresh sample – As adsorbed on heated sample)/(As adsorbed on fresh sample)
[c)] The remaining amorphous iron content after heat treatment at 360 ^{o} C for 12 h.

6.2.3.8 Relationship between Transformation and Arsenic Adsorption

Figure 6.21 shows a relationship between arsenic adsorption and 2-line ferrihydrite transformation into hematite after heat treatment. The relationship was evaluated on the ratio of reduction in arsenic adsorption ([As adsorbed on the fresh FH2s - As adsorbed on the heated FH2s]/[As adsorbed on the fresh FH2s]) (at pH 7, 0.0534 mol As(III)/kg, and 0.1068 mol As(V)/kg) and the ratio of 2-line ferrihydrite transformation into hematite (1-$[Fe_o]/[Fe_t]$) after heat treating at 360 ^oC.

After heat treatment, the FH2, FH2-Ci, FH2-Ti, and FH2-Mg series transformed completely by above 98% while the ratio of transformation was 57.11~96.19% for the FH2-Si series and 72.02~87.21% for the FH2-Al series, respectively. With arsenite, the FH2-Mg series showed lower reduction ratios (2.62~5.58%) in spite of nearly complete 2-line ferrihydrite transformation to hematite. The PZC value of the heated FH2-Mg-2 was determined to be 8.90 (section 5.2.6). Therefore, the lower reduction ratios in arsenite adsorption may be in part due to higher PZC value of the FH-Mg series than the other FH2 series.

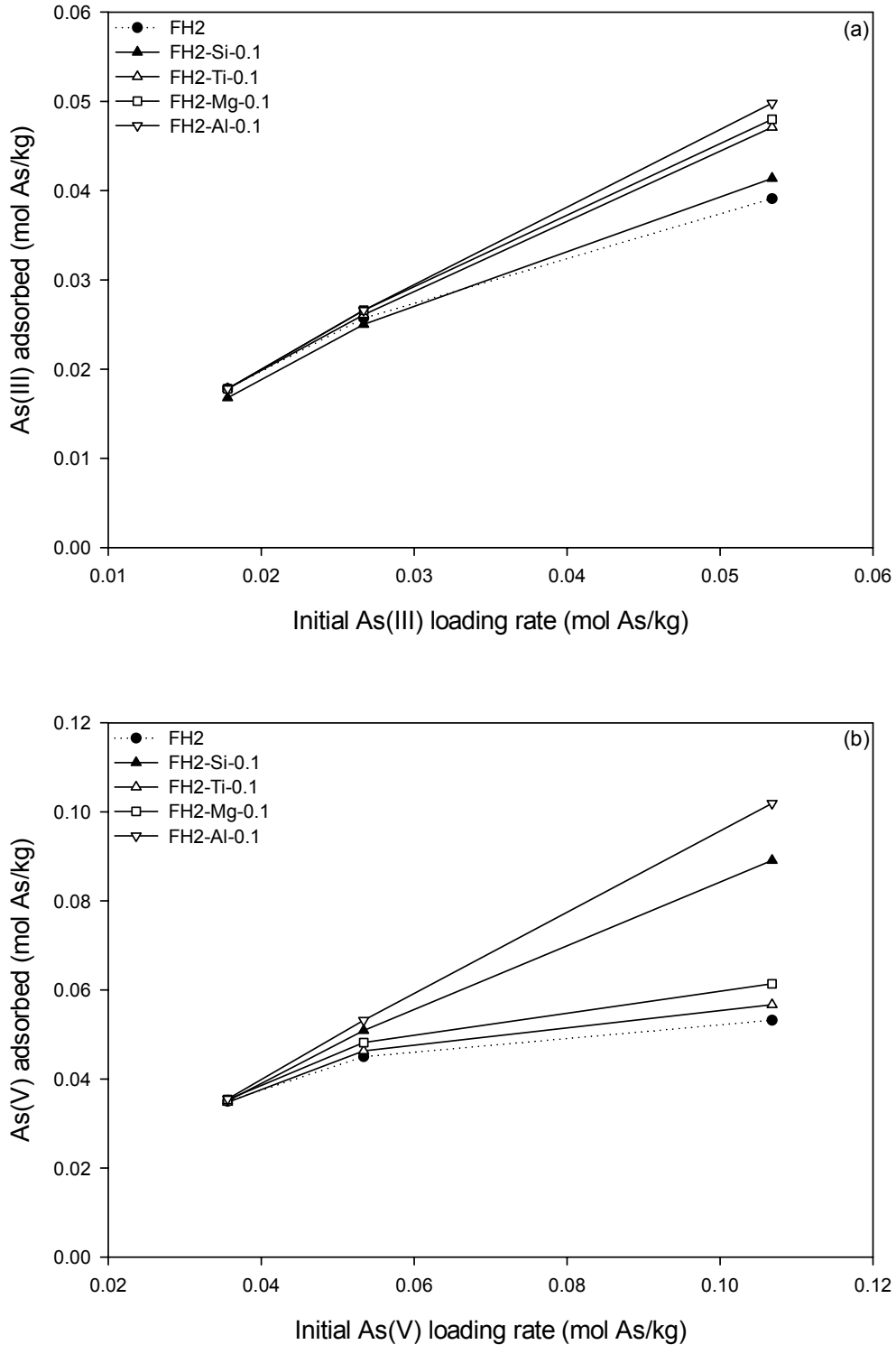

Figure 6.20 Adsorption of As(III) (a) and As(V) (b) on Heat-Treated 2-line Ferrihydrites with an Inhibitor/Fe Molar Ratio of 0.1 at pH 7 after Heat-Treating at 360 ^{o}C for 12 h.

On the other hand, an appreciable drop (34~53%) in arsenate adsorption on the FH2, FH2-Ci, FH2-Ti, and FH2-Mg series was observed. However, the reduction ratio in arsenate adsorption for the FH2-Al and FH2-Si series was much lower than those of the other FH2 series. Especially, the FH2-Al series showed the smallest reduction ratio in arsenate adsorption after heat treatment. As discussed in section 6.2.3.6, the smallest reduction ratio in arsenate adsorption on the FH-Al series may be attributed to the combined effect of the high fraction of the remaining 2-line ferrihydrite, the abundance of highly reactive edges of gibbsite and boehmite, and the net positive surface charge (at pH 7). Although the PZC value (6.3) of the heated FH2-Si-0.1 was lower than that of the heated FH2 (8.7) and FH2-Mg-2 (8.9), the FH2-Si series showed lower arsenate reduction ratios than the FH2, FH2-Ci, FH2-Ti, and FH2-Mg series. The lower arsenate reduction ratios may be attributed to larger amounts (3.81~42.89%) of the remaining 2-line ferrihydrite after heat treatment with respect to the other heated FH2 series. Based on the above analysis, it can be concluded that the less 2-line ferrihydrite transforms into hematite, the larger arsenate is adsorbed on the FH2s at pH 7. However, there was no evident relationship between the extent of transformation of 2-line ferrihydrite to hematite and the reduction in arsenite adsorption on the FH2s at pH 7.

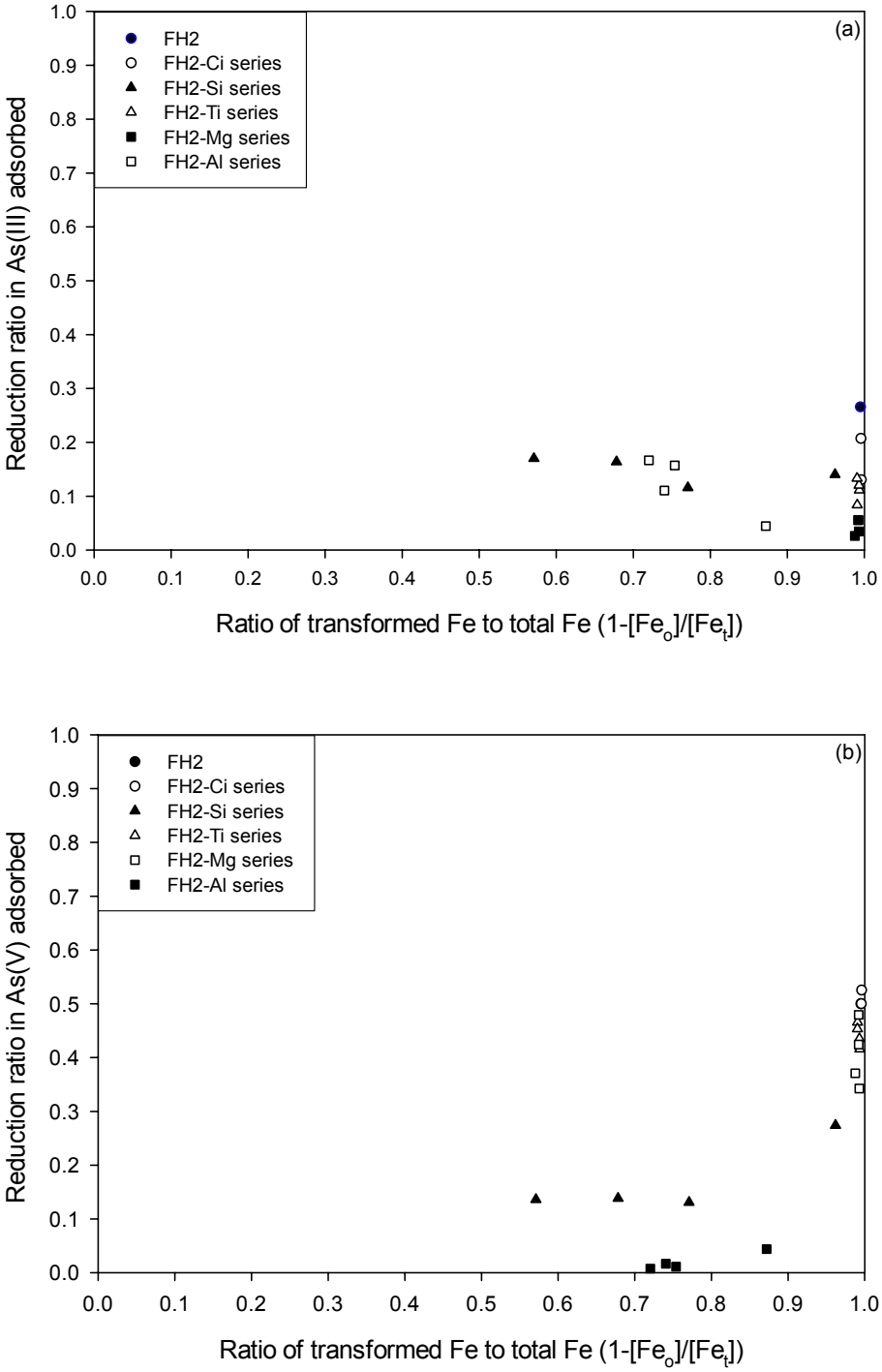

Figure 6.21 Relationships between the Rate of Transformation (1-[Fe_o]/[Fe_t]) and the Reduction Ratio in Arsenic Adsorption ([As Adsorbed on the Fresh FH2s - As Adsorbed on the Heated FH2s]/[As Adsorbed on the Fresh FH2s]) at pH 7, 0.0534 mol As(III)/kg (a) and 0.1068 mol As(V)/kg (b) after Heat-Treating at 360 ^oC for 12 h.

6.2.4 Effect of pH on Arsenic Adsorption

All of the FH2s aged at RT for ~20 days ("fresh") at RT were evaluated to investigate arsenic adsorption at different pH values (about 3, 5, 7, and 9). The pH influence on arsenic adsorption on the fresh FH2s at a low initial As loading equivalent to 0.0178 mol As(III)/kg and 0.02225 mol As(V)/kg is given Figures 6.22 to 6.26.

6.2.4.1 Effect of pH on Arsenic Adsorption on FH2-Si Series

The pH influence on arsenic adsorption on the fresh FH2-Si series is shown in Figure 6.22. The percentage of arsenite adsorption was greater than 99.76% for FH2, 98.92% for FH2-Si-0.025, 99.22% for FH2-Si-0.05, 98.21% for FH2-Si-0.075, and 97.26% for FH2-Si-0.1 throughout the pH range of 5.08 to 9.08 with an initial loading of 0.0178 mol As(III)/kg sample while arsenate was almost completely adsorbed on both the FH2 and FH2-Si series throughout the pH range of 2.98 to 7.13 with an initial loading of 0.02225 mol As(V)/kg sample.

With increasing the Si/Fe molar ratio from 0 to 1, the percentage arsenite removal decreased by 1.71~3.27% throughout the pH range of 3.01 to 9.08. The decrease in percentage removal at pH 3.01 (3.27%) was larger than that at pH 9.08 (1.71%). In contrast, there was no discernable difference in the percentage arsenate removal with increasing the Si/Fe molar in the range of pH 2.98 to 7.13. However, at pH 9.16 the percentage arsenate removal decreased sharply by 13.17% with increasing the Si/Fe molar ratio from 0 to 0.1. Both co-precipitated silica [186] and dissolved Si species [187~189] can adversely affect the arsenic adsorption on hydrous ferric iron oxides (HFO). The co-precipitated silica may cover active sites on HFO through polymerization

of silicic acid and hence lead to a considerable decrease of arsenic adsorption with increasing the Si/Fe molar ratio [33, 187].

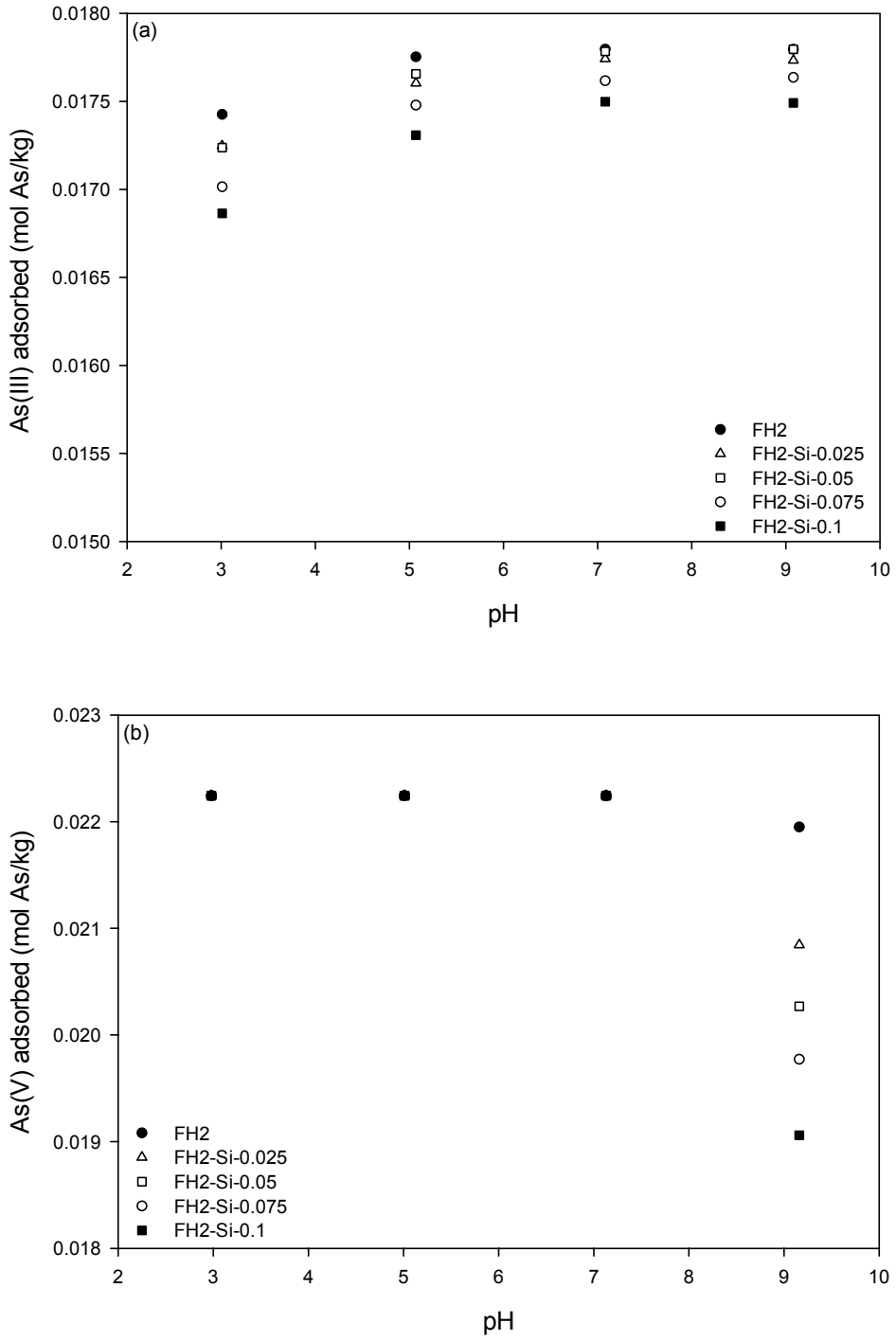

Figure 6.22 Effect of pH on Adsorption of As(III) (a) and As(V) (b) on Fresh FH2-Si Series at an As Loading of 0.01780 for As(III) and 0.02225 mol As/g Sample for As(V).

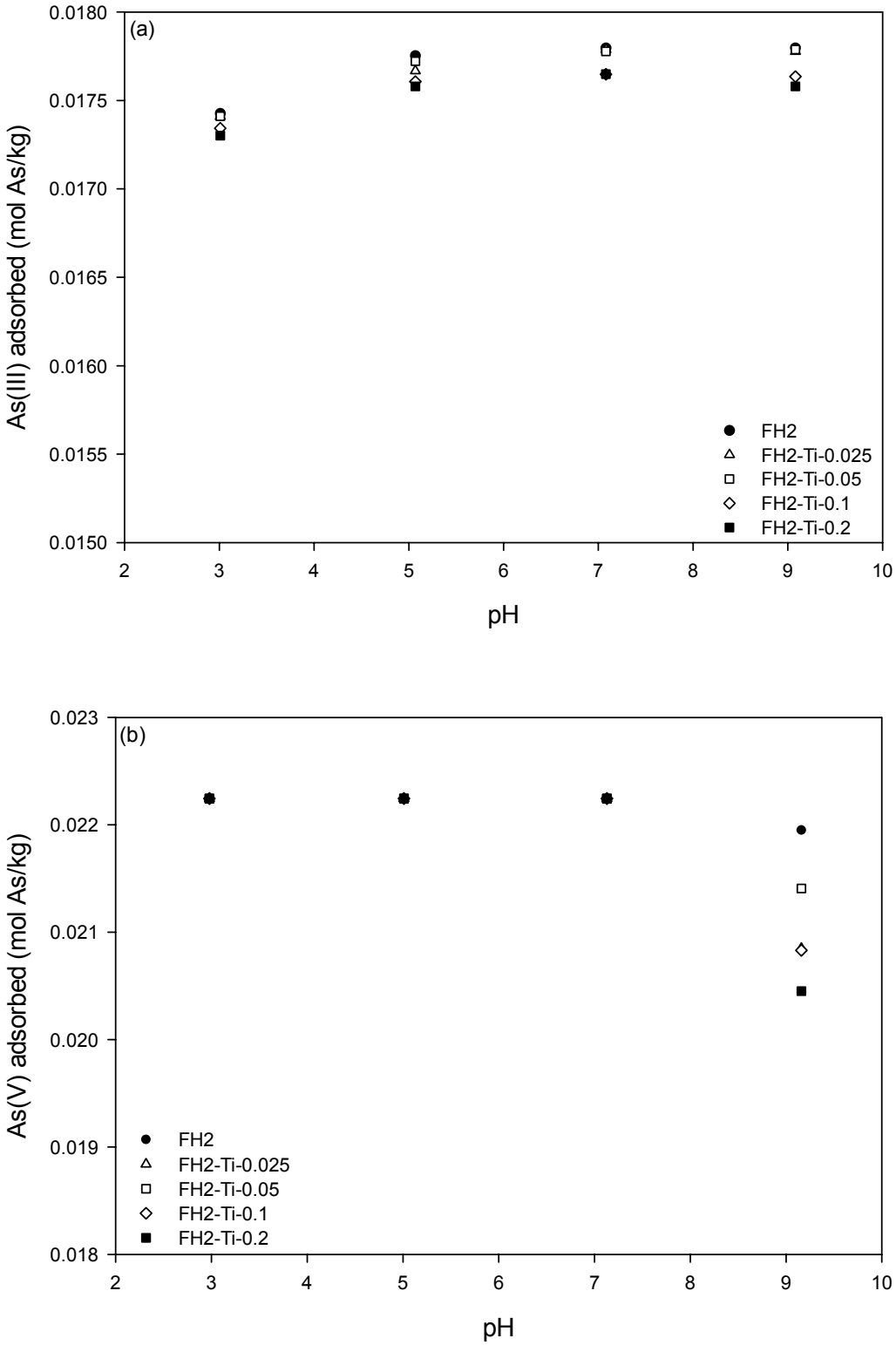

Figure 6.23 Effect of pH on Adsorption of As(III) (a) and As(V) (b) on Fresh FH2-Ti Series at an As Loading of 0.01780 for As(III) and 0.02225 mol As/g Sample for As(V).

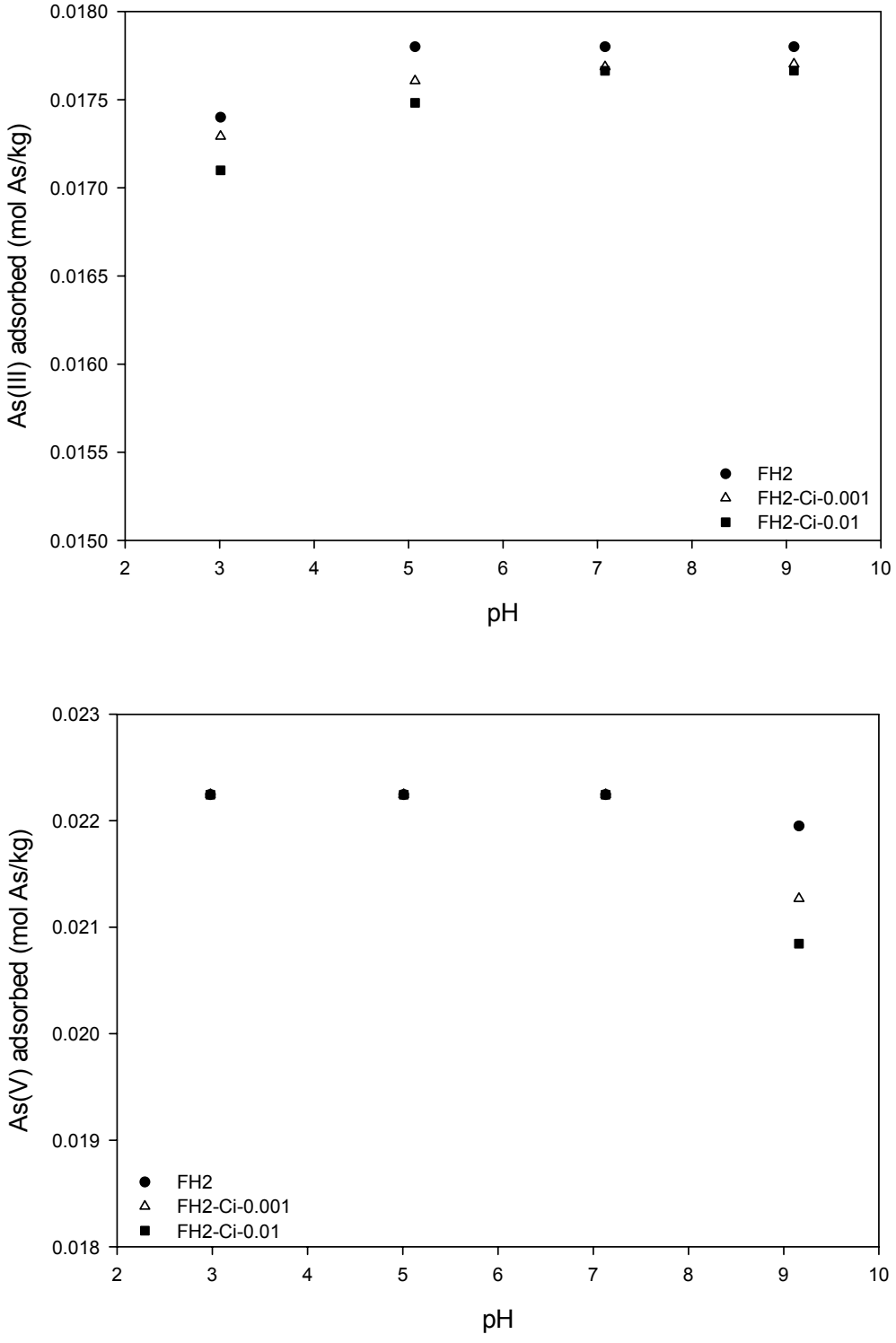

Figure 6.24 Effect of pH on Adsorption of As(III) (a) and As(V) (b) on Fresh FH2-Ci Series at an As Loading of 0.01780 for As(III) and 0.02225 mol As/g Sample for As(V).

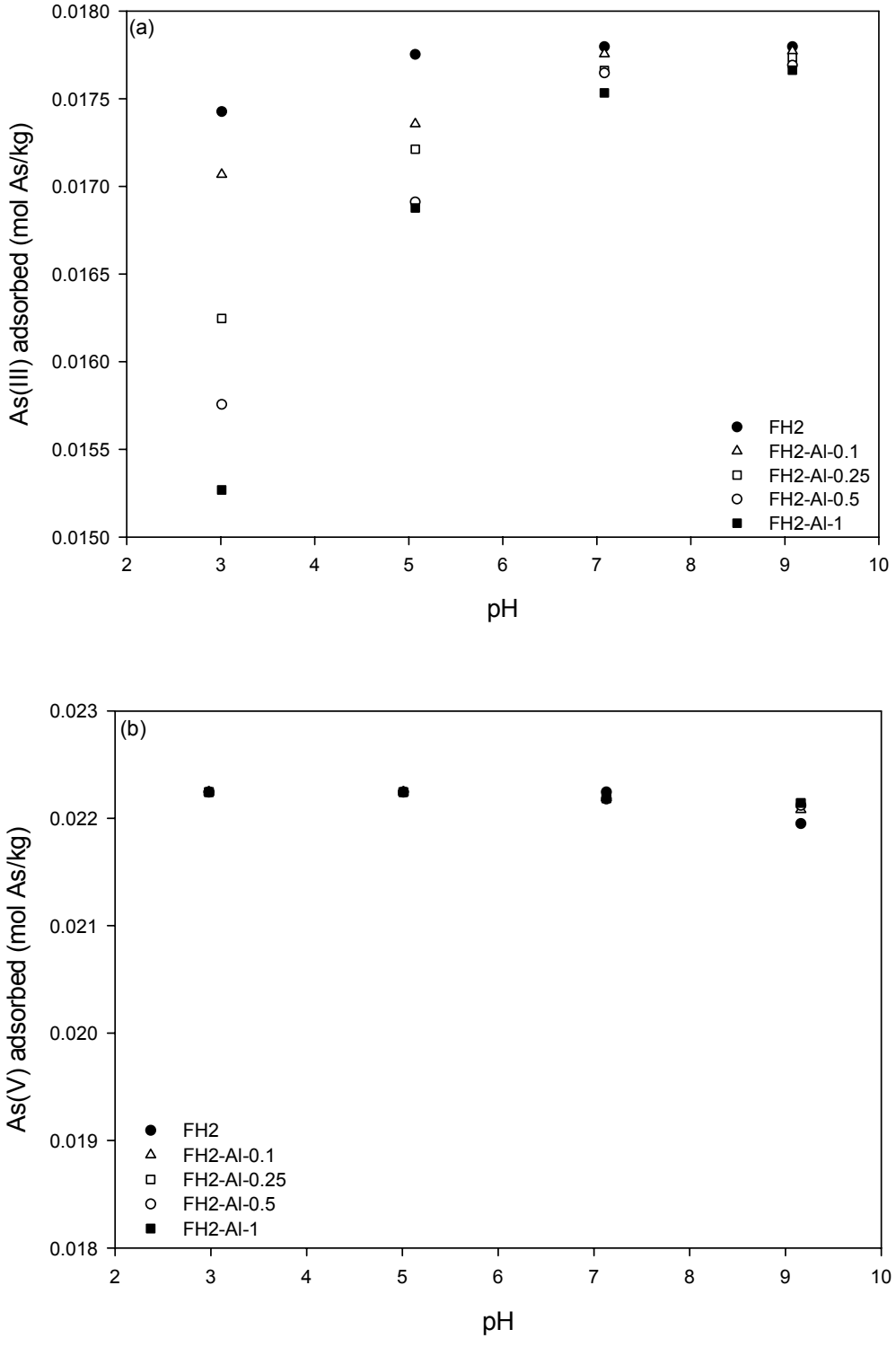

Figure 6.25 Effect of pH on Adsorption of As(III) (a) and As(V) (b) on Fresh FH2-Al Series at an As Loading of 0.01780 for As(III) and 0.02225 mol As/g Sample for As(V).

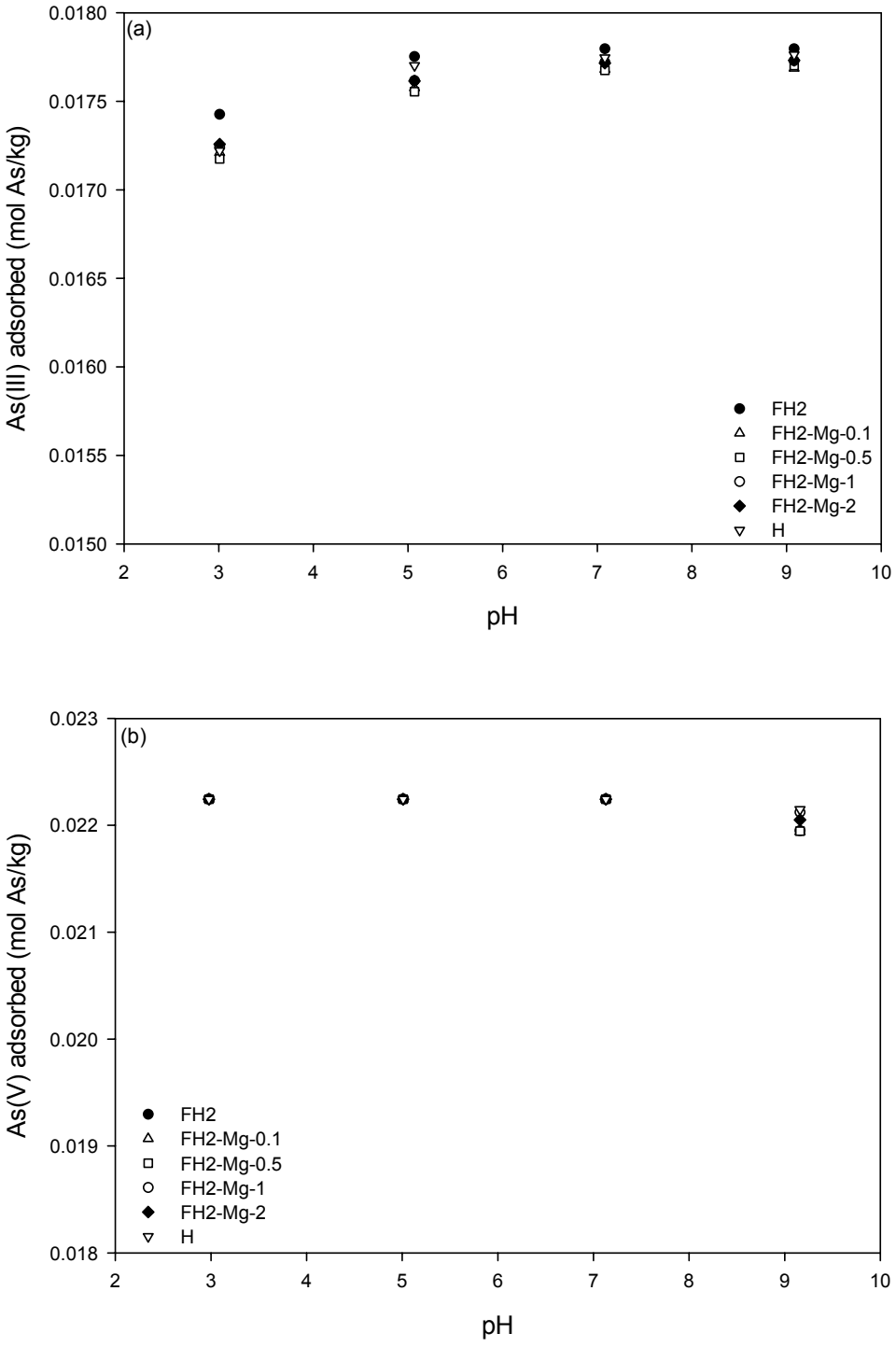

Figure 6.26 Effect of pH on Adsorption of As(III) (a) and As(V) (b) on Fresh FH2-Mg Series and HTlc at an As Loading of 0.01780 for As(III) and 0.02225 mol As/g Sample for As(V).

With arsenite, there was a trend of increasing adsorption with increasing pH, with the maximum adsorption occurring at pH 7.08 to 9.08. In contrast, arsenate adsorption reached broad maxima from pH 2.98 to 7.13 but sharply decreased at pH 9.16. The pH ranges of both arsenite and arsenate adsorption maxima are in agreement with those (at 0.267 mol As/kg ferrihydrite) obtained by other research [44]. The results of this study about the pH effect on arsenic adsorption on the dried solids of the fresh FH2 and FH2-Si series are in agreement with those obtained by using both the single iron (III) oxides such as 2-line ferrihydrite solutions [44**]** and hydrous ferric oxide solutions [151, 153, 154**]**. Compared with the results obtained by the single iron (III) oxides, the iron (III) oxide of the dried FH2-Si series in this study was still a principal adsorbent for arsenic adsorption. Also the pH effect on arsenic adsorption in this study was similar to that observed in the arsenic adsorption on the dried Fe (III)-Si binary adsorbent [191].

With increasing the initial arsenic loading, adsorption envelope for arsenite has been reported with contrasting trends. Raven et al. [44] reported that arsenite adsorption (at initial As(III) loadings of 0.028, 0.083, and 1.383 mol As(III)/kg Fe) increased with increasing pH up to 9.0~9.5 and then decreased at above this pH, with adsorption maxima at pH 9~9.5. On the other hand, Pierce et al. [151] observed that at initial low As loadings of 0.014~0.29 mol As(III)/mol Fe, arsenite adsorption increased with increasing pH to 7.0 and then reduced at above this pH, but at initial higher As loadings of 0.0.725~14 mol As(III)/mol Fe, arsenite adsorption decreased continuously with increasing pH. The disagreement in adsorption envelopes for arsenite might be possibly attributable to differences in experimental conditions such as the initial arsenite loading. In our study, the results about the pH effect on arsenic adsorption (0.00185 mol As(III)/mol Fe and

0.00231 mol As(V)/mol Fe) were in agreement with those obtained by Zeng (0.00245 mol As/mol Fe) [91] due to the close range of initial As loadings.

The pH ranges of both maximum arsenite and arsenate adsorption were not influenced by differences in surface charge of FH2 and FH2-Si-0.1 although the PZC (6.90) of FH2-Si-0.1 was smaller than that (7.82) of FH2 (section 4.2.5). The result indicates that both arsenite and arsenate adsorptions were independent of PZC value of FH2 and FH2-Si-0.1 at the low arsenic loadings in this study. Therefore, each species (arsenite and arsenate) may be retained dominantly as an inner-sphere complex on FH2 and FH2-Si series via a ligand exchange reaction between arsenic and a surface functional group.

Maximum arsenite adsorption in the pH range of 7.08~9.08 may be at least in part due to H^+ dissociation from arsenite (pK_{a1} = 9.22), inducing protonation of surface OH^- on both the FH2 and FH2-Si series to form OH_2. Since the surface OH_2 group is more contributive than the charged OH^- group to ligand exchange, the surface of both FH2 and FH2-Si series is likely more effective for arsenite adsorption near the pK_{a1}. Maxima in the adsorption envelopes at a pH near their pK_a are well-recognized phenomenon [62].

On the other hand, maximum arsenate adsorption at pH < 7.13 is due to ligand exchange of surface OH_2 groups on both the FH2 and FH2-Si series. At about pH 7, close to the pK_{a2} of arsenate, H^+ dissociation from arsenate (pK_{a2} = 6.97) may lead to arsenate adsorption by inducing protanation of surface OH^- group on both the FH2 and FH2-Si series to form OH_2. At above a pH > PZC (7.82 for FH2 and 6.90 for FH2-Si-0.1), enhanced electrostatic repulsion between the negatively charged arsenate ($HAsO_4^{2-}$ and $H_2AsO_4^-$) and the negatively charged surface of both the FH2 and FH2-Si series can lead

to decreased arsenate adsorption. Considerably decreased arsenate adsorption at pH 9.16 was observed due to the increased repulsion between the more negatively charged arsenate species and the negatively charged surface of FH2-Si-0.1, whereas the arsenite adsorption decreased less because of the less negative charge character of arsenite compared with arsenate [44].

The reduction in adsorption of both arsenite at pH 3.01 and arsenate at pH 9.16 may be in part attributable to the release of arsenic resulting from the increased solubility of the 2-line ferrihydrite at these pH extremes. It was reported by Zeng [191] that the dissolved Fe from a Fe (III)-Si binary adsorbent was largest at about pH 3, dropped to the lowest solubility at pH 6.0 to 6.5, and then increased with increasing pH. Additionally with increasing pH, an increase in competing OH^- for adsorption sites may be also responsible for the reduction in arsenate adsorption on the FH2 and FH2-Si series [204].

Both arsenite and arsenate have been known to induce a shift in the PZC to more acidic pH value [62], leading to the surface of iron oxides at a given pH to be more negative. However, a significant decrease in both arsenite and arsenate adsorption in this study was not observed. The result is likely due to higher concentration of adsorption sites per unit weight of the FH2-Si series with the poorly crystalline 2-line ferrihydrite. The 2-line ferrihydrite of the dried FH2-Si series in this study was still a principal adsorbent for arsenic adsorption, although an increase in the Si/Fe molar ratio from 0 to 0.1, which corresponded to an decrease in total iron content by 12 % (section 5.2.1), led to lower concentrations of surface adsorption Fe sites due to polymerization of silicic acid on the FH2-Si series.

6.2.4.2 Effect of pH on Arsenic Adsorption on FH2-Ti Series

The pH influence on arsenic adsorption on the fresh FH2-Ti series is shown in Figure 6.23. The percentage arsenite adsorption was greater than 99.76% for FH2, 99.27% for FH2-Ti-0.025, 99.58% for FH2-Ti-0.05, 98.94% for FH2-Ti-0.1, and 98.78% for FH2-Ti-0.2 throughout the pH range of 5.08 to 9.08 with an initial loading of 0.0178 mol As(III)/kg sample, whereas arsenate was almost completely adsorbed on both the FH2 and FH2-Ti series throughout the pH range of 2.98 to 7.13 with an initial loading of 0.02225 mole As(V)/kg sample.

The percentage arsenite removal decreased at all pH values by 0.71~1.22% with increasing the Ti/Fe molar ratio from 0 to 0.2 while there was no significant difference in the percentage arsenate removal in the range of pH 2.98 to 7.13. However, at pH 9.16 the percentage arsenate removal decreased from 98.68% to 91.94% with increasing the Ti/Fe molar ratio from 0 to 0.1. The slight decrease in arsenic removal with increasing the Ti/Fe molar ratio may be due to formation of amorphous titanium hydroxide ($Ti(OH)_4$) during the preparation of the FH2-Ti series as discussed in section 5.2.1.

With arsenite, there was a trend of increasing adsorption with increasing pH, with the maximum adsorption occurring at pH 7.08 to 9.08. In contrast, arsenate adsorption reached broad maxima from pH 2.98 to 7.13 but decreased at pH 9.16. The results of this study about the pH effects on arsenic adsorption on the dried solids of the fresh FH-Ti series were in agreement with those obtained by using 2-line ferrihydrite solutions [44] and hydrous ferric oxide solutions [151, 153, 154].

The pH ranges of both maximum arsenite and arsenate adsorption were not affected by differences in the surface charge of the FH2 and FH2-Ti series, although the PZC of

FH2-Ti-0.2 was estimated to be smaller than that (7.82) of FH2 due to the formation of amorphous titanium hydroxide (section 5.2.5), the PZC of which was reported 4.6 [252]. The results indicate that both arsenite and arsenate adsorptions were independent of PZC value for the FH2 and FH2-Ti series at the low arsenic loadings in this study. Therefore, arsenite and arsenate may be adsorbed dominantly on the FH2 and FH2-Ti series as an inner-sphere complex via a ligand exchange reaction between arsenic and a surface functional group.

A significant decrease in arsenite and arsenate adsorptions in this study was not observed. The result is likely due to the higher concentration of adsorption sites per unit weight of the FH2-Ti series with the poorly crystalline 2-line ferrihydrite. The 2-line ferrihydrite of the dried FH2-Ti series in this study was still a principal adsorbent for arsenic adsorption, although an increase in the Ti/Fe molar ratio from 0 to 0.2, which corresponded to an decrease in total iron content by 20% (section 5.2.1), led to lower concentration of surface adsorption Fe sites due to the formation of $Ti(OH)_4$ (section 5.2.5).

6.2.4.3 Effect of pH on Arsenic Adsorption on FH2-Ci Series

The pH influence on the arsenic adsorption on the fresh FH2-Ci series is shown in Figure 6.24. The percentage arsenite adsorption was greater than 99.76% for FH2, 98.93% for FH2-Ci-0.001, and 98.23% for FH2-Ci-0.01 throughout the pH range of 5.08 to 9.08 with an initial loading of 0.0178 mol As(III)/kg sample, whereas arsenate was almost completely adsorbed on both the FH2 and FH2-Ci series throughout the pH range of 2.98 to 7.13 with an initial loading of 0.02225 mol As(V)/kg sample.

The percentage arsenite removal decreased at all pH values by 0.74~1.88% with increasing the Ci/Fe molar ratio from 0 to 0.01. The decrease in percentage removal at pH 3.01 (1.88%) was more than that at pH 9.08 (0.74%). There was no significant difference in the percentage arsenate removal in the range of pH 2.98 to 7.13. However, at pH 9.16 the percentage arsenate removal decreased from 98.68% to 93.71% with increasing the Ci/Fe molar ratio from 0 to 0.01. The decrease in arsenic removal with increasing the Ci/Fe molar ratio is attributable to a function of the surface activity of the functional groups (three COOH groups and one OH group) on citrate [49, 192]. Both arsenite and arsenate adsorptions on 2-line ferrihydrite decreased in the presence of citrate [49].

With arsenite, there was a trend of increasing adsorption with increasing pH, with the maximum adsorption occurring at pH 7.08 to 9.08. In contrast, arsenate adsorption reached broad maxima from pH 2.98 to 7.13 but decreased at pH 9.16. The results about the pH influence on arsenic adsorption on the dried solids of the fresh FH-Ci series were generally in agreement with those obtained by using 2-line ferrihydrite solutions [44] and hydrous ferric oxide solutions [151, 153, 154].

The pH ranges of both maximum arsenite and arsenate adsorption were not affected by differences in the surface charge of the FH2 and FH2-Ci series, although the PZC of the FH2-Ci series was estimated to be smaller than that (7.82) of FH2 due to the specific adsorption of Ci on the 2-line ferrihydrite surface. The results indicate that both arsenite and arsenate adsorption were independent of PZC values of the FH2 and FH2-Ci series at the above arsenic loadings. Therefore, arsenite and arsenate may be adsorbed dominantly on the FH2 and FH2-Ci series as an inner-sphere complex via a ligand exchange reaction between arsenic and a surface functional group.

A significant decrease in arsenite and arsenate adsorptions in this study was not observed. The result is likely due to the higher concentration of adsorption sites per unit weight of the FH2-Ci series with the poorly crystalline 2-line ferrihydrite. The 2-line ferrihydrite of the dried FH2-Ci series in this study was still a principal adsorbent for arsenic adsorption, although both arsenite and arsenate adsorption on the FH2-Ci series decreased in the presence of citrate.

6.2.4.4 Effect of pH on Arsenic Adsorption on FH2-Al Series

The pH influence of arsenic adsorption on the fresh FH2-Al series is shown in Figure 6.25. The percentage of arsenite adsorption was greater than 99.76% for FH2, 97.53% for FH2-Al-0.1, 96.71% for FH2-Al-0.25, 95.03% for FH2-Al-0.5, and 94.83% for FH2-Al-1 throughout the pH range of 5.08 to 9.08 at an initial loading of 0.0178 mol As(III)/kg sample whereas arsenate was almost adsorbed on both the FH2 and FH2-Al series throughout the pH range of 2.98 to 7.13 at an initial loading of 0.02225 mol As(V)/kg sample.

The percentage of arsenite removal decreased by 0.75~12.38% throughout the pH range of 3.01 to 9.08 with increasing the Al/Fe molar ratio from 0 to 1. The decrease in the percentage arsenite removal at pH 3.01 (12.38%) was much larger than at pH 9.08 (0.75%). However, there was no discernable difference in the percentage arsenate removal in the range of pH 2.98 to 9.16 with increasing the Al/Fe molar. It was reported by other research [64] that both arsenite and arsenate adsorption (at 0.05 mol As/mol Al+Fe) decreased with increasing the Al/Fe molar ratio. The discrepancy in the results between this study and other study [64] may be attributable to different experimental

conditions (adsorbent type and initial arsenic/adsorbent loading rate) and the different degree of transformation of adsorbent during aging at room temperature. A detailed comparison of arsenate adsorptions on the fresh FH2 and FH2-Al series will be given later in section 6.2.5.

The adsorption capacity of arsenate reached broad maxima from pH 2.98 to 7.13, but decreased slightly at pH 9.16. In contrast, the adsorption capacity of arsenite increased with increasing pH, with the maximum adsorption occurring at pH 7.08 to 9.08. However, the maximum arsenite adsorption occurred at pH 9 with increasing the Al/Fe molar ratio. The result may be explained by the mode of arsenite bonding by the FH2-Al series that arsenite adsorbs strongly on surface Fe sites of 2-line ferrihydrite via inner-sphere complexation whereas arsenite forms predominantly outer-sphere complexes on amorphous Al hydroxide [168] and inner- or outer-sphere complexes on crystalline Al hydrooxide (gibbsite) at a pH of > 5.5 [196] and shows a weak affinity for gibbsite surface [195]. It was also reported that arsenate adsorbed strongly on both surface Fe and Al sites by inner-sphere complexation [15, 155, 168, 196].

Maximum arsenite adsorption in the pH range of 7.08~9.08 may be at least in part due to H^+ dissociation from arsenite (pK_{a1} = 9.22), inducing protonation of surface OH^- on the FH2 and FH2-Al series to form OH_2. It was reported that arsenate adsorption on amorphous Al oxide exhibited 100 % adsorption from pH 3 to 9 whereas arsenite adsorption on amorphous Al oxide showed a parabolic adsorption curve with a maximum at a pH of 8 [257]. At pH 3.01, arsenite adsorption was sharply decreased with increasing the Al/Fe molar ratio. The results may be in part attributable to an increase in solubility of the FH2 and FH2-Al series, which is likely to lead to the decreased arsenite adsorption. It

was reported by others [191, 258] that the dissolved Fe from a Fe(III)-Si binary adsorbent was the largest at about pH 3 and Al hydroxides was subjected greater dissolution at pH < 4.5. Therefore, FH2-Al-1 showed smaller adsorption capacity at pH 3.01 due to the combined effect of dissolution of Fe(III) and Al(III).

On the other hand, maximum arsenate adsorption at low pH (< 7.13) or at pH values near the pK_{a2} (6.97) of arsenate may be due to ligand exchange of surface OH_2 groups on the FH2 and FH2-Al series for arsenate. At above pH > PZC (7.82 for FH2 and 8.70 for FH2-Al-1), enhanced electrostatic repulsion between negatively charged arsenate ($HAsO_4^{2-}$ and $H_2AsO_4^-$) and the negatively charged surface of both the FH2 and FH2-Al series led to decreased arsenate adsorption. Additionally with increasing pH, an increase in competing OH^- for adsorption sites may be responsible for the reduction in arsenate adsorption on the FH2 and FH2-Al series [204].

6.2.4.5 Effect of pH on Arsenic Adsorption on FH2-Mg Series and HTlc

The pH influence on arsenic adsorption on the fresh FH2-Mg series and HTlc is shown in Figure 6.26. The percentage arsenite adsorption was greater than 99.76% for FH2, 98.76% for FH2-Mg-0.1, 98.64% for FH2-Mg-0.5, 98.99% for FH2-Mg-1, 98.98% for FH2-Mg-2, and 99.47% for HTlc throughout the pH range of 5.08 to 9.08 at an initial loading of 0.0178 mol As(III)/kg sample. Arsenate was completely adsorbed on the FH2, FH2-Mg series, and HTlc throughout the pH range of 2.98 to 7.13 at an initial loading of 0.02225 mol As(V)/kg sample.

The percentage arsenite removal of the FH2-Mg series decreased by 0.37~0.96% throughout the pH range of 3.01 to 9.08 with increasing the Mg/Fe molar ratio from 0 to

2. The decrease in the percentage arsenite removal at pH 3.01 (0.96%) was slightly larger than at pH 9.08 (0.37%). There was no significant difference in percentage arsenate removal in the range of pH 2.98 to 7.13. However, at pH 9.16 the percentage arsenate removal increased slightly by 0.46 % with increasing the Mg/Fe molar ratio from 0 to 2. The slight increase in arsenate removal with increasing the Mg/Fe molar ratio may be explained by an observation that the PZC of FH2-Mg-2 (7.90) was slightly higher than that of FH2 (7.82) (section 4.2.5), that is, FH2-Mg-2 had more positively charged surface sites than FH2 due to the specific adsorption of Mg on the 2-line ferrihydrite surface. With increasing pH from 3.01 to 9.08 for arsenite and from 2.98 to 9.16 for arsenate, the percentage arsenite removal of HTlc increased by 2.04% whereas the percentage arsenate removal of HTlc decreased by 0.43%. Higher arsenate removal for HTlc may be attributable to the ion exchange of the interlayer anions (carbonate ions) by arsenate ions [247~250] as well as a high PZC value of 8.94 [73].

With arsenite, there was a trend of increasing adsorption with increasing pH, with the maximum adsorption occurring at pH 7.08 to 9.08. In contrast, arsenate adsorption reached broad maxima from pH 2.98 to 7.13, but slightly decreased at pH 9.16. The results of this study concerning the pH effect on arsenic adsorption on the dried solids of the fresh FH-Mg series and HTlc were generally in agreement with those obtained by using 2-line ferrihydrite solutions [44] and hydrous ferric oxide solutions [151, 153, 154]. Since the PZC value (7.90) of FH2-Mg-2 was very close to that (7.82) of FH2 (7.82) as shown in section 4.2.5 and the arsenic adsorption capacity of the FH2-Mg series was close to that of FH2, the pH ranges of both maximum arsenite and arsenate adsorption were little influenced by differences in the surface charge of the FH2 and FH2-Mg series.

The result indicates that both arsenite and arsenate adsorption were independent of PZC of the FH2 and FH2-Mg series at the low arsenic loadings in this study. Therefore, both arsenite and arsenate predominantly formed inner-sphere complexes on the FH2 and FH2-Mg series via a ligand exchange reaction between arsenic and a surface functional group.

A significant decrease in both arsenite and ar senate adsorption in this study was not observed. The result is likely due to the higher concentration of adsorption sites per unit weight of sample with the poorly crystalline 2-line ferrihydrite. The 2-line ferrihydrite of the dried FH2-Mg series in this study was still a principal adsorbent for arsenic adsorption since the ratio for total iron content of the FH2 to FH2-Mg series ranged from 95.33 to 99.22% (section 5.2.1).

6.2.4.6 Effect of Extreme pH on Arsenic Adsorption

The influence of extreme pHs (pH 3.01 for As(III) and pH 9.16 for As(V)) on arsenic adsorption on the fresh FH2s at a low initial As loading (equivalent to 0.0178 mol As(III)/kg or 0.02225 mol As(V)/kg) is given in Figure 6.27. At pH 3.01, the adsorption capacity of arsenite decreased with increasing the Ci/Fe, Si/Fe, Ti/Fe, and Al/Fe molar ratio. With increasing the inhibitor/Fe molar ratio, the decrease in the adsorption capacity of arsenite followed the order: FH2-Al > FH2-Si > FH2-Ci > FH2-Mg > FH2-Ti series. However, arsenite adsorption on the FH2-Mg series was less subjected to the influence of the low pH. As discussed in the previous sections, the sharper decrease for the FH2-Al series with increasing the Al/Fe molar ratio may be attributable to an increase in both solubility of the FH2-Al series and weak affinity of arsenite toward Al hydroxides, which

is likely to lead to the decreased arsenite adsorption. It was reported by other researches that the dissolved Fe from an iron oxide adsorbent was the largest at about pH 3, Al hydroxides were subjected to greater dissolution at pH < 4.5 [191, 258,] and the solubility of amorphous Al hydroxide was greater than that of Fe(III) at low pHs [259]. Also arsenite adsorption on amorphous Al oxide showed a parabolic adsorption curve with a maximum at a pH of 8; adsorption increased with increasing solution pH from 3 to 8 and then decreased with increasing pH from 8 to 10.5 [257]. Compared to the other FH2 series, the FH2-Al series, therefore, exhibited the smaller adsorption capacity of arsenite at pH 3.01 partly due to a combined effect of dissolutions of both Fe(III) and Al(III).

On the other hand, at pH 9.16, the adsorption capacity of arsenate decreased with increasing the Si/Fe, Ti/Fe, and Ci/Fe molar ratio. With increasing the inhibitor/Fe molar, the decrease in the adsorption capacity of arsenate decreased in the order of FH2-Si > FH2-Ti > FH2-Ci series. However, arsenate adsorptions on the FH2-Mg and FH2-Al series were less affected by the high pH. As shown in the precious sections, the sharper decrease for the FH2-Si series with increasing the Si/Fe molar ratio may be attributable to an increase in solubility of the FH2-Si series. Compared to the other FH2 series, the decreased arsenate adsorption on the FH2-Si series may be due to the increased repulsion between the more negatively charged arsenate species and the negatively charged surface of the FH2-Si series [44].

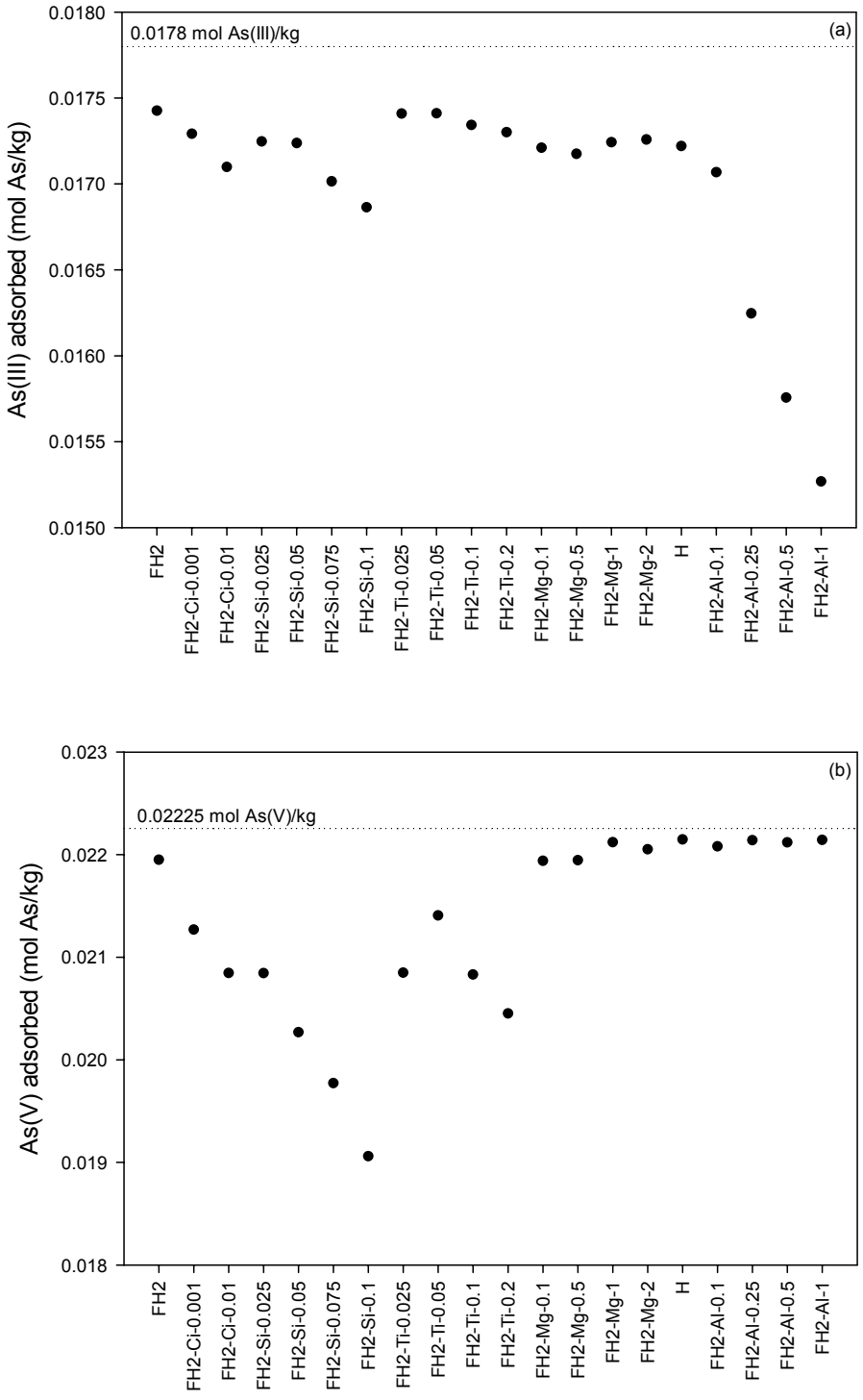

Figure 6.27 Effect of pH Extremes (pH 3.01 for As(III) and pH 9.16 for As(V)) on Adsorption of As(III) (a) and As(V) (b) on Fresh FH2s at an As Loading of 0.01780 for As(III) and 0.02225 mol As/g Sample for As(V).

6.2.5 Effect of High Arsenic Loading on Arsenic Adsorption

Based on the results of the screening adsorption experiments, four types of samples (FH2, FH2-Mg-2, FH2-Al-1, and HTlc) aged at RT for 40 days were selected as adsorbents to evaluate their adsorption capacities of arsenic at pH 7 and at high arsenic loadings in the range of 5~400 mg arsenic/g sample (corresponding to 0.06674~5.3389 mol As/kg). The influence of high arsenic loadings on arsenic adsorption is shown in Figure 6.28.

6.2.5.1 Comparison of Arsenite Adsorption and Arsenate Adsorption

With increasing the initial arsenic loading from 0.06674 to 5.3389 mol As/kg, the percentage arsenite adsorption decreased to 42.39% for FH2, 43.64% for FH2-Mg-2, 33.85% for FH2-Al-1, and 39.63% for HTlc, respectively while the percentage of arsenate adsorption reduced to 29.05% for FH2, 29.38% for FH2-Mg-2, 30.58% for FH2-Al-1, and 37.92% for HTlc, respectively. The results indicate that arsenite was adsorbed in larger amounts than arsenate at high arsenic loadings whereas arsenite was adsorbed in smaller amounts than arsenate at low arsenic loadings as shown in the screening adsorption experiments (section 6.2.1), which were performed at low arsenic loadings (0.0067~0.0534 mol As (III)/kg sample and 0.0133~0.1068 mol As (V)/kg sample). In our study, arsenite was adsorbed in larger amounts than aesenate from 0.2669 mol As/kg for both FH2 and FH2-Mg-2 and 5.3389 mol As/kg for both FH2-Al-1 and HTlc.

The results were agreement with other researches [44, 191], where arsenite was adsorbed on an Fe(III)-Si binary oxide adsorbent in larger amounts than arsenate above 0.13347 mol As/kg [91] and the adsorption capacity of arsenite was much larger than that

of arsenate at an higher initial concentration of 13.3 mol As/kg [44]. Raven et al. [44] have proposed that the very high arsenite retention levels prevented the possibility of its retention entirely as a surface adsorbed monomeric species, that is, ferrihydrite was transformed into a ferric arsenite phase during arsenite adsorption. There was a trend in arsenic adsorption in our study: the adsorption density for arsenite more continuously increased than that for arsenate at high arsenic loadings and did not attain a maximum even at the highest arsenic loading of 5.3389 As mol/kg. An additional surface precipitation of arsenite on the surface of samples might be occurring after surface complexation of arsenite although this hypothesis would require more experiments at higher initial arsenite loadings and verification by other techniques.

6.2.5.2 Arsenic Adsorption Isotherm and Adsorption Density

Two-parameter isotherm equations (Freundlich, Langmuir, and Temkin) were used for fitting the experimental data. The isotherm data from Figure 6.28 were fitted to the above three models by linear regression. The correlation coefficient (R^2) and sum of squared errors (SS_{Error}) for the different models are shown in Table 6.7. It was found that the Freundlich equation provided a better fitting for isotherm data for both arsenite and arsenate with respect to the Langmuir and Temkin equations. Generally, the applicability of the two-parameter isotherm models for the present data approximately followed the order: Freundlich > Langmuir > Temkin. However, the Langmuir equation may not be suitable for estimating the maximum arsenic adsorption capacity ($q_{e,max}$) since both arsenite and arsenate adsorptions on all the samples did not attain a maximum even at the highest initial arsenic loading of 5.3389 mol As/kg and the correlation coefficients for the

Langmuir equation ranged from 0.8580 to 0.9698, which were lower than those (0.981~0.993) obtained by other research [191].

The highest observed adsorption density (q_e) for arsenite in this study was 2.2633 for FH2, 2.3301 for FH2-Mg-2, 1.8075 for FH2-Al-1, and 2.1160 mol As(III)/kg for HTlc, respectively while that for arsenate was 1.5508 for FH2, 1.5688 for FH2-Mg-2, 1.6329 for FH2-Al-1, and 2.0244 mol As(V)/kg for HTlc, respectively. The highest adsorption density for both arsenite and arsenate in this study did not exceed the maximum number of surface sites (0.25 mol sites/mol Fe ≈ 2.809 mol sites/kg Fe) on hydrous iron oxides [260].

Compared to four samples in this study, larger maximum adsorption densities for arsenic were reported by other researches: 0.60(0.58) and 0.25(0.16) mol As/mol Fe for arsenite and arsenate, respectively, at pH 4.6(9.2) [44], 0.25 mol As/mol Fe for arsenate [148], 5.0 mol As/mol Fe for both arsenite and arsenate [151]. The discrepancy in adsorption density between this study and other researches may be attributable to different experimental conditions (adsorbent type, initial arsenic/adsorbent loading rate, and pH adjustment) and the different degree of transformation of adsorbent. Especially, the air-dried solid were used as adsorbents in this study whereas solution phase ferrihydrite was used in other researches. It was reported by a research [47] that freeze-dried ferrihydrite adsorbed Cu and Pb much slower than ferrihydrite gel since the ferrihydrite gel had open, easily accessible surfaces and removal of surface water by freeze-drying caused the open structure to collapse. Therefore, air entrapped in micro-pores in this study caused in part to lower the arsenic adsorption capacity due to incomplete saturation of water into the micro-pores.

On the other hand, arsenic adsorption experiments [157, 191] using a dried solid as an adsorbent showed smaller maximum adsorption densities for arsenic with respect to four samples in this study: 0.171 mol As(III)/kg and 0.164 mol As(V)/kg for an Fe-Si binary oxide (dried at a temperature between 120 and 150 ^{o}C and sieved through 0.088 mm) at pH 6.5 [191] and 0.00149 mol As(III)/kg and 0.00212 mol As(V)/kg for granular ferric hydroxide (sieved to a size of 0.8 to 1.2 mm) at pH 7.6 [157].

Table 6.7 Correlation Coefficient (R^2) and Sum of Squared Error (SS_{Error}) for the Fit of Arsenite and Arsenate Adsorption Data

	As(III)				As(V)			
	FH2	FH2-Mg-2	FH2-Al-1	HTlc	FH2	FH2-Mg-2	FH2-Al-1	HTlc
Freundlich[a]								
R^2[b]	0.9838	0.9776	0.9776	0.9949	0.9622	0.9798	0.9848	0.9867
SS_{Error}	0.1743	0.2428	0.2141	0.0524	0.3132	0.1727	0.1321	0.1391
Langmuir[d]								
R^2	0.9232	0.9024	0.9698	0.9440	0.8580	0.9515	0.8744	0.9607
SS_{Error}	0.0026	0.0033	0.0013	0.0018	0.0043	0.0015	0.0039	0.0013
Temkin[e]								
R^2	0.8153	0.8272	0.7596	0.8033	0.7144	0.7953	0.7976	0.8409
SS_{Error}	4079.49	4023.31	3234.72	3752.86	2888.68	2153.41	2288.06	2981.93

[a] Linear plot of ln(equilibrium As solution concentration) vs ln(equilibrium adsorbed As)
[b] SS_{Model}/SS_{Total} = (Model sum of squares)/(Total sum of squares)
[c] SS_{Error} = Sum of squared errors = $\sum_{i=1}^{n}(Y_i - \hat{Y}_i)^2$, Y_i : observed value, $\hat{Y}_i$: predicted value
[d] Linear plot of 1/(equilibrium As solution concentration) vs 1/(equilibrium adsorbed As)
[e] Linear plot of ln(equilibrium As solution concentration) vs equilibrium adsorbed As

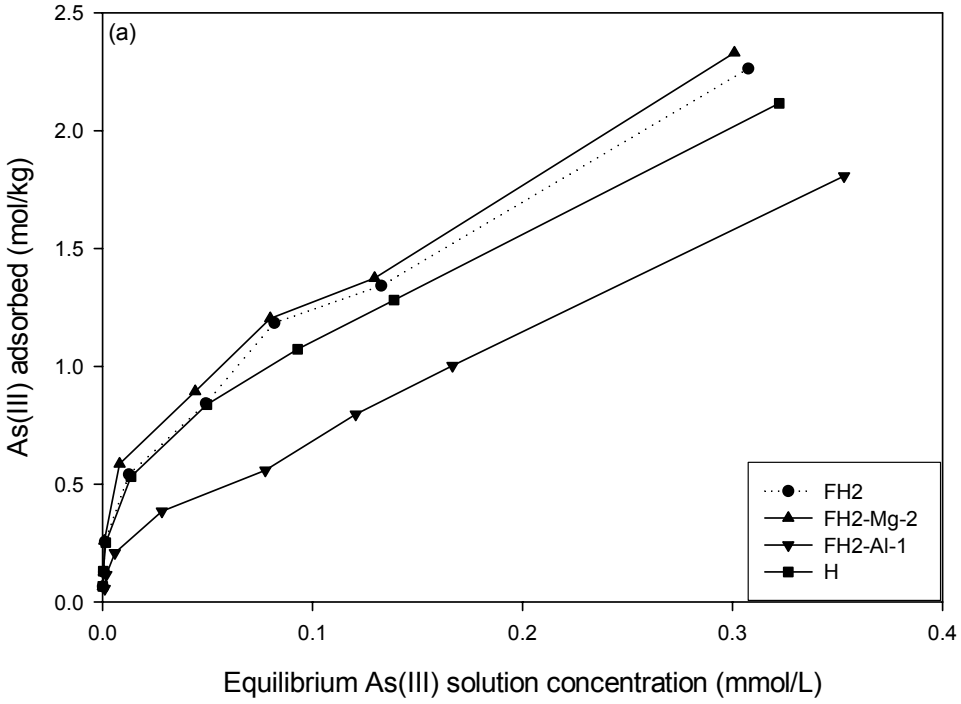

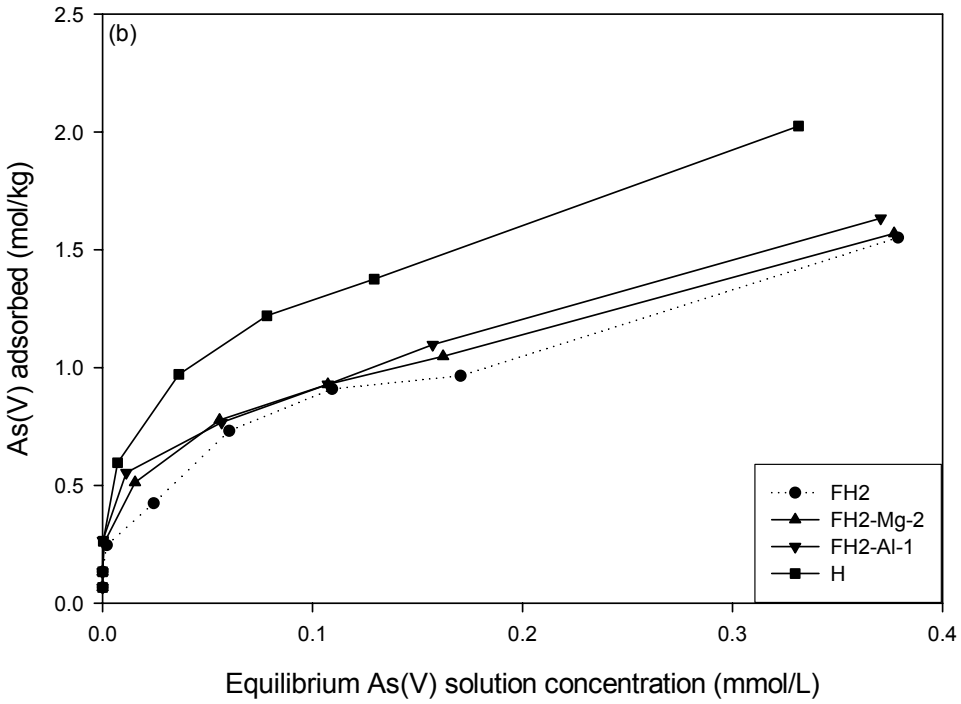

Figure 6.28 Arsenic Adsorption at pH 7 and at Initial High As Loadings (0.06674, 0.13347, 0.2669, 0.6674, 1.3347, 2.0021, 2.6694, and 5.3389 mol As/kg).

6.2.5.3 Comparison of Adsorption Capacities of Arsenic

The highest observed adsorption density for arsenite decreased in the order of FH2-Mg-2 > FH2 > HTlc > FH2-Al-1 while for arsenate it followed the order: HTlc > FH2-Al-1 > FH2-Mg-2 > FH2. FH2-Mg-2 exhibited slightly higher adsorption density for both arsenite and arsenate than FH2. Compared to FH2 (325.8 m^2/g, the PZC of 7.82, 2.389 μm), the higher arsenic adsorption density of FH2-Mg-2 may be due to larger specific surface area (340.2 m^2/g), more positively charged surface (the PZC of 7.90), and smaller particle size (2.175 μm) although FH2-Mg-2 was very similar to FH2 from the viewpoint of structure. High arsenate adsorption density for HTlc may be due to ion exchange of interlayer anions (carbonate ions) by arsenate ions [247~250] as well as a high PZC value of 8.94 [73].

For FH2-Al-1, the lowest arsenite adsorption density may be attributable to a weak affinity of arsenite toward gibbsite [195] and amorphous Al hydroxide [257]: outer-sphere complexes on amorphous Al hydroxide [168] and inner- or outer-sphere complexes on crystalline Al hydroxide (gibbsite) at a pH of > 5.5 [196]. However, FH2-Al-1, which consisted of poorly crystalline 2-line ferrihydrite, poorly crystalline Al hydroxide, and crystalline Al hydroxides (gibbsite and bayerite) (section 4.2.1), showed a higher adsorption density of arsenate with respect to FH2 and FH2-Mg-2. The higher adsorption density of arsenate for FH2-Al-1 may be explained as follows: First, arsenate adsorbed strongly on FH2-Al-1, forming an inner-spehere complex on poorly crystalline Al hydroxide, crystalline Al hydroxides (gibbsite and bayerite) [168, 196], poorly crystalline 2-line ferrihydrite. Second, although the OH^- groups on the planar surfaces of gibbsite are fully charge-satisfied and relatively inert [53, 253], the edges of gibbsite have

a lot of undercoordinated O atoms which are active sites for oxyanion sorption reactions [53]. The abundance of highly reactive, undercoordinated O atoms on the edges of gibbsite and over much of surface of poorly crystalline Al hydroxide may be responsible for the higher arsenate adsorption on FH2-Al-1 [228]. Third, the higher arsenate adsorption for FH2-Al-1 may be attributable to the high PZC value of poorly crystalline Al hydroxide (8.5~9.4) [168, 228], gibbsite (9.0~9.9) and bayerite (9.1) [196, 228~230]. Finally, the large specific surface area (> 600 m^2/g) of poorly crystalline Al hydroxide may in part lead to increase the arsenate adsorption capability for FH2-Al-1[218].

Previously, arsenate adsorption on different Al(III) derived phases has been reported with contrasting results. It was generally reported that arsenate adsorption on hydrous ferric oxide suspension at pH 5 to 8 exceeded the arsenate adsorption on hydrous aluminum oxide suspension [259, 261] due to incomplete precipitation of added aluminum as an amorphous hydroxide [262] and greater solubility of amorphous hydroxide of aluminum at both low and high pH values with respect to Fe (III) [259]. Arsenate adsorption on 0:1 Al:Fe hydroxide (2-line ferrihydrite) suspension was higher than that on both 1:0 Al:Fe hydroxide (Al hydroxides) suspension and 1:1 Al:Fe hydroxide suspension (at 0.01~0.5 $mol_{As(V)}/(mol_{Al+Fe})$ [98]. However, the maximum levels of PO_4 adsorption on Al and Fe hydroxide solutions at pH 6 were reported to be 1.86 (2-line ferrihydrite solution), 2.50 (1:1 mixture of 2-line ferrihydrite/noncrystalline Al hydroxide solution), and 3.40 mol PO_4/kg (noncrystalline Al hydroxide solution) [263].

On the other hand, arsenate adsorption on amorphous Al hydroxide solid was slightly higher than that on amorphous Fe hydroxide solid (at pH 7 and at 0.25 and 2 mol As(V)/kg) [168]. Removal of arsenate by adsorption on synthetic Al hydroxide solid was

more effective than on synthetic Fe hydroxide (2-line ferrihydrite) solid (at pH 5 and at 0~2.67 mol As(V)/kg) due to a smaller degree of crystallinity of amorphous Al hydroxide than amorphous Fe hydroxide (2-line ferrihydrite) [264]: The adsorption capacity of arsenate was determined to be 1.63 mol As(V)/kg for amorphous Al hydroxide solid and 1.01 mol As(V)/kg for 2-line ferrihydrite solid, respectively.

We do not have an explanation for the discrepancy in adsorption capacity of arsenate between this study and other studies [98, 259, 261] other than that it could be due to different experimental conditions such as the type of adsorbent (solid vs solution) and the degree of transformation of adsorbent. However, the experimental results in this study presented here led us to suggest the following scenarios. First, arsenate adsorption on Al hydroxide solid was larger than that on Fe hydroxide solid [168, 264] whereas removal of arsenate by adsorption on Fe hydroxide solution was larger than that on Al hydroxide solution [30, 259, 261]. In this study, air-dried solids were used as adsorbents. Therefore, it may be assumed that adsorption of arsenate on FH2-Al-1 was larger than that on FH2. Second, the observed difference in arsenate adsorption capacities between FH2 and FH2-Al-1 may be due to a smaller degree of crystallinity of FH2-Al-1 with respect to FH2. The fraction ($[Fe_o]/[Fe_t]$) of amorphous Fe remaining in FH2 (aged at RT for 30 days) and FH2-Al-1 (aged at RT for 40 days) was 93.17 and 97.32%, respectively. The result indicates that Al (III) exhibited a strong retarding effect on the transformation of amorphous Fe in FH2-Al-1 due to the presence of Al(III) at the 2-line ferrihydrite through the complexation of stable Al(III) species [96] and the adsorption/reprecipitation of Al(III) species [220]. The smaller degree of cryatllinity of FH2-Al-1 was also confirmed by a comparison of XRD patterns for FH2 and FH2-Al-1 during aging (air-

drying) at RT as shown in Figure 6.29. It was observed that peaks of 2-line ferrihydrite for FH2-Al-1's aged for both 4 and 135 days were much broader than those for FH2 aged for 20 days and peaks of gibbsite and bayerite for FH2-Al-1 aged for 4 days were less sharper than those for FH2-Al-1 aged for 135 days. The results indicates that FH2-Al-1 at an initial aging time (for example 4 days) might contain more poorly crystalline 2-line ferrihydrite than FH2 and less crystalline Al hydroxides than FH2-Al-1 aged for 135 days: FH2-Al-1 consisted of poorly crystalline/less crystalline Al hydroxides and more poorly crystalline 2-line ferrihydrite whereas FH2 was composed of poorly crystalline 2-line ferrihydrite. Therefore, FH2-Al-1 showed a smaller degree of crystallinity than FH2.

In summary, the higher arsenate adsorption on FH2-Al-1 with respect to FH2 might be attributable to the smaller degree of crystallinity, the abundance of highly reactive, unsaturated O atoms on the edges of gibbsite, the high PZC value, the large specific surface area of poorly crystalline Al hydroxide.

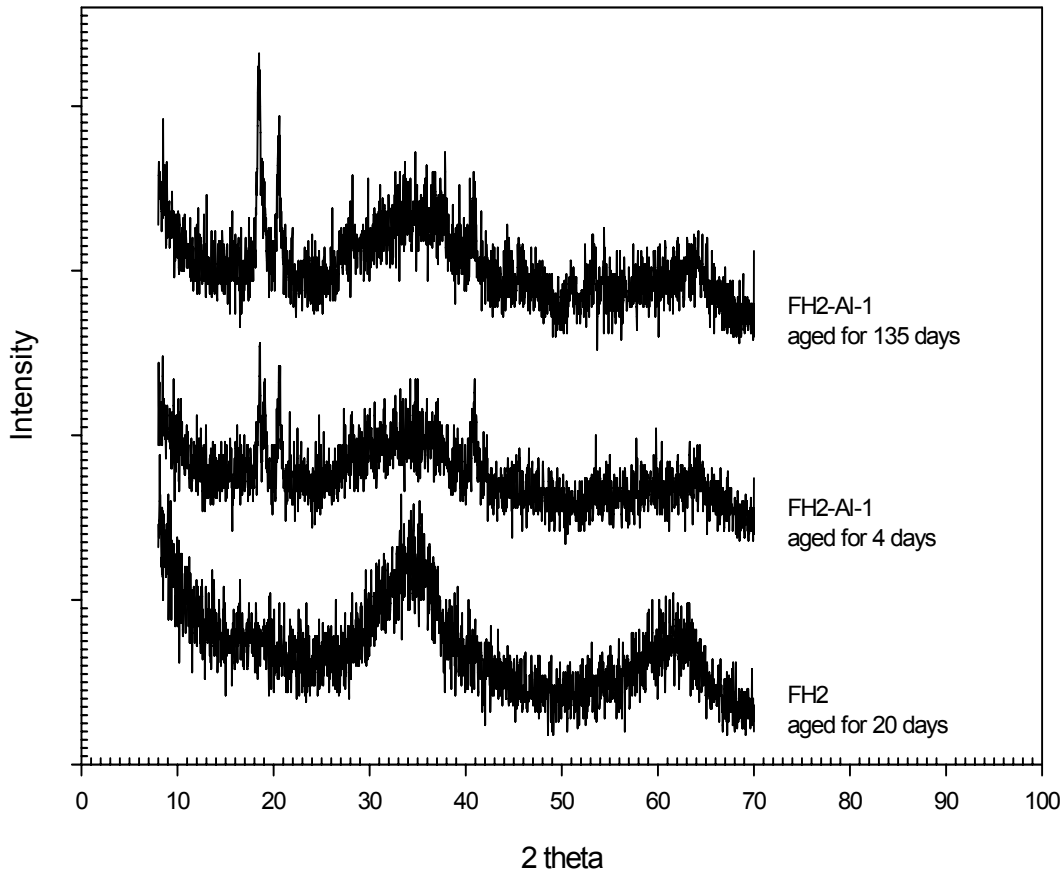

Figure 6.29 A Comparison of XRD Patterns of FH2 and FH2-Al-1 during Aging at Room Temperature.

6.2.6 Environmental Implications

The adsorption study has shown that arsenic adsorption on the fresh, aged, and heated FH2s was influenced by their chemical composition (inhibitor/Fe ratio, $[Fe_o]/[Fe_t]$, and products) and surface properties (surface charge and surface area). Compared to the fresh FH2, the fresh HTlc, FH2-Al-1, and FH2-Mg-2 showed higher adsorption densities for As(V), while the fresh Mg-2 exhibited a larger adsorption density for As(III). In water treatment, more efficient As(V) removal could potentially be achieved using HTlc, FH2-Al-1, and FH2-Mg-2 as filter media for column adsorption compared to FH2 due to a

more positively charged surface and a smaller degree of crystallinity. As(III) might be also more effectively removed using FH2-Mg-2 as a filter medium compared to FH2.

The positive effect of inhibitor (except Ci) on amorphous Fe transformation during heat treatment and arsenic adsorption on the heated FH2s was evident. Considering both amorphous Fe transformation and arsenic retention, use of other FH2s instead of FH2 in water treatment will likely result in enhancing arsenic retention at waste disposal sites. Under reduced conditions as might occurring at a disposal site of arsenic waste, a reductive dissolution of FH2 and a reduction of As(V) to As(III) would be expected, resulting in a release of arsenic into the disposal site. Compared to pure FH2, arsenic might be more strongly retained over time due to a slower rate of reductive dissolution at the disposal site when FH2 with a coprecipitated inhibitor (Si(IV) or Al(III)) is used for removing As(V) or FH2 with an adsorbed inhibitor (Mg(II)) is used for removing As(III) in water treatment. Since As(V) species occur as the most stable forms of arsenic in oxidized surface water, As(V) waste may be generally produced in water treatment. Therefore, use of the FH2-Al and FH-Si series for As(V) and the FH2-Mg series for As(III) in water treatment might be more advantageous compared to the other FH2s. Also, use of HTlc in water treatment will likely lead to improve arsenic retention at waste disposal sites compared to the other FH2s due to a higher adsorption capacity of arsenic on the heated HTlc, almost equal to that for the fresh HTlc. In order to obtain an improved understanding of the probable fate of arsenic at disposal sites, the rate and products of reductive dissolution of the FH2-Al, FH2-Si, FH2-Mg series and HTlc in the presence of arsenic must be investigated.

6.3 Conclusions

Arsenic adsorption on the fresh FH2s at pH 7 was decreased with increasing the Ci(citrate)/Fe, Al/Fe, Si/Fe, and Ti/Fe molar ratios for As(III), while for As(V) adsorption was reduced with increasing the Ci/Fe, Si/Fe, and Ti/Fe molar ratios. An increase in the Ci/Fe molar ratio resulted in a considerable decrease in arsenic adsorption. The adsorption density for As(III) was 2.33, 2.26, and 1.81 mol/kg for FH2-Mg-2, FH2, and FH2-Al-1, respectively, while for As(V) adsorption density was 1.63, 1.57, and 1.55 mol/kg for FH2-Al-1, FH2-Mg-2, and FH2, respectively. Aging at RT for 235 d led to slightly decreased arsenic adsorption, whereas heat treatment at 360 ^{o}C resulted in considerably reduced arsenic adsorption. The heated FH2 showed a smaller adsorption capacity of arsenic than the other heated FH2s (except the FH2-Ci series). The heated FH2-Al and FH2-Si series showed much higher adsorption capacities for As(V) than any other FH2, whereas the heated FH2-Mg series exhibited the largest adsorption capacity of As(III) among the heated FH2s. As(III) adsorption on the fresh FH2s increased with increasing pH, whereas As(V) adsorption reached broad maxima from pH 3 to 7, but decreased at pH 9. With increasing inhibitor/Fe molar ratio, As(III) adsorption on the fresh FH2-Mg series was less sensitive to low pH (3), whereas As(V) adsorption on the fresh FH2-Al and FH2-Mg series were less affected by high pH (9). In water treatment, more efficient arsenic removal might potentially be achieved by using FH2-Al-1 and FH2-Mg-2 for As(V) and FH2-Mg-2 for As(III) as filter media, and the use of the FH2-Al and FH-Si series for As(V) and the FH2-Mg series for As(III) will likely result in enhanced arsenic retention at waste disposal sites.

CHAPTER VII

SUMMARY AND CONCLUSIONS

Two-line ferrihydrite was observed as the sole phase in the fresh FH2, FH2-Si, FH2-Ti, FH2-Ci(citrate), and FH2-Mg series (aged for 20 d), whereas the FH2-Al series (aged for 135 d) consisted of mixed solid phases (2-line ferrihydrite, gibbsite, bayerite, and poorly crystalline Al hydroxide). For FH2, FH2-Si-0.1, FH2-Mg-2, and FH2-Al-1 sieved to a grain size of smaller than the No. 100 (0.15 mm), each sample showed a nearly normal distribution of particle size with volume means of 2.175~2.389 μm, while the BET specific surface areas ranged from 229.3 (FH2-Al-1) to 393.8 m^2/g (FH2-Si-0.1). The coprecipitation of Si(IV) with Fe(III) shifted the PZC (7.82 for FH2) to a more acidic pH (6.90 for FH2-Si-0.1), whereas the specific adsorption of Mg(II) or the coprecipitation of Al(III) with Fe(III) promoted a shift of the PZC to more basic pH values (7.90 for FH2-Mg-2 and 8.70 for FH2-Al-1). A positive effect of inhibitor on mechanical strength was obtained only for FH2-Si-0.1. The characterization study has shown that inhibitor/Fe molar ratio can play a significant role in determining chemical and physical characteristics. Therefore, before any realistic application of the FH2s as adsorbents, they need to first be evaluated for extent of transformation and the adsorption capacity of arsenic.

After aging the FH2s (except for the FH2-Al series) at RT for 235 d, 13~32% of the amorphous Fe oxide had transformed into other iron oxides. The transformation of amorphous Fe oxide was retarded in the presence of Si(IV) or at high molar ratios of Mg(II) and citrate. However, there were no distinct differences between inhibitor-specific

influences on the transformation (except for Si). Compared to aging at RT, heat treatment at high temperatures had much more significant effects on transformation of the FH2s. Upon heating the FH2, FH2-Mg, FH2-Ti, and FH2-Ci series at 360 ^{o}C, most of the amorphous Fe oxide was transformed to hematite, whereas Si(IV) and Al(III) had stronger retarding effects on the transformation of amorphous Fe oxide than any of the other inhibitors. Si(IV) was much more pronounced than Al(III) in retarding the transformation. Hematite and 2-line ferrihydrite were identified with increasing Al/Fe molar ratio, while at higher Al/Fe molar ratios $\geq$ 0.5, greater than 25% of the 2-line ferrihydrite remained untransformed, gibbsite and bayerite were decomposed, and very tiny peaks indicative of boehmite appeared as a trace component. Heat treatment at 360 ^{o}C resulted in a basic shift of the PZC for FH2 and FH2-Mg-2, whereas for FH2-Si-0.1 and FH2-Al-1, the PZC dropped to slightly more acidic pH values. In summary, heat treatment at high temperatures had considerable impacts on the transformation, structure, and PZC of the FH2s compared to aging ar RT. The influence of inhibitor on the transformation was related to its affinity for the 2-line ferrihydrite surface. Transformation inhibitors that have the ability to coprecipitate with Fe(III) or specially adsorb on the 2-line ferrihydrite surface could retard the overall transformation. Especially, both coprecipitated Si(IV) and Al(III) had stronger retarding effects on the transformation of amorphous Fe oxide than any of the other inhibitors during heat treatment at high temperatures. The concentration of the inhibitor also exerted a signicant influence on surface charge and composition of the product, with hematite formation being favored at lower inhibitor/Fe molar ratios.

Arsenic adsorption on the fresh FH2s at pH 7 decreased with increasing Ci/Fe, Al/Fe, Si/Fe, and Ti/Fe molar ratio for As(III), while for As(V) adsorption was reduced with increasing Ci/Fe, Si/Fe, and Ti/Fe molar ratio. The adsorption density for As(III) on the FH2s decreased in the order: FH2-Mg-2 > FH2 > FH2-Al-1, whereas for As(V) adsorption was decreased in the order: FH2-Al-1 > FH2-Mg-2 > FH2. Compared to the fresh FH2s, aging at RT for 235 d had only a slight effect on arsenic adsorption, whereas heat treatment at 360 ^{o}C resulted in considerably reduced arsenic adsorption. The heated FH2s containing an inhibitor (except citrate for As(V)) showed larger adsorption capacities for arsenic than the heated FH2. The heated FH2-Al and FH2-Si series showed much higher adsorption capacities of As(V) than any of the other FH2s, whereas the heated FH2-Mg series exhibited the largest adsorption capacity of As(III) among the heated FH2s. There was a trend of increasing As(III) adsorption on the fresh FH2s with increasing pH, whereas As(V) adsorption reached broad maxima from pH 3 to 7, but decreased at pH 9. With increases in the inhibitor/Fe molar ratio, As(III) adsorption on the fresh FH2-Mg series was less affected by low pH (3), and As(V) adsorption on the fresh FH2-Al and FH2-Mg series were less sensitive to high pH (9). The adsorption study has shown that arsenic adsorptions on the fresh, aged, and heated FH2s were influenced by their chemical composition (inhibitor/Fe ratio, $[Fe_o]/[Fe_t]$, and mineralogy) and surface properties (surface charge and surface area).

The results of this study showed that inhibitors (except for citrate) had a positive influence on FH2 transformation during heat treatment and arsenic adsorption. Therefore, the inhibitors can play a significant role in both arsenic removal in water treatment and sludge transformation behavior at waste-disposal sites. Compared to the traditional

coagulation process with FH2 suspension alone in water treatment, the use of FH2 coprecipitated with an inhibitor or specifically adsorbed by an inhibitor as a filter medium might be advantageous for arsenic removal and waste management. In water treatment, more effective arsenic removal could potentially be achieved using FH2-Al-1 and FH2-Mg-2 for As(V) and FH2-Mg-2 for As(III) as filter media and the use of the FH2-Al and FH-Si series for As(V) and the FH2-Mg series for As(III) will likely result in improved arsenic retention at waste-disposal sites. To obtain an improved understanding of the fate of arsenic at disposal sites, the rate and products of transformation of the FH2-Al, FH2-Si, and FH2-Mg series in the presence of arsenic must be investigated. Before any realistic application as filter media in water treatment, these materials need to be further evaluated for the desorption behavior of arsenic and the effect of counterion on arsenic adsorption.

REFERENCES

[1] R.M. Cornell, U. Schwertmann, The Iron Oxides: Structure, Properties, Reactions, Occurrences, and Uses, VCH, Weinheim, 1996, p. 7-432.

[2] R.M. Cornell, U. Schwertmann, The Iron Oxides: Structure, Properties, Reactions, Occurrences and Uses, WILEY-VCH, Weinheim, 2003, p. 1-540.

[3] U. Schwertmann, Adv. Soil Sci. 1 (1985) 172.

[4] J.L. Jambor, J.E. Dutrizac, Chem. Rev. 98 (1998) 2549.

[5] F.V. Chukhrov, B.B. Zvyagin, A.I. Gorshkov, L.P. Ermilova, V.V. Balashova, Izvest. Akad. Nauk, SSSR, Ser. Geol. 4 (1973) 23.

[6] W. Feitknecht, W. Michaelis, Helv. Chim. Acta 45 (1962) 212.

[7] K.M. Towe, W.F. Bradley, J. Colloid Interface Sci. 24 (1967) 384.

[8] U. Schwertmann, J. Friedl, H. Stanjek, J. Colloid Interface Sci. 209 (1999) 215.

[9] F.V. Chukhrov, B.B. Zvyagin, A.I. Gorshkov, L.P. Ermilova, V.V. Korovushkin, E.S. Rudnitskaya, Yakubovskaya, Izvest. Akad. Nauk, SSSR, Ser. Geol. 5 (1976) 5.

[10] R.A. Eggleton, R.W. Fitzpatrick, Clays Clay Miner. 36 (1988) 111.

[11] A. Manceau, J.M. Combes, G. Calas, Clays Clay Miner. 38 (1990) 331.

[12] V.A. Drits, B.A. Sakharov, A.L. Salyn, A. Manceau, Clay Miner. 28 (1993) 185.

[13] A. Manceau, V.A. Drits, Clay Miner. 28 (1993) 165.

[14] J.M. Combes, A. Manceau, G. Calas, J.Y. Bottero, Geochim. Cosmochim. Acta 53 (1989) 583.

[15] G.A. Waychunas, B.A. Rea, C.C. Fuller, J.A. Davis, Geochim. Cosmochim. Acta 57 (1993) 2251.

[16] G.A. Waychunas, C.C. Fuller, B.A. Rea, J.A. Davis, Geochim. Cosmochim. Acta 60 (1996) 1765.

[17] J.M. Combes, A. Manceau, G. Calas, Geochim. Cosmochim. Acta, 54 (1990) 1083.

[18] D.E. Janney, J.M. Cowley, P.R. Buseck, Am. Min. 85 (2000) 1180.

[19] J. Zhao, F.E. Huggins, Z. Feng, F. Lu, N. Shah, G.P. Huffman, J. Catal. 143 (1993) 499.

[20] J. Zhao, F.E. Huggins, Z. Feng, G.P. Huffman, Clays Clay Miner. 42 (1994) 737.

[21] A. Manceau, W.P. Gates, Clays Clay Miner. 45 (1997) 448.

[22] D.E. Janney, J.M. Cowley, P.R. Buseck, Clays Clay Miner. 48 (2000) 111.

[23] D.G. Lewis, C.M. Cardile, Austr. J. Soil Res. 27 (1989) 103.

[24] U. Schwertmann, J. Friedl, A. Kyek, Clays Clay Miner. 52 (2004) 221.

[25] R.K. Kukkadapu, J.M. Zachara, J.K. Fredrickson, S.C. Smith, A.C. Dohnalkova, C.K. Russell, Am. Min. 88 (2003) 1903.

[26] M.S. Seehra, P. Roy, A. Raman, A. Manivannan, Solid State Commun. 130 (2004) 597.

[27] T. Ishikawa, T. Ueno, A. Yasukawa, K. Kandori, T. Nakayama, T. Tsubota, J. Mater. Chem. 12 (2002) 2416.

[28] U. Schwertmann, J. Friedl, H. Stanjek, D.G. Schulze, Clays Clay Miner. 48 (2000) 159.

[29] A. Violante, M. Ricciardella, M. Pigna, Water Air Soil Pollut. 145 (2003) 289.

[30] Y. Masue, R.H. Loeppert, T.A. Kramer, Environ. Sci. Technol. (2006) (In press).

[31] U. Schwertmann, R.M. Cornell, Iron Oxides in the Laboratory, VCH, New York, 1991, p. 54-110.

[32] F.V. Chukhrov, B.B. Zvyagin, A.I. Gorshkov, L.P. Yermilova, V.V. Balashova, Int. Geol. Rev. 16 (1973) 1131.

[33] J.D. Russell, Clay Miner. 14 (1979) 109.

[34] S. Brunauer, P.H. Emmett, E. Teller, J. Am. Chem. Soc. 60 (1938) 309.

[35] L. Clausen, I. Fabricius, J. Colloid Interface Sci. 227 (2000) 7.

[36] P.G. Weidler, J. Porous Materials 4 (1997) 165.

[37] A.A. Van der Giessen, J. Inorg. Nucl. Chem. 28 (1966) 2155.

[38] L. Carlson, U. Schwertmann, Geochim. Cosmochim. Acta 45 (1981) 421.

[39] R.J. Davies-Colley, P.O. Nelson, K.J. Williamson, Environ. Sci. Technol. 18 (1984) 491.

[40] A. Hofmann, M. Pelletier, L. Michot, A. Stradner, P. Schurtenberger, R. Kretzschmar, J. Colloid Interface Sci. 271 (2004) 163.

[41] H. Stanjek, P.G. Weidler, Clay Miner. 27 (1992) 397.

[42] H.C. Bruun Hansen, B. Raben-Lange, K. Raulund-Rasmussen, O.K. Borggaard, Soil Sci. 158 (1994) 40.

[43] L. Axe, P.R. Anderson, J. Colloid Interface Sci. 175 (1995) 157.

[44] K.P. Raven, A. Jain, R.H. Loeppert, Environ. Sci. Technol. 32 (1998) 344.

[45] C.E. Martínez, S. Sauvé, A. Jacobson, M.B. Mcbride, Environ. Sci. Technol. 33 (1999) 2016.

[46] O. Larsen, D. Postma, Geochim. Cosmoch. Acta 65 (2001) 1367.

[47] A.C. Scheinost, S. Abend, K.I. Pandya, D.L. Sparks, Environ. Sci. Technol. 35 (2001) 1090.

[48] P. Leone, M. Gennari, M. Nègre, V. Boero, J. Agric. Food Chem. 49 (2001) 1315.

[49] M. Grafe, M.J. Eick, P.R. Grossl, A.M. Saunders, J. Environ. Qual. 31 (2002) 1115.

[50] A. Voegelin, S.J. Hug, Environ. Sci. Technol. 37 (2003) 972.

[51] L. Charlet, A.A. Manceau, J. Colloid Interface Sci. 148 (1992) 443.

[52] M.B. McBride, in: J.B. Dixon, S.B. Weed (Eds.), Surface Chemistry of Soil Minerals, SSSA, Inc., Madison, WI, 1989, p. 35-87.

[53] C.T. Johnston, E. Tombácz, in: J.B. Dixon, S.B. Weed (Eds.), Surface Chemistry of Soil Minerals, SSSA, Inc., Madison, WI, 2002, p. 37-67.

[54] G.H. Bolt, W.H. Van Riemsdijk, in: G.B. Bolt (Eds.), Ion Adsorption in Inorganic Variable Charge Constituents, Elsevier Scientific Publishing Company, Amsterdam, 1982, p. 459-504.

[55] J.A. Dyer, P. Trivedi, N,C, Scrivner, D.L. Sparks, Environ. Sci. Technol. 37 (2003) 915.

[56] P. Trivedi, J.A. Dyer, D.L. Sparks, Environ. Sci. Technol. 37 (2003) 908.

[57] H.C.B. Hansen, T.P. Wetche, K. Raulund-Rasmussen, O.K. Borggaard, Clay Miner. 29 (1994) 341.

[58] H.H. Huang, M.C. Lu, J.N. Chen, Wat. Res. 35 (2001) 2291.

[59] G.A. Parks, Chem. Rev. 39 (1965) 177.

[60] P.H. Tewari, A.W. Mclean, J. Colloid Interface Sci. 40 (1972) 267.

[61] N.H.G. Penners, L.K. Koopal, Colloids & Surfaces 19 (1986) 337.

[62] W. Stumm, Chemistry of the Solid-Water Interface, Wiley & Sons Inc., New York, 1992, p. 428.

[63] P. Hesleitner, D. Babić, N. Kallay, E. Matijević, Langmuir 3 (1987) 815.

[64] U. Schwertmann, H. Fechter, Clay Miner. 17 (1982) 471.

[65] P.R. Anderson, M.M. Benjamin, Environ. Sci. Technol. 19 (1985) 1048.

[66] M. Ohmori, E. Matijević, J. Colloid Interface Sci. 150 (1992) 594.

[67] A. Garg, E. Matijević, Langmuir 4 (1988) 38.

[68] P. Tartaj, A. Cerpa, M.T. García-González, C.J. Serna, Clays Clay Miner. 50 (2002) 342.

[69] A. Cerpa, M.T. García-González, C.J. Serna, P. Tartaj, The Canadian Journal of Chemical Engineering 79 (2001) 608.

[70] T.D. Evans, J.R. Leal, P.W. Arnold, J. Electroanal. Chem. 105 (1979) 161.

[71] W.A. Zeltner, M.A. Anderson, Langmuir 4 (1988) 469.

[72] A. Jain, K.P. Raven, R.H. Loeppert, Environ. Sci. Technol. 33 (1999) 1179.

[73] W. Stumm, J.J. Morgan, Aquatic Chemistry – Chemical Equilibria and Rates in Natural Waters, John Wiley & Sons, Inc., New York, 1996, p. 516-613.

[74] R.M. Cornell, R. Giovanoli, W. Schneider, J. Chem. Tech. Biotechnol. 46 (1989) 115.

[75] U. Schwertmann, R.M. Taylor, in: J.B. Dixon, S.B. Weed (Eds.), Iron Oxides, SSSA, Inc., Madison, WI, 1989, p. 379-438.

[76] D. Postma, R. Jakobsen, Geochim. Cosmochim. Acta 60 (1996) 3169.

[77] M.A. Sørensen, M.M. Stackpoole, A.I. Frenkel, R.K. Bordia, G.V. Korshin, T.H. Christensen, Environ. Sci. Technol. 34 (2000) 3991.

[78] M.A. Blesa, E. Matijević, Adv. Colloid Interface Sci. 29 (1989) 173.

[79] U. Schwertmann, E. Murad, Clays Clay Miner. 31 (1983) 277.

[80] R.M. Cornell, U. Schwertmann, Clays Clay Miner. 27 (1979) 402.

[81] U. Schwertmann, R.M. Cornell, Iron Oxides in the Laboratory, VCH, Weinheim, 2000, p. 51.

[82] U. Schwertmann, Plant & Soil 130 (1991) 1.

[83] R.M. Cornell, R. Giovanoli, Clays Clay Miner. 33 (1985) 424.

[84] K.A. Baltpurvins, R.C. Burns, G.A. Lawrence, Environ. Sci. Technol. 30 (1996) 939.

[85] H. Lengweiler, W. Buser, W. Feitknecht, Helv. Chim. Acta 44 (1961) 796.

[86] H. Lengweiler, W. Buser, W. Feitknecht, Helv. Chim. Acta 44 (1961) 805.

[87] R.J. Knight, R.N. Sylva, J. inorg. nucl. Chem. 36 (1974) 591.

[88] W.R. Fischer, U. Schwertmann, Clays Clay Miner. 23 (1975) 33.

[89] H. Bao, P.L. Koch, Geochim. Cosmochim. Acta 63 (1999) 599.

[90] R. Giovanoli, R.M. Cornell, Z. Pfanzenernähr. Bodenk 155 (1992) 455.

[91] G. Bondietti, J. Sinniger, W. Stumm, Colloids Surf. A 79 (1993) 157.

[92] R.M. Cornell, R. Giovanoli, P.W. Schindler, Clays Clay Miner. 35 (1987) 21.

[93] S. Glasauer, J. Friedl, U. Schwertmann, J. Colloid Interface Sci. 216 (1999) 106.

[94] U. Schwertmann, R.M. Taylor, Clays Clay Miner. 20 (1972) 159.

[95] U. Schwertmann, H. Thalmann, Clay Miner. 11 (1976) 189.

[96] R.M. Taylor, Geoderma 42 (1988) 65.

[97] D.G. Lewis, U. Schwertmann, Clays Clay Miner. 27 (1979) 195.

[98] R.W. Fitzpatrick, J. Le Roux, U. Schwertmann, Clays Clay Miner. 26 (1978) 189.

[99] R.M. Cornell, R. Giovanoli, W. Schneider, J. Chem. Tech. Biotechnol. 53 (1992) 73.

[100] R.M. Cornell, Clay Miner. 23 (1988) 329.

[101] R.G. Ford, K.M. Kemner, P.M. Bertsch, Geochim. Cosmochim. Acta 63 (1999) 39.

[102] J.K. Fredrickson, J.M. Zachara, R.K. Kukkadapu, Y.A. Gorby, S.C. Smith, C.F. Brown, Environ. Sci. Technol. 35 (2001) 703.

[103] R.M. Cornell, Clays Clay Miner. 33 (1985) 219.

[104] R.M. Cornell, Z. Pfanzenernähr. Bodenk 150 (1987) 304.

[105] R.M. Cornell, R. Giovanoli, Clays Clay Miner. 37 (1989) 65.

[106] V. Barrón, J. Torrent, E. De Grave, Am. Min. 88 (2003) 1679.

[107] D.G. Schulze, U. Schwertmann, Clay Miner. 19 (1984) 521.

[108] P.G. Weidler, H. Stanjek, Clay Miner. 33 (1998) 277.

[109] C.W. Childs, N. Kanasaki, N. Yoshinaga, Clay Sci. 9 (1993) 65.

[110] A.S. Campbell, U. Schwertmann, H. Stanjek, J. Friedl, A. Kyek, P.A. Campbell, Langmuir 18 (2002) 7804.

[111] C.R.A. Catlow, J. Corish, J. Hennessy, W.C. Mackrodt, J. Am. Ceram. Soc. 71 (1988) 42.

[112] F. Watari, P. Delavignette, J. Van Landuyt, S. Amelinckx, J. Solid State Chem. 48 (1983) 49.

[113] A.J. Herbillon, J. Tran Vian An, J. Soil Sci. 20 (1969) 223.

[114] S.M. Glasauer, P. Hug, P.G. Weidler, A.U. Gehring, Clays Clay Miner. 48 (2000) 51.

[115] R.K. Vempati, R.H. Loeppert, D.C. Dufner, D.L. Cocke, Soil Sci. Soc. Am. J. 54 (1990) 695.

[116] N. Yoshinaga, N. Kanasaki, Clay Sci. 9 (1993) 43.

[117] R.L. Parfitt, S.J. Van der Gaast, C.W. Childs, Clays Clay Miner. 40 (1992) 675.

[118] M. Soma, H. Seyama, N. Yoshinaga, B.K.G. Theng, C.W. Childs, Clay Sci. 9 (1996) 385.

[119] WHO, Toxicity Effects of Arsenic in Humans, www.who.int/peh-super/Oth.lec/Arsenic/series4/0002.htm, Washington, DC, 1999.

[120] EPA, Arsenic in Drinking Water: Health Effects Research, www.epa.gov/OGWDW/ars/ars10.html, Washington, DC, 1999.

[121] J. Farrell, J. Wang, P. O'day, M. Conklin, Environ. Sci. Technol. 35 (2001) 2026.

[122] N.E. Korte, Q. Fernando, Crit. Rev. Environ. Control 21 (1991) 1.

[123] J.F. Ferguson, J. Gavis, Water Res. 6 (1972) 1259.

[124] J.G. Hering, P.Y. Chen, J.A. Wilkie, M. Elimelech, S. Liang, J. AWWA, 88 (1996) 155.

[125] J.Q. Jiang, Water Sci. Technol. 44 (2001) 89.

[126] P.H. Masscheleyn, R.D. Delaune, W.H. Patrick Jr., Environ. Sci. Technol. 25 (1991) 1414.

[127] M. Edwards, J. AWWA 86 (1994) 64.

[128] L. Wang, A.S.C. Chen, T.J. Sorg, K.A. Fields, J. AWWA 94 (2002) 161.

[129] S.K. Gupta, K.Y. Chen, J. Water Pollu. Control Fed. 50 (1978) 493.

[130] E. Korngold, N. Belayev, L. Aronov, Desalination 141 (2001) 81.

[131] J.J. Waypa, M. Elimelech, J.G. Hering, J. AWWA 89 (1997) 102.

[132] P. Brandhuber, G. Amy, Desalination 117 (1998) 1.

[133] A. Seidel, J.J. Waypa, M. Elimelech, Environ. Eng. Sci. 18 (2001) 105.

[134] P. Brandhuber, G. Amy, Desalination 140 (2001) 1.

[135] Y. Sato, M. Kang, T. Kamei, Y. Magara, Water Res. 36 (2002) 3371.

[136] T. Budinova, N. Petrov, M. Razvigorova, J. Parra, P. Galiatsatou, Ind. Eng. Chem. Res. 45 (2006) 1896.

[137] A. Joshi, M. Chaudhuri, J. Environ. Eng. 122 (1996) 769.

[138] S. Bajpai, M. Chaudhuri, J. Environ. Eng. 125 (1999) 782.

[139] S. Chakravarty, V. Dureja, G. Bhattacharyya, S. Maity, S. Bhattacharjee, Water Res. 36 (2002) 625.

[140] B.A. Manning, S. Goldberg, Environ. Sci. Technol. 31 (1997) 2005.

[141] S. Fendorf, M.J. Eick, P. Grossl, D.L. Sparks, Environ. Sci. Technol. 31 (1997) 315.

[142] C. Su, R.W. Puls, Environ. Sci. Technol. 35 (2001) 1487.

[143] M.V.B. Krishna, K. Chandrasekaran, D. Karunasagar, J. Arunachalam, J. Hazard. Mater. B 84 (2001) 229.

[144] R.C. Cheng, S. Liang, H.C. Wang, M.D. Beuhler, J. AWWA, 86 (1994) 79.

[145] K.N. Scott, J.F. Green, H.D. Do, S.J. McLean, J. AWWA 87 (1995) 114.

[146] M. Bissen, F.H. Frimmel, Acta Hydrochim. Hydrobiol. 31 (2003) 97.

[147] M.C.F. Magalhães, Pure Appl. Chem. 74 (2002) 1843.

[148] C.C. Fuller, J.A. Davis, G.A. Waychunas, Geochim. Cosmochim. Acta 57 (1993) 2271.

[149] S. Dixit, J.G. Hering, Environ. Sci. Technol. 37 (2003) 4182.

[150] M.L. Pierce, C.B. Moore, Environ. Sci. Technol. 14 (1980) 214.

[151] M.L. Pierce, C.B. Moore, Water Res. 16 (1982) 1247.

[152] T.H. Hsia, S.L. Lo, C.F. Lin, Chemosphere 25 (1992) 1825.

[153] T.H. Hsia, S.L. Lo, C.F. Lin, D.Y. Lee, Colloids Surf. A 85 (1994) 1.

[154] J.A. Wilkie, J.G. Hering, Colloids Surf. A 107 (1996) 97.

[155] B.A. Manning, S.E. Fendorf, S. Goldberg, Environ. Sci. Technol. 32 (1998) 2383.

[156] W. Driehaus, M. Jekel, U. Hildebrandt, J. Water SRT-Aqua 47 (1998) 30,

[157] O.S. Thirunavukkarasu, T. Viraraghavan, K.S. Subramanian, Water SA 29 (2003) 161.

[158] D.B. Singh, G. Prasad, D.C. Rupainwar, V.N. Singh, Water Air Soil Pollut. 42 (1988) 373.

[159] S.E. O'Reilly, D.G. Strawn, D.L. Sparks, Soil Sci. Soc. Am. J. 65 (2001) 67.

[160] W.R. Richmond, M. Loan, J. Morton, G.M. Parkinson, Environ. Sci. Technol. 38 (2004) 2368.

[161] A. Manceau, Geochim. Cosmochim. Acta 59 (1995) 3647.

[162] S.R. Randall, D.M. Sherman, K.V. Ragnarsdottir, C.R. Collins, Geochim. Cosmochim. Acta 63 (1999) 2971.

[163] A. Manceau, K.L. Nagy, L. Spadini, K.V. Ragnarsdottir, J. Colloid Interface Sci. 228 (2000) 306.

[164] M.A. Anderson, D.T. Malotky, J. Colloid Interface Sci. 72 (1979) 413.

[165] X. Sun, H.E. Doner, Soil Sci. 161 (1996) 865.

[166] X. Sun, H.E. Doner, Soil Sci. 163 (1998) 278.

[167] J.B. Harrison, V.E. Berkheiser, Clays Clay Minner. 30 (1982) 97.

[168] S. Goldberg, C.T. Johnston, J. Colloid Interface Sci. 234 (2001) 204.

[169] L. Sigg, W. Stumm, Coll. Surf. 2 (1981) 101.

[170] U. Schwertmann, W.R. Fischer, Geoderma 10 (1973) 237.

[171] R.M. Cornell, R. Giovanoli, J. Chem. Soc., Chem. Commu. (1987), 413.

[172] R.K. Vempati, R.H. Loeppert, Clays Clay Miner. 37 (1989) 273.

[173] R.L. Parfitt, S.J. Van der Gaast, C.W. Childs, Clays Clay Miner. 40 (1992) 675.

[174] G.S.R. Krishnamurti, P.M. Huang, Clays Clay Miner. 39 (1991) 28.

[175] G.S.R. Krishnamurti, P.M. Huang, Soil Sci. Soc. Am. J. 57 (1993) 861.

[176] J.D. Filius, T. Hiemstra, W.H. Van Riemsdijk, J. Colloid Interface Sci. 195 (1997) 368.

[177] R.M. Cornell, P.W. Schindler, Colloid & Polymer Sci. 258 (1980) 1171.

[178] D.L. Jones, D.S. Brassington, European Journal of Soil Science 49 (1998) 447.

[179] N. Kallay, E. Matijević, Langmuir 1 (1985) 195.

[180] L. Lövgren, S. Sjöberg, P.W. Schindler, Geochim. Cosmochim. Acta 54 (1990) 1301.

[181] L. Lövgren, Geochim. Cosmochim. Acta 55 (1991) 3639.

[182] D.G. Schulze, U. Schwertmann, Clay Miner. 22 (1987) 83.

[183] Y. Zhang, L. Charlet, P.W. Schindler, Colloids & Surfaces 63 (1992) 259.

[184] W.F. Bleam, M.B. McBride, J. Colloid Interface Sci. 103 (1985) 124.

[185] T. Ishikawa, T. Ueno, A. Yasukawa, K. Kandori, T. Nakayama, T. Tsubota, Corrosion Science 45 (2003) 1037.

[186] L. Zeng, Wat. Res. 37 (2003) 4351.

[187] P.J. Swedlund, J.G. Webster, Wat. Res. 33 (1999) 3413.

[188] X. Meng, S. Bang, G.P. Korfiatis, Wat. Res. 34 (2000) 1225.

[189] T.R. Holm, J. AWWA 94 (2002) 174.

[190] X. Meng, G.P. Korfiatis, C. Christodoulatos, S. Bang, Wat. Res. 35 (2001) 2805.

[191] L. Zeng, Water Qual. Res. J. Canada 39 (2004) 267.

[192] M. Grafe, M.J. Eric, P.R. Grossl, Soil Sci. Soc. Am. J. 65 (2001) 1680.

[193] K. Kaiser, G. Guggenberger, L. Haumaier, W. Zech, Eur. J. Soil Sci. 48 (1997) 301.

[194] P.H. Hsu, in: J.B. Dixon, S.B. Weed (Eds.), Aluminum Hydroxides and Oxyhydroxides, SSSA, Inc., Madison, WI, 1989, p. 331-378.

[195] R. Weerasooriya, H.J. Tobschall, H.K.D.K. Wijesekara, E.K.I.A.U.K. Arachchige, K.A.S. Pathiratne, Chemosphere 51 (2003) 1001.

[196] Y. Arai, E.J. Elzinga, D.L. Sparks, J. Colloid Interface Sci. 235 (2001) 80.

[197] R.G. Robins, P. Singh, R.P. Das, in: R.G. Reddy, V. Ramachandran (Eds.), Coprecipitation of Arsenic with Fe(III), Al(III) and Mixtures of Both in a Chloride System, TMS, Warrendale, PA, 2005.

[198] P.K. Dutta, A.K. Ray, V.K. Sharma, F.J. Millero, J. Colloid Interface Sci. 278 (2004) 270.

[199] R.C. Vaishya, S.K. Gupta, Sep. Sci. and Technol. 39 (2004) 645.

[200] L.S. McNeill, M. Edwards, J. Environ. Eng. 123 (1997) 453.

[201] T.L. Theis, R. Iyer, S.K. Ellis, J. AWWA 84 (1992) 101.

[202] T.L. Theis, R. Iyer, S.K. Ellis, Environ. Progress 13 (1994) 72.

[203] S.S. Lin, M.D. Gurol, Environ. Sci. Technol. 32 (1998) 1417.

[204] B.R. Manna, S. Dey, S. Debnath, U.C. Ghosh, Water Qual. Res. J. Canada 38 (2003) 193.

[205] I.A. Katsoyiannis, A.I. Zouboulis, Wat. Res. 36 (2002) 5141.

[206] S. Khaodhiar, M.F. Azizian, K. Osathaphan, P.O. Nelson, Water Air Soil Pollut. 119 (2000) 105.

[207] O.S. Thirunavukkarasu, T. Viraraghavan, K.S. Subramanian, Water Qual. Res. J. Canada 36 (2001) 55.

[208] Y. Xu, L. Axe, J. Colloid Interface Sci. 282 (2005) 11.

[209] M. Webb, in: J.A. Greig (Eds.), Synthetic Clay Anion Exchangers: Their Structure, Modification and Application in Removing Colour and Toxins from Textile Process Waters, The Royal Society of Chemistry Information Services, London, 1996, p. 135-142.

[210] S. Abend, N. Bonnke, U. Gutschner, G. Lagaly, Colloid Polym Sci. 276 (1998) 730.

[211] W.G. Hou, Y.L. Su, D.J. Sun, C.G. Zhang, Langmuir 17 (2001) 1885.

[212] J. Das, D. Das, G.P. Dash, K.M. Parida, J. Colloid Interface Sci. 251 (2002) 26.

[213] ASTM, Annual Book of ASTM Standards-Section 4-Construction, American Society for Testing and Materials, Philadelphia, PA, 1990, p. 168-1010.

[214] APHA, AWWA, WEF, Standard Methods for the Examination of Water and Wastewater, American Public Health Association, Washington, DC, 1995, 2.80-2.81.

[215] S. Han, W. Hou, C. Zhang, D. Sun, X. Huang, G. Wang, J. Chem. Soc., Faraday Trans. 94(7) (1998) 915.

[216] G.N. White, J.B. Dixon, Soil Mineralogy Laboratory Manual Agronomy 626, Texas A&M University, College Station, TX, 2003, P. 159-162.

[217] G. Lefèvre, M. Fédoroff, Materials Letters 56 (2002) 978.

[218] P.M. Huang, M.K. Wang, N. Kämpf, D.G. Schulze, in: J.B. Dixon, D. Schulze, (Eds.), Aluminum Hydroxides, SSSA, Inc., Madison, WI, 2002, p. 261-289.

[219] D.G. Lewis, U. Schwertmann, Clay Miner. 14 (1979) 115.

[220] P.R. Anderson, M.M. Benjamin, Environ. Sci. Technol. 24 (1990) 692.

[221] Daren Cline, Statistics 601-Statistical Analysis, Texas A&M University, College Station, TX, 2003, p. 15-16.

[222] X. Meng, R.D. Letterman, Environ. Sci. Technol. 27 (1993) 1924.

[223] H.A.B. Potter, R.N. Yong, Applied Clay Science 14 (1999) 1.

[224] K. Kaiser, G. Guggenberger, European Journal of Soil Science 54 (2003) 219.

[225] J. Berkowitz, M.A. Anderson, C. Amrhein, Wat. Res. 40 (2006) 911.

[226] N. Koga, S. Yamada, Solid State Ionics 172 (2004) 253.

[227] J.E. Schenk, W.J. Weber Jr., J. AWWA 2 (1968) 199.

[228] S. Goldberg, J.A. Davis, J.D. Hem, in: G. Sposito (Eds.), The Surface Chemistry of Aluminum Oxides and Hydroxides, CRC Press/Lewis Publ., Boca Raton, FL, 1996, p. 271-331.

[229] T. Hiemstra, H. Yong, W.H. Van Riemsdijk, Langmuir 15 (1999) 5942.

[230] C. Su, D.L. Suarez, Clays Clay Miner. 45 (1997) 814.

[231] C.M. Douglas, C.R. George, Applied Statistics and Probability for Engineers, John Wiley & Sons, Inc., New York, 2002, p. 171-177.

[232] T. Sugimoto, X. Zhou, A. Muramatsu, J. Colloid Interface Sci. 252 (2002) 339.

[233] Z. Feng, J. Zhao, F.E. Huggins, G.P. Huffman, J. Catal. 143 (1993) 510.

[234] T.G. Quin, G.J. Long, C.G. Benson, Clays Clay Miner. 36 (1988) 165.

[235] W.T. Reichle, S.Y. Kang, D.S. Everhardt, J. Catal. 101 (1986) 352.

[236] N. Uekawa, J. Kajiwara, K. Kakegawa, Y. Sasaki, J. Colloid Interface Sci. 250 (2002) 285.

[237] A.R. Hind, S.K. Bhargava, S.C. Grocott, Colloids Surf. A 146 (1999) 359.

[238] K. Wefers, C. Misra, Oxides and Hydroxides of Aluminum, Aloca Technical Paper No. 19, Aloca Laboratories, Pittsburgh, PA, 1987

[239] T. Sato, J. Therm. Anal. 32 (1987) 61.

[240] J. Rouquerol, F. Rouquerol, M. Ganteaume, J. Catal. 36 (1975) 99.

[241] I.N. Bhattacharya, S.C. Das, P.S. Mukherjee, S. Paul, P.K. Mitra, Scandinavian J. of Metallurgy 33 (2004) 211.

[242] X. Gong, Z. Nie, M. Qian, J. Liu, L.A. Pederson, D.T. Hobbs, N.G. McDuffie, Ind. Eng. Chem. Res. 42 (2003) 2163.

[243] L. Liang, J.J. Morgan, Aquatic Sci. 52 (1990) 32.

[244] M. Schudel, S.H. Behrens, H. Holthoff, R. Kretzschmar, M. Borkovec, J. Colloid Interface Sci. 196 (1997) 241.

[245] N.F. Bogdanova, A.V. Klebanov, L.E. Ermakova, M.P. Sidorova, Colloid J. 64 (2002) 389.

[246] N.F. Bogdanova, L.E. Ermakova, P.S. Chikhachev, M.P. Sidorova, Colloid J. 67 (2005) 422.

[247] N.K. Lazaridis, K.A. Matis, M. Webb, Chemosphere 42 (2001) 373.

[248] N.K. Lazaridis, A. Hourzemanoglou, K.A. Matis, Chemosphere 47 (2002) 319.

[249] Y. Seida, Y. Nakano, Wat. Res. 34 (2000) 1487.

[250] T. Sato, T. Wakabayashi, M. Shimada, Ind. Eng. Chem. Prod. Res. Dev. 25 (1986) 89.

[251] S. Miyata, Clays Clay Minner. 28 (1980) 50.

[252] T. Sugimoto, X. Zhou, J. Colloid Interface Sci. 252 (2002) 347.

[253] D.G. Schulze, in: J.B. Dixon, D.G. Schulze (Eds.), An Introduction to Soil Mineralogy, SSSA, Inc., Madison, WI, 2002, p. 1-35.

[254] P. Alphonse, M. Courty, Thermochimica Acta 425 (2005) 75.

[255] B. Doušová, V. Machovič, D. Koloušek, F. Kovanda, V. Dorničák, Water Air Soil Pollut. 149 (2003) 251.

[256] F. Ogata, N. Kawasaki, T. Nakamura, S. Tanada, J. Colloid Interface Sci. 300 (2006) 88.

[257] S. Goldberg, Soil Sci. Soc. Am. J. 66 (2002) 413.

[258] W.L. Lindsay, Chemical Equilibria in Soils, John Wiley & Sons, New York, 1979, p. 34-49.

[259] J.G. Hering, P.Y. Chen, J.A. Wilkie, M. Elimelech, J. Environ. Eng. 123 (1997) 800.

[260] D.A. Dzombak, F.M.M. Morel, Surface Complexation Modeling, Hydrous Ferric Oxide, John Wiley & Sons, New York, 1990, p. 43-64.

[261] J.H. Gulledge, J.T. O'connor, J. AWWA 65 (1973) 548.

[262] L.S. McNeill, M. Edwards, J. AWWA, 89 (1997) 75.

[263] N. Khare, D. Hesterberg, J.D. Martin, Environ. Sci. Technol. 39 (2005) 2152.

[264] A. García-Sanchez, E. Alvarez-Ayuso, F. Rodriguez-Martin, Clay Miner. 37 (2002) 187.

VITA

Namryong Her

Academic History

- Ph.D. Civil Engineering, Texas A&M University, Texas USA
  August 2007
  Dissertation: "Transformation of 2-Line Ferrihydrite and Its Effect on Arsenic Adsorption"
  Advisor: Dr. Robin Autenrieth & Dr. Richard H. Loeppert
- M.S. Civil Engineering, Korea Advanced Institute of Science & Technology, Korea (Feb 1988)
- B.S. Civil Engineering, Korea University, Korea (Feb 1986)

Experience

- Research Assistant, Texas A&M University (January 2003 to April 2006)
- Manager, Hyundai E&C Co., Seoul, South Korea (May 1992 to July 2001)
- Researcher, Korea Institute of Science & Technology, Seoul, South Korea (April 1991 to May 1992)
- Assistant Manager, Daewoo Engineering Co., Seoul, South Korea (March 1988 to April 1991)

Publications

"A study on Treatment of Composting Toilet Effluent Using Ozonation and Activated Carbon Adsorption", N. Her, W. C. Park, and J. M. Oh (1993), *J. of Water Purification & Liquid Waste Treatment (Japan)*, 34(10), 15-21.

"Design Optimization for Solidification of Hazardous Wastes", N. Her, H. S. Shin, and J. K. Koo (1988), *Hazardous Waste & Hazardous Materials*, 5(3), 239-250.

"Solidification of Hazardous Waste from Electroplating Industry", N. Her, H. S. Shin, and J. K. Koo (1988), *J. of Korea Society of Civil Engineers*, 8(2), 89-98.

Professional Registration

- Professional Engineer (PE), Registrated No. 9414101251, Water Supply & Sewage, Civil Engineering, Korea (1994)